THIRD EDITION

ECHOCARDIOGRAPHY IN PEDIATRIC AND CONGENITAL HEART DISEASE

FROM FETUS TO ADULT

EDITED BY

WYMAN W. LAI | LUC L. MERTENS | MERYL S. COHEN | TAL GEVA

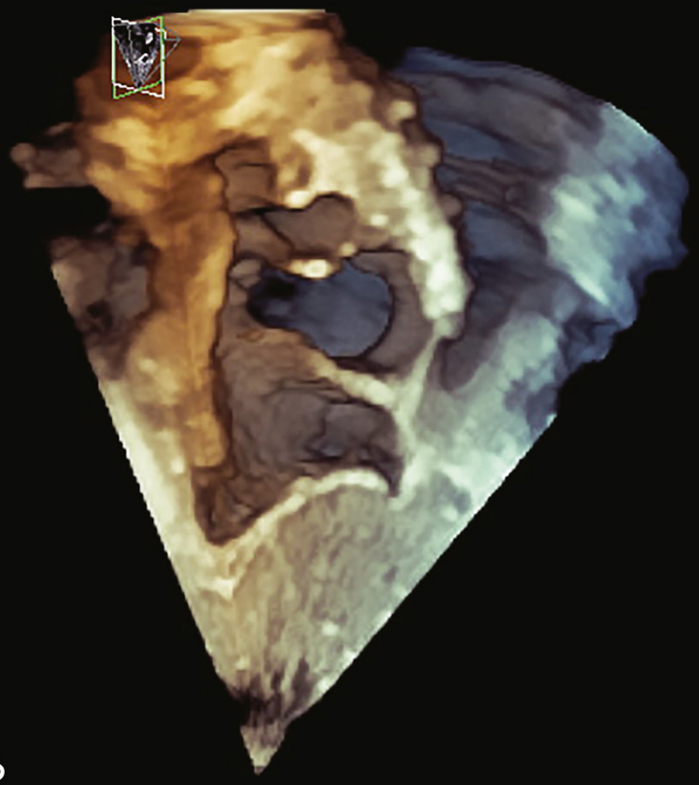

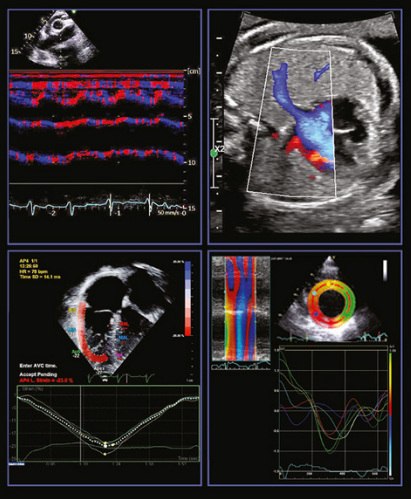

with website

WILEY Blackwell

Echocardiography in Pediatric and Congenital Heart Disease

Dedications

To my parents, CheToo and SoFa Lai; my wonderful wife, Lydia; and my children, Justin and Amanda.

Wyman W. Lai

To the team I have the privilege of working with every day. They inspire me and keep me humble. To the pediatric echo family in Europe and North America: what an amazing group of professional friends you have become. Not in the least: to my children Francis and Virginie; for all the time I could not spend with them.

Luc L. Mertens

To my husband Bruce Randazzo and my children Jake, Isabel, and Ethan for supporting me always.

Meryl S. Cohen

To my wife Judith and sons Omri and Alon with love.

Tal Geva

Echocardiography in Pediatric and Congenital Heart Disease

From Fetus to Adult

Third Edition

Edited by

Wyman W. Lai MD, MPH, MBA

Co-Medical Director
CHOC Children's Heart Institute
Orange, CA;
Clinical Professor
Department of Pediatrics
University of California, Irvine School of Medicine
Irvine, CA, USA

Luc L. Mertens MD, PhD

Section Head, Echocardiography
Cardiology
The Hospital for Sick Children;
Professor of Pediatrics
Department of Pediatrics
University of Toronto
Toronto, ON, Canada

Meryl S. Cohen MD, MS Ed

Professor of Pediatrics
Perelman School of Medicine
University of Pennsylvania;
Associate Chief, Division of Cardiology
The Cardiac Center
The Children's Hospital of Philadelphia
Philadelphia, PA, USA

Tal Geva MD

Alexander S. Nadas Professor of Pediatrics
Harvard Medical School;
Cardiologist-in-Chief and Chair
Department of Cardiology
Boston Children's Hospital
Boston, MA, USA

WILEY Blackwell

This edition first published 2022

Edition History
2009 (1e John Wiley & Sons Ltd.); 2016 (2e John Wiley & Sons Ltd.)

Registered Offices
John Wiley & Sons, Inc., 111 River Street, Hoboken, NJ 07030, USA
John Wiley & Sons Ltd, The Atrium, Southern Gate, Chichester, West Sussex, PO19 8SQ, UK

Editorial Office
9600 Garsington Road, Oxford, OX4 2DQ, UK

For details of our global editorial offices, customer services, and more information about Wiley products visit us at www.wiley.com.

Wiley also publishes its books in a variety of electronic formats and by print-on-demand. Some content that appears in standard print versions of this book may not be available in other formats.

Library of Congress Cataloging-in-Publication Data

Names: Lai, Wyman W., editor. | Mertens, Luc, editor. | Cohen, Meryl, editor. | Geva, Tal, editor.
Title: Echocardiography in pediatric and congenital heart disease : from fetus to adult / edited by Wyman W. Lai, Luc L. Mertens, Meryl S. Cohen, Tal Geva.
Description: Third edition. | Hoboken, NJ : Wiley-Blackwell, 2022. | Includes bibliographical references and index.
Identifiers: LCCN 2021028306 (print) | LCCN 2021028307 (ebook) | ISBN 9781119612803 (cloth) | ISBN 9781119612889 (adobe pdf) | ISBN 9781119612872 (epub)
Subjects: MESH: Heart Defects, Congenital–diagnostic imaging | Echocardiography–methods
Classification: LCC RC683.5.U5 (print) | LCC RC683.5.U5 (ebook) | NLM WG 220 | DDC 616.1/207543–dc23
LC record available at https://lccn.loc.gov/2021028306
LC ebook record available at https://lccn.loc.gov/2021028307

Cover Design: Wiley
Cover Images: © Tal Geva

Set in 9.5/12pt Minion by Straive, Pondicherry, India

10 9 8 7 6 5 4 3 2 1

Contents

Contributors

Vivekanand Allada MD
Professor of Clinical Pediatrics
Perelman School of Medicine
University of Pennsylvania;
Medical Director, Outpatient and Community Cardiology
Associate Chief, Cardiology
Director of Strategic Operations, Cardiac Center
The Children's Hospital of Philadelphia
Philadelphia, PA, USA

Gabriel Altit MD
Neonatology
Department of Pediatrics
McGill University
Montreal, QC, Canada

Bhawna Arya MD, FASE, FACC
Director, Fetal Cardiology
Seattle Children's Hospital;
Associate Professor of Pediatrics
Division of Cardiology
University of Washington School of Medicine
Seattle, WA, USA

Amir H. Ashrafi MD, FASE, FACC
Neonatal-Cardiac Intensive Care
Division of Neonatology
CHOC Children's Hospital
Orange, CA, USA

Piers C. A. Barker MD
Professor of Pediatrics and Obstetrics/Gynecology
Section Head, Pediatric Cardiac Non-Invasive Imaging
Duke University School of Medicine
Durham, NC, USA

Rebecca S. Beroukhim MD
Co-Director, Heart Tumor Program
Assistant Professor of Pediatrics
Harvard Medical School;
Boston Children's Hospital
Boston, MA, USA

William L. Border MBChB, MPH, FASE
Director of Noninvasive Cardiac Imaging
Children's Healthcare of Atlanta Sibley Heart Center;
Professor of Pediatrics
Emory University School of Medicine
Atlanta, GA, USA

David W. Brown MD
Associate Professor of Pediatrics
Department of Cardiology
Boston Children's Hospital;
Department of Pediatrics
Harvard Medical School
Boston, MA, USA

Dale A. Burkett MD
Assistant Professor
University of Colorado;
The Heart Institute
Children's Hospital Colorado
Aurora, CO, USA

Elizabeth Caris MD
Assistant Professor
Department of Pediatrics
University of Washington School of Medicine
Seattle Children's Hospital
Seattle, WA, USA

Frank Cetta MD, FACC, FASE
Professor of Medicine and Pediatrics
Mayo Clinic
Rochester, MN, USA

Meryl S. Cohen MD, MS Ed
Professor of Pediatrics
Perelman School of Medicine
University of Pennsylvania;
Associate Chief, Division of Cardiology
The Cardiac Center
The Children's Hospital of Philadelphia
Philadelphia, PA, USA

Steven D. Colan MD
Professor of Pediatrics
Harvard Medical School;
Boston Children's Hospital
Boston, MA, USA

Julie De Backer MD, PhD
Professor
Department of Cardiology and Center for Medical Genetics
Ghent University Hospital
Ghent, Belgium

Jan D'hooge MD
Professor
Department of Cardiovascular Sciences
Catholic University of Leuven;
Medical Imaging Research Center
University Hospitals Leuven
Leuven, Belgium

Andreea Dragulescu MD, PhD
Labatt Family Heart Center
Division of Cardiology
The Hospital for Sick Children;
Staff Cardiologist, Associate Professor
Department of Pediatrics
University of Toronto
Toronto, ON, Canada

Stacey Drant MD
Professor of Pediatrics
Division of Pediatric Cardiology
Perelman School of Medicine
University of Pennsylvania;
The Children's Hospital of Philadelphia
Philadelphia, PA, USA

Benjamin W. Eidem MD, FACC, FASE
Professor of Pediatrics and Medicine
Mayo Clinic
Rochester, MN, USA

Matthew Fenton MB, BS, BSc
Consultant Paediatric Cardiologist
Cardiothoracic Unit
Great Ormond Street Hospital for Children;
Institute of Cardiovascular Sciences
University College London
London, UK

Lindsay R. Freud MD
Associate Professor of Pediatrics
University of Toronto;
Associate Director of Fetal Cardiology
The Hospital for Sick Children;
Toronto, ON, Canada

Mark K. Friedberg MD
Professor of Pediatrics
Labatt Family Heart Center
Department of Pediatrics
The Hospital for Sick Children;
University of Toronto
Toronto, ON, Canada

Kevin G. Friedman MD
Pediatric Medicine
Boston Children's Hospital;
Associate Professor
Harvard Medical School
Boston, MA, USA

Michele A. Frommelt MD
Professor of Pediatrics
Division of Pediatric Cardiology
Medical College of Wisconsin;
Children's Hospital of Wisconsin
Milwaukee, WI, USA

Peter C. Frommelt MD
Professor of Pediatrics
Director of Echocardiography
Division of Pediatric Cardiology
Medical College of Wisconsin;
Children's Hospital of Wisconsin
Milwaukee, WI, USA

Javier Ganame MD, PhD
Associate Professor of Medicine
Department of Medicine
Division of Cardiology
McMaster University
Hamilton, ON, Canada

Tal Geva MD
Alexander S. Nadas Professor of Pediatrics
Harvard Medical School;
Cardiologist-in-Chief and Chair
Department of Cardiology
Boston Children's Hospital
Boston, MA, USA

Marc Gewillig MD, PhD, FESC, FACC, FSCAI
Professor of Paediatric and Congenital Cardiology
University Hospitals Leuven
Leuven, Belgium

David J. Goldberg MD
Associate Professor of Pediatrics
Division of Pediatric Cardiology
The Children's Hospital of Philadelphia;
Perelman School of Medicine
University of Pennsylvania
Philadelphia, PA USA

Lisa K. Hornberger MD
Professor of Pediatrics and Obstetrics and Gynecology
Director, Fetal and Neonatal Cardiology Program
Section Head, Pediatric Echocardiography
Stollery Children's Hospital;
Mazankowski Alberta Heart Institute;
Women's and Children's Health Research Institute
University of Alberta
Edmonton, AB, Canada

Xavier Iriart MD
Section Head, Echocardiography
Department of Pediatric and Adult Congenital Cardiology
Bordeaux University Hospital (CHU)
Pessac, France

Pei-Ni Jone MD
Professor of Pediatrics
Pediatric Cardiology
Director of Echocardiography Quality
Director of 3D Echocardiography
Division of Pediatric Cardiology
Children's Hospital Colorado;
University of Colorado School of Medicine
Denver, CO, USA

Sachin Khambadkone MD
Interventional Cardiologist
Paediatric and Adolescent Cardiology
Great Ormond Street Hospital for Children;
Hon. Associate Professor
Institute of Cardiovascular Sciences
University College London
London, UK

Joe R. Kreeger ACS, RDCS, RCCS
Senior Sonographer
Children's Healthcare of Atlanta Sibley Heart Center
Atlanta, GA, USA

Andreas Kühn MD
Senior Consultant Pediatric Cardiology
Department of Pediatric Cardiology and Congenital Heart Disease
German Heart Center Munich;
Special Practice for Pediatric Cardiology and Congenital Heart Defects
Munich, Germany

Wyman W. Lai MD, MPH, MBA
Co-Medical Director
CHOC Children's Heart Institute
Orange, CA;
Clinical Professor
Department of Pediatrics
University of California, Irvine School of Medicine
Irvine, CA, USA

Matthew S. Lemler MD
Professor of Pediatrics
Division of Cardiology
University of Texas Southwestern;
Clinical Director, Pediatric Cardiology
Children's Medical Center of Dallas
Dallas, TX, USA

Jami C. Levine MS, MD
Assistant Professor of Pediatrics
Boston Children's Hospital
Boston, MA, USA

Leo Lopez MD
Clinical Professor of Pediatrics
Stanford University School of Medicine
Stanford, CA;
Medical Director of Echocardiography
Lucile Packard Children's Hospital Stanford
Palo Alto, CA, USA

Jan Marek MD, PhD, FESC
Professor of Cardiology
Institute of Cardiovasular Sciences
University College London;
Director of Echocardiography
Consultant Pediatric and Fetal Cardiologist
Great Ormond Street Hospital for Children
London, UK

Renee Margossian MD
Assistant Professor of Pediatrics
Harvard Medical School;
Department of Cardiology
Boston Children's Hospital
Boston, MA, USA

Colin J. McMahon MD, MHPE, FACC
Consultant Paediatric Cardiologist
Department of Paediatric Cardiology
Children's Health Ireland
Dublin, Ireland

Patrick J. McNamara MD
Chair of Neonatology
Department of Pediatrics
University of Iowa
Iowa City, IA, USA

Luc L. Mertens MD, PhD
Section Head, Echocardiography
Cardiology
The Hospital for Sick Children;
Professor of Pediatrics
Department of Pediatrics
University of Toronto
Toronto, ON, Canada

Owen I. Miller FRACP, FRCPCH
Consultant in Pediatric and Fetal Cardiology
Department of Congenital Heart Disease
Evelina London Children's Hospital
Guy's and St Thomas' NHS Foundation Trust
London, UK

Shaine A. Morris MD, MPH
Associate Professor, Pediatrics-Cardiology
Medical Director, Cardiovascular Genetics
Medical Director, Fetal Cardiology
Department of Pediatrics
Section of Cardiology
Texas Children's Hospital and Baylor College of Medicine
Houston, TX, USA

Shobha Natarajan MD
Associate Professor of Clinical Pediatrics
The University of Pennsylvania School of Medicine;
Division of Cardiology
The Children's Hospital of Philadelphia
Philadelphia, PA, USA

James C. Nielsen MD
Clinical Professor of Pediatrics
NYU Grossman School of Medicine;
Associate Director, Pediatric Cardiology
Hassenfeld Children's Hospital at NYU Langone
New York, NY, USA

Erwin Oechslin MD, FRCPC, FESC
Professor of Medicine
Toronto Adult Congenital Heart Disease Program
University of Toronto;
Bitove Family Professor of Adult Congenital Heart Disease
Peter Munk Cardiac Centre
University Health Network/Toronto General Hospital
Toronto, ON, Canada

Ira A. Parness MD
Director of Pediatric Echocardiography
Cohen's Children's Medical Center/Northwell Health;
Professor of Pediatrics
Donald and Barbara Zucker School of Medicine at Hofstra/Northwell
New York, NY, USA

Maria A. Pernetz RDCS, RVT, RCCS
Technical Director, Adult Congenital Heart Center
Emory Healthcare
Atlanta, GA, USA

Andrew J. Powell MD
Chief, Cardiac Imaging Division
Department of Cardiology
Boston Children's Hospital;
Professor of Pediatrics
Harvard Medical School
Boston, MA, USA

Ashwin Prakash MD
Director, Cardiac MRI and CT
Department of Cardiology
Boston Children's Hospital;
Associate Professor of Pediatrics
Harvard, Medical School
Boston, MA, USA

Kuberan Pushparajah MD
Consultant Paediatric Cardiologist and Clinical Senior Lecturer
King's College London;
Congenital Cardiac MRI Programme Lead
Evelina London Children's Hospital
Guy's and St Thomas' NHS Foundation Trust
London, UK

Michael D. Quartermain MD, FASE
Associate Professor of Clinical Pediatrics
Perelman School of Medicine
University of Pennsylvania;
Medical Director, Pediatric Echocardiography Laboratory
Division of Cardiology
The Children's Hospital of Philadelphia
Philadelphia, PA, USA

Daniela Y. Rafii MD
Assistant Professor of Clinical Pediatrics
Hassenfeld Children's Hospital at NYU Langone
Associate Director, Pediatric Cardiology
Maimonides Children's Hospital
New York, NY, USA

Claudio Ramaciotti MD
Professor of Pediatrics
Division of Cardiology
Director, Echocardiography Laboratory
University of Texas Southwestern;
Children's Medical Center of Dallas
Dallas, TX, USA

Pierangelo Renella MD
Department of Cardiology
CHOC Children's Heart Institute
Orange, CA;
Associate Professor of Pediatrics
University of California, Irvine School of Medicine
Irvine, CA, USA

Lindsey S. Rogers MD, MS Ed
Associate Professor of Clinical Pediatrics
Perelman School of Medicine
University of Pennsylvania;
Division of Cardiology
The Children's Hospital of Philadelphia
Philadelphia, PA, USA

Jack Rychik MD
Professor of Pediatrics
Division of Pediatric Cardiology
The Children's Hospital of Philadelphia;
Perelman School of Medicine
University of Pennsylvania
Philadelphia, PA USA

Craig Sable MD
Associate Chief, Division of Cardiology
Children's National Hospital;
Professor of Pediatrics
George Washington University School of Medicine
Washington, DC, USA

Ritu Sachdeva MD
Medical Director, Cardiovascular Imaging Research Core
Children's Healthcare of Atlanta Sibley Heart Center;
Professor of Pediatrics
Emory University School of Medicine
Atlanta, GA, USA

Stephen P. Sanders MD
Professor of Pediatrics (Cardiology)
Harvard Medical School;
Director, Cardiac Registry
Departments of Cardiology, Pathology, and Cardiac Surgery
Boston Children's Hospital
Boston, MA, USA

Jill J. Savla MD, MSCE
Assistant Professor of Pediatrics
Perelman School of Medicine
University of Pennsylvania;
Division of Cardiology
The Children's Hospital of Philadelphia
Philadelphia, PA, USA

David N. Schidlow MD, MMus
Assistant Professor of Pediatrics
Harvard Medical School;
Department of Cardiology
Boston Children's Hospital
Boston, MA, USA

John M. Simpson MD, FRCP
Professor of Paediatric and Fetal Cardiology
Department of Congenital Heart Disease
Evelina London Children's Hospital
Guy's and St Thomas' NHS Foundation Trust
London, UK

Timothy C. Slesnick MD
Director of Cardiac MRI
Children's Healthcare of Atlanta Sibley Heart Center;
Associate Professor of Pediatrics
Emory University School of Medicine
Atlanta, GA, USA

Shubhika Srivastava MBBS
Professor of Pediatrics
Sidney Kimmel School of Medicine
Thomas Jefferson University;
Chief of Cardiology
Nemours/Alfred I. duPont Hospital for Children
Wilmington, DE, USA

Poonam P. Thankavel MD
Director of Cardiac Imaging
Medical City Children's Hospital
Dallas, TX, USA

Anne Marie Valente MD
Associate Professor of Pediatrics and Internal Medicine
Departments of Cardiology and Pediatrics
Boston Children's Hospital;
Division of Cardiology, Department of Medicine
Brigham and Women's Hospital;
Harvard Medical School
Boston, MA, USA

Olivier Villemain MD, MSc, PhD
Assistant Professor of Pediatrics
Labatt Family Heart Center
Department of Pediatrics
The Hospital for Sick Children;
Department of Pediatrics
University of Toronto
Toronto, ON, Canada

Manfred Otto Vogt MD, PhD
Professor of Pediatric Cardiology
Technische Universität München;
Special Practice for Pediatric Cardiology and Congenital Heart Defects
Munich, Germany

Jacqueline Wheatley DMS, RDCS, FASE
Pediatric Cardiac Sonographer
The Hospital for Sick Children
Toronto, ON;
Skills Instructor, Diagnostic Cardiac Sonography Program
Mohawk College
Hamilton, ON, Canada

Brian R. White MD, PhD
Instructor of Pediatrics
Division of Pediatric Cardiology
The Children's Hospital of Philadelphia;
Perelman School of Medicine
University of Pennsylvania
Philadelphia, PA, USA

Adel K. Younoszai MD
Associate Dean of Child Health
Professor of Pediatric Cardiology
University of Colorado School of Medicine;
Associate Director of Child Health, CU Medicine
Assistant Director of Ambulatory Care
Children's Hospital Colorado
Aurora, CO, USA

Meghan Zimmerman MD, MPH
Department of Pediatrics
Dartmouth-Hitchcock Medical Center;
Assistant Professor of Pediatrics
Geisel School of Medicine
Lebanon, NH, USA

Preface

This textbook was designed to be a resource on echocardiography in pediatric and congenital heart disease. When first published in 2009, this book filled a void of nearly 10 years between major textbooks in the field. In this textbook we strived to provide a comprehensive source of information for both beginners and advanced practitioners. At the time of the first edition, the "special" topics included 3D echocardiography and fetal echocardiography. When we updated the textbook in 2016, the newer topics were post-Fontan imaging and pregnancy with heart disease.

In this updated third edition of our comprehensive textbook, we focused on consolidating recent advances in echocardiography into routine practice. We have incorporated the topics of speckle tracking echocardiography and 3D echocardiography into the chapters discussing ventricular function and cardiovascular lesions. To highlight the progress in our profession, we added new chapters on assessment of the right ventricle, the transitional neonatal circulation, and the role of multimodality imaging. In our "key elements" sections, we continued to emphasize echocardiographic predictors of important clinical outcomes. Many, if not most, of the images and videos have been replaced to give the readers up-to-date examples of essential clinical images.

The pediatric echocardiography community is small but cohesive. We are indebted to all the authors – both physicians and sonographers – who contributed to the success of this textbook. The authors have volunteered their time, imparted their expertise, and provided images of the highest quality. Cooperation and the willingness to share information provides a constant source of quality improvement to all of our laboratories. The editors are also grateful for the support and aid provided by the staff at Wiley Blackwell. In addition to their editing and publishing efforts, they have served as a wonderful link between the authors, editors, and printers.

We would like to recognize the "founders" of pediatric echocardiography who pioneered the use of ultrasound in the investigation of congenital heart disease. Many of these founders wrote or edited excellent textbooks on pediatric echocardiography, including Stanley Goldberg, Geoffrey Stevenson, Roberta Williams, Stephen Sanders, Norman Silverman, David Sahn, Rebecca Snider, Gerald Serwer, and Alvin Chin. Without the outstanding work of these pioneers and others who followed them, we would have much less to write about in our field.

Finally, as with all work endeavors, we would not have succeeded without the unwavering support of our families, friends, and colleagues. We owe them so much more than we express here.

Wyman W. Lai, MD, MPH, MBA
Luc L. Mertens, MD, PhD
Meryl S. Cohen, MD, MS Ed
Tal Geva, MD

About the Companion Website

This book is accompanied by a companion website:

www.wiley.com/go/lai-echo3

The companion website includes over 700 video clips, referenced at the end of the chapters throughout the book.

PART I

Introduction to Cardiac Ultrasound Imaging

CHAPTER 1

Ultrasound Physics

Jan D'hooge[1], Olivier Villemain[2], and Luc L. Mertens[2]
[1]Catholic University of Leuven; University Hospitals Leuven, Leuven, Belgium
[2]The Hospital for Sick Children; University of Toronto, Toronto, ON, Canada

Physics and technology of echocardiography

In echocardiography images of the cardiovascular structures are created by using ultrasound waves. Knowledge of the physics of ultrasound helps us to understand how the different ultrasound imaging modalities operate and is also important when operating an ultrasound machine as it can help with image optimization during acquisition and a better understanding of machine operation.

This chapter describes the essential concepts of how ultrasound waves can be used to generate an image of the heart. Certain technological developments are discussed, as well as how machine settings influence image characteristics. For a more detailed description of ultrasound physics in imaging we refer the readers to dedicated literature on the topic [1,2].

How the ultrasound image is created

The pulse–echo experiment

To illustrate how ultrasound imaging works, the acoustic "pulse–echo" experiment can be used:

1. A short electric pulse is applied to a piezoelectric crystal. This electric field will induce a shape change of the crystal through reorientation of its polar molecules. Thus, the application of an electric field deforms the crystal.
2. The deformation of the piezoelectric crystal induces a local compression of the tissue with which the crystal is in contact. Thus, the superficial tissue layer is briefly compressed resulting in an increase in local pressure (acoustic pressure) (Figure 1.1).
3. Due to an interplay between tissue elasticity and inertia, this local tissue compression (with subsequent decompression or rarefaction) propagates away from the piezoelectric crystal at a speed of approximately 1530 m/s in human soft tissue (Figure 1.2). This is called the acoustic wave. The rate of compression/decompression determines the frequency of the wave and typically is between 1 and 15 MHz for human diagnostic ultrasonic imaging. As these frequencies cannot be perceived by the human ear, these waves are named "ultrasonic" (the range of human perceivable frequencies is between 20 and 20 kHz). The spatial distance between subsequent compressions is called the wavelength (λ) and relates to the frequency (f) and sound velocity (c) as: $\lambda \cdot f = c$. During propagation, acoustic energy is lost mostly as a result of absorption resulting in a reduction in amplitude of the wave with propagation distance. The shorter the wavelength (i.e., the higher the frequency), the faster the particle motion and the larger the absorption effects. Higher frequency waves will thus attenuate more and penetrate less deeply into the tissue. This explains why the "high" frequency probes have less penetration.
4. Spatial changes in tissue density or tissue elasticity will result in a disturbance of the propagating compression (i.e., acoustic) wave and will cause part of the energy in the wave to be reflected. These so-called "specular reflections" occur, for example, at the interface between different types of tissue (i.e., acoustic impedance difference), such as between blood and myocardium. The reflected waves behave similarly to optic waves as the direction is determined by the angle between the reflecting surface and the incident wave. This is similar to the reflection of optic waves on the water surface. When the spatial dimensions of the changes in density or compressibility become small relative to the wavelength (i.e., below ~100 μm), these inhomogeneities will cause part of the energy in the wave to be scattered and transmitted in different directions. Part of the scattered energy is transmitted back in the direction of source and is called *backscatter*. Both the specular and backscattered reflections propagate back towards the piezoelectric crystal.
5. When the reflected waves reach the piezoelectric crystal this causes deformation and results in relative motion of its (polar) molecules and generation of an electric field, which can be detected and measured. The amplitude of this electric signal is directly proportional to the amount of compression of the crystal, which is determined by the amplitude of the reflected/backscattered waves. This electric signal is the radiofrequency (RF) signal and can be represented as the amplitude of the reflected ultrasound wave as a function of time (Figure 1.3). Because reflections occurring further away

Echocardiography in Pediatric and Congenital Heart Disease: From Fetus to Adult, Third Edition. Edited by Wyman W. Lai, Luc L. Mertens, Meryl S. Cohen and Tal Geva.

Companion website: www.wiley.com/go/lai-echo3

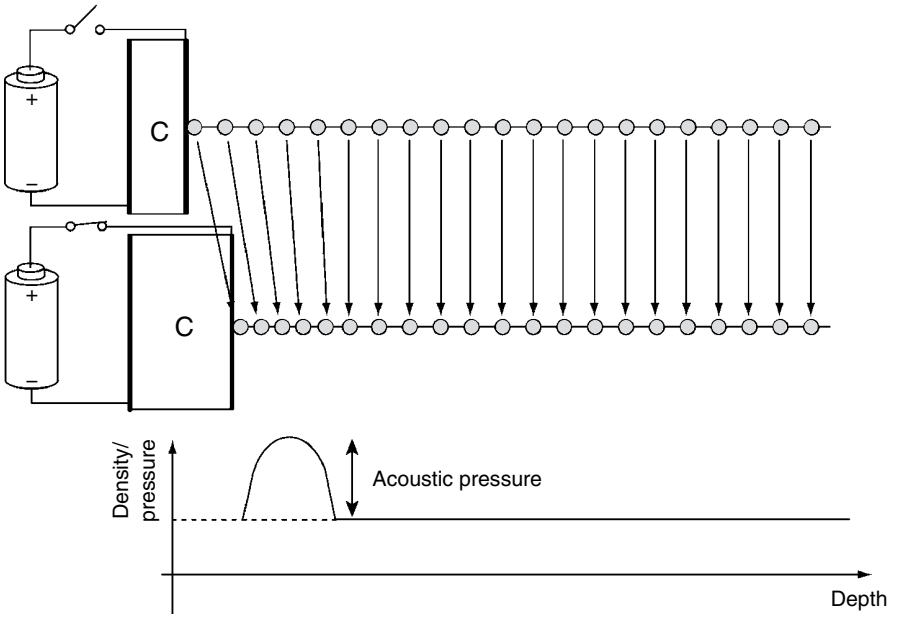

Figure 1.1 Local tissue compression due to deformation of the piezoelectric crystal (C) when applying an electric field.

from the transducer need to propagate further, they will be received later. As such, the time axis in Figure 1.3 can be replaced by the propagation distance of the wave (i.e., depth). The signal detected by the transducer is typically electronically amplified. The amount of amplification has a preset value but can be modified on an ultrasound system by using the "gain" button. Importantly, the overall gain will amplify both the signal and potential noise and will thus not impact the signal-to-noise ratio.

In the example shown in Figure 1.3, taken from a water tank experiment, two strong specular reflections can be observed (around 50 and 82 μs) while the lower amplitude reflections in between are scatter reflections. In clinical echocardiography, the most obvious specular reflection is the strong reflection coming from the pericardium observed in the parasternal views as a consequence of the high acoustic impedance difference. The direction of propagation of the specular reflection is determined by the angle between the incident wave and the reflecting

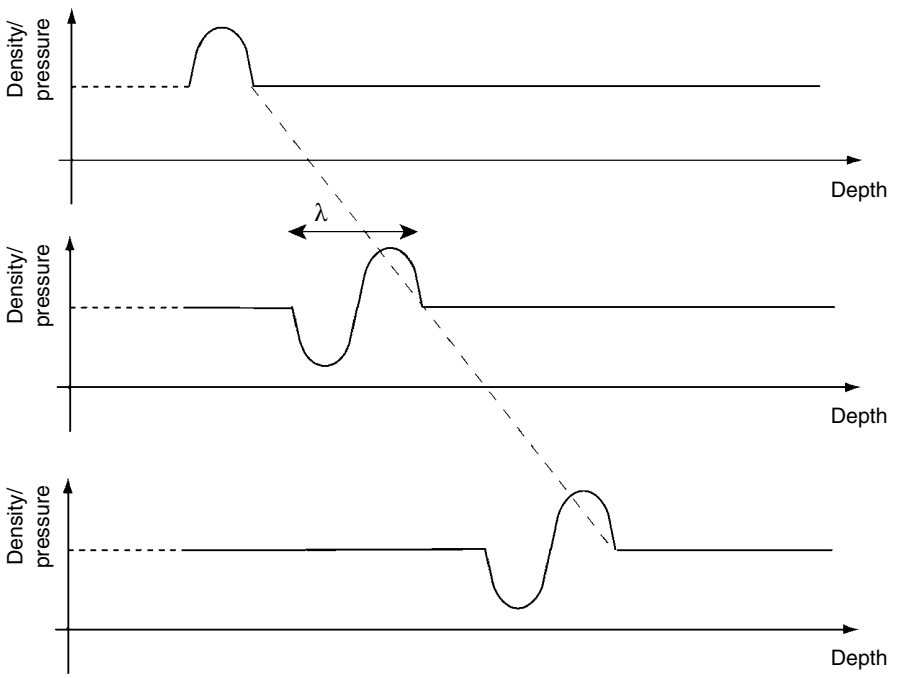

Figure 1.2 The local tissue compression/decompression propagates away from its source at a speed of approximately 1530 m/s in soft tissue.

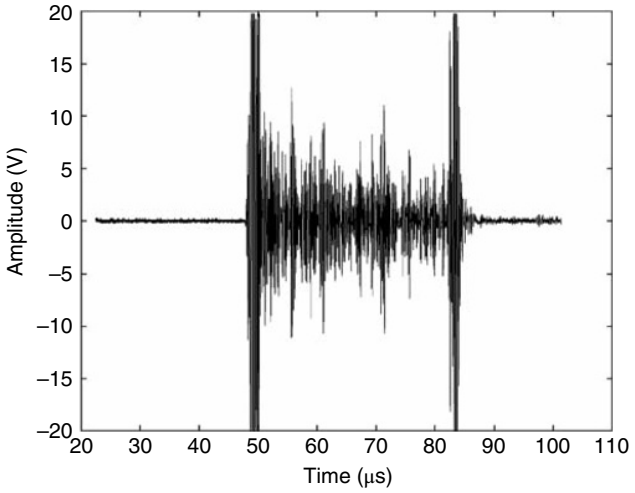

Figure 1.3 The reflected amplitude of the reflected ultrasound waves as a function of time after transmission of the ultrasound pulse is called the radiofrequency signal.

surface. Thus, the strength of the observed reflection will depend on: (i) the exact transducer position; (ii) orientation with respect to the pericardium; and (iii) the acoustic impedance difference between the two structures. Indeed, for given transducer positions/orientations, the strong specular reflection might propagate in a direction not detectable by the transducer. For this reason, the pericardium typically does not show as bright in the images taken from an apical transducer position. In contrast, scatter reflections are not angle dependent and will always be visible for a given structure independent of the exact transducer position.

The total duration of the above described pulse–echo experiment is about 100 μs when imaging at 5 MHz The reflected signal in Figure 1.3 is referred to as an A-mode image ("A" referring to "amplitude") and is the most fundamental form of imaging given it tells us something about the acoustic characteristics of the materials in front of the transducer. For example, Figure 1.3 clearly shows that at distance of ~3.7 cm in front of the transducer the propagation medium changes density and/or compressibility, with a similar change occurring at a distance of ~6.3 cm (these distances correspond to 50 and 82 μs, respectively, times 1530 m/s – which is the total propagation distance of the wave – divided by 2 as the wave has to travel back and forth). The 2.6 cm of material in between these strong reflections is acoustically inhomogeneous (i.e., shows scatter reflections) and thus contains local (very small) fluctuations in mass density and/or compressibility, while the regions closer and further away from the transducer do not cause significant scatter and would thus be acoustically homogeneous. Indeed, this A-mode image was taken from a 2.6-cm thick tissue-mimicking material (i.e., gelatin in which small graphite particles were dissolved) put in a water tank.

Grayscale encoding

Since the A-mode image just presented is not visually attractive, the RF signal resulting from a pulse–echo experiment is further processed:

1. *Envelope detection*: The high-frequency information of the RF signal is selected by detecting the envelope of the signal (Figure 1.4). This process is also referred to as "demodulation."
2. *Grayscale encoding*: The signal is subdivided as a function of time in small intervals. Each pixel/voxel is attributed a number, defined by the local amplitude of the signal, ranging between 0 and 255 (2^8 or 8-bit image). "0" represents "black," "255" represents "white," and a value in between is represented by a grayscale. By definition, bright pixels correspond to high-amplitude reflections (i.e., high acoustic impedance difference). This process is illustrated in Figure 1.4. Note that a different color encoding is also possible simply by coding different color intensities in a range of values between 0 and 255. On clinical scanners the color map can be easily selected and is a preference of the operator. Typically shades of blue or bronze can be used to represent the image. More modern ultrasound systems have higher resolution encoding with 12- or 16-bit resolution images (i.e., encoding 4096 or 65,536 gray/color levels).
3. *Attenuation correction*: As wave amplitude decreases with propagation distance due to attenuation (mostly due to conversion of acoustic energy to heat, i.e., acoustic absorption), reflections from deeper structures are intrinsically smaller in amplitude and therefore show less bright. In order to give identical structures located at different distances from the transducer a similar gray value (i.e., reflected amplitude), compensation for this attenuation must occur. Thus, an attenuation profile as a function of distance from the transducer is assumed, which allows for automatic amplification of the signals from deeper regions – the so-called *automated* time gain compensation (TGC), also referred to as depth gain compensation. As the preassumed attenuation profile might be incorrect mainly due to variable reflections and absorptions, sliders on the ultrasound scanner (TGC toggles) allow for manual correction of the automatic compensation and will result in more or less local amplification of the received signal as required to obtain a more homogenous brightness of the image. In this way, the operator can optimize local image brightness. It is recommended to start scanning using a neutral setting of these sliders, as attenuation characteristics will be patient and view specific. For every view the TGC can be optimized manually.
4. *Log compression*: In order to increase the image contrast in the darker (i.e., less bright) regions, gray values in the image may be redistributed according to a logarithmic curve (Figure 1.5). The characteristics of this compression (i.e., local contrast enhancement) can be changed on the

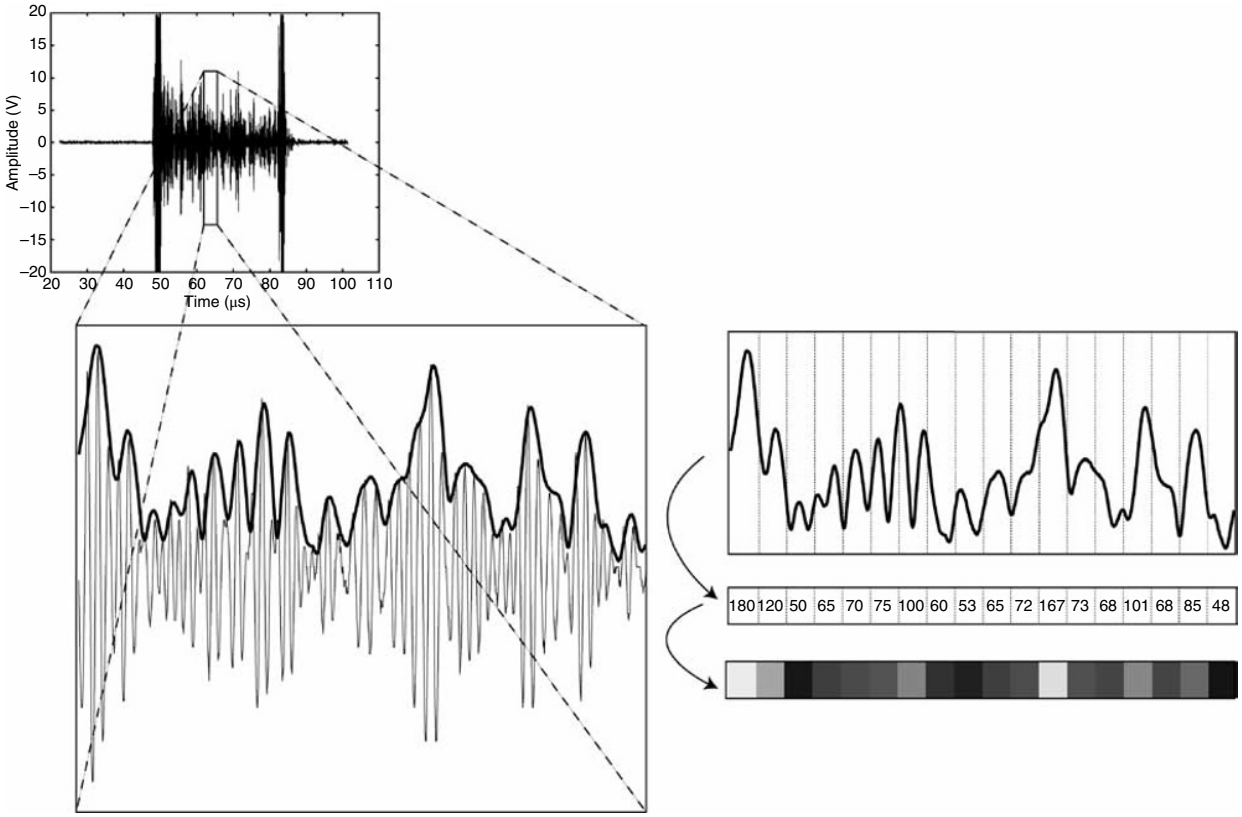

Figure 1.4 The radiofrequency signal is demodulated in order to detect its envelope. This envelope signal (bold) is color encoded based on the local signal amplitude.

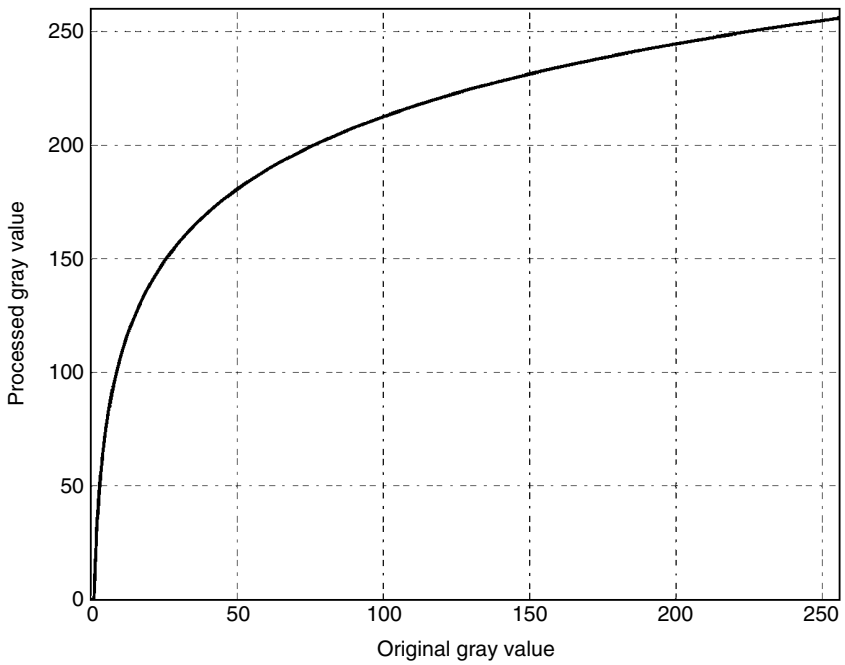

Figure 1.5 The logarithmic compression curve.

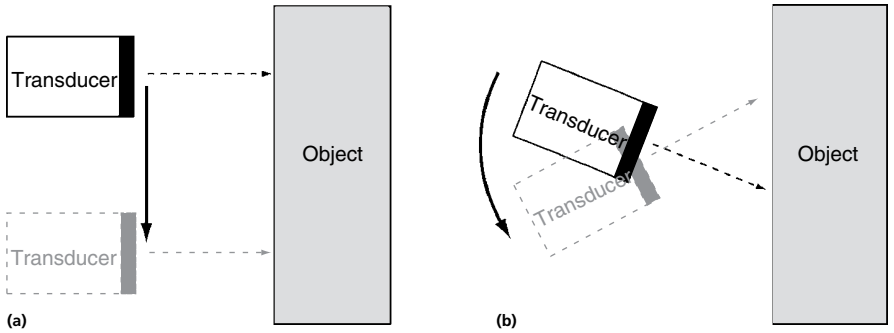

Figure 1.6 Translation of the ultrasound source results in a linear image format **(a)** whereas pivoting results in sector images **(b)**.

ultrasound scanner (contrast or compression). These setting changes do not affect the ultrasound acquisition but only influence the visual representation of the created image. This is similar to contrast adaptation used in digital photography, where ambient lighting and/or contrast can be retrospectively enhanced independent of the acquisition settings. The setting on the system impacting the visual aspect of the image is the so-called "dynamic range." Adjustment of the dynamic range, or compression, settings changes the number of gray values used and therefore results in high contrast (i.e., almost black and white images without much gray) or low-contrast images.

Image construction

In order to obtain an ultrasound image, the procedures of signal acquisition and post-processing are repeated.

For conventional B-mode imaging ("B" referring to "brightness"), the transducer can either be translated (Figure 1.6a) or tilted (Figure 1.6b) within a plane between two subsequent pulse–echo experiments. In this way, a conventional 2D cross-sectional image is constructed. The same principle can be used for 3D imaging by moving the ultrasound beam in 3D space between subsequent acquisitions.

Alternatively, the ultrasound beam is transmitted in the same direction for each transmitted pulse. In that case, an image line is obtained as a function of time, which is particularly useful when looking at motion. This modality is therefore referred to as M-mode ("M" referring to "motion") imaging.

Image artifacts

Side lobe artifacts

In the construction of an ultrasound image by focused waves, the assumption is made that all reflections originate from a region directly in front of the transducer. Although most of the ultrasound energy is indeed centered on an axis in front of the transducer, in practice part of the energy is also directed sideways (i.e., directed off-axis). The former part of the ultrasound beam is called the main lobe whereas the latter is referred to as the side lobes (Figure 1.7, Videos 1.1 and 1.2).

Because the reflections originating from these side lobes are much smaller in amplitude than the ones coming from the main lobe, they can typically be neglected. However, image artifacts can arise when the main lobe is in an anechoic region (e.g., a cyst or inside the left ventricular cavity) causing the relative contribution of the side lobes to become significant. In this way, a small cyst or lesion may be more difficult to detect, as it appears

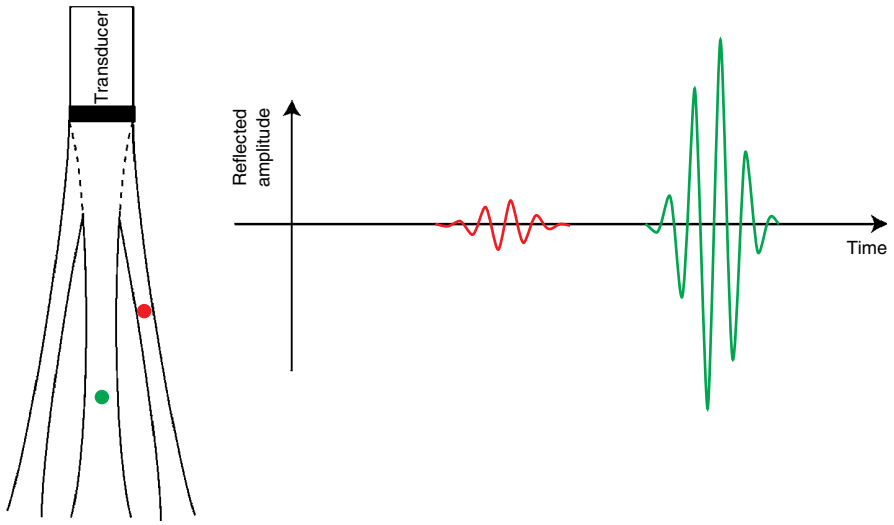

Figure 1.7 Reflections caused by side lobes (red) will induce image artifacts because all reflections are assumed to arrive from the main ultrasound lobe (green).

brighter due to spillover of (side lobe) energy from neighboring regions. Similarly, when using contrast agents, the reflections resulting from small side lobes may become more significant as these agents strongly reflect ultrasound energy. As such, increased brightness may appear in regions adjacent to regions filled with contrast without contrast being present in the region.

Reverberation artifacts

When the reflected wave arrives at the transducer, part of the energy is converted to electric energy as described in the previous section. However, due to the acoustic impedance difference between the tissue and the transducer, another part of the wave is simply reflected on the transducer surface and will start propagating away from the transducer as if it was another ultrasound transmission. This secondary "transmission" will propagate in a way similar to that of the original pulse, which means that it is reflected by the tissue and detected again (Figure 1.8, Video 1.3).

These higher order reflections are called reverberations and give rise to ghost (mirror image) structures in the image (Video 1.4). These ghost images typically occur when strongly reflecting structures such as ribs or the pericardium are present in the image (Video 1.5). Similarly, as the reflected wave coming from the pericardium is very strong, its backscatter (i.e., propagating again towards the pericardium) will be sufficiently strong as well. This wave will reflect on the pericardium and can be detected by the transducer after the actual pericardial reflection arrives. In clinical practice, this causes a ghost image to be created behind the pericardial reflection that typically appears as a mirror image of the left ventricle around the pericardium in a parasternal long-axis view.

Shadowing and dropout artifacts

When complete reflections occur due to high acoustic impedance difference, no acoustic energy is transmitted to more distal structures and – as a consequence – no reflections from these distal structures can be obtained. As a result, a very bright structure will appear in the image followed by a signal void, i.e., an acoustic shadow (Video 1.6). For example, when a metallic prosthetic valve has been implanted, the metal (being very dense and extremely stiff) can cause almost complete ultrasound reflections, resulting in an apparently anechoic region distal to the valve. This occurs because no ultrasound energy reaches the deeper regions. Similarly, some regions in the image may receive little ultrasound energy due to superficial structures blocking ultrasound penetration. Commonly, ribs (being more dense and stiffer than soft tissue) are strong reflectors at cardiac diagnostic frequencies and can impair proper visualization of some regions of the image. Or, even more obviously, the absence of ultrasound gel may allow air to be in contact with the transducer. As air has a very different acoustic impedance from biological tissues, the acoustic wave (at the emission frequency in medical imaging) cannot propagate at all. These artifacts are most commonly referred to as "dropout" and can only be avoided by changing the transducer position/orientation.

When signal dropout occurs at deeper regions only, the acoustic power transmitted can be increased. This will obviously result in more energy penetrating to deeper regions and will increase the overall signal-to-noise ratio of the image (in contrast to increasing the overall gain of the received signals as explained earlier). However, the maximal transmit power allowed is limited in order to avoid potential adverse biological effects. Indeed, at higher energy levels, ultrasound waves can

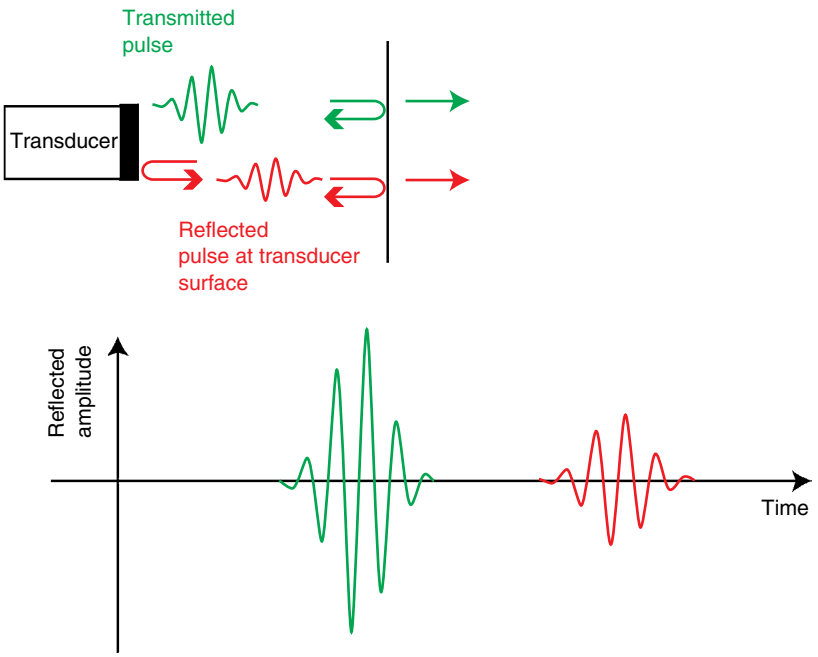

Figure 1.8 A transmitted wave (green) will reflect and result in an echo signal (green). The reflected wave will, however, partially reflect at the transducer surface (red) and generate secondary signals (red).

cause tissue damage either due to cavitation (i.e., the formation of vapor cavities that subsequently implode and generate very high local pressures and temperatures) or tissue heating. The former risk is quantified in the mechanical index (MI) and should not pass a value of 1.9, while the latter is estimated through a thermal index (TI) and should not pass – depending on whether it is for nonobstetric or non-neonatal applications – a value of a 1.0 for too long (the higher the value, the shorter the examination time should be). Overall, the acoustic power output of the system should not exceed 720 mW/cm^2, in accordance with US Food and Drug Administration (FDA) recommendations. This value is verified by the regulatory bodies to allow manufacturers to enter the market and thus does not have to be verified by the operator. Both MI and TI are always displayed on the monitor during scanning and will increase with increasing power output. The operator has to find a compromise between image quality (including penetration depth) and the risk of adverse biological effects. In case penetration is not appropriate at maximal transmit power, the operator should choose a transducer with a lower transmit frequency.

Ultrasound technology and image characteristics

Ultrasound technology

Phased-array transducers

Rather than mechanically moving or tilting the transducers, as in the early-generation ultrasound machines, modern ultrasound devices use electronic beam steering. To do this, an array of piezoelectric crystals is used. By introducing time delays between the excitation of different crystals in the array, the ultrasound wave can be sent in a specific direction without mechanical motion of the transducer (Figure 1.9). The RF signal for a transmission in a particular direction is then simply the sum of the signals received by the individual elements. These individual contributions can be filtered, scaled, and time delayed separately before summing. This process is referred to as *beam forming* and is a crucial element for obtaining high-quality images. The scaling of the individual contributions is typically referred to as *apodization* and is critical in suppressing side lobes and thus avoiding the associated artifacts.

This concept can be generalized by creating a 2D matrix of elements that enables steering of the ultrasound beam in three dimensions. This type of transducer is referred to as a matrix array or 2D array transducer. Because each of the individual elements of such an array needs electrical wiring, manufacturing such a 2D array was technically challenging for many years because of the limitation of the thickness of the transducer cable. These obstacles have been overcome and 3D arrays are now available on high-end ultrasound systems.

Second harmonic imaging

Wave propagation as illustrated in Figure 1.2 only happens when the amplitude of the ultrasound wave is relatively small (i.e., the acoustic pressures involved are small). Indeed, when the amplitude of the transmitted wave becomes significant, the shape of the ultrasound wave will change during propagation, as illustrated in Figure 1.10. The phenomenon of wave distortion during propagation is referred to as nonlinear wave propagation. This wave distortion results in the generation of harmonic frequencies which are integer multiples of the transmitted frequency. Transmitting a 1.7-MHz ultrasound pulse will thus result in the spontaneous generation of frequency components of 3.4, 5.1, 6.8, and 8.5 MHz, and so on. These harmonic components become stronger with propagation distance. The rate at which the waveform distorts for a specific wave amplitude is tissue dependent and characterized by the nonlinearity parameter, β (or the so-called "B/A" parameter).

The ultrasound scanner can be set up to receive only the second harmonic component through filtering of the received RF signal. If further post-processing of the RF signal is done in exactly the same way as described earlier, a second harmonic image is obtained. Such an image typically has a better signal-to-noise ratio by avoiding clutter noise due to (rib or air) reverberation artifacts. As second harmonic waves are increasingly present with increasing depth, second harmonic imaging results in better images at deeper depths. This harmonic image is commonly used in patients with poor acoustic windows and poor penetration. Although harmonic imaging increases the

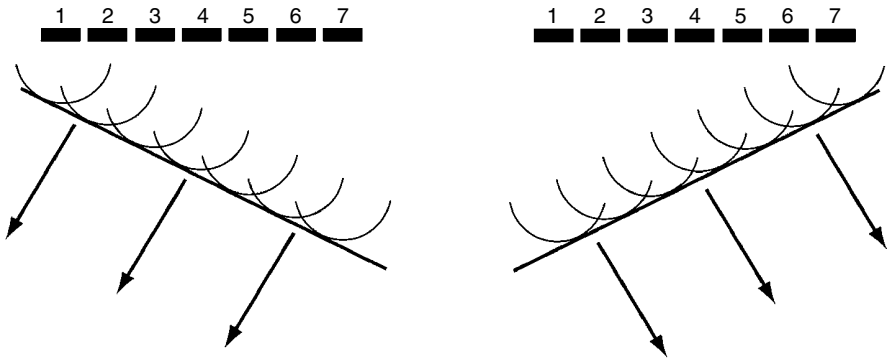

Figure 1.9 An array of crystals can be used to steer the ultrasound beam electronically by introducing time delays between the activation of individual elements in the array.

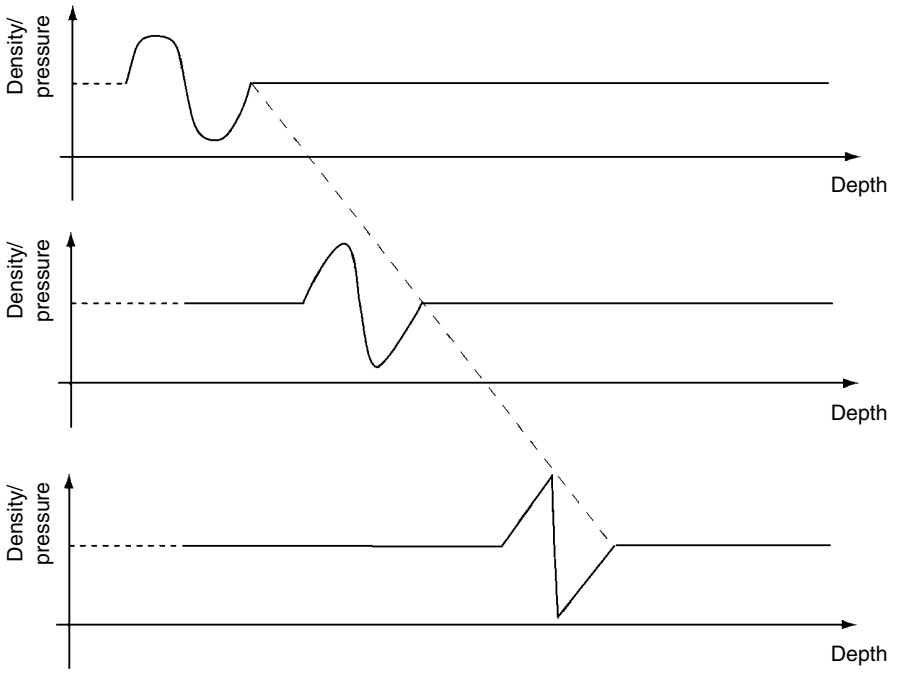

Figure 1.10 Nonlinear wave behavior results in changes in shape of the waveform during propagation.

signal-to-noise ratio, it has intrinsically poorer axial resolution as further discussed later in this chapter. Higher harmonics (i.e., third, fourth, etc.) are also present but typically fall outside the bandwidth of the transducer, which is the range of analyzable frequencies, and thus are not detected by the transducer. Harmonic imaging has become the default cardiac imaging mode for adult scanning on many systems. It is typically unnecessary to use harmonic imaging in young infants as it reduces axial resolution. Switching between conventional and harmonic imaging is done by changing the transmit frequency of the system. For lower frequency transmits, the default setting is usually a harmonic imaging mode, which is indicated on the display by showing both transmit and receive frequencies (e.g., 1.7/3.4 MHz). When a single frequency is displayed, the scanner is in a conventional (i.e., fundamental) imaging mode. For pediatric scanning, especially in smaller infants, fundamental imaging is the preferred mode due to its better spatial resolution, and presets for higher frequency probes are typically programmed in the fundamental frequency.

Contrast imaging

As blood is a poor reflector of ultrasound energy (i.e., relative homogeneity of the acoustic impedance), it shows dark in the image. For some applications, like myocardial perfusion assessment, it can be useful to artificially increase blood reflectivity. This can be achieved by using an ultrasound contrast agent. As air is a very strong reflector of ultrasound energy due its relative high compressibility and low density when compared with soft tissue, it often is used as a contrast agent. The injection of small air bubbles with diameters similar to those of red blood cells, significantly increases blood reflectivity. Agitated saline can be used or ultrasound contrast agents that contain encapsulated air bubbles to limit the diffusion of air in blood. Contrast imaging can be helpful for visualizing the endocardial border as it enhances the difference in gray value between the myocardium and the blood pool. It can be used in patients with poor image penetration to better visualize the endocardial border. Contrast injection can also be used for detecting shunts. As in pediatrics, right-to-left shunting can be present; typically carbon dioxide is the preferred gas to create agitated saline. Contrast agents can also be used to increase the brightness of the perfused myocardial tissue, although artifacts can be present which can make the interpretation of the perfusion images less obvious. At present, different contrast agents are commercially available for clinical use but regulatory approval for pediatric use differs between countries. In the presence of right-to-left shunting, contrast agents should be used cautiously and only by experienced operators.

Image resolution

Resolution is defined as the shortest distance at which two adjacent objects can be distinguished as separate. The spatial resolution of an ultrasound image varies depending on the position of the object relative to the transducer. Also, the resolution in the direction of the image line (range or *axial resolution*) is different from the one perpendicular to the image – within the 2D image plane (azimuth or *lateral resolution*) – which is different again from the resolution in the direction perpendicular to the image plane (*elevation resolution*).

Axial resolution

In order to obtain an optimal axial resolution, a short ultrasound pulse (high frequency) needs to be transmitted. The length of the transmitted pulse is mainly determined by the characteristics of the transducer, i.e., the range of frequencies that can be generated/detected – referred to as its bandwidth. The bandwidth is most commonly expressed relative to the center frequency of the transducer. A typical value would be 80%, implying that for a 5 MHz transducer the absolute bandwidth is about 4 MHz. This type of transducer can thus generate/receive frequencies in the range of 3–7 MHz. The absolute transducer bandwidth is typically proportional to the mean transmission frequency. A higher frequency transducer will thus produce shorter ultrasound pulses and, thus, better axial resolution. Unfortunately, as discussed previously, higher frequencies are attenuated more by soft tissue and are impacted by depth. As such, a compromise needs to be made between image resolution and penetration depth. In pediatric and neonatal cardiology where the acquisition depth is less, higher frequency transducers can be used to increase image spatial resolution. Typically for infants 10–12 MHz transducers are used, resulting in a typical axial resolution of the order of 150 μm, knowing that the axial resolution is roughly equal to λ.

Most systems allow changing the transmit frequency of the ultrasound pulse within the bandwidth of the transducer. As such, a 5-MHz transducer can be used to transmit a 3.5-MHz pulse which can be practical when penetration is not sufficient at 5 MHz. The lower frequency will result in a longer transmit pulse with a negative impact on axial resolution. Similarly, for second harmonic imaging, a narrower band pulse needs to be transmitted, as part of the bandwidth of the transducer needs to be used to be able to receive the second harmonic. As such, in harmonic imaging mode, a longer ultrasound pulse is transmitted (i.e., less broad band) resulting in a worse axial resolution of the second harmonic image despite improvement of the signal-to-noise ratio. Therefore, some of the cardiac structures appear thicker, especially valve leaflets. This should be considered when interpreting the images.

Lateral resolution

Lateral resolution is determined by the width of the ultrasound beam (i.e., the width of the main lobe). The narrower the ultrasound beam, the better the lateral resolution. In order to narrow the ultrasound beam, several methods can be used but the most obvious one is focusing. This is achieved by introducing time delays between the firing of individual array elements (similar to that done for beam steering) in order to make sure that the transmitted wavelets of all individual array elements arrive at the same position at the same time and will thus constructively interfere (Figure 1.11). Similarly, time delaying the reflections of the individual crystals in the array will make sure that reflections coming from a particular point in front of the transducer will sum in phase and therefore create a strong echo signal

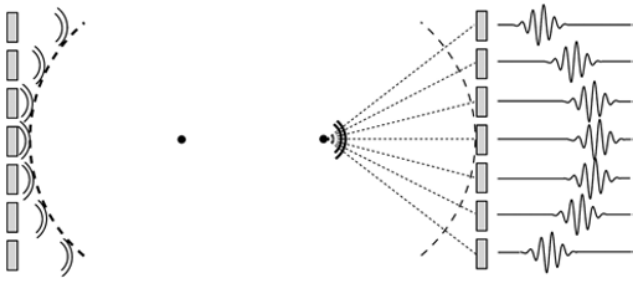

Figure 1.11 Introducing time delays during the transmission of individual array elements (left) allows for all wavelets to arrive at a particular point (focus) simultaneously. Similarly, received echo signals can be time delayed so that they constructively interfere (receive focus).

(Figure 1.11). Because the sound velocity in soft tissue is known and is considered homogeneous, the position from which reflections can be expected is known at each time instance after transmission of the ultrasound pulse. As such, the time delays applied in receive can be changed dynamically in order to move the focus point to the appropriate position. This process is referred to as *dynamic (receive) focusing*. In practice, dynamic receive focusing is always used and does not need adjustments by the operator, in contrast to the transmit focus point whose position should be set manually. Obviously, to resolve most morphologic detail, the transmit focus should always be positioned close to the structure/region of interest. Most ultrasound systems allow the selection of multiple transmit focal points. In this setting, each image line will be created multiple times with a transmit pulse at each of the set focus positions, and the resulting echo signals will be combined in order to generate a single line in the image. Although this results in a more homogeneous distribution of the lateral resolution with depth, it takes more time to generate a single image and thus will result in lowering the frame rate (i.e., temporal resolution).

The easiest way to improve the focus performance of a transducer is by increasing its size (i.e., aperture). Unfortunately, the footprint needs to fit between the patient's ribs, thereby limiting the size of the transducer and thus limiting lateral resolution of the imaging system. This parameter is essential for phased-array probes used in cardiology, which have a small aperture in order to thwart anatomic obstacles (ribs).

Ultimately, the lateral resolution depends on the wavelength and shape of the wave dictated by the geometry of the probe and/or by the emission parameters (i.e., time delays) of the wave beam. As an example, for an 8-MHz pediatric transducer, realistic numbers for the lateral resolution of the system are depth dependent and are approximately 0.3 mm at 2 cm, going up to 1.2 mm at 7 cm depth.

Elevation resolution

For elevation resolution, the same principles hold as for lateral resolution in the sense that the dimension of the ultrasound beam in the elevation direction will be determinant. However,

most ultrasound devices are still equipped with 1D array transducers. As such, focusing in the elevation direction needs to be done by the use of acoustic lenses (similar to optic lenses, acoustic lenses concentrate energy in a given spatial position), which implies that the focus point is fixed in both transmit and receive (i.e., dynamic focusing is not possible in the elevation direction). This results in a resolution in the elevation direction that is worse than the lateral resolution. The homogeneity of the resolution is also worse with depth. Moreover, the transducer aperture in the elevation direction is typically somewhat smaller (in order to fit in between the ribs of the patient) resulting in a further decrease of elevation resolution compared with the lateral component. Newer systems with 2D array transducer technology have more similar lateral and elevation image resolution. Matrix-array transducers not only create 3D images but also allow the generation of 2D images of higher/more homogeneous spatial resolution.

Temporal resolution

By definition, temporal resolution in medical imaging is the number of images obtained per second (i.e., frame rate). This parameter should be differentiated from the transmission/reception frequency of the acoustic wave (i.e., pulse repetition frequency, PRF). In conventional ultrasound imaging, which requires focused transmissions (as described later), a large number of transmissions/receptions must be repeated before an image can be obtained, so the frame rate is much lower than the PRF. Typically, a 2D pediatric cardiac image consists of 300 lines. The construction of a single image thus takes about $300 \times 100\,\mu s$ (the time required to acquire one line) or 30 ms. In this example, the PRF is 10,000 Hz while the frame rate is 33 Hz. Thus, 33 images can be produced per second, which is sufficient to look at motion (e.g., old television displays based on cathode ray tubes only displayed 25 frames per second). With more advanced imaging techniques such as parallel beam forming, higher frame rates can be obtained (70–80 Hz). In order to increase frame rate further, either the field of view can be reduced (i.e., a smaller sector will require less image lines to be formed and will thus speed up the acquisition of a single frame) or the number of lines per frame (i.e., the line density) can be reduced. The latter comes at the cost of spatial resolution, as image lines will be further apart. There is thus an intrinsic trade-off between the image field of view, spatial resolution, image contrast, and temporal resolution. Most systems have a "frame rate" button nowadays that allows changing the frame rate, although this always comes at the expense of image quality. Higher frame rates are important when the heart rate is higher as is often the case in pediatric patients and when studying short-lived events (e.g., isovolumetric contraction) or fast-moving structures (e.g., valve leaflets).

High frame rate imaging

In order to increase the frame rate for a given PRF, several techniques can be applied, including those described in the previous section.

1 *Ultrafast ultrasound*: In conventional imaging, the need to focus the emissions and repeat this process hundreds of times (i.e., once per image line) to obtain an image makes high frame rates impossible. To overcome this, ultrafast imaging has been developed over the last two decades [3]. It is based on transmitting unfocused (i.e., plane) or even defocused (i.e., diverging) waves, which enable the reconstruction of an image with much fewer transmit events by reconstructing image lines on receive for the entire insonified region. In the extreme, the entire field of view can be insonified on transmit so that an entire image can be reconstructed from a single ultrasound transmission (Figure 1.12). In that situation, frame rate and PRF thus become the same, implying that imaging is enabled at a frame rate of 5–10 kHz (depending on the frequency and imaging depth). However, spatial resolution as well as image contrast are reduced because of the broad transmit wave. Although this can (partially) be overcome by using multiple (plane or diverging) transmit waves under slightly different angles and taking the average image as the result (called coherent wave compounding), this will negatively impact frame rate. The ability to investigate the heart at high temporal resolution enables new imaging modalities that give additional information on blood and

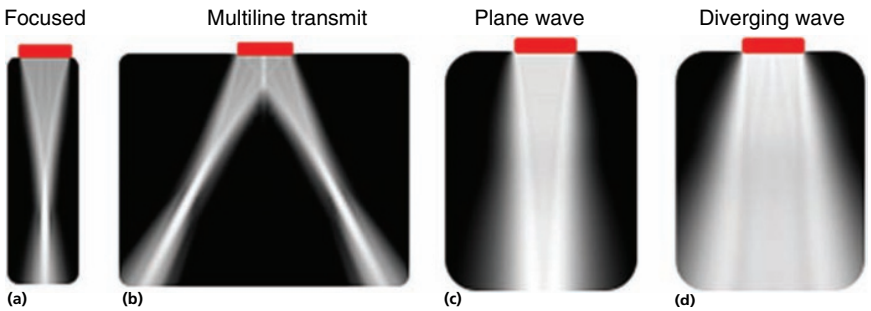

Figure 1.12 Conventional versus high frame rate ultrasound. **(a)** Traditional echocardiography makes use of focused transmit beams. **(b–d)** High frame rate imaging either transmits several focused beams in parallel (two in the example in **(b)**); unfocused or plane waves **(c)**; or defocused/diverging waves **(d)**. For the high frame rate imaging techniques, image lines are created in the insonified region by receive beam forming.

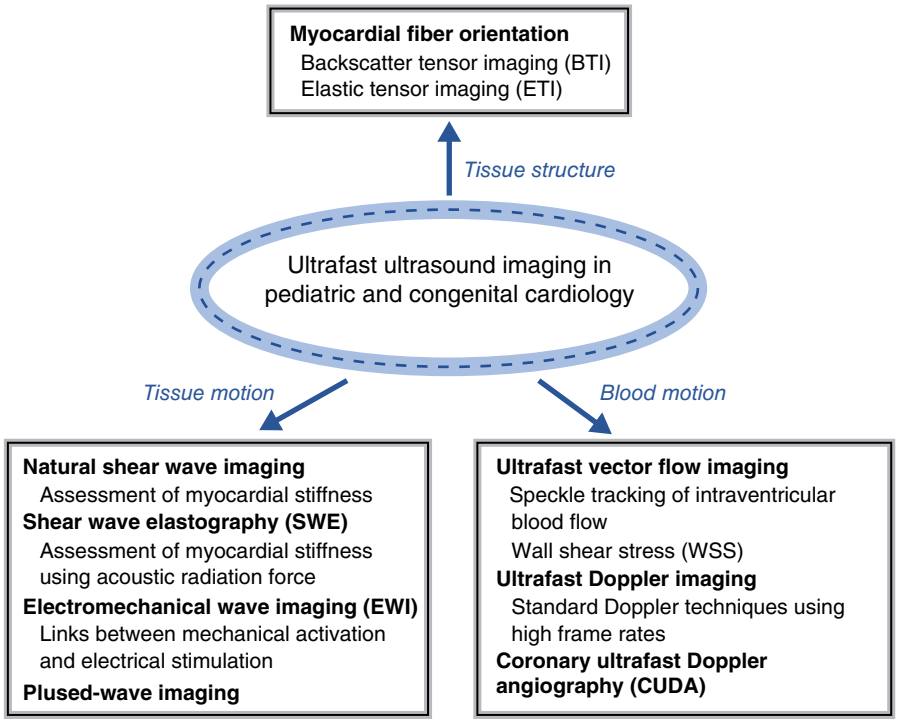

Figure 1.13 Potential applications of ultrafast ultrasound imaging in pediatric and congenital cardiology.

tissue motion as well as on tissue mechanical properties and structure (see Figure 1.13 for applications in pediatric cardiology).

2 *Multiline transmit*: Alternatively, multiline transmit beam forming has been proposed in which the transmitted beams remain focused (as in conventional imaging) but in which several focused beams are transmitted simultaneously into different directions. As in plane/diverging wave imaging, image lines are then reconstructed on receive for the spatial regions insonified. As only a part of the field of view gets insonified in this approach, the process needs to be repeated by moving the transmit beams around (as in conventional imaging). The more transmit beams that are generated in parallel, the faster a single frame can be acquired (and thus the higher the frame rate), but increased cross-talk between the beams can occur thereby lowering image quality.

Overall, for both plane/diverging wave and multiline transmit imaging, a compromise needs to be found between image quality and frame rate, as in conventional imaging. However, for these high frame rate modes, this compromise gets intrinsically skewed towards higher frame rates. In general, for comparable frame rates, both high frame rate methodologies have been shown to be very competitive and choosing one or the other approach may mostly be determined by how easily it can be implemented on a given system (given its electronic hardware constraints). To date, these high frame rate solutions are not commercially available although this is likely to change in the near future. For a more elaborate discussion of these novel imaging modalities and their (potential) clinical use, the reader is referred to a review by Cikes et al. [4].

Image optimization in pediatric echocardiography

All the principles mentioned so far can be used to optimize image acquisition for the pediatric population. As children are smaller, less penetration is required. The heart rates are higher, requiring higher temporal resolution and, as structural heart disease is more common in the pediatric age group, spatial resolution needs to be optimized to obtain the best possible diagnostic images. Image optimization will always be a compromise between image quality and temporal resolution. A few general recommendations can be made which can help in image optimization:

1 Always use the highest possible transducer frequency to optimize spatial resolution. For infants, high-frequency probes (8–12 MHz) must be available and used. Often, different transducers have to be used for different parts of the examination. So, for instance, for subxiphoid imaging in a newborn, a 5- or 8-MHz probe can be used, while for the apical and parasternal windows a 10–12-MHz probe often provides better spatial resolution. For larger children and young adults, 5-MHz and rarely 2.5–3.5-MHz probes can be used, although for the parasternal windows the higher frequency probes can generate good-quality images also in this population.

2 In smaller children in particular, harmonic imaging does not necessarily result in better image quality due to its intrinsically lower axial resolution. Generally, fundamental frequencies provide good-quality images. Harmonic imaging is generally more useful in larger children and adults.
3 Gain and dynamic range settings are adjusted to optimize image contrast so that the structures of interest can be seen with the highest possible definition. TGCs are used to make the images as homogeneous as possible at different depths. Image depth and focus are always optimized to image the structures of interest.
4 For optimizing temporal resolution the narrowest sector possible should be used.
5 Depth settings are minimized to include the region of interest.

Doppler imaging

Continuous-wave Doppler

When an acoustic source moves relative to an observer, the frequencies of the transmitted and the observed waves are different. This phenomenon is known as the Doppler effect. A well-known example is that of an ambulance passing a static observer: the observed pitch of the siren is higher when the car approaches than when it moves away.

The Doppler phenomenon can be used to measure tissue and blood velocities by comparing the transmitted with the received ultrasound frequency. Indeed, when ultrasound scattering occurs at stationary tissues, the transmitted and reflected frequencies are identical. This statement is only true when attenuation effects are negligible. In soft tissue there will be an intrinsic frequency shift due to frequency-dependent attenuation. When scattering occurs at tissues in motion (Figure 1.14), a (additional) frequency shift – the Doppler shift (f_D) – will be induced that is directly proportional to the velocity (v) by which the tissue is moving:

$$f_D = -2v\cos\theta\, f_T/c$$

where f_T is the transmit frequency, θ is the angle between the direction of wave propagation and the tissue motion, and c is the velocity of sound in soft tissue (i.e. 1530 m/s). Note that for motion orthogonal to the image line, θ = 90° and the Doppler shift is zero regardless of the amplitude of the tissue velocity v. The Doppler phenomenon thus only allows measurement of the magnitude of the velocity along or parallel to the image line (i.e., motion towards or away from the transducer) while motion orthogonal (perpendicular) to the line is not detected. In practice, an angle up to 20° is considered acceptable in order to obtain clinically relevant Doppler measurements. Ideally, the angle should always be minimized by selecting the proper image line for the Doppler recording or by repositioning the ultrasound transducer. Notably, the velocities can never be overestimated due to angle dependency, and therefore the highest value recorded is closest to the truth. Where the angle between the flow and the ultrasound line is known (θ in the Doppler equation), the velocity estimate can be corrected for this angle. Although this is possible in laminar flow conditions as observed in nonstenosed vessels, the flow direction is typically not known in cardiac applications. Therefore, angle correction is typically not used for cardiac ultrasound and should be used with care, especially in the presence of turbulent flows.

In order to make a Doppler measurement by using CW Doppler, one piezoelectric crystal (or a group of crystals) is used for transmitting a continuous wave at a fixed frequency and a second crystal (or group of crystals) is used to continuously record the reflected signals in order to record a reception frequency. All the crystals are embedded in the same transducer, and the frequency difference, that is, the Doppler shift, is continuously measured. The instantaneous frequency shift is converted to a velocity by applying the Doppler equation and is displayed as a function of time in a so-called *spectrogram*. However, because different velocities are present within the ultrasound beam for any given time instance during the cardiac cycle, a range of Doppler frequencies (or Doppler shift) is typically detected. Thus, there is a spectrum of Doppler shifts measured and displayed in the spectrogram (Figure 1.15) – hence the term "spectral Doppler" is often used. Depending on the clinical application, the speed at which the spectrogram is updated can be modified (i.e., the sweep speed). For example, to look at beat-to-beat variations during the respiratory cycle, a low sweep speed can be used while a high sweep speed is needed when looking at flow characteristics within a single cardiac cycle.

Finally, as typical blood velocities cause a Doppler shift in the sonic range (20 Hz to 20 kHz), the Doppler shift itself can be made audible to the user. A high pitch (large Doppler shift) corresponds to a high velocity whereas a low pitch (small Doppler shift) corresponds to a low velocity. As such, the user gets both

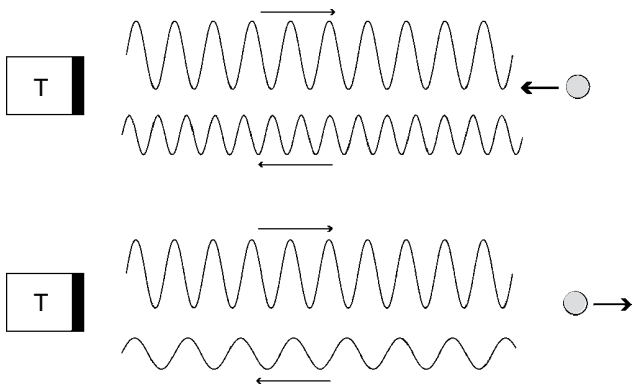

Figure 1.14 The Doppler effect will induce a frequency shift of the transmitted ultrasound wave when the reflecting object is in motion. T, transmitter.

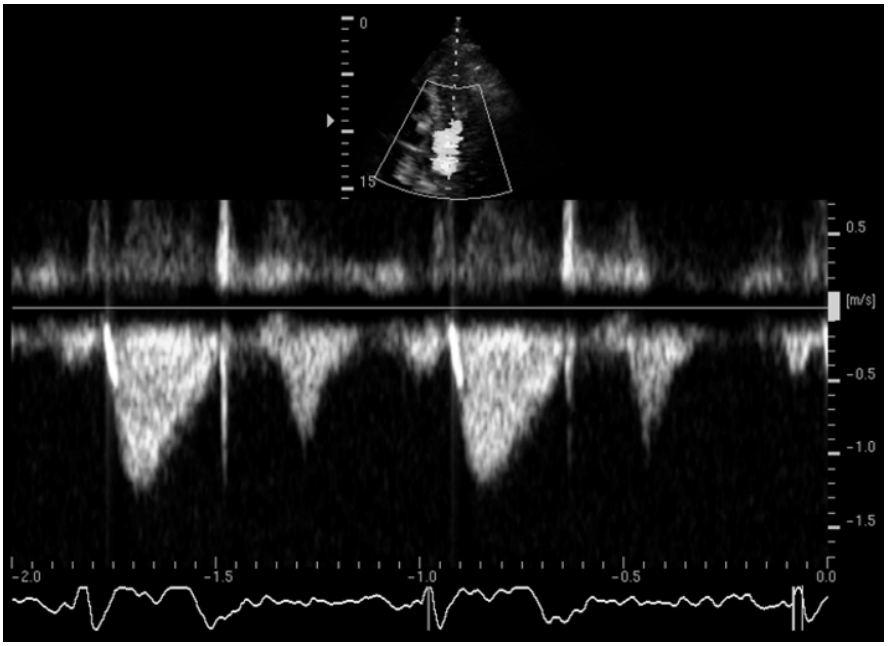

Figure 1.15 Example of a continuous-wave Doppler spectrogram of the left ventricular outflow tract.

visual (spectrogram) and aural information on the velocities instantaneously present in the ultrasound beam.

The system described here is referred to as the CW Doppler system. As an ultrasound wave is transmitted continuously, no spatial information is obtained. Indeed, all velocities occurring anywhere within the ultrasound beam (i.e., on the selected ultrasound line of interrogation) will contribute to the reflected signal and appear in the spectrogram. As the ultrasound signal weakens with depth due to attenuation, velocities close to the transducer will intrinsically contribute more than the ones occurring further away. For most applications CW Doppler is combined with 2D imaging which allows the operator to align the Doppler signal based on the anatomic information. Sometimes the relatively large footprint of the probe does not allow a good Doppler alignment, so the use of a small blind probe can help with obtaining better Doppler alignment. This can be used for instance for measurement of a peak gradient across the aortic valve in the case of aortic valve stenosis.

Optimization of CW Doppler

1 Alignment with the direction of the measured velocity should be optimized.
2 The gain control affects the ratio of the output signal strength to the input signal strength. The gain controls should be manipulated to produce a clean uniform profile without any "blooming." The gain controls should be turned up to overemphasize the image and then adjusted down. This will prevent any loss of information due to too little gain.
3 The compress control assigns the varying amplitudes a certain shade of gray. If the compress control is very low or high the quality of the spectral analysis graph will be affected, and this may lead to erroneous interpretation.
4 The reject button eliminates the smaller amplitude signals that are below a certain threshold level. This will help to provide a cleaner image and may make measurements more obvious.
5 The filter is used to reduce the noise that occurs from reflectors that are produced from walls and other structures that are within the range of the ultrasound beam.

Pulsed-wave Doppler

The pulse–echo measurement described previously can be repeated along a particular line in the ultrasound image at a given repetition rate (i.e., PRF). Rather than acquiring the complete RF signal as a function of time, in pulsed-wave (PW) Doppler mode, a single sample of each reflected pulse is taken at a fixed time after the transmission of the pulse (the so-called range gate or sample volume). Assuming the position of the scattering sites relative to the transducer remains constant over time, all reflections (therefore all samples taken at the range gate) will be identical. However, when the tissue is moving relative to the transducer, the ultrasound wave will have to travel further (motion away from the transducer) or less far (motion toward the transducer) between subsequent acquisitions. As a result, the reflected signal will shift in time and the sample taken at the range gate will change (Figure 1.16).

It can be demonstrated that the frequency of the signal constructed in this way is directly proportional to the velocity of the reflecting object following the same mathematical relationship that is given in the Doppler equation. For this reason, this imaging mode is referred to as PW *Doppler* imaging despite the fact that the Doppler phenomenon as such is not exploited.

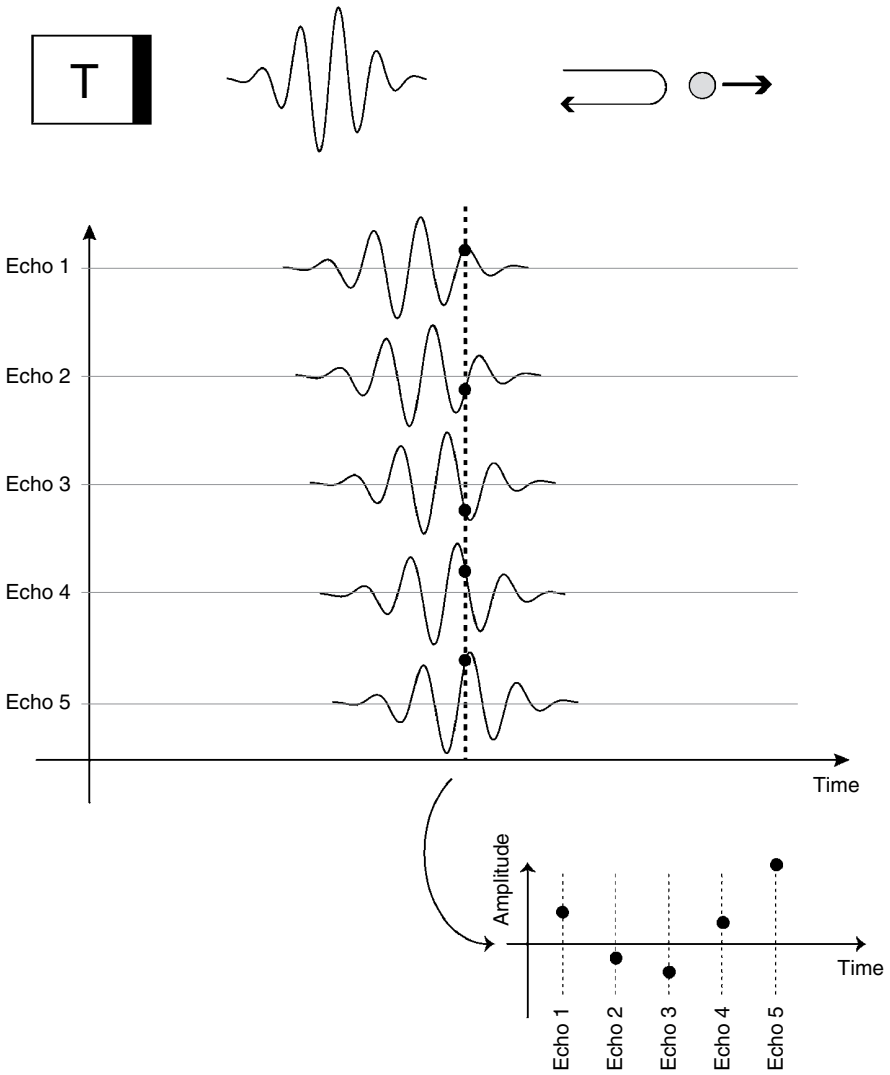

Figure 1.16 Schematic illustration of the principle of the pulsed-wave Doppler system. T, transmitter.

Note that motion orthogonal to the direction of wave propagation will not induce a significant change in propagation distance for the ultrasound wave; it will not result in a significant time shift of the reflected signal and will thus not be detected by the system.

For a PW Doppler system, velocities are displayed as a function of time in a spectrogram similar to that done for the CW Doppler system (Figure 1.17). However, the velocities displayed in a PW spectrogram occur within a specific region (the sample volume) within the 2D image.

In practice, more than one sample is taken at the range gate. Moreover, it can be demonstrated that the accuracy of the velocity estimate is better for narrow band pulses (i.e., ultrasound pulses containing relative few frequencies). By changing the size of the range gate, the bandwidth of the transmitted pulse can be changed. A larger range gate will improve the accuracy of the velocity estimate and will improve the signal-to-noise ratio of the spectrogram but will obviously result in a less localized measurement. The operator can change the size of the range gate as appropriate.

As explained previously, blood is relatively homogeneous in acoustic impedance making it appear dark in the B-mode image. As a result, echo signals obtained from the blood are sensitive to side lobe artifacts and may thus contain echo signals coming from the wall. In order to avoid displaying these "spilled over" velocities in the spectrogram, low shift frequencies (i.e., low velocities) are removed from the spectrogram using a high-pass filter typically referred to as the "wall filter." The cut-off frequency of this high-pass filter can be manually selected and should be chosen such that strong, low velocities from the wall are adequately removed without significantly impacting the velocity spectrum of the blood itself.

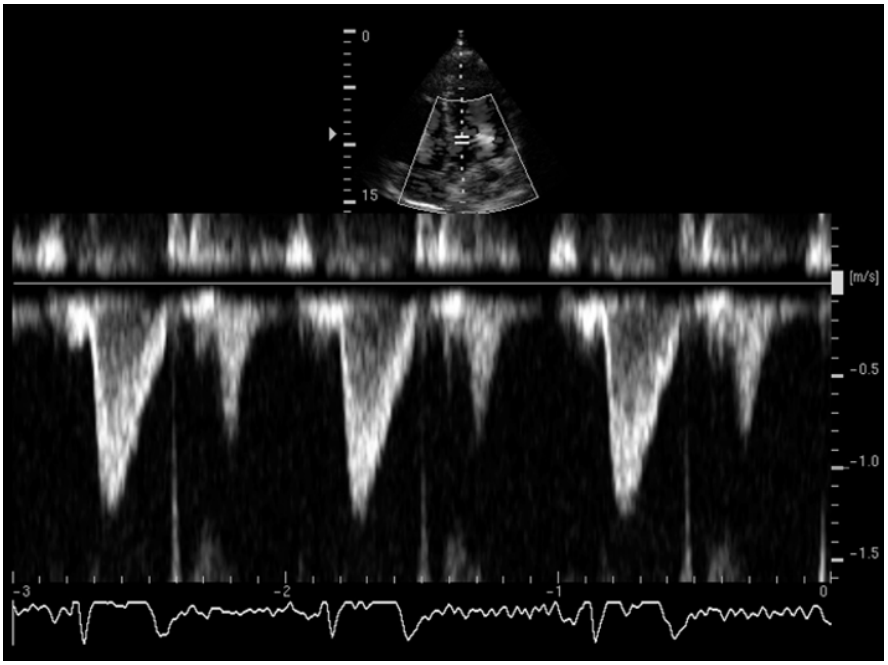

Figure 1.17 Example of a pulsed-wave Doppler spectrogram of the left ventricular outflow tract.

Aliasing

If the velocity of the scattering object is relatively large and the shift between two subsequent acquisitions is larger than half a wavelength, the PW Doppler system cannot differentiate this high velocity (Figure 1.18a – red signal) from a low velocity (Figure 1.18a – green signal) because the extracted samples at the range gate are identical. This effect is known as aliasing, and a clinical example is given in Figure 1.18b. To avoid aliasing, either the PRF needs to be increased or the transmit frequency needs to be decreased. The latter option is not commonly used in practice, while the former can be adjusted as required. Depending on the system, the PRF setting is referred to as "Nyquist velocity," "scale," or "velocity range." Moreover, where the direction of flow is known, most systems allow shifting the baseline of the spectrogram, thereby increasing the maximal velocity that can be measured without introducing aliasing.

Velocity resolution

A high PRF will ensure that aliasing will not occur when the maximal detectable velocity is high. However, as the ultrasound system can only measure a fixed number of velocity amplitudes, the smallest difference between two velocity amplitudes detectable by the system will decrease with increasing PRF. As such, a compromise needs to be made between velocity resolution and maximal detectable velocity. For this reason, it is important in practice to keep the PRF as small as possible while still avoiding aliasing in order to have maximal accuracy of the velocity measurement. When the maximum velocity is high, PW

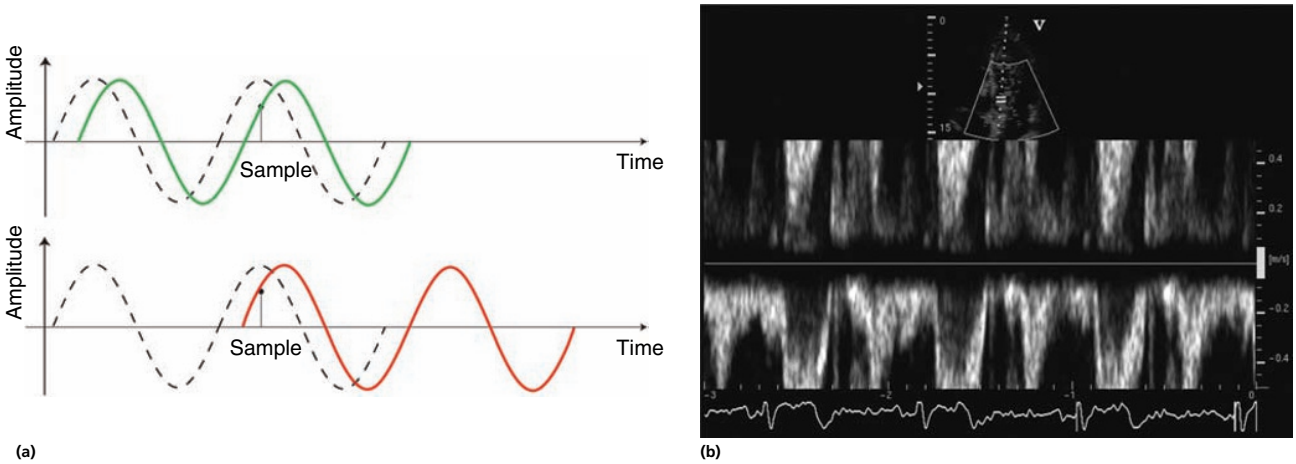

Figure 1.18 Principle of aliasing in Doppler acquisitions **(a)** and a practical example **(b)**.

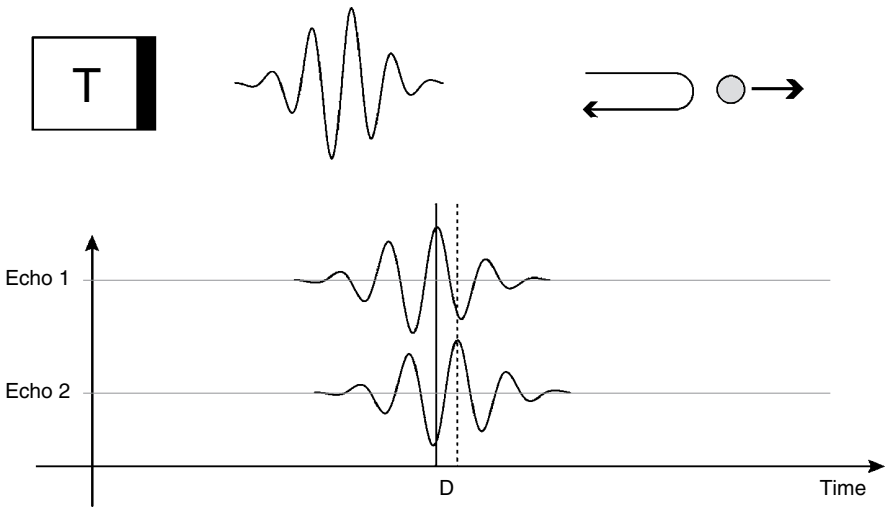

Figure 1.19 Principle of color flow imaging. T, transmitter.

Doppler will not be able to detect the highest velocity without aliasing and CW Doppler will be required to measure true peak velocities. Thus, in turbulent flow, both PW and CW Doppler interrogations are needed to make an accurate interpretation of location and maximum velocity, respectively. The velocity amplitude at which PW Doppler is no longer capable of measuring the velocity without aliasing is dependent on the transmit frequency, the PRF, and the depth at which these velocities occur (the closer to the transducer, the higher the maximal velocity that can correctly be measured).

Optimizing PW Doppler signals

1. As for any Doppler technique, alignment with the direction of the velocity is important.
2. The gain control, compress, and filter settings are similar to those of CW Doppler.
3. Shift of the baseline allows the whole display to be used for either forward or reverse flow, which is useful if the flow is only in one direction.
4. The Nyquist limit should always be optimized and set no higher or lower than necessary to display the measured flow velocities.
5. An increase in sample volume increases the strength of the signal and gives more velocity information at the expense of a lower spatial resolution. In general, the smallest sample volume that results in adequate signal-to-noise ratio should be used.

Color flow imaging

Pulsed-wave Doppler measurements can be implemented for several range gates along the image line and can be repeated for each image line in order to obtain velocity information within a 2D region of interest. However, many ultrasound pulses need to be transmitted to reconstruct a single image line (as explained earlier), therefore the temporal resolution of such a system would be extremely poor (a maximal frame rate of a few Hertz is obtained). In order to overcome this problem, color flow (CF) imaging has been developed. CF imaging allows estimation of the flow velocity based on only two ultrasound transmissions in the same direction. Although in theory two pulses are indeed sufficient, in practice more pulses are used to improve the quality of the measurement. Similar to PW Doppler, motion of the scattering sites between acquisitions will result in a time delay between both reflected signals if motion of the scattering (i.e., blood) is present (Figure 1.19). By measuring this time delay between both reflections, the amount of blood displacement between both acquisitions is obtained. The local velocity is then simply calculated as this displacement divided by the time interval between both acquisitions (= 1/PRF).

This procedure can be applied along the whole RF line in order to obtain local velocity estimates along the line (from close to the transducer to the deepest structures). Moreover, it is repeated between subsequent image lines within the 2D image. In this way, CF imaging can visualize the spatial distribution of the velocities by means of color superimposed onto the gray-scale image. By convention, red represents velocities toward the transducer and blue represents velocities away from the transducer, whereby different shades of red/blue indicate different velocity amplitudes. High variance of the velocity estimate measured in a given pixel is typically encoded by adding yellow or green to the color in this pixel. In this way, regions with high variance in the velocity estimate are highlighted as they indicate disturbed (i.e., turbulent) flow.

Similar to the PW Doppler technique, aliasing can occur with CF imaging and can be reduced by increasing PRF (allowing less time for motion between the two acquisitions) or reducing the transmission frequency. However, PRF settings are linked to the velocity resolution in the same way as for the PW Doppler system. An important difference with the PW Doppler technique is that the local average velocity rather than the local spectrum in velocities is measured. Peak velocity values measured with both techniques will thus be different, with CF imaging giving lower peak values.

Finally, it should be noted that creating a CF image takes more time than creating a B-mode image, as several pulses need to be sent along each image line. In order to keep the temporal resolution of the CF dataset acceptable, the region in which velocities are effectively estimated should be minimized to the anatomically relevant region only. All systems enable this by buttons affecting the size of the so-called "color box."

Optimizing color Doppler imaging

1 Use the smallest color Doppler sector as necessary. Large-sector color Doppler has lower temporal resolution.
2 Gain settings should be adjusted until background noise is detected in the color image and then reducing it so that the background noise disappears.
3 The Nyquist limit (scale) should be adapted depending on the velocities of the flows measured. When looking at high-velocity flows, the scale should be adjusted so a high Nyquist limit is chosen. When low velocities are studied (coronary flow, venous flows), the scale needs to be lowered to allow the display of these lower velocities.

Imaging of myocardial displacement or deformation

Doppler myocardial imaging

The exact same Doppler systems as described can be used to measure myocardial velocities rather than blood velocities. The only difference is related to filtering: when imaging blood velocities the goal is to filter out slowly moving, strongly reflecting structures (i.e., velocities originating from the myocardium), whereas myocardial velocity imaging requires filtering structures that are moving at high velocity and that have low scattering power (i.e., blood). On occasion, Doppler myocardial imaging displays slowly moving blood as these velocities do not only fall within the typical myocardial velocity range but also have brightness similar to that of the myocardium due to blood aggregation. To measure tissue Doppler velocities, both PW Doppler and color Doppler can be used. For both techniques, optimization of the Doppler beam alignment with the direction of motion is important. As color Doppler velocities do not represent peak velocities, the velocities measured are generally lower compared with the velocities measured by PW Doppler. As in pediatric heart tissue, Doppler velocities can be higher than in the adult population, so attention should be paid to avoid aliasing during image acquisition. Also, for color tissue Doppler, acquiring at the highest possible frame rate is important. This can be achieved by reducing the sector width and by using the frame rate button, which reduces the number of echo beams used to generate the images thus reducing spatial resolution.

Estimation of motion in 2D: speckle tracking

A limitation of the conventional Doppler techniques (CW, PW, and CF) is that they only detect motion along the image line. Indeed, motion perpendicular to the image line will not be detected.

In order to overcome this limitation several methods have been proposed, but a very popular one is a technique commonly referred to as "speckle tracking." The principle of speckle tracking is very simple: a particular segment of tissue (or blood) is displayed in the ultrasound image as a pattern of gray values (Figure 1.20). Such a pattern, resulting from the spatial distribution of gray values, is commonly referred to as a "speckle pattern." This pattern characterizes the underlying myocardial tissue acoustically and is (assumed to be) unique for each tissue segment. It can therefore serve as a fingerprint of the tissue segment within the ultrasound image.

If the position of the tissue segment within the ultrasound image changes, we can assume that the position of its acoustic fingerprint will change accordingly. Tracking of the acoustic pattern during the cardiac cycle thus allows detection of the motion of this myocardial segment within the 2D image. The same approach can be taken when 3D datasets are available. Fundamental to this methodology is that speckle patterns are preserved between image frames. It can be shown that this is indeed the case if tissue rotation, deformation, and out-of-plane motion between subsequent image frames are limited. An obvious way to achieve this is by acquiring grayscale data at a sufficiently high frame rate in order to make the time interval between subsequent image acquisitions short, thus avoiding the above effects.

Although these methods were initially proposed to measure 2D myocardial velocities, they have more recently also been

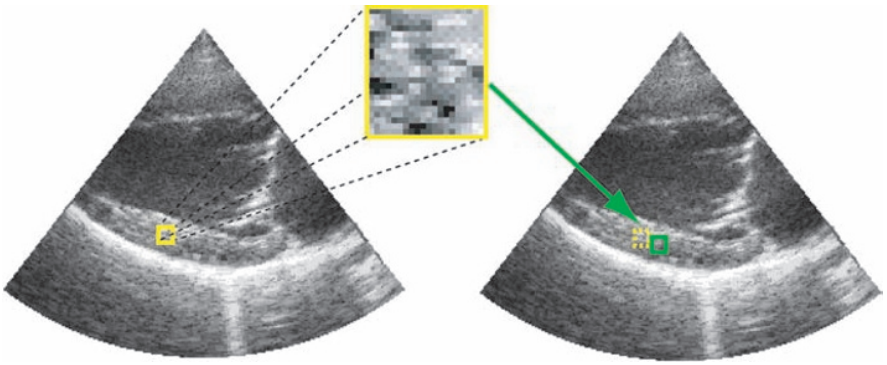

Figure 1.20 A particular segment of soft tissue (here, in the heart) results in a specific spatial distribution of gray values (i.e., speckle pattern) in this ultrasound image. This pattern can be used as an acoustic marker of the tissue.

applied to measure 2D blood-flow patterns based on ultrafast ultrasound methods. More information on ultrasound velocity estimation methodologies can be found in a review by Jensen [5].

Videos

To access the video clips for this chapter, please go to wiley.com/go/lai-echo3.

Video 1.1 Side lobe artifact. The probe cannot generate a pulse in one direction only. There is a strong side lobe artifact in this image.

Video 1.2 Side lobe artifact resolved by harmonic imaging. The heart in Video 1.1 was reimaged using harmonic imaging which resolved the side lobe artifact.

Video 1.3 Reverberation. A strong reflector at the surface, likely a rib, causes a strong reverberation line.

Video 1.4 Refraction. Due to refraction a structure is misplaced, resulting in a ghost image.

Video 1.5 Reflector. A strong reflector (pericardium) imaged at an angle causes structures that lie in front of it and at the side of it appear as if they lie behind it, creating a mirror artifact.

Video 1.6 Acoustic shadowing. A calcified ventricular septal defect patch causes an acoustic shadow.

References

1 Suetens P. Ultrasonic imaging. In: *Fundamentals of Medical Imaging*. Cambridge, UK: Cambridge University Press, 2002, pp. 145–83.
2 Szabo T. *Diagnostic Ultrasound Imaging: Inside Out*. Elsevier Academic Press, London, 2004.
3 Tanter M, Fink M. Ultrafast imaging in biomedical ultrasound. *IEEE Trans Ultrason Ferroelectr Freq Control* 2014;**61**(1):102–19.
4 Cikes M, Tong L, Sutherland GR, D'hooge J. Ultrafast cardiac ultrasound imaging: technical principles, applications, and clinical benefits. *JACC Cardiovasc Imaging* 2014;**7**(8):812–23.
5 Jensen JA. Medical ultrasound imaging. *Prog Biophys Mol Biol* 2007;**93**(1–3):153–65.

CHAPTER 2

Instrumentation, Patient Preparation, and Patient Safety

Stacey Drant and Vivekanand Allada
The Children's Hospital of Philadelphia, Philadelphia, PA, USA

Introduction

With continued advances in ultrasound technology and accreditation requirements, establishing and maintaining a pediatric echocardiography laboratory (echo lab) has become progressively more complex. Echo labs have become increasingly "digital" requiring sophisticated information technology for digital acquisition, reporting, and archiving. Lab accreditation has become more widespread to establish consistency within and amongst pediatric echo labs in an effort to assure quality. Guidelines and recommendations for pediatric echo labs have been published and incorporated into the requirements for accreditation. This chapter serves as a reference guide to establishing and maintaining a pediatric echo lab.

A variety of published recommendations exist pertaining to the organization and function of a pediatric echo lab from several medical societies including the American College of Cardiology (ACC), American Heart Association (AHA), American Academy of Pediatrics (AAP), and the American Society of Echocardiography (ASE). These recommendations have substantial overlap and form the basis for the requirements of the Intersocietal Accreditation Commission (IAC) necessary to achieve accreditation of a pediatric echo lab. For more detailed information, readers are referred to the applicable references and websites cited.

Structure and organization

Pediatric echo labs vary substantially in size and composition of the staff, from individual office practices performing outpatient echocardiograms to large hospital-based labs that combine inpatient and outpatient imaging. In general, pediatric echo labs include physical space, ultrasound machines, pediatric cardiologists, and sonographers. Most pediatric echo labs – including all IAC accredited labs – have medical and technical directors to provide administrative functions.

Personnel and supervision

Physicians

The performance and interpretation of transthoracic echocardiograms is a requirement for cardiology fellowship training. Echocardiography is an operator-dependent imaging technique that requires skill in both performance and interpretation of studies. The recommendations of the American Society of Pediatric Cardiology Training Program Directors/ACC/AAP/AHA Training Statement on Pediatric Cardiology Fellowship Training in Noninvasive Cardiac Imaging 2015 represent the most recent guidelines for echocardiography training [1]. These guidelines describe two levels of expertise, core and advanced, that are appropriate for different career goals. Core level training recommendations represent the minimum that should be achieved by all pediatric cardiology fellows during their standard 3-year cardiology fellowship. Core training allows each fellow to achieve competency to allow for independent use of transthoracic echocardiography to diagnose simple congenital heart disease and acquired pediatric heart disease. Physicians with core level training are not expected to develop expertise in transesophageal and fetal echocardiography; however, exposure to these during core training is recommended as this allows for familiarity with techniques, indications, and limitations, with many fellows becoming competent in these areas. Advanced fellowship (generally requiring an additional year of training) allows for the development of skill and expertise in the echocardiographic diagnosis of complex congenital heart disease, transesophageal, and fetal echocardiography with the goal of assuming positions as independent noninvasive imaging physicians and is also often obtained when a faculty position in academic echocardiography is the goal.

While the current guidelines define specific minimum procedure numbers as a guide to achieving core and advanced levels of training, emphasis is placed primarily on competency-based benchmarks as listed in Tables 2.1 and 2.2 [1]. At present in North America, there is no formal examination that can be used to determine competency in pediatric echocardiography;

Echocardiography in Pediatric and Congenital Heart Disease: From Fetus to Adult, Third Edition. Edited by Wyman W. Lai, Luc L. Mertens, Meryl S. Cohen and Tal Geva.

Companion website: www.wiley.com/go/lai-echo3

Table 2.1 Pediatric echocardiography training: minimal procedural numbers for competency assessment

Level of training	Number of studies
Core training	
TTE perform and interpret	150
TTE review and interpret	100
Advanced training*	
TTE perform and interpret	100
TTE review and interpret	100
TEE perform and interpret	50
Fetal echocardiogram perform and interpret†	50
Fetal echocardiogram review and interpret†	50

*Numbers are in addition to those obtained during core training.
†Fetal echocardiogram: 50 should have congenital heart disease and/or abnormality of fetal circulation.
TEE, transesophageal echocardiogram; TTE, transthoracic echocardiogram.
Source: Srivastava S, Printz BF, Geva T, et al. Task Force 2: Pediatric Cardiology Fellowship Training in Noninvasive Cardiac Imaging. *J Am Coll Cardiol* 2015;6:687–98. © Elsevier.

thus, evaluation is based solely upon an assessment of the trainee's skills during fellowship training. Continued performance and interpretation of echocardiograms and participation in intramural conferences and continuing medical education is necessary to maintain clinical competency. In order to be accredited by the IAC in pediatric echocardiography, medical staff of the laboratory are required to meet the training guidelines outlined, demonstrate continuing medical education specific to pediatric echocardiography, and to maintain an annual procedure volume sufficient to maintain proficiency in examination performance and interpretation, but no specific benchmarks are defined [2].

Sonographers

With continued advances in cardiac ultrasound, performing a pediatric echocardiogram continues to become increasingly sophisticated. This places added educational and professional demands on sonographers. The ASE has published minimum qualifications for cardiac sonographers [3,4], which are reflected in the IAC standards for technical staff summarized in Table 2.3. Despite the fact that training in cardiac sonography has historically been heterogeneous, current standards mandated for credentialing reflect the importance of a formal verifiable education in cardiac sonography. This guarantees that new sonographers have adequate knowledge and technical skills to be competent in contemporary pediatric echocardiography. Current IAC guidelines recommend that each sonographer achieves and maintains minimum standards in education and credentialing in pediatric and/or fetal echocardiography within 1–2 years of the start of employment. Current IAC requirements for credentialing and maintenance of competence are listed in Table 2.4 [2].

Facility

The facility must meet the standards set out by the Occupational Safety and Health Administration and by the Joint Commission where applicable.

Space requirements

The ASE [5] and the IAC [2] recommend that echo laboratories should be large enough to accommodate an area for scanning, a designated space for the interpretation and preparation of reports, and space for the storage of images and reports to remain compliant with state laws (Figure 2.1). The scanning space needs to be large enough to accommodate a patient bed that allows for position changes, an echocardiography imaging system, and patient privacy; a scanning room is generally recommended to be at least 150 square feet [2]. In addition, a sink and antiseptic soap must be readily available and used for hand washing in accordance with the infection control policy of the facility. For the practice of transesophageal echocardiography, space must be available to perform high-level disinfection and to store transesophageal echocardiography probes.

Equipment

Pediatric echo labs require a variety of equipment to function effectively (Table 2.5) including a specialized bed, gel warmer, and blood pressure machine in addition to the ultrasound systems. Forms of distraction such as DVD players or televisions are also recommended to entertain young children during the performance of the studies. All imaging equipment should be tested on a regular basis; the manufacturer's recommendations regarding preventative maintenance should be followed. Echo labs that perform special procedures, including transesophageal echocardiography (TEE), stress echo, and sedated echocardiograms, should also have written procedures in place to handle acute medical emergencies including maintaining a fully equipped crash cart and other pediatric-specific medical equipment in a variety of sizes to accommodate patients of varying sizes [2].

Ultrasound systems

Ultrasound systems dedicated to echocardiography must include the hardware and software to perform M-mode and 2D imaging, color flow and spectral Doppler, along with electrocardiogram (ECG) gating [2,5,6]. There should also be a system setting for tissue Doppler imaging [2]. Many echo labs have added routine 3D imaging and speckle tracking echocardiography into their protocols. The image display may include the name of the institution, patient name, date and time of the study, the ECG tracing, and range and depth markers. Echocardiography has specific transducer requirements, including the ability for the transducer head to fit between rib spaces for a variety of patient sizes as well as the wedge-shaped sector display. Transducers ranging from 2.0 to 12 MHz, providing both low- and high-frequency imaging, are required for pediatric imaging due to the range in patient size

Table 2.2 Core competencies and evaluation tools for noninvasive imaging

Medical knowledge
Know the physical properties of ultrasound and Doppler principles
Know the principles of echocardiographic image construction and factors that influence image composition
Know the ultrasound imaging devices, including "knobology," appropriate transducer and settings to optimize images, and proper and safe use of the ultrasound equipment
Know the proper use of different echocardiographic techniques (2D, M-mode, 3D, color, and spectral Doppler) to thoroughly evaluate cardiac anatomy, physiology, and function
Know the standard transthoracic imaging planes (subxiphoid, apical, parasternal, suprasternal)
Know the effects of patient positioning on image acquisition and how to move them to optimize echocardiographic images
Know the indications for a pediatric TTE
Know the hemodynamic and physiologic changes from fetus to adult
Know the full spectrum of pediatric cardiac surgical procedures, including the components of a complete preoperative and postoperative echocardiographic assessment, as well as potential postoperative complications of each procedure
Know the techniques for imaging abnormal situs and dextrocardia, as well as the associated terminology of complex disease
Know the basic TEE imaging views and indications, including the use of TEE for guidance of intraoperative and catheter-based interventions, and be aware of the limitations of TEE imaging
Know the basic fetal imaging views and indications and limitations of fetal echocardiographic imaging
Know the basic principles used to generate MR images
Know the indications and contraindications for cardiac MR in patients with CHD, including children and adults
Know the indications and contraindications for cardiac MR in children with acquired heart disease
Evaluation tools: direct observation, conference participation and presentation, and in-training examination
Patient care or procedural skills
Have the skills to do a clinical history, know the indications for study, review prior studies, and interim procedures
Have the skills to identify the goals of each study
Have the skills to consistently obtain adequate images from all planes on a standard TTE in a timely manner
Have the skills to identify cardiac structures displayed by echocardiography and how echocardiographic images correlate with cardiac anatomy
Have the skills to recognize imaging artifacts
Have the skills to obtain appropriate measurements of ventricular, valvar, and vascular dimensions
Have the skills to obtain appropriate measurements of ventricular function
Have the skills to evaluate valvar stenosis and regurgitation with spectral (pulsed and continuous wave) and color Doppler
Have the skills to identify and describe common lesions: atrial septal defect, ventricular septal defect, patent ductus arteriosus, aortic stenosis, and pulmonary stenosis
Have the skills to complete a full examination of patients with simple congenital defects, including full Doppler assessment, along with a detailed, concise report
Have the skills to perform a comprehensive 2D and Doppler examination of a newborn with previously undiagnosed complex CHD and be able to assess the need for prostaglandin without assistance. Complete description of complex anatomic details is encouraged, but not required, of a trainee completing core fellowship; accurate imaging/interpretation of complex CHD may require advanced training and/or post-fellowship experience
Have the skills to identify and describe pericardial disease
Have the skills to demonstrate familiarity with indications, use, and limitations of TEE
Have the skills to demonstrate familiarity with indications, use, and limitations of basic imaging skills for fetal echocardiography
Have the skills to read basic cardiac MR images acquired in infants, children, and young adults with either structurally normal or abnormal hearts
Evaluation tools: conference participation, direct observation, and procedure logs

CHD, congenital heart disease; MR, magnetic resonance; TEE, transesophageal echocardiogram; TTE, transthoracic echocardiogram.
Source: Srivastava S, Printz BF, Geva T, et al. Task Force 2: Pediatric Cardiology Fellowship Training in Noninvasive Cardiac Imaging. *J Am Coll Cardiol* 2015;6:687–98. © Elsevier.

from premature infants to adults with congenital heart disease. In addition, a dedicated nonimaging continuous-wave Doppler transducer (Pedoff) must be available. All machines should have harmonic imaging capability and other instrument settings that enable the optimization of both standard and contrast-enhanced ultrasound examinations.

Echo lab personnel, including sonographers, trainees, and physicians, must be able to adjust the system settings for image optimization; thus, an in-depth familiarity with each system is ideal. Pediatric echocardiography often incorporates significantly more vascular imaging than in adult labs to evaluate the systemic venous return, pulmonary veins, branch pulmonary arteries, coronary arteries, and aortic arch. These static structures benefit from different system settings than those for the more mobile intracardiac structures, and thus the ability to readily adjust the depth and gain along with the persistence, log compression, sector angle, gate, and Doppler filters becomes imperative. Most vendors have systems specialists who can provide training in the utilization and adjustment of the system settings in order to create optimal preset packages for each machine according to the institutional preferences.

Scheduling

Sufficient time should be allotted for each study according to the procedure type. Performance time for an uncomplicated complete pediatric transthoracic echocardiogram is generally 45–60 minutes from patient encounter to departure. Additional time may be required for: (i) patients with complex disease;

Table 2.3 American Society of Echocardiography (ASE) guidelines for pediatric cardiac sonographers

Comprehensive understanding of:
Cardiovascular and thoracic anatomy, pathophysiology, hemodynamics, and embryology
Congenital and acquired heart defects
Segmental approach to the diagnosis of congenital heart defects
Surgical procedures for repair and palliation of congenital heart defects
Ultrasound physics
Instrumentation
Tissue characteristics
Biological effects of ultrasound
Measurements of cardiac structures and blood flow
Making appropriate quantitative calculations from echo measurements
Communication and safety-related skills:
Ability to interact and communicate effectively both orally and in writing
Be well versed in medical terminology
Capable of explaining the purpose of the echo exam to the patient and answer questions
Utilize proper infection control procedures
Comply with patient confidentiality and privacy laws
Competent in first aid and basic life support
Familiar with other types of diagnostic tests

Table 2.4 Intersocietal Accreditation Commission (IAC) guidelines for credentialing and maintenance of competence in pediatric echocardiography

Credentialing and education
Credentialing includes:
• RDCS: Registered Diagnostic Cardiac Sonographer from American Registry of Diagnostic Medical Sonography (ARDMS)
• RCS or RCCS: Registered Cardiac Sonographer or Registered Congenital Cardiac Sonographer from Cardiovascular Credentialing International (CCI)
• CRCS: Canadian Registered Cardiac Sonographer from Sonography Canada
• ACS: Advanced Cardiac Sonographer from Cardiovascular Credentialing International (CCI)
Provisional staff employed in an accredited facility:
• New graduates of cardiac ultrasound program must obtain an appropriate credential within 1 year of date of graduation
• Individuals cross training in echocardiography to fulfill clinical experience prerequisites for a credentialing exam must obtain appropriate credential within 2 years from the start of training
Technical expertise
Must be able to properly display cardiac and/or vascular structures and blood flow in each of the imaging views within a standardized protocol
Proficiency in 2D, M-mode, and Doppler echocardiography
Ability to accurately document abnormal echocardiography and Doppler velocities indicative of abnormal cardiovascular pathophysiology
Demonstrate knowledge and competency in specialty areas of echocardiography when required in practice
Maintenance of competence
Annual procedure volume sufficient to maintain proficiency in examination performance
Document at least 15 hours of echocardiography-related continuing medical education over a period of 3 years

(ii) when other modalities such as 3D imaging or speckle tracking imaging are required; or (iii) studies performed on sedated patients. An "urgent" study must be performed in the next available time slot while a "stat" study must be performed as soon as possible, pre-empting routine studies. Qualified personnel and equipment must be available for urgent or "stat" studies outside normal working hours in inpatient facilities or

Figure 2.1 Echocardiography reading room with live imaging displayed on wall screens and dual screen work stations for efficient review of images and reporting.

Table 2.5 Pediatric echocardiography laboratory equipment

Ultrasound system: • Hardware and software to perform M-mode, 2D, Doppler (including color, spectral (pulsed wave and continuous wave) and tissue Doppler modalities) • Image display including name of institution, patient name, date and time of study, electrocardiogram tracing, range and depth markers • Transducers: ◦ Frequency range 2.0–12.0 MHz ◦ Dedicated nonimaging continuous-wave Doppler (Pedoff) ◦ Transesophageal probes (if performed in the lab)
Digital image storage method
Imaging bed with dropout section of mattress
Gel warmer
Blood pressure machine (including age-appropriate cuff sizes)
Distraction equipment (e.g., TV, DVD player, music player)
Contrast agents and intravenous supplies
Equipment to treat medical emergencies (e.g., suction, oxygen, code cart)

somewhere appropriate. Routine inpatient echocardiograms should be performed on the same working day as they are ordered unless otherwise specified, while outpatient studies should be assigned priority as defined by the referring physician and/or indication of the study [2,5,6]. Many busy pediatric echo labs have systems that schedule patients in time slots during the course of the day while others use a "first come, first served" type of schedule. The echocardiogram order and requisition must clearly indicate the type of study to be performed, the reason(s) for the study, and the clinical question to be answered, and the signed order/requisition must be present in the patient's medical record.

Storage

A permanent record of both echocardiographic images and the final echocardiographic report must be produced and retained in accordance with applicable state and federal guidelines. Federal guidelines fall under the Healthcare Insurance Portability and Accountability Act (HIPAA) passed in 1996 and directs that facilities retain records for 6 years from the date of creation [7]. State laws also govern the length of time medical records need to be retained and vary from state to state; however, HIPAA requirements supersede state laws if the state law requires shorter retention periods.

Images must be archived as moving images in the original format that they were acquired. The current standard format has changed from analog media utilizing videotape to digital storage. The ASE has published guidelines for digital echocardiography [8] which describe digital archiving in detail. The DICOM (Digital Imaging and Communications in Medicine) standard was created through a collaboration of the National Electrical Manufacturers' Association and various professional organizations and serves to standardize the exchange of digital images allowing interoperability within and between echo labs. In order to accommodate the large storage requirements, both clinical and digital compression is often required. Clinical compression is at the discretion of the imager and can be accomplished by limiting the time length of a clip or the number of clips. Digital compression is accomplished utilizing JPEG compression, currently the only compression approved by the DICOM committee, which provides more efficient storage of individual frames and loops without significant distortion of the images. Quantitative image analysis has shown little degradation at compression ratios as high as 20 : 1 [9]. DICOM standards now also need to be applied to 3D echocardiograms. Thus, the DICOM Working Group is rewriting the standard to allow exchange of multidimensional datasets.

Optimal transfer of images for interpretation and archiving is performed using high-speed networks with a minimum speed of 100 megabits per second; heavily trafficked lines benefit from gigabit per second capacity. Echocardiographic data should initially be stored locally on a high-capacity hard disk array that supports rapid access to handle both recent studies and returning patients. A long-term archive is needed, which may take the form of a jukebox of optical disks, CD ROMs, DVDs, digital linear tape, advanced intelligent tape, or videotape. The archive should simultaneously generate a second copy of each study to serve as a back-up, which should be stored in a separate location to provide recovery in case of archive failure.

Software systems that connect the echocardiographic reports to the hospital information systems for scheduling, reporting, and billing are becoming more common. As more hospitals move toward electronic scheduling, registration, and medical record keeping, the ability to interface information electronically between the hospital system and the echocardiography machine has become a reality. DICOM worklists allow patient demographics to directly populate the echocardiography machine, eliminating the risk of manual entry errors.

Patient preparation and safety

Proper patient preparation is an essential step to ensure a quality echocardiogram; this is particularly important in the pediatric population where lack of cooperation can be a major obstacle to obtaining adequate images. A system for transferring patients to and from the echo lab should be a part of the operations manual. A parent or guardian should accompany a minor to and from the echo lab and be present during the study, except where privacy issues supersede. Having a brief discussion with the patient and family to explain the procedure helps to guide expectations and allay fears. ECG leads can be placed during this discussion. The importance of patient position for optimal imaging can also be explained (Figure 2.2). In addition, the caregiver can be asked to help calm or distract their child during the procedure. A calm environment sometimes helps avoid the need for sedation in young children. Each echo room should use dimmed lighting, use warmed ultrasound gel, and provide visual distractions (e.g., bubbles, toys, TV, DVD player). In some cases, bundling (in

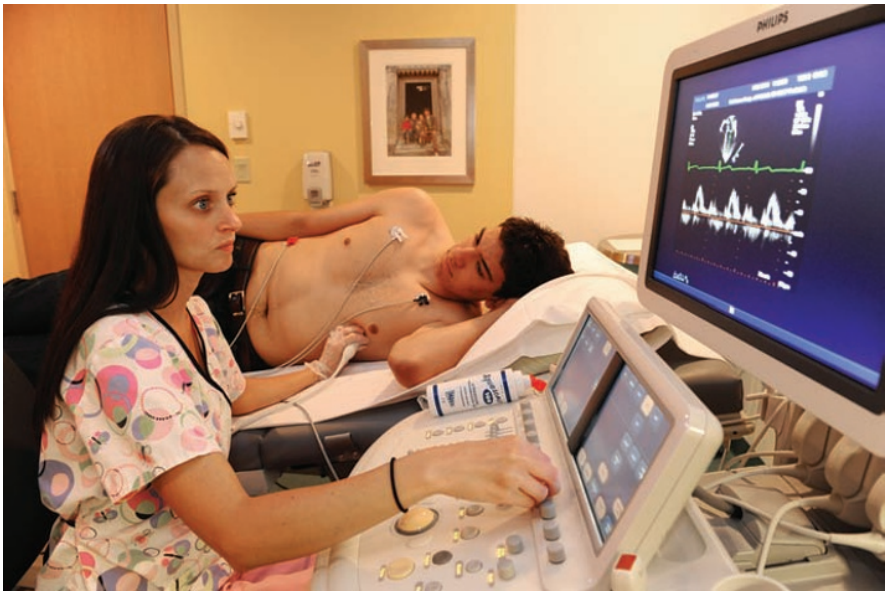

Figure 2.2 Pediatric echocardiograms are performed in rooms with enough space for the ultrasound machine and for the sonographer to have comfortable seating. During the examination, the patient is often required to move into various positions including left decubitus position as seen here. An apical four-chamber view is being performed in this study.

neonates) or a parent lying on the bed next to their child can help keep the child still for the study. Moreover, small rewards (such as a sticker) are often used as positive reinforcement.

Sedation

The performance of high-quality transthoracic echocardiography is more likely to yield the necessary diagnostic information when the patient does not move and when any associated anxiety is effectively controlled. This has become increasingly important because the initial diagnosis of both structural and functional cardiac abnormalities are generally made by echocardiography and a substantial percentage of interventional decisions rely solely upon this data.

Historically, sedation for transthoracic echocardiograms was provided under the supervision of pediatric cardiologists using a variety of medications with varied success [10–15]. However, with the subsequent involvement of anesthesiologists and the development of hospital sedation services, procedural sedation for nonpainful procedures such as echocardiography has evolved with the use of newer medications and novel routes of administration. A recent review "Selection of medications for pediatric procedural sedation outside of the operating room" is available in UpToDate and provides a comprehensive review for patient management during nonpainful procedures [16]. Nonpharmacologic interventions including distraction, relaxation, and positive reinforcement are the preferred methods for pediatric patients undergoing echocardiography and can be employed solely or as a complement to sedation [17–20]. When nonpharmacologic interventions are not sufficient, sedation becomes necessary and the authors of this chapter recommend sedation with oral, sublingual, or intranasal midazolam or dexmedetomidine rather than short-acting barbiturates in healthy children. Ultimately, the choice of medication and route of administration are determined by several factors including patient characteristics, duration of imaging, and availability of personnel to administer specific medications that may be restricted. Typically, sedation for pediatric echocardiography is performed in a hospital setting that provides the necessary trained personnel, medications and equipment. Hospital policies and accreditation requirements for echo labs require that each echo lab has a written policy for sedation protocols in addition to the appropriate staff for the performance of sedation.

Examinations and procedures

Transthoracic echocardiography

The standard pediatric echocardiogram involves 2D imaging of all cardiac structures along with spectral and color Doppler hemodynamic assessment of the valves and vessels and an evaluation of ventricular function. A protocol should be in place that defines the components of the standard examination, including the order in which the imaging planes will be interrogated, the structures to be examined, and the measurements to be made. It is helpful to have a list of structures to be interrogated within each imaging plane. Optimally, recorded images are a combination of complete sweeps and selected single planes

to assure that the segmental anatomy of the heart is accurately determined. Guidelines for a standard pediatric transthoracic echocardiogram protocol have been published by the Task Force of the Pediatric Council of the ASE and are used by the IAC for pediatric accreditation [21]. If a required element cannot be adequately imaged, it should be documented in the report. Due to the complexity of congenital heart disease, a complete examination may require custom planes to completely display and interrogate an abnormality.

Transesophageal echocardiography

Detailed description of and guidelines for the performance of TEE in pediatric patients with acquired and congenital heart disease have been updated [22]. The purpose of this section is to focus on the practical aspects of echo lab requirements to perform TEE in pediatric or adult patients with congenital heart disease within a facility. The location and indication for pediatric TEE often differ from those performed in adult labs and require a specialized fund of knowledge and skills. Pediatric TEE is occasionally performed in an outpatient setting; however, the majority of these studies are performed in the operating room, cardiac catheterization lab, intensive care unit, or sedation unit. These studies require ongoing communication and close collaboration with surgeons, interventionalists, anesthesiologists, and intensivists.

The knowledge, skill, and training needed to perform pediatric TEE are quite different from those required to perform TEE in the adult patient. Comprehensive knowledge of congenital heart disease and surgical repairs as well as experience in TEE imaging are crucial to adequately demonstrate and interrogate structures in the nonstandard views necessary. Thus, it is recommended that physicians who perform TEE independently on pediatric or adult patients with congenital heart disease achieve additional training and experience as outlined in Table 2.6 [22]. IAC certification exists for pediatric TEE [2], and these requirements are outlined in Table 2.7. Because TEE is an invasive procedure, an explanation of the procedure along with indications, risks, and benefits should be provided to the patient and/or their legal guardian and informed consent obtained. If TEE is being performed in conjunction with a surgical or catheterization procedure, the consent may be obtained and documented with the consent for the primary procedure or anesthesia.

Probe size is largely determined by patient size; each probe comes with guidelines regarding use based on weight of the patient.

TEE probe disinfection and maintenance are integral to assure patient safety. Integrity of the insulating layers of the transducer must be routinely checked before and after each use. Probe cleaning technique and specific brands of disinfectants are recommended by probe manufacturers, and a policy should be in place to follow these guidelines. In addition to cleaning, it is recommended that the TEE probe be intermittently tested for electrical safety utilizing a saline bath connected to a leakage current analyzer. Guidelines, similar to those in place for gastrointestinal endoscopy, have been published by the British Society of Echocardiography in 2011 [23] and provide detailed information regarding TEE probe decontamination. The Centers for Disease Control and Prevention (CDC) also published "Guidelines for disinfection and sterilization in healthcare facilities" in 2008 and updated them in May 2019 [24], but there are no specific recommendations for TEE probes.

Fetal echocardiography

A detailed description of and guidelines for the performance of a fetal echocardiogram have been published [25]. Fetal echocardiography is described in detail in Chapter 44. Fetal echocardiography requires additional knowledge to that for pediatric transthoracic echocardiography including understanding of maternal–fetal physiology, fetal anatomic and physiologic changes throughout gestation, and fetal arrhythmias. Advanced training is recommended for fetal echocardiography. IAC certification exists for performance of fetal echocardiograms [2] and these requirements are outlined in Table 2.8. Space, ultrasound equipment, information technology, and staff requirements are similar to those required for pediatric echocardiography. Many fetal echocardiography laboratories are housed within the pediatric echo lab. Others are located in areas that perform other types of fetal imaging (e.g., maternal–fetal medicine units).

Table 2.6 Guidelines for training and maintenance of competence in transesophageal echocardiography in pediatric and congenital heart disease

Component	Objective	Duration	Number of cases
Echocardiography	Prior experience in performing/interpreting TTE	6 months or equivalent	Minimum of 450 cases across all ages
Esophageal intubation	TEE probe insertion	Variable	25 cases (50% under 2 years old)
TEE exam	Perform and interpret with supervision	Variable	50 cases
Ongoing TEE experience (Level 3)	Maintenance of competency	Annual	25–50 cases/year; or achievement of laboratory-established outcome variables

TEE, transesophageal echocardiography; TTE, transthoracic echocardiography.
Source: Puchalski MD, Liu GK, Miller-Hance WC, et al. Guidelines for performing a comprehensive transesophageal echocardiographic examination in children and all patients with congenital heart disease: recommendations from the American Society of Echocardiography. *J Am Soc Echocardiogr* 2019;32(2):173–215. © 2019, Elsevier.

Table 2.7 Pediatric transesophageal echocardiography (TEE): IAC requirements summary

Ordering and scheduling:
- Process in place for obtaining and recording indication for test
- Order must be present in the patient's medical record and include:
  - Type of study to be performed
  - Reason for the study
  - Clinical question to be answered
- Scheduling:
  - Uncomplicated complete study (outside the operating room) – 45–60 minutes
  - Complicated studies – additional 15–30 minutes
  - Time for adequate post-sedation monitoring should be included
  - Urgent or stat – studies performed as soon as possible
  - Availability for emergencies – qualified personnel and equipment should be available outside normal working hours

Training: see Table 2.6

Components of transesophageal examination:
- Technical personnel – to assist the physician and may include:
  - Sonographer
  - Nurse
  - Trainee
- Preparation of the patient:
  - Consent must be obtained
  - Safety guidelines (including intravenous access, cardiac monitor with electrocardiogram telemetry, pulse oximetry, oxygen with appropriate delivery devices)
- Moderate sedation – written policies must exist for the use of moderate sedation including:
  - Type of sedatives and appropriate dosing
  - Monitoring during and after the examination
- Monitoring the patient – facility guidelines for the monitoring of patients who receive anesthetic agents are required
- Recovery of the patient – the patient must be monitored for sufficient time to assure that no complications have arisen from the procedure or the sedation used
- Components of the examination – protocol must be in place defining standard views and components of a comprehensive TEE examination

Procedure volumes – annual procedure volume must be sufficient to maintain proficiency in examination performance and interpretation

Probe safety and maintenance – manufacturer's guidelines must be followed for care and cleansing of the TEE transducer and adhere to appropriate infectious disease standards:
- Structural and electrical integrity of the transducer must be checked between each use and "Passed" or "Failed" documented in the maintenance log along with action taken if "Failed"

A list of peri-procedural complications must be maintained

Reporting – report must include:
- Complications of the procedure ("Yes" or "No")
- Components of the procedure (2D, color, or spectral Doppler)
- Comment on all structures evaluated in the examination:
  - Note any structure not well visualized
  - Note if examination is abbreviated for any reason
- Summary of the examination including pertinent positive and negative findings

Intracardiac echocardiography

One of the more recent applications of echocardiography, intracardiac echocardiography (ICE), has become integral to many cardiac catheterization interventions including device placement, mitral valve interventions, and electrophysiology

Table 2.8 Fetal echocardiography: IAC requirements summary

A technical protocol must be written and adhered to in the facility including:
- Components of the examination
- Indications for performance of a fetal echocardiogram

Complete examination – standard views from multiple planes including views of all cardiac and selected extracardiac structures and may include:
- Presence of single or multiple gestations and locations of fetuses relative to the mother and one another
- Survey of fetal lie and position defining fetal orientation
- Measurement to estimate fetal size/gestational age (e.g., biparietal diameter or head circumference, abdominal circumference, femur length)
- Fetal cardiac position and visceral situs
- Measurement of chest and heart circumference and area for calculation of size ratios
- Assessment of fetal heart rate and rhythm using M-mode and Doppler techniques
- Short-axis view of umbilical cord vasculature with spectral Doppler evaluation of flow in the umbilical vessels and ductus venosus
- Imaging of pericardial and pleural space, abdomen, and skin for fluid or edema
- Imaging and Doppler/color flow of systemic veins, their course, and cardiac connection
- Imaging and Doppler/color flow of pulmonary veins, their course, and cardiac connection
- Multiple imaging planes of and Doppler assessment of flow direction and velocity
  - Atria
  - Atrial septum
  - Foramen ovale
  - Ductus arteriosus
  - Ventricular septum
  - Atrioventricular valves
  - Ventricular outflow tracts
  - Semilunar valves
- Four-chamber and short-axis view of the heart for assessment of cardiac chamber size and function
- Short- and long-axis views of:
  - Ascending, descending, and transverse arch of the aorta
  - Ductus arteriosus
  - Main and proximal branch pulmonary arteries
- Additional fetal elements:
  - Middle cerebral arterial blood flow

Report components – must include but may not be limited to:
- Measurements performed where normal values are known
- Interpretation of measurements appropriate to the area of abnormality or clinical issue
- Doppler values both normal and abnormal appropriate to the area of abnormality or clinical issue
- Text must include comment on:
  - Components of procedure
  - All structures evaluated in the exam (as specified above)
  - Text must be consistent with quantitative and Doppler data including localization and quantification of abnormal findings
  - Notation of structures that were not well visualized

Procedure volumes – annual procedure volume sufficient to maintain proficiency in examination performance and interpretation

Scheduling – sufficient time must be allotted for each study according to procedure type (complete or follow-up). Performance time for an uncomplicated complete study is 30–60 minutes

procedures. Current guidelines for use of ICE in catheter interventions have been published by the ASE [26]. The advantage of ICE over TEE in the adult population is that it obviates the need for general anesthesia. Moreover, ICE catheters are manipulated by the interventionalist so that an echocardiography physician is not always needed during the procedure. ICE has been utilized sparingly in pediatrics primarily due to the limitations imposed by patient size; ICE catheters range in size from 8 to 10 Fr and require a 10 Fr venous sheath. Current ICE catheters are steerable and employ a monoplane 64-element phased-array transducer with grayscale, color, spectral, and tissue Doppler capabilities. Views are obtained by rotating the catheter within the right atrium or right ventricle and steering the catheter tip. ICE catheters are also expensive and have only a single use. In the adult population this cost is offset by avoiding the costs for an anesthesiologist and an echocardiography physician; however, it is unclear whether this can be duplicated in the pediatric population. Currently, ICE is being used in pediatrics primarily for atrial septal defect device closure and evaluation of percutaneous pulmonary valve placement [27]. ICE catheters have also been used as TEE probes in very small infants. In one adult study, ICE catheters were used as a nasogastric TEE probe to image the atria in patients being evaluated for intracardiac thrombus prior to cardioversion [28]. The use of ICE during interventional and electrophysiology procedures has been published [29,30].

Research protocols

Research activities that require echocardiography are common in academic centers. In general, single-center investigator-initiated research studies are organized within the laboratory structure and do not require oversight outside of the local institutional review board. If a specific protocol is being utilized, there may be designated sonographers and physicians who obtain and interpret the images and make the necessary measurements or calculations. In larger multicenter studies, a core lab is often utilized. Core labs provide image storage, consistency in measurements, quality assurance, and feedback to participating echo labs to achieve the highest quality echo studies. Guidelines for echocardiography in clinical trials have been published by ASE and serve to outline the different levels of core lab requirements. These guidelines also provide recommendations regarding study design, image analysis, data management, quality assurance, statistical analysis plan, and regulatory considerations [31].

Telemedicine

Telemedicine is the use of telecommunication and information technology to provide remote echocardiography services. Echocardiograms performed on pediatric patients at one site can be transferred electronically to another site for interpretation by an experienced pediatric echocardiographer. This allows for more efficient use of the physician's time by obviating the need for travel between different locations to read echocardiograms. Telemedicine also allows for after-hours review by on-call cardiologists from their homes. After-hours echocardiography review is accomplished either by direct digital transfer utilizing network connections or cloud-based systems, depending upon the vendor.

Telemedicine places significant demands on hospital-based networks. The speed of transfer is often dependent upon the network speed of the transferring facility. Some examples of modes of transmission include ISDN phone lines, DSL, cable modem, T1 lines, and fiberoptic cable. The rate of transfer for a T1 line is 1.5 Mbps while that of fiberoptic cable is often 50–100 Mbps. Actual rates of transfer may be significantly slower depending upon other network traffic. The rate of transfer of an entire study can be improved utilizing incremental transfer of each image as it is captured from the echocardiography machine rather than downloading the entire study at its conclusion [9].

Indications/reporting/billing

The indications for performing a pediatric transthoracic echocardiogram were published by the ACC/AHA/ASE Association Task Force on Practice Guidelines in 1997 [32] and were updated in 2003 [33]. The role of echocardiography has expanded from its role in screening, diagnosis, and monitoring of patients with congenital or acquired heart disease to include assessment of those at risk for the development of myocardial dysfunction and pulmonary hypertension. The increasing scope of transthoracic echo in pediatrics has raised concerns for overutilization.

Appropriate use criteria for pediatric echocardiography in the outpatient setting have been published [34] and are being introduced into quality improvement processes by the ACC and the IAC. Studies evaluating the appropriateness and diagnostic yield of transthoracic echocardiography for pediatrics have been done in both the inpatient and outpatient settings [35,36], and more recently appropriate use criteria have been published for multimodality imaging in patients with congenital heart disease [37]. This will likely lead to further refinement of the current criteria for outpatient echocardiography as well as the creation of appropriate use criteria for inpatient echocardiography.

Requirements for the reporting of a pediatric echocardiogram are dictated not only by the clinical question but also by the requirements for echo lab accreditation (IAC) as well as billing (CPT codes). The indication for an echocardiogram, regardless of modality, must be verified prior to performing the study to appropriately direct the examination. The echocardiogram order must clearly indicate the type of study to be performed, the reason for the study, the underlying diagnosis, and the clinical question(s) to be answered.

Table 2.9 Definitions of complete and limited echocardiograms

Complete study
CPT definition: A comprehensive procedure that includes 2D and, when performed, selected M-mode examination of the left and right atria, left and right ventricles, the aortic, mitral, and tricuspid valves, the pericardium, and adjacent portions of the aorta in addition to spectral and color flow Doppler providing information regarding intracardiac blood flow and hemodynamics
IAC definition: Imaging study that defines the cardiac and visceral position and a complete segmental image analysis of the heart from multiple views and also defines the cardiac anatomy and physiology as fully as possible using imaging and Doppler modalities
Limited or follow-up study
CPT definition: An examination that does not evaluate or document or attempt to evaluate all the structures that comprise the complete echocardiographic exam. Typically limited to, or performed in follow-up of, a focused clinical concern
IAC definition: A study that generally examines a specific region of interest of the heart and/or addresses a defined clinical question

The definition of a complete and a limited study based on CPT and IAC criteria is outlined in Table 2.9. The distinction is often ambiguous; a focused question may require a thorough evaluation of multiple structures and thus meet the definition of a complete echocardiogram. From a billing standpoint, the CPT codes for complete and limited echocardiograms are divided into noncongenital and congenital designations; however, these definitions are not always explicitly differentiated. Echocardiography reporting guidelines and requirements have been published by the Task Force of the Pediatric Council of the ASE [21] as well as the IAC [2] in an attempt to improve quality and consistency. Descriptions of an abnormality of a cardiac structure should include comments on both anatomy and function (if appropriate). The interpretation summary should highlight the key abnormalities and compare with prior studies (if appropriate) to determine if findings are unchanged, progressive, or improved. The final report must be reviewed and signed by the interpreting physician and include the date and time of the signature. Amended reports must include the time and date of the amendment and action taken if there was a significant change from the original study. Timeliness of reporting has specific requirements for accreditation: (i) routine inpatient echocardiograms must be interpreted by the medical staff within 24 hours of completion of the exam; (ii) outpatient studies must be interpreted by the end of the next business day; and (iii) the report must be signed and verified within 48 hours of the interpretation.

Preliminary findings on urgent studies should be immediately available, and the final report should be available by the end of the next business day, while findings of a stat echo must be made available immediately by the interpreting physician. A policy and procedure must be in place for reporting and documentation of critical values including documentation of physician-to-physician communication. Preliminary reports should be prepared under IAC guidelines. Sufficient support staff should be available to assist with scheduling and distribution of finalized echocardiography reports.

IAC accreditation

The IAC provides accreditation for a variety of cardiovascular testing including echocardiography. This organization is sponsored by the ASE, ACC, Society of Diagnostic Medical Sonography (SDMS), and Society of Pediatric Echocardiography (SOPE) with a mission to improve healthcare through accreditation. The IAC provides accreditation in specific areas of pediatric echocardiography including transthoracic, transesophageal, and fetal echocardiography. The ASE states that "existing echo labs should be accredited by the IAC" while new labs should be expected to submit applications within 2 years of the onset of operation. Increasingly, IAC accreditation has become linked to reimbursement for Medicare and Medicaid as well as many private insurers. Completion of the application requires both detailed information of echo lab operations as well as submission of case studies for review. This process requires facilities to adopt or revise policies and protocols, ensure adequate personnel training and expertise, and validate quality improvement (QI) programs. Once accredited, reaccreditation is required every 3 years with demonstration of compliance with updated standards. Current IAC Standards and Guidelines for Pediatric Echocardiography Accreditation are available for download on the IAC website and define the minimum requirements for all echocardiography facilities [2]. Case studies for submission can be identified prospectively or retrospectively. The review process generally takes approximately 12–16 weeks. Audits of institutions may occur at any time during accreditation.

Quality improvement

The establishment and maintenance of a robust QI program is essential to maintaining quality and consistency in any pediatric echo lab. The process encourages continuous feedback for the lab as a unit as well as for each individual sonographer and physician. Along with continued medical education, the quality improvement process also serves an educational role.

Quality improvement has increasingly become a standard within both pediatric and adult congenital heart disease centers and the ACC has established the Adult Congenital and Pediatric Quality Network (ACPC) which is dedicated to collecting and sharing data, collaborating, and developing best practices for patients with congenital heart disease [38]. The ACPC collaborative requires centers to enroll and contribute data. There are seven quality metrics that have been published for echocardiography including: (1) results reporting in pediatric echocardiography, (2) adverse events with sedated pediatric

echocardiography, (3) echocardiogram for exertional chest pain, (4) echocardiogram performed as an outpatient during the first year of life for arterial switch operation patients, (5) echocardiographic diagnostic accuracy, (6) initial transthoracic echocardiogram image quality, and (7) comprehensive echocardiographic examination. Additional quality metrics are being developed for appropriate use in pediatric echocardiography and fetal echocardiography.

The IAC independently includes QI requirements for accreditation that reflect recommendations published in the ASE publication "Recommendations for quality echocardiography laboratory operations" in 2011 [5].

The IAC requirements are briefly summarized in Table 2.10. Each facility must have a QI program in place. Biannual meetings are required, and minutes of the meetings must be maintained and made available to all personnel. A policy to address discrepancies must be in place. All medical and technical staff are required to attend at least one of the two meetings each year. Correlation and confirmation of results must be maintained for each physician and each modality. Correlation with other modalities or with surgical or autopsy findings is generally warranted as outlined in Table 2.11. Guidelines published by the ASE in 2011, "Recommendations for quality echocardiography laboratory operations," include quality assessment recommendations [5]. The goal of these recommendations is "to provide feedback to the lab members in the spirit of learning and quality improvement while keeping in mind that reasonable and equally competent people can sometimes differ in their review of echocardiographic results."

Table 2.10 Intersocietal Accreditation Commission (IAC) quality improvement measures

- Physician interpretation variability – must be assessed on a minimum of two cases per modality (transthoracic echocardiogram (TTE), transesophageal echocardiogram (TEE), fetal) per quarter for:
  - Quality and accuracy of the interpretation based upon the acquired images
- Technical quality review – must evaluate the technical quality of the images and, if applicable, the safety of the procedure on a minimum of two cases per modality (TTE, TEE, fetal) per quarter. Review must include:
  - Clarity of images and/or evaluation for suboptimal images or artifact
  - Completeness of the study
  - Adherence to facility image acquisition protocols
- Final report timeliness and completeness – minimum of two cases per modality (TTE, TEE, fetal) per quarter for:
  - Timeliness: interpretation time:
    - Stat: immediately available by interpreting physician (verbal or written sonographer findings/comments must not be provided to anyone other than the interpreting physician)
    - Routine inpatient: within 24 hours of exam completion
    - Outpatient: by the end of the next business day and verified signed report within 48 hours of interpretation
  - Critical results – there must be a policy in place for communicating critical results
  - Appropriate use – evaluate the appropriateness of the initial outpatient echocardiogram as "appropriate," "may be appropriate," or "rarely appropriate"
  - Report completeness:
    - Demographics: date of study, date of birth, gender, name/identifier of the facility, name/identifier of the patient, performing sonographer, ordering physician
    - Clinical data: including indication for study, height, weight, blood pressure
    - Must accurately reflect the content and results of the study
    - Must comment on whether a given dimension is normal or abnormal
    - If any structure is not well visualized this must be noted
    - Report text must be consistent with the quantitative and Doppler data and must include localization and quantification of abnormal findings
    - 2D and/or M-mode numeric data: measurements performed in the course of the exam and/or interpretation
    - Doppler evaluation: peak and mean gradients (if stenosis present) and degree regurgitation, peak tricuspid regurgitation velocity for estimation of right ventricular systolic pressure
    - Summary of results including pertinent positive and negative findings
  - Pediatric TTE – must include left ventricular internal dimension or volume at end diastole and end systole, left ventricular posterobasal free wall and septal thickness, and aortic root dimension unless underlying pathology prohibits
  - Pediatric TEE – report text must also include complications of procedure (yes or no)
  - Fetal echocardiogram:
    - Clinical data: including indication for study, last menstrual period or estimated date of delivery, and fetal number
- Correlation will be performed with any appropriate imaging modality, surgical findings, or clinical outcomes on a minimum of four cases annually with at least two cases per relevant testing area to be reviewed in quality improvement meetings

Echocardiography laboratory productivity

An important resource for pediatric echocardiography directors and administrators is the ASE (https://www.asecho.org/). Under the auspices of the ASE, the Committee on Pediatric Echocardiography Laboratory Productivity (C-PELP), comprised of academic pediatric echo lab directors, studied how echo lab structure influenced productivity for physicians and sonographers. Using a national survey of academic pediatric echo labs, the committee generated benchmark data and trends. To date, three surveys have been published (with plans for futures surveys in the works).

Each survey determined: (i) the annual laboratory volume and types of echocardiographic studies performed; (ii) physician productivity defined as the average number of studies interpreted per day by a full-time echocardiography physician dedicated to the laboratory; and (iii) the average number of studies performed by a pediatric cardiac sonographer in a year. Finally, each survey addressed factors (personnel, resources, education, equipment, PAC (programmable automation controller) systems, and IT) that influence echo lab productivity.

In the first survey, C-PELP I [39] sought to identify factors – programmatic or laboratory related – that affected clinical productivity. C-PELP II [40] further delved into echo machine utilization (echocardiograms per machine per year) and factors

Table 2.11 Quality improvement correlation requirements

Transthoracic echocardiograms
Correlate with:
- Other diagnostic procedures:
  - Cardiac catheterization
  - Magnetic resonance imaging
  - Computed tomography
- Surgical intervention
- Postmortem examination

Components and areas for correlation include:
- Semilunar valve stenosis
- Selected anomalies of functional evaluation of diagnostic interest to the facility
- Echo studies which are the primary diagnostic imaging prior to surgical repair

Transesophageal echocardiograms (if performed)
Correlate with:
- Other diagnostic procedures
- Surgical repair

Components for correlation include:
- Left ventricular function and regional wall motion analysis
- Left or right ventricular function
- Presence and severity of valvar dysfunction
- Defects of atrial and ventricular septation
- Presence or absence of thrombi or vegetations
- Presence or absence of anomalous venous connections
- Abnormalities of the aorta

Fetal echocardiograms (if performed)
Correlate with:
- Postnatal transthoracic echocardiogram
- Postnatal cardiac catheterization
- Postmortem examination

influencing work flow and workforce (program size, trainees, scheduling formats, use of sedation). C-PELP III [41] was designed to assess how clinical productivity was associated with laboratory infrastructure elements such as training, administrative tasks, quality improvement, research, and use of focused cardiac ultrasound. While further details are beyond the scope of this chapter, the ASE C-PELP survey results are available in the *Journal of the American Society of Echocardiography*.

References

1 Srivastava S, Printz BF, Geva T, et al. Task Force 2: Pediatric Cardiology Fellowship Training in Noninvasive Cardiac Imaging. *J Am Coll Cardiol* 2015;**6**:687–98.
2 IAC (Intersocietal Accreditation Commission). IAC Standards and Guidelines for Pediatric Echocardiography Accreditation. Published 2017, revised 2018. https://www.intersocietal.org/echo/seeking/echo_standards.htm (accessed January 2020).
3 Ehler D, Carney DK, Dempsey AL, et al. Guidelines for cardiac sonographer education. *J Am Soc Echocardiogr* 2001;**14**:77–84.
4 Bierig SM, Ehler D, Knoll ML, Waggoner AD. ASE minimum standards for the cardiac sonographer: a position paper. Raleigh, NC, USA: American Society of Echocardiography, 2005. http://www.asecho.org/wordpress/wp-content/uploads/2013/05/Minimum-Standards-for-the-Cardiac-Sonographer.pdf (accessed December 2020).
5 Picard MH, Adams D, Bierig SM, et al. American Society of Echocardiography recommendations for quality echocardiography laboratory operations. *J Am Soc Echocardiogr* 2011;**24**:1–10.
6 Kisslo J, Byrd BF, Geiser EA, et al. Recommendations for continuous quality improvement in echocardiography. *J Am Soc Echocardiog* 1995;**8**:S1–S28.
7 US Code of Federal Regulations. 45 CFR 164.316(b)(2). https://www.govregs.com/regulations/expand/title45_chapterA_part164_subpartC_section164.316 (accessed December 2020).
8 Thomas JD, Adams DB, DeVries S, et al. Guidelines and recommendations for digital echocardiography. *J Am Soc Echocardiogr* 2005;**18**:287–97.
9 Karson TH, Zepp RC, Chandra S, et al. Digital storage of echocardiograms offers superior image quality to analog storage, even with 20:1 digital compression: results of the Digital Echo Record Access Study. *J Am Soc Echocardiogr* 1996;**9**:769–78.
10 Warden CN, Bernard PK, Kimball TR. The efficacy and safety of oral pentobarbital sedation in pediatric echocardiography. *J Am Soc Echocardiogr* 2010;**22**:33–7.
11 Lazol JP, DeGroff CG. Minimal sedation second dose strategy with intranasal midazolam in an outpatient pediatric echocardiographic setting. *J Am Soc Echocardiogr* 2009;**22**:383–7.
12 Cooper L, Candiotti K, Gallagher C, et al. A randomized, controlled trial on dexmedetomidine for providing adequate sedation and hemodynamic control for awake, diagnostic transesophageal echocardiography. *J Cardiothorac Vasc Anesth* 2011;**25**: 233–7.
13 Nicholson SC, Montenegro LM, Cohen MS, et al. A comparison of the efficacy and safety of chloral hydrate versus inhaled anesthesia for sedating infants and toddlers for transthoracic echocardiograms. *J Am Soc Echocardiogr* 2010;**23**:38–42.
14 Roach CL, Husain N, Zabinsky J, et al. Moderate sedation for echocardiography of preschoolers. *Pediatr Cardiol* 2010;**31**:469–73.
15 Heistein LC, Ramaciotti C, Scott WA, et al. Chloral hydrate sedation for pediatric echocardiography: physiologic responses, adverse events, and risk factors. *Pediatrics* 2006;**117**:e434–41.
16 Cravero JP, Roback MG. Selection of medications for pediatric procedural sedation outside of the operating room. In: Wiley JF (ed.) UpToDate. Waltham, MA: UpToDate, 2020. https://www.uptodate.com/contents/selection-of-medications-for-pediatric-procedural-sedation-outside-of-the-operating-room/print (accessed December 2020).
17 Stouffer JW, Shirk BJ, Polomano RC. Practice guidelines for music interventions with hospitalized pediatric patients. *J Pediatr Nurs* 2007;**22**:448–56.
18 Walworth DD. Procedural-support music therapy in the healthcare setting: a cost-effectiveness analysis. *J Pediatr Nurs* 2005;**20**:276–84.
19 McGee K. The role of a child life specialist in a pediatric radiology department. *Pediatr Radiol* 2003;**33**:467–74.
20 Etzel-Hardman D, Kapsin K, Jones S, et al. Sedation reduction in a pediatric radiology department. *J Healthc Qual* 2009;**31**:34–9.
21 Lai WW, Geva T, Shirali GS, et al. Guidelines and standards for performance of a pediatric echocardiogram. *J Am Soc Echocardiogr* 2006;**19**:1413–30.
22 Puchalski MD, Liu GK, Miller-Hance WC, et al. Guidelines for performing a comprehensive transesophageal echocardiographic examination in children and all patients with congenital heart disease: recommendations from the American Society of Echocardiography. *J Am Soc Echocardiogr* 2019;**32**(2):173–215.

23 Kanagala P, Bradley C, Hoffman P, et al. Guidelines for transoesophageal echocardiographic probe cleaning and disinfection from the British Society of Echocardiography. *Eur J Echocardiogr* 2011;**12**:17–23.

24 CDC (Centers for Disease Control and Prevention). Guideline for disinfection and sterilization in healthcare facilities (2008). http://www.cdc.gov/infectioncontrol/guidelines/disinfection/ (last accessed December 2020).

25 Rychik J, Ayres N, Cuneo B, et al. American Society of Echocardiography guidelines and standards for performance of the fetal echocardiogram. *J Am Soc Echocardiogr* 2004;**17**:803–10.

26 Silvestry FE, Kerber RE, Brook MM, et al. Echocardiography-guided interventions. *J Am Soc Echocardiogr* 2009;**22**:213–31.

27 Baker PC. Intracardiac echocardiography in congenital heart disease. *J Cardiovasc Trans Res* 2009;**2**:19–23.

28 Schuster P, Chen J, Hoff PI. TEE time? ICE TEE time! IntraCardiac Echocardiography probe used for TransoEsophageal Echocardiography. *Europace* 2010;**12**:1787–8.

29 Hijazi ZM, Shivkumar K, Sahn DJ. Intracardiac echocardiography during interventional and electrophysiological cardiac catheterization. *Circulation* 2009;**119**:587–96.

30 Kliger C, Cruz-Gonzalez I, Ruiz CE. The present and future of intracardiac echocardiography for guiding structural heart disease interventions. *Rev Esp Cardiol* 2012;**65**:791–4.

31 Douglas PS, DeCara JM, Devereux RB, et al. Echocardiographic imaging in clinical trials: American Society of Echocardiography standards for echocardiography core laboratories. *J Am Soc Echocardiogr* 2009;**22**(7):755–65.

32 Cheitlin MD, Alpert JS, Armstrong WF, et al. ACC/AHA Guidelines for the clinical application of echocardiography: a report of the American College of Cardiology/American Heart Association Task Force on Practice Guidelines (Committee on Clinical Application of Echocardiography). *Circulation* 1997;**18**:1686–744.

33 Cheitlin MD, Armstrong WF, Aurigemma GP, et al. ACC/AHA/ASE 2003 Guideline update for the clinical application of echocardiography summary article. *J Am Soc Echocardiogr* 2003;**16**:1091–110.

34 Campbell, RM, Douglas PS, Eidem BW, et al. ACC/AAP/AHA/ASE/HRS/SCAI/SCCT/SCMR/SOPE 2014 Appropriate use criteria for initial transthoracic echocardiography in outpatient pediatric cardiology. *J Am Coll Cardiol* 2014;**64**:2039–60.

35 Lang SM, Bolin E, Daily JA, et al. Appropriateness and diagnostic yield of inpatient pediatric echocardiograms. *Congenit Heart Dis* 2017;**12**:210–17.

36 Rose-Felker K, Kelleman MS, Campbell RM, et al. Appropriateness of outpatient echocardiograms ordered by pediatric cardiologists and other clinicians. *J Pediatr* 2017;**184**:137–42.

37 Sachdeva R, Valente AM, Han BK, et al. ACC/AHA/ASE/HRS/ISACHD/SCAI/SCCT/SCMR/SOPE 2020 Appropriate use criteria for multimodality imaging during the follow-up care of patients with congenital heart disease. *J Am Coll Cardiol* 2020;**75**:657–703.

38 ACPC (Adult Congenital and Pediatric Cardiology). Adult Congenital and Pediatric Quality Network, 2020. https://cvquality.acc.org/initiatives/acpc-quality-network (accessed December 2020).

39 Lai WW, Srivastava S, Cohen MS, Frommelt PC, Allada V. Pediatric echocardiography laboratory organization and clinical productivity. *J Am Soc Echocardiogr* 2013;**26**:1180–6.

40 Srivastava S, Allada V, Younoszai A, et al. Determinants of pediatric echocardiography laboratory productivity: analysis from the Second Survey of the American Society of Echocardiography Committee on Echocardiography Laboratory Productivity. *J Am Soc Echocardiogr* 2016;**29**:1009–15.

41 Soriano BD, Fleishman CE, Van Hoever AM, et al. Determinants of physician, sonographer, and laboratory productivity: analysis of the Third Survey from the American Society of Echocardiography Committee on Pediatric Echocardiography Laboratory Productivity. *J Am Soc Echocardiogr* 2018;**31**:976–82.

CHAPTER 3

Segmental Approach to Congenital Heart Disease

Tal Geva
Boston Children's Hospital; Harvard Medical School, Boston, MA, USA

Introduction

Before the advent of surgical treatment for patients with congenital heart disease (CHD), physicians generally regarded these conditions as hopeless. In 1936, Abbott, who worked at McGill University, published the first systematic classification of CHD based on a study 1000 heart specimens [1]. Two years later in 1938, Gross, who worked at Boston Children's Hospital, performed the first successful cardiovascular operation – ligation of a patent ductus arteriosus in a 7.5-year-old girl [2]. This breakthrough procedure was followed by Blalock and Taussig's landmark establishment of a systemic-to-pulmonary artery shunt to alleviate cyanosis in tetralogy of Fallot [3]; resection of aortic coarctation by Gross and Hufnagel and by Crafoord and Nylin; and the first open heart surgery to close an atrial septal defect by Gibbon in 1953 [4]. These and other landmark advances in the treatment of patients with CHD during the 1940s and 1950s inspired interest in the study of CHD morphology and stimulated the development of several taxonomies for its classification.

The highly variable spectrum of congenital anomalies of the cardiovascular system presents a challenge for those who care for these patients. A comprehensive classification scheme of CHD based on clear and internally consistent nomenclature is, therefore, essential for diagnosis, management, research, and education. The goals of any CHD taxonomy are:

1 To provide a consistent nomenclature based on readily identifiable anatomic-morphologic features of the cardiac chambers.
2 To devise a systematic analytical approach that produces a specific and unique set of diagnoses for each cardiac malformation.
3 To be applicable to all forms of CHD, including cardiac malformations that have not yet been described.
4 To promote understanding and exchange of data among clinicians and researchers.

This chapter describes a segment-by-segment approach, known as the *segmental approach to congenital heart disease*, to the classification and nomenclature of congenital anomalies of the heart and great vessels. Inspired by Lev, Van Praagh and his colleagues originally proposed this classification system in the 1960s and early 1970s [5–7] and have since refined it [8,9]. Importantly, notable modifications and alternative taxonomies have been proposed by pathologists, geneticists, embryologists, cardiologists, cardiovascular surgeons, radiologists, and others [9–22]. In particular, many practitioners favor the nomenclature advocated by Anderson and colleagues [23]. However, despite numerous efforts by individuals and professional groups to advocate the use of a single classification system, none has achieved uniform acceptance. A potentially more successful approach, currently being developed, is to acknowledge the major taxonomies and to create a system that cross-links individual malformations and therapeutic procedures to common codes [24–26]. Although this chapter emphasizes the taxonomy advocated by Van Praagh et al., readers should also familiarize themselves with Anderson's nomenclature and, most importantly, maintain a clear and consistent method of communication within their institutions.

Segmental analysis of congenital heart disease

Analysis of CHD is based upon an understanding of the developmental, morphologic, and segmental anatomy of the heart and great vessels. The cardiac segments are the anatomic and embryologic "building blocks" that form the mammalian heart (Figure 3.1). The three main segments are: (i) veins and atria; (ii) ventricles; and (iii) great arteries. There are two connecting segments between the main segments: (i) the atrioventricular (AV) canal; and (ii) the conus or infundibulum. The AV canal consists of the AV valves (the mitral and tricuspid valves in normally formed hearts) and the atrioventricular septum. The infundibulum (or conus) is the connecting segment between the ventricles and the great arteries. In normally formed hearts, the infundibulum consists of a circumferential subpulmonary myocardium shaped like a prolate cone (as viewed externally; hence conus) or a funnel (as viewed internally; hence infundibulum). The normal subpulmonary infundibular myocardium separates the pulmonary and tricuspid valves. The normal subaortic

Echocardiography in Pediatric and Congenital Heart Disease: From Fetus to Adult, Third Edition. Edited by Wyman W. Lai, Luc L. Mertens, Meryl S. Cohen and Tal Geva.

Companion website: www.wiley.com/go/lai-echo3

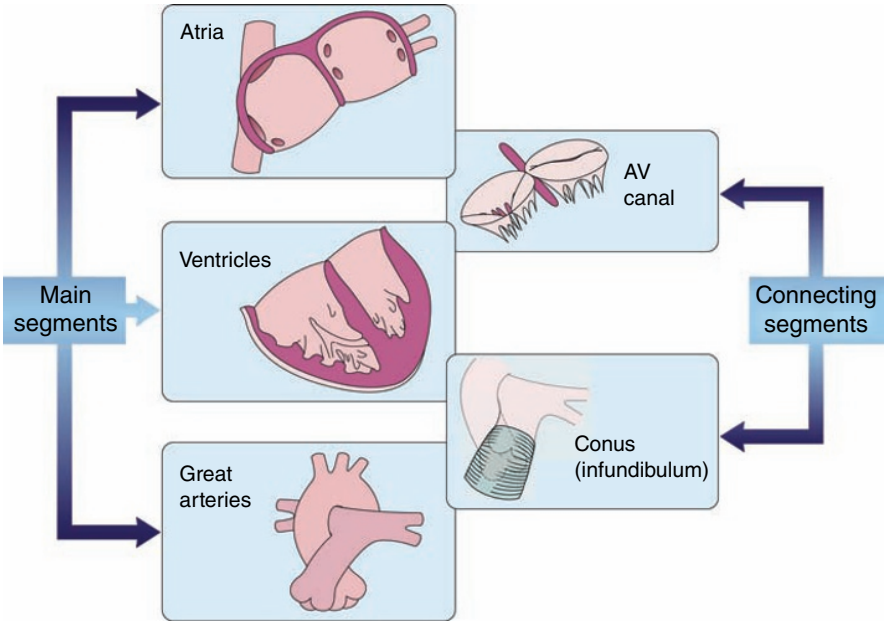

Figure 3.1 Anatomic segments of the heart. The three main cardiac segments are the atria, ventricles, and great arteries. There are two connecting segments: the atrioventricular (AV) canal (including the AV valves, the interatrial and interventricular components of the AV canal septum), and the conus (or infundibulum). The connecting segments may be viewed as multidirectional joints between the main cardiac segments allowing infinite possibilities of AV and ventriculoarterial alignments. In the segmental approach to congenital heart disease it is essential that each cardiac segment is analyzed separately and independently of adjacent segments.

infundibulum consists mostly of a conal septum (the myocardium that separates the left and right ventricular outflow tracts). The posterior aspect of the subaortic infundibular free wall is normally absent, resulting in fibrous continuity between the left and noncoronary aortic valve leaflets and the anterior leaflet of the mitral valve.

The fundamental principle of segmental analysis of CHD is to analyze each of the aforementioned components of the heart in a sequential step-by-step fashion. First, the anatomic pattern (i.e., situs) of the abdominal and thoracic organs is defined and the position of the heart is described. Then, each of the main cardiac segments is examined, described, and assigned a designation based upon its unique morphologic features, independent of its neighboring segments (Figure 3.2). For example, each ventricle is defined according to its intrinsic morphology and not by the entering AV valve or the exiting great artery. Analysis of the main cardiac chambers – veins and atria, ventricles, and great arteries – involves two steps. First, the *identity* of the chamber or great vessel is determined based upon its morphology and intrinsic myocardial architecture. Second, the *situs* of the cardiac segment is determined. In the case of the atria, their situs may be solitus (normal), inversus (mirror image of solitus), or ambiguous (indeterminate, or lacking unique anatomic features that identify the atria). Once the three main cardiac segments are characterized according to their unique morphologic features, the connecting segments are evaluated and defined. Finally, a complete set of diagnoses is formulated by combining the five cardiac segments and all associated cardiovascular anomalies as described in the following section.

Step-by-step segmental analysis

The following 10 steps are taken as part of the segmental analysis of CHD.

Thoracoabdominal situs

Before analyzing intracardiac anatomy, the situs of the thoracic and abdominal organs is determined to provide an "anatomic framework" for further analysis (Figure 3.3). Normally, the visceral organs are "lateralized." In other words, the pattern of anatomic organization of the abdominal organs, tracheobronchial tree, and lungs is asymmetric. In *situs solitus* (normal arrangement), the spleen, pancreas, stomach, and sigmoid colon are left-sided, and the liver, cecum, and appendix are right-sided. The left lung comprises two lobes and the left mainstem bronchus is longer, more horizontal, and hyparterial (courses inferior to the left pulmonary artery) (Figure 3.4). The right lung comprises three lobes and the right mainstem bronchus is shorter and eparterial (courses posterior to the right pulmonary artery). In visceral *situs inversus*, the spatial organization of the abdominal and thoracic organs is the mirror image of normal. In other words, there is complete left–right reversal of the position and orientation of the organs. It is worth noting that in visceral situs inversus the pattern of anatomic

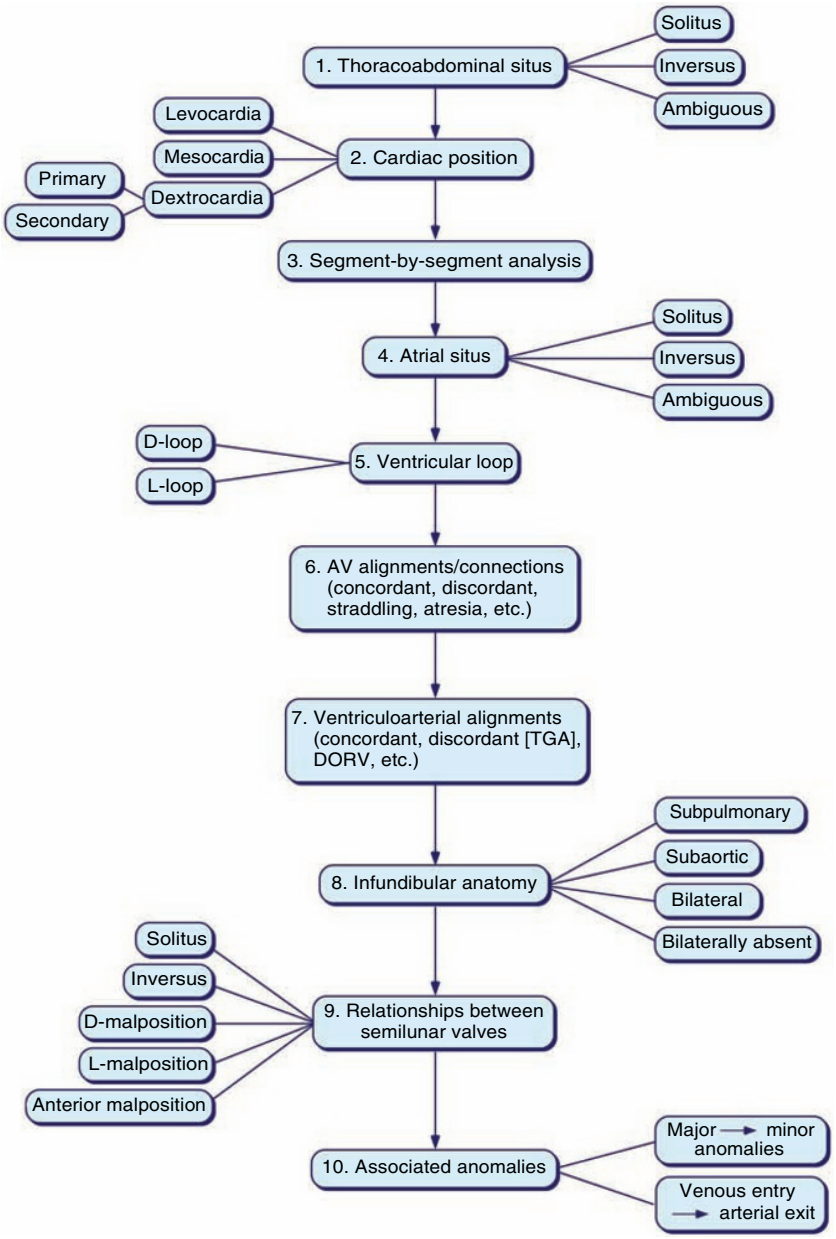

Figure 3.2 The 10 steps of the segmental approach to the diagnosis of congenital heart disease. Before analyzing intracardiac anatomy, the situs of the thoracic and abdominal organs and cardiac position within the thorax are determined to provide an "anatomic framework" for further analysis (steps 1 and 2). When describing cardiac anatomy, the three following principles apply. (i) Each cardiac segment must be described in terms of its own unique anatomic features and not according to those of adjacent segments (steps 3–9). For example, the left ventricle is determined according to its internal morphology, particularly its smooth superior septal surface, and not according to the AV valve that connects it with the atria (usually it is the mitral valve but it may be both mitral and tricuspid valves, as in a double-inlet left ventricle, or it may be a common AV valve or even a tricuspid valve). (ii) For each cardiac segment, both its situs and connections must be described specifically and not inferred from each other. (iii) Associated malformations (step 10) may be described in order of their hemodynamic importance or in an anatomic order (progressing from the venous entry to the arterial exit of the heart). DORV, double-outlet right ventricle; TGA, transposition of the great arteries.

organization is asymmetric, similar to situs solitus but in mirror image. Ciliary disorders are often associated with situs inversus. In *situs ambiguous*, the spatial position and orientation of the abdominal and thoracic organs are abnormally symmetric and inconsistent. For example, the spleen may be absent, the liver is often midline, both lungs may have two or three lobes, and the bronchi may be similar to each other in length and orientation. Situs ambiguous is typically associated with heterotaxy syndrome, a condition characterized by partial or complete lack of lateralization of the visceral organs leading to an abnormal degree of symmetry, anomalies of the spleen (e.g., polysplenia, asplenia), CHD, and extracardiac anomalies [27–29]. In many patients with heterotaxy syndrome, visceral situs cannot be clearly designated as solitus or inversus, hence the term *situs ambiguous* is used. However, the anatomic organization of the visceral organs in these patients is often partially lateralized, allowing for determination of a "predominant situs." For example, when the stomach is right-sided and the inferior vena cava is left-sided, the predominant abdominal situs is inversus even though the liver may be midline.

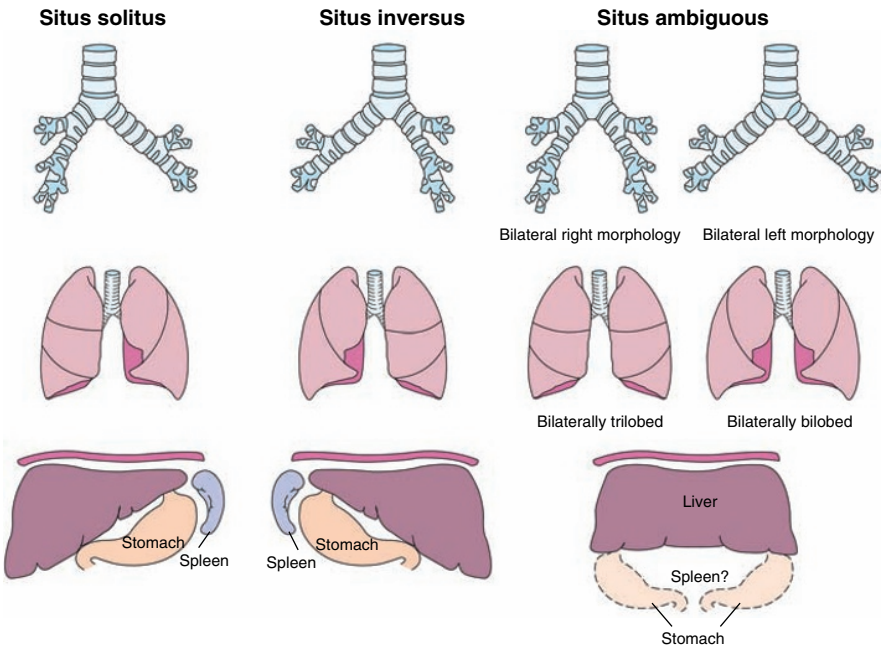

Figure 3.3 Thoracoabdominal situs. **(Top)** Morphology of the tracheobronchial tree. In situs solitus, the right mainstem bronchus is short and eparterial (its branch for the right upper lobe is over the second branch of the right pulmonary artery) and the left mainstem bronchus is longer and hyparterial (it courses underneath the left pulmonary artery). In situs inversus, there is mirror imaging of the anatomy seen in situs solitus. In situs ambiguous, the bronchi can have a bilaterally right or bilaterally left morphology. Bilaterally hyparterial left bronchial morphology is often seen in patients with heterotaxy syndrome and polysplenia, whereas bilaterally eparterial right bronchial morphology is often seen in patients with heterotaxy syndrome and asplenia. **(Middle)** Lung lobation. A bilobed left lung and a trilobed right lung are typical in situs solitus. In situs inversus, the right lung is bilobed and the left lung is trilobed. As with the tracheobronchial tree, in situs ambiguous the lungs may be bilaterally bilobed or bilaterally trilobed. **(Bottom)** In visceral situs solitus the liver is right-sided and the stomach and spleen are left-sided. Incomplete lateralization of the abdominal organs with a midline liver and stomach may be seen in patients with heterotaxy syndrome. Splenic anomalies (asplenia, polysplenia, hyposplenia, and a single right-sided spleen) and complex cardiac anomalies are frequent. In patients with heterotaxy syndrome and visceral situs ambiguous, the disposition of the abdominal situs predicts atrial situs less reliably then bronchial anatomy.

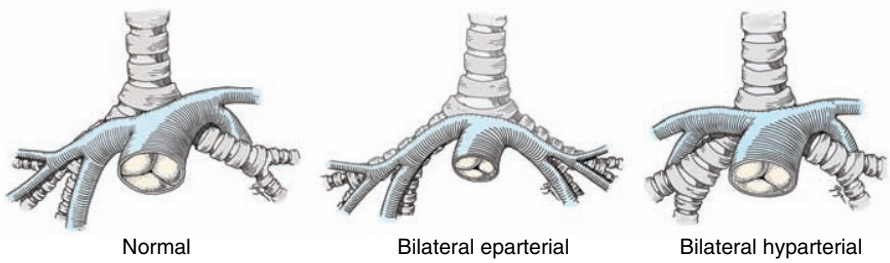

Figure 3.4 Relationships between the mainstem bronchi and the pulmonary arteries. In normal anatomy, the right pulmonary artery courses anterior to the right mainstem bronchus (the bronchus is said to be eparterial) and left pulmonary artery courses over the left mainstem bronchus (the bronchus is said to be hyparterial). In the majority of patients with asplenia syndrome both mainstem bronchi are eparterial and in most patients with polysplenia syndrome both mainstem bronchi are hyparterial.

Cardiac position

The position of the heart within the thorax can be described as levocardia, mesocardia, or dextrocardia (Figure 3.5). This designation is based on the spatial location of the majority of the cardiac mass relative to a sagittal plane that crosses the thoracic midline from the sternum to the spine. In addition, the orientation of the long axis of the heart (the orientation of the axis connecting the AV junction and the ventricular apex) should be described. Although the position of the heart within the thorax and the orientation of the base-to-apex axis are often

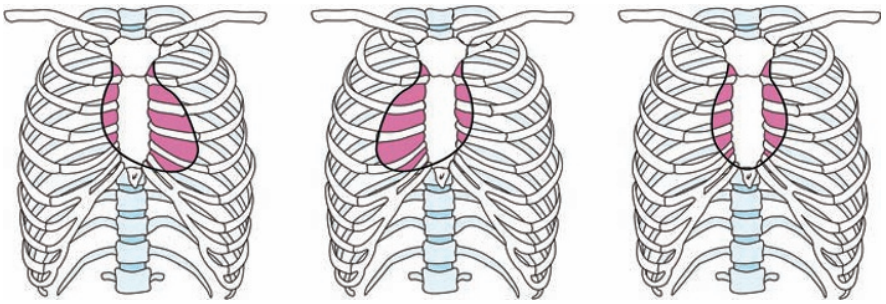

Figure 3.5 Cardiac position within the thorax. In levocardia, the heart is predominantly in the left hemithorax. In dextrocardia, the heart is predominantly in the right hemithorax. In mesocardia, the heart is midline and the apex typically points anteriorly or inferiorly. The orientation of the apex should be explicitly described because the position of the heart within the thorax and the orientation of the apex may not be concordant (e.g., dextrocardia with a leftward pointing apex).

concordant (e.g., levocardia and a leftward pointing apex), occasional exceptions occur (e.g., dextrocardia and a leftward pointing apex).

In levocardia, the heart is positioned predominantly in the left hemithorax. In dextrocardia, the heart is predominantly in the right hemithorax. In mesocardia, the heart is midline with approximately equal proportions of the cardiac mass on each side of the sternum. The base-to-apex axis in mesocardia is usually oriented anteriorly or sometimes inferiorly. The terms *primary* and *secondary* dextrocardia are used to distinguish between cardiac malposition related primarily to cardiac anomalies and secondary to noncardiac anomalies. *Primary dextrocardia* is defined as a condition in which the heart is in the right hemithorax in association with a structural congenital heart defect. In primary dextrocardia the apex usually points to the right. *Secondary dextrocardia* is a condition in which the heart is either "pushed" or "pulled" toward the right hemithorax due to extracardiac abnormalities. Examples of circumstances where the heart is "pushed" to the right hemithorax include left-sided tension pneumothorax, left congenital lobar emphysema, and left-sided diaphragmatic hernia. Conditions where the heart is pulled toward the right hemithorax include hypoplasia or agenesis of the right lung. In secondary dextrocardia the cardiac apex may point to the left or anteriorly. Leftward malposition of the heart occurs in patients with right diaphragmatic hernia or hypoplasia or agenesis of the left lung. In the latter condition, the heart is displaced toward the left superior hemithorax and the base-to-apex orientation points toward the left axilla.

In addition to malposition of the heart within the thorax, the heart can rarely be partially or completely exteriorized, a condition termed *ectopia cordis*. The extent of the midline defect allows the heart to be partially or completely outside the thoracic cavity varies. A known association of anomalies, of which ectopia cordis is a component, is termed *pentalogy of Cantrell*. This group of defects includes: deficiency of the anterior diaphragm; a midline supraumbilical abdominal wall defect; a defect in the diaphragmatic pericardium; congenital cardiac abnormalities; and a defect of the lower sternum [30].

Segment-by-segment analysis of cardiac anatomy

At this stage of the segmental analysis, the three main segments and the two connecting segments are analyzed individually (steps 4–9 in Figure 3.2).

Atrial situs

The first step in determining atrial situs is to identify the atria according to their morphologic characteristics (Table 3.1, Figure 3.6). The atria are not designated based on systemic and/or pulmonary venous connections because these can be variable. Instead, the atria are defined by their intrinsic anatomy. The right atrial myocardium includes the crista terminalis and tinea sagittalis (Figure 3.6a). The septal surface of the right atrium features the superior and inferior limbic bands of the fossa ovale. The right atrial appendage is typically broad-based, it has a triangular shape, and its position is anterior relative to the left atrial appendage. The pectinate muscles of the right atrial appendage extend toward the AV valve annulus and the Eustachian valve. The left atrium is characterized by an elongated, narrow appendage (Figure 3.6b). The left atrial appendage is located posterior relative to the right atrial appendage. In contrast to the right atrial appendage, the pectinate muscles of the left atrium are confined to the appendage. The left atrial septal surface features the septum primum (the valve of the foramen ovale).

In atrial situs solitus (Figure 3.7), the right atrium is right-sided whereas in atrial situs inversus it is left-sided. In individuals with normal anatomy, the right atrium receives the right and left horns of the sinus venosus, including the superior vena cava, inferior vena cava, and the orifice of the coronary sinus (the cardiac termination of the left horn of the sinus venosus). The left atrium normally receives the pulmonary veins. In atrial situs ambiguous, typically seen in patients with heterotaxy syndrome, the anatomic landmarks characteristic of the right and left atria are not sufficient to determine situs (either situs solitus

Table 3.1 Morphologic criteria for the identification of the right atrium and left atrium

	Right atrium	Left atrium
Myocardial features	Crista terminalis, tinea sagittalis, extension of pectinate muscles toward AV valve	Pectinate muscles confined to appendage*
Appendage	Broad base, triangular, anterior	Long and narrow (finger-like), posterior
Septum	Septum secundum (limbus of the fossa ovale)	Septum primum (valve of the foramen ovale)
Veins	Receives the right and left terminations of the sinus venosus: IVC†, SVC‡, CS§	Normally receives all pulmonary veins¶

*When a persistent left superior vena cava (LSVC) drains directly into the left atrium (LA) a muscle bar similar to a crista terminalis may be present in the LSVC–LA junction.
†In cases with interrupted IVC, the right atrium receives the CS.
‡The SVC is not a reliable marker of the right atrium because a persistent left superior vena cava may drain directly into the left atrium [39].
§When the coronary sinus is unroofed, the drainage site of the IVC may incorrectly identify the right atrium. In such circumstance, drainage of the IVC to the unroofed coronary sinus creates the appearance of an IVC to left atrium connection. When the CS is unroofed and the IVC is interrupted, the shape, size, and location of the atrial appendages may be used for identification of atrial situs.
¶The pulmonary veins are not a reliable marker of the left atrium due to their potential for variable connections.
CS, coronary sinus; IVC, inferior vena cava; SVC, superior vena cava.

or situs inversus). Variations of anatomy may include a common atrium with an absence (or presence of only remnants) of the atrial septum, interruption of the inferior vena cava between the renal and hepatic segments, bilateral superior venae cavae, and an unroofed or absent coronary sinus. The atrial appendages can be similar to each other; however, in most cases of heterotaxy syndrome the atrial appendages are not identical (i.e., they are not "isomeric"). Although the distribution of the pectinate muscles has been proposed as a useful marker of atrial identity [31], imaging of the pectinate muscle in living patients has not been consistently achieved.

Ventricular loop

The first step in determining the ventricular loop (situs) is to identify the left and right ventricles. It is important to recognize that between the AV and semilunar valves (what is generally considered the ventricular mass of the heart) there are three distinct chambers: the left ventricle, the right ventricular sinus, and the infundibulum (or conus) [6,7,32,33]. The normal right ventricle comprises two distinct chambers, which are well incorporated into each other: the right ventricular sinus and the infundibulum. Externally, the normal right ventricle is triangular in shape and the diaphragmatic (inferior) wall makes an acute angle with the anterior wall. Internally, the normal right ventricle is characterized by septal attachments of the tricuspid valve, coarse trabeculations, and a distinct septal surface that includes the septal and moderator bands (Figure 3.8a). The infundibulum is normally well incorporated with the right ventricular sinus, such that their separate identities may be obscured (Figure 3.8). However, these chambers have different embryologic and developmental origins. Moreover, in several congenital cardiac anomalies the infundibulum is either poorly incorporated with the right ventricular sinus (e.g., double-chambered right ventricle [34]) or is completely dissociated from the right ventricular sinus and completely associated with the left ventricle (e.g., anatomically corrected malposition of the great arteries and transposition of the great arteries with posterior aorta [32,35]).

The anatomic features of the normal left ventricle are illustrated in Figure 3.9. Externally, the shape of the normal left ventricle approximates that of a cone. Internally, the myocardial architecture exhibits fine apical trabeculations, and attachments of the mitral valve to two distinct papillary muscles that attach to the left ventricular free wall without attachments to the interventricular septum. The aortic valve is in fibrous continuity with the mitral valve due to the absence of an intervening conal musculature in this region. It is important to recognize, however, that variations in anatomy and physiology can greatly alter left ventricular morphology, and many of the morphologic characteristics of the normal left ventricle can be altered. For example, in a markedly hypertrophied left ventricle, or in a double- or common-inlet left ventricle, the apical trabeculations may be prominently hypertrophied, similar to the trabeculations of the right ventricle. Also, the normal attachments of the mitral valve to the left ventricular free wall papillary muscles are usually altered in common AV canal defects, a straddling mitral valve, and other malformations. Therefore, the most reliable morphologic feature of the left ventricle is its smooth superior septal surface.

Once ventricular identity has been established based on morphologic criteria, the type of ventricular loop can be determined (Figure 3.10). The type of ventricular loop is clinically relevant in that it determines the pattern of coronary artery distribution, the disposition of the conduction system, and the internal organization of the ventricular myocardium. Furthermore, a L- (or levo-) ventricular loop is associated with increased risks of AV block (either congenital or acquired), Ebstein-like malformation of the left-sided tricuspid valve, and hypoplasia of the left-sided right ventricular sinus. Because the spatial position of the ventricles varies widely, a right–left location relative to each other cannot be used reliably to determine the ventricular

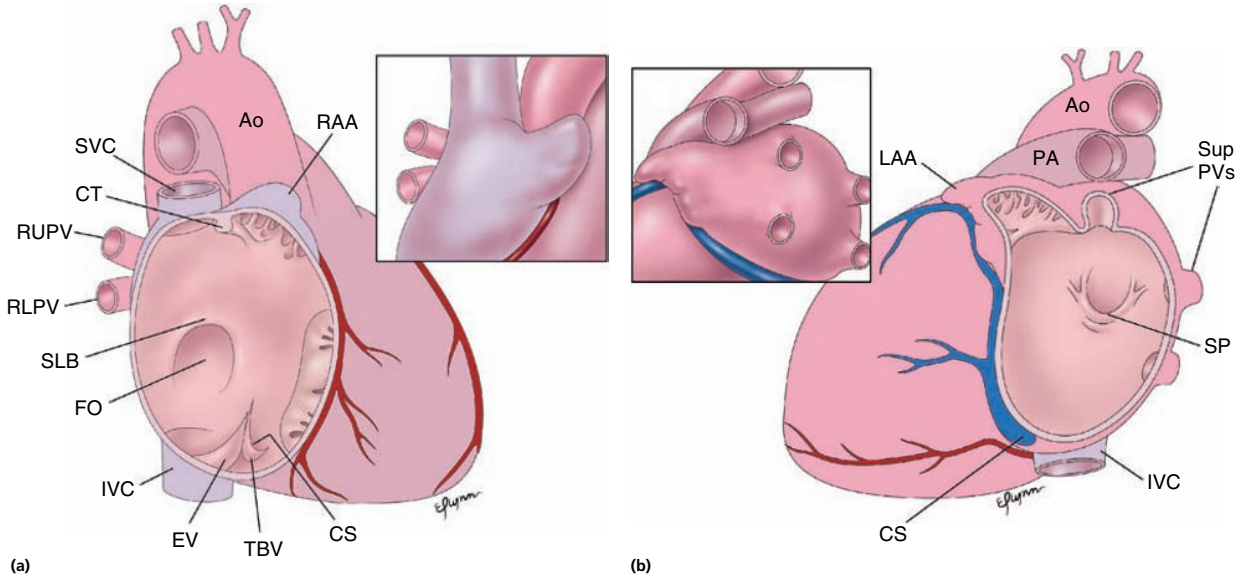

Figure 3.6 Atrial morphology. **(a)** Right atrial morphology: The right atrium (RA) can be divided into three components. (i) The *sinus venosus*, including the orifices of the inferior vena cava (IVC), superior vena cava (SVC), and coronary sinus (CS), is characterized by its smooth surface (absence of muscular trabeculations). The sinus venosus is partially separated from the other components of the RA by remnants of the embryonic right venous valve system, which includes the Thebesian valve (TBV) of the CS and the Eustachian valve (EV) of the IVC. (ii) The *right atrial appendage* is characterized by a broad-based triangular shape and coarse trabeculations (pectinate muscle). The crista terminalis (CT) is a prominent muscle bar that separates the sinus venosus component of the RA from the trabeculated right atrial appendage and is the site of the sinoatrial node. (iii) The *interatrial portion of the atrioventricular (AV) canal* includes the base of the atrial septum and the tricuspid valve annulus. The fossa ovalis (FO) forms the right atrial side of the interatrial septum and is characterized by an oval-shaped muscular boundary (termed *septum secundum* or *limbus of the fossa ovalis*) whereas the floor of the fossa is covered by septum primum. **(b)** Left atrial morphology. Similar to the RA, the left atrium can also be divided into three components: (i) a pulmonary venous component; (ii) a left atrial appendage (LAA), which is narrow-based and elongated; and (iii) the AV canal region, which is bordered distally by the mitral valve annulus. Note the attachments of septum primum (SP) are located on the left atrial septal surface. Ao, aorta; PA, pulmonary artery; RLPV, right lower pulmonary vein; RUPV, right upper pulmonary vein; SLB, superior limbic band of fossa ovale; Sup PVs, superior pulmonary veins.

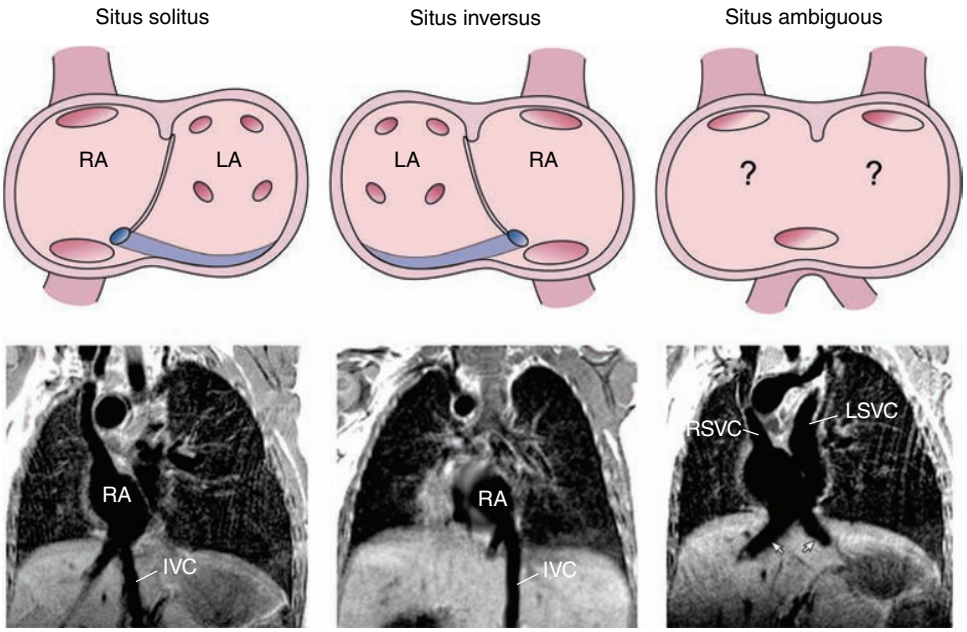

Figure 3.7 Visceral and atrial situs. **(Top)** In *atrial situs solitus*, the right-sided right atrium (RA) receives the major horn of the sinus venosus, including the superior vena cava, inferior vena cava, and the orifice of the coronary sinus. The left-sided left atrium (LA) normally receives the pulmonary veins, its septum features septum primum (the flap valve of the foramen ovale) and a narrow-based, elongated, and posterior appendage (Table 3.1). In *atrial situs inversus*, the right atrium is left-sided and the left atrium is right-sided. In *atrial situs ambiguous*, typically seen in patients with heterotaxy syndrome, the anatomic landmarks characteristics of the right and left atria are not sufficient to determine situs (either situs solitus or situs inversus). Often in this situation, the atria are in common with an absence (or presence of only remnants) of the atrial septum, the inferior vena cava may be interrupted between the renal and hepatic segments, there may be bilateral superior venae cavae, and the coronary sinus may be unroofed or absent. The atrial appendages may be quite similar to each other. **(Bottom)** Coronal plane spin echo magnetic resonance imaging (MRI) in patients with heterotaxy syndrome and atrial situs solitus (left panel), atrial situs inversus (central panel), and atrial situs ambiguous (right panel). IVC, inferior vena cava; LSVC, left superior vena cava; RSVC, right superior vena cava.

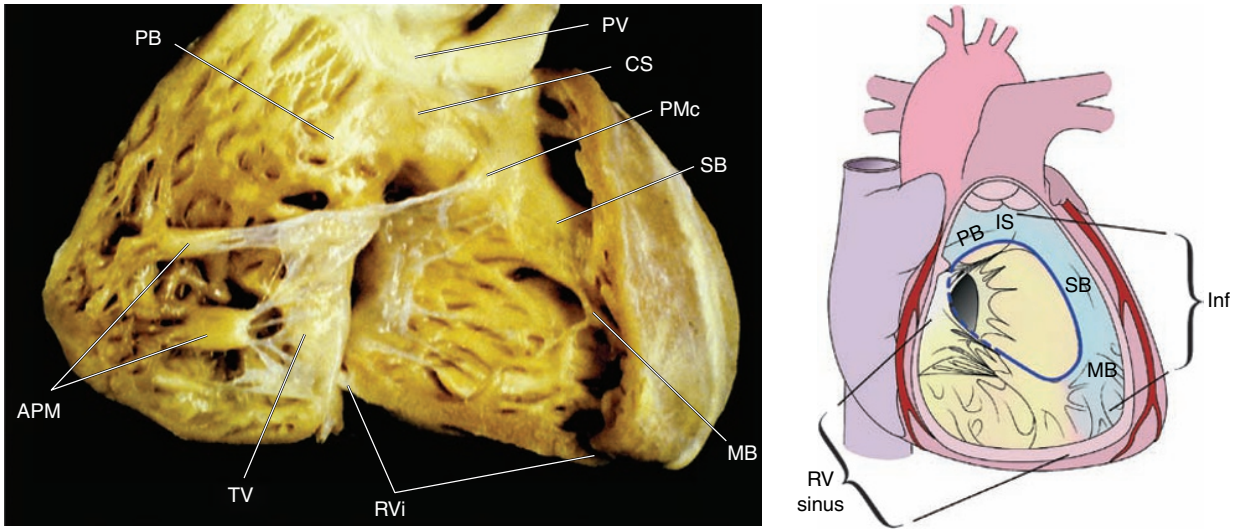

Figure 3.8 Right ventricular (RV) morphology. **(a)** Anatomic specimen showing normal RV morphology. Note the coarse trabeculations and the chordal attachments of the tricuspid valve (TV) to the trabeculated septal surface. **(b)** The normal right ventricle comprises two distinct chambers, which are well incorporated into each other: the RV sinus and the infundibulum (Inf). The boundary between the RV sinus and the infundibulum is termed the *proximal os infundibulum* (shown as a dark blue ring) and comprises the parietal band (PB), infundibular septum (IS), septal band (SB), moderator band (MB), and the anterior papillary muscle of the tricuspid valve (APM). The RV sinus may be subdivided into two parts: (i) an atrioventricular canal portion (underneath the septal leaflet of the tricuspid valve); and (ii) the trabecular portion, which extends to the RV apex. The infundibulum may be similarly subdivided into two components: (i) a distal (subpulmonary) segment, which includes the distal portion of the SB, the IS, and the PB; and (ii) the proximal infundibulum, which is typically trabeculated and has its own apex located anterior to the RV sinus apex. CS, conal septum; PMc, papillary muscle of the conus; PV, pulmonary vein; RVi, right ventricular inflow (sinus).

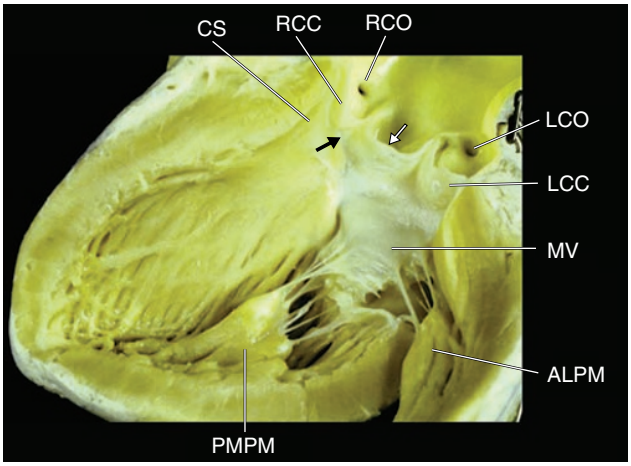

Figure 3.9 Left ventricular morphology. The most reliable morphologic feature of the left ventricle is its smooth superior septal surface. In the normal left ventricle, the finely trabeculated apex (trabeculae carneae) are quite characteristic. However, in a markedly hypertrophied left ventricle, or in double- or common-inlet left ventricle, the apical trabeculations may be prominently hypertrophied (similar to the trabeculations seen in the right ventricle). In the normal left ventricle, the mitral valve (MV) attaches to two large groups of papillary muscles, which attach to the left ventricular free wall. The aortic valve is in fibrous continuity with the MV due to the absence of an intervening conal musculature in this region. More anteriorly, under the right coronary cusp of the aortic valve, the conal musculature comprises the infundibular septum (CS). The black arrow denotes the location of the membranous septum under the right noncoronary commissure. The white arrow denotes the noncoronary cusp of the aortic valve. ALPM, anterolateral papillary muscle; LCC, left coronary cusp, LCO, left coronary orifice; PMPM, posteromedial papillary muscle; RCC, right coronary cusp; RCO, right coronary orifice.

loop [36,37]. Instead, the principle of *chirality* is used. This method can be applied regardless of the spatial position of the ventricles and requires only the identification of the inflow, outflow, and septal surface of one of the ventricles (Figure 3.10). The only circumstance where the type of ventricular loop cannot be reliably determined is in an anatomically single right ventricle without a recognizable left ventricle or an interventricular septum.

Atrioventricular alignments and connections

Once the identity and situs of the atria and the ventricles have been established, attention is then focused on the first connecting segment, the AV canal. Figure 3.11 illustrates several representative types of AV alignments and connections. However, it is important to recognize that these examples are only samples of an anatomic continuum. Although the morphology of the AV valve generally follows the type of ventricle which it enters, exceptions are not rare (e.g., AV canal, double-inlet ventricle, and straddling AV valve).

Ventriculoarterial alignments

Next, the outflow of the heart is examined to determine from which cardiac chamber each great artery originates. Ventriculoarterial alignment describes how the semilunar valves and their respective great vessels align with the underlying ventricles. Figure 3.12 illustrates several representative types of ventriculoarterial alignments. However, as with AV

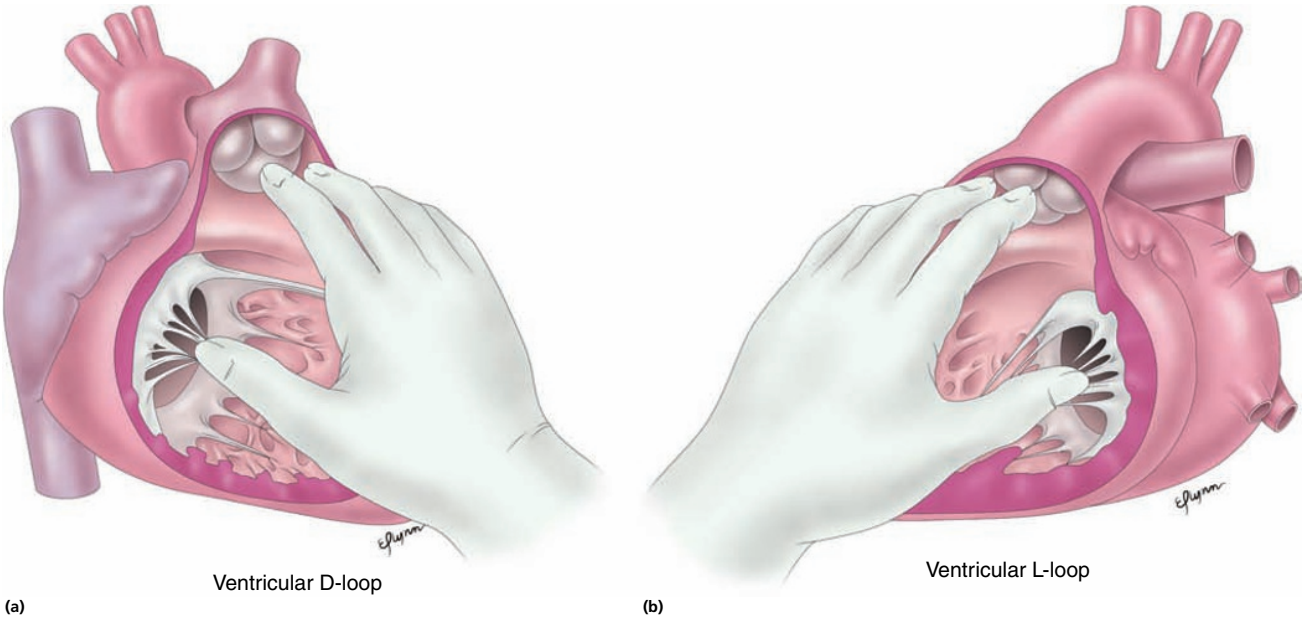

Figure 3.10 Determination of ventricular situs. **(a)** In a ventricular D-loop the palmar aspect of the right hand is placed over the right ventricular septal surface with the thumb in the tricuspid valve, the fingers in the right ventricular outflow, and the dorsum of the right hand facing the right ventricular free wall. **(b)** In a ventricular L-loop the palmar aspect of the left hand faces the right ventricular septal surface with the thumb in the tricuspid valve (or inflow), the fingers in the right ventricular outflow, and the dorsum of the left hand facing the right ventricular free wall. Using this principal, ventricular situs can be determined regardless of ventricular position in the chest. The same principle also applies to the left ventricle. When using the left ventricle, a right-handed left ventricle will be L-looped and a left-handed left ventricle will be D-looped.

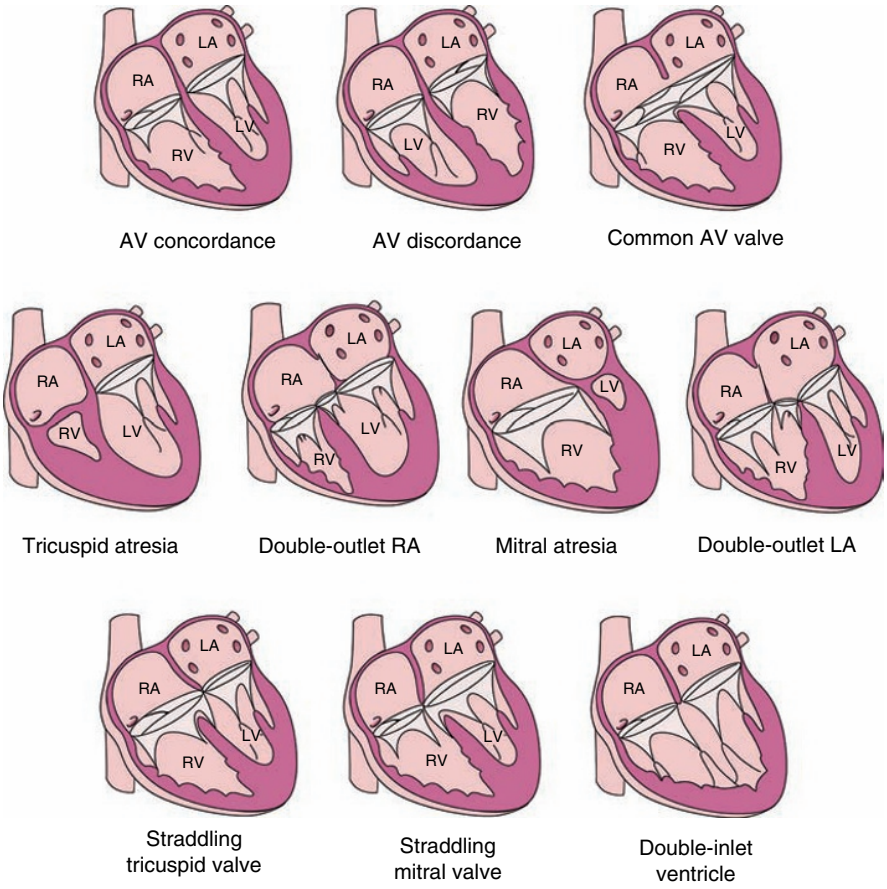

Figure 3.11 Diagram illustrating some of the possible atrioventricular (AV) alignments and connections. This step in the segmental approach to congenital heart disease follows identification of atrial and ventricular morphology and situs. LA, left atrium; LV, left ventricle; RA, right atrium; RV, right ventricle.

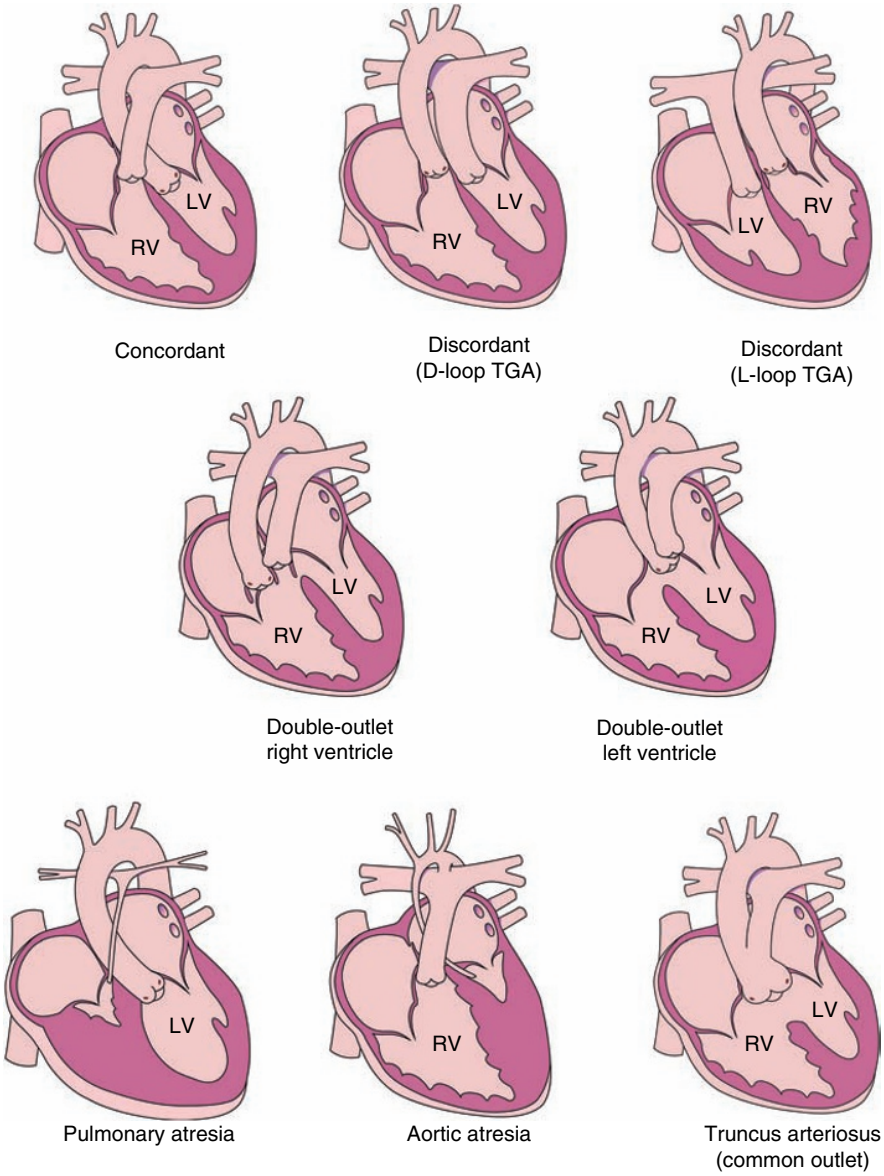

Figure 3.12 Diagram illustrating some of the possible ventriculoarterial alignments and connections. Note that the type of ventriculoarterial alignment is determined by which great artery arises entirely or predominantly from which ventricle. It is clinically impractical to accurately and reproducibly determine the great arterial origin from either ventricle in terms of percent origin. Specifically, the so-called "50% rule" is not applicable in vivo;. This is due to complex 3D relations between the ventricles and the great arteries, the complex geometric nature of the ventricular septum, and cardiac motion in systole and diastole and with respiration. LV, left ventricle; RV, right ventricle; TGA, transposition of the great arteries.

alignments, it is important to recognize that the spectrum of possible alignments between the great arteries and the underlying ventricles is a continuum and sometimes difficult to determine. Classification of ventriculoarterial alignment into discrete groups requires drawing sharp borders within transition zones, which inevitably leaves certain anatomic variations straddling some categories. The preferred approach is to assign a great vessel to an underlying ventricle when it completely or nearly completely relates to that chamber. In cases where a semilunar valve significantly overrides the ventricular septum, the preferred approach is to describe the anatomy (e.g., right ventricular origin of the aorta and biventricular origin of the main pulmonary artery). Specifically, the so-called "50% rule" is not practicably applicable in vivo; due to complex 3D relations between the ventricles and the great arteries, the curved geometry of the ventricular septum, and rotational and translational cardiac motion. It is important to note that determination of ventriculoarterial alignment is based on the spatial relationships between the semilunar valves and the underlying ventricles and is not based on the type of infundibulum present (see next section).

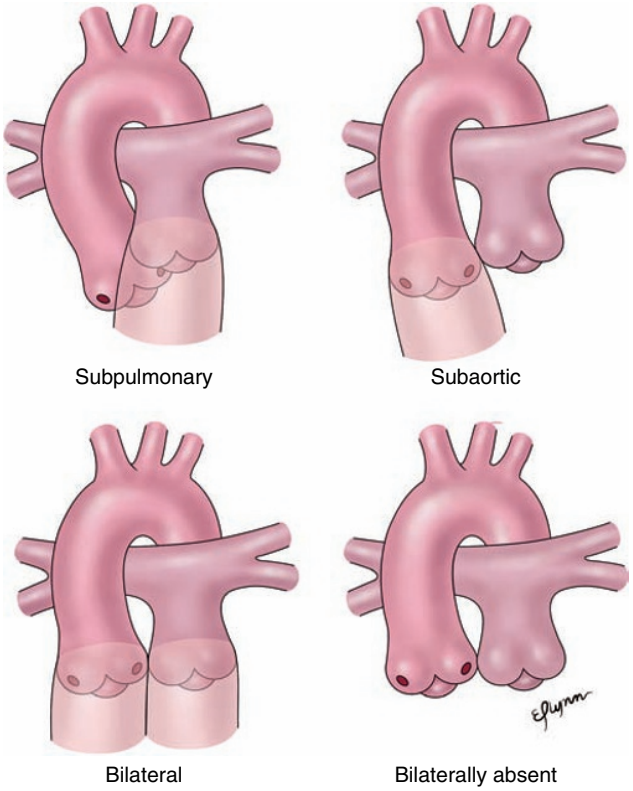

Figure 3.13 Type of infundibulum (conus). In general, there are four types of infundibulum: (i) *subpulmonary* with an absence of the subaortic infundibular free wall (found in the normal heart); (ii) *subaortic* with an absence of the subpulmonary infundibular free wall (often found in transposition of the great arteries); (iii) *bilateral conus* (commonly found in patients with double-outlet right ventricle, but can be rarely found in patients with transposition of the great arteries and even in patients with normally related great arteries); and (iv) *bilaterally absent* (found in some patients with double-outlet left ventricle).

Type of infundibulum (conus)

The infundibulum is the connecting segment between the ventricles and the great arteries (Figure 3.13). In normal anatomy, there is a complete *subpulmonary conus* with muscular separation between the pulmonary and the AV valves (see Figure 3.8), whereas the subaortic conus is incomplete, allowing fibrous continuity between the left and noncoronary cusps of the aortic valve and the anterior leaflet of the mitral valve (see Figure 3.9). Part of the subaortic conus is normally present in the form of a conal septum represented by the myocardium that separates the anterolateral aspect of the left ventricular outflow (the myocardium under the right coronary cusp of the aortic valve) and the right ventricular outflow tract. In some patients, there is an increased distance between the left coronary cusp and the anterior mitral leaflet due to elongation of the intervalvular fibrosa. In this circumstance, the aortic and mitral valves are said to have fibrous contiguity as opposed to fibrous continuity.

Normal conal anatomy is termed *subpulmonary conus* indicating the presence of a complete subpulmonary infundibular myocardium and partial absence of the subaortic infundibular free wall. Abnormal conal anatomy includes complete subaortic conus, bilateral conus, and bilaterally absent conus. A *subaortic conus* is present when the aortic valve is entirely supported by infundibular myocardium completely separating it from the AV valve(s). The subpulmonary conus is incomplete with an absence of infundibular myocardium between the pulmonary and AV valve(s). A subaortic conus is often found in transposition of the great arteries. However, it is important to recognize that: (i) transposition of the great arteries is a specific type of ventriculoarterial alignment (which great artery originates from which ventricle?) and is not defined by the type of conus; and (ii) any type of conus may be present in transposition of the great arteries or in any other type of ventriculoarterial alignment (other than normal) [38].

Bilateral conus is present when both semilunar valves are completely separated from the AV valve(s) by infundibular myocardium. Although a bilateral conus is commonly associated with a double-outlet right ventricle, it is important to recognize that, similar to transposition: (i) a double-outlet right ventricle is a specific type of ventriculoarterial alignment (which great artery originates from which ventricle?) and is not defined by the type of conus; and (ii) any type of conus may be present in a double-outlet right ventricle.

Bilaterally absent conus is the least common type of infundibular anatomy. It is present when both semilunar valves are in direct fibrous continuity with the AV valve(s) and in direct fibrous continuity with each other as a result of the absence of infundibular myocardium. It is the rarest type of conal anatomy and most commonly seen in double-outlet left ventricle.

Relationship between semilunar valves

This step in the segmental approach to CHD describes the spatial relationships between the aortic and pulmonary valves (Figure 3.14). Although the spatial relationships between the

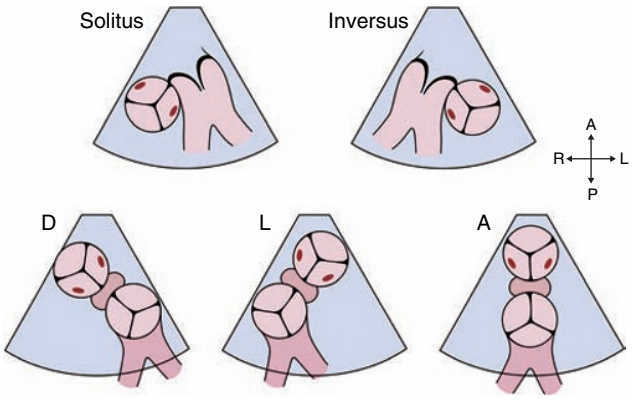

Figure 3.14 Relationships between semilunar valves. The diagram illustrates several common interrelations between the semilunar valves as seen by a transthoracic echocardiographic parasternal short-axis view. It must be recognized, however, that the interrelations between the semilunar valves form an anatomic continuum. A, anterior; D, dextro (rightward); L, levo (leftward).

semilunar valves are often associated with predictable patterns of ventriculoarterial alignments, there are many exceptions to these rules. Moreover, it is important to recognize that the designation of "D" and "L" to describe the spatial relationships between the semilunar valves does not provide information regarding the anterior–posterior and the superior–inferior orientations. Therefore, it is important to provide this additional information as part of comprehensive description of the anatomy.

Associated anomalies

Once the three main cardiac segments and the two connecting segments have been evaluated and categorized, all associated cardiovascular anomalies are systematically examined and described. To provide a logical and consistent description of all associated anomalies, they can either be described in order of their hemodynamic importance (from major to minor anomalies) or in an anatomic order (progressing from the venous entry to the arterial exit of the heart) (see Figure 3.2).

Conclusion

The segmental approach to anatomic analysis of CHD allows accurate description of all known forms of cardiac anomalies and can be applied to patients of all ages using diagnostic imaging modalities such as echocardiography, angiography, computed tomography, and magnetic resonance imaging. In rare circumstances when the morphology does not conform to a clearly defined diagnostic category, it is essential to provide an accurate, detailed description of the anatomy using tools provided by the segmental approach to CHD.

References

1 Abbott ME. *Atlas of Congenital Cardiac Disease*. New York: American Heart Association, 1936.

2 Gross RE. Surgical management of the patent ductus arteriosus: with summary of four surgically treated cases. *Ann Surg* 1939;**110**:321–56.

3 Blalock A, Taussig HB. Landmark article May 19, 1945: The surgical treatment of malformations of the heart in which there is pulmonary stenosis or pulmonary atresia. By Alfred Blalock and Helen B. Taussig. *JAMA* 1984;**251**:2123–38.

4 Gibbon JH, Jr. Application of a mechanical heart and lung apparatus to cardiac surgery. *Minn Med* 1954;**37**:171–85.

5 Van Praagh R. The segmental approach to diagnosis of congenital heart disease. In: Bergsma D (ed.) *Birth Defects: Original Article Series*, VIII no. 5. Baltimore: Williams & Wilkins, 1972, pp. 4–23.

6 Van Praagh R, Van Praagh, S, Vlad P, Keith JD. Anatomic types of congenital dextrocardia: diagnostic and embryologic implications. *Am J Cardiol* 1964;**13**:510–31.

7 Van Praagh R, Van Praagh S. Isolated ventricular inversion. A consideration of the morphogenesis, definition and diagnosis of nontransposed and transposed great arteries. *Am J Cardiol* 1966;**17**:395–406.

8 Van Praagh R, Santini F, Geva T. Segmental situs in congenital heart disease: a fundamental concept. *G Ital Cardiol* 1990;**20**:246–53.

9 Van Praagh R. The segmental approach clarified. *Cardiovasc Intervent Radiol* 1984;**7**:320–5.

10 Lev M. Some newer concepts of the pathology of congenital heart disease. *Med Clin North Am* 1966;**50**:3–14.

11 Lev M, Liberthson RR, Golden JG, Eckner FA, Arcilla RA. The pathologic anatomy of mesocardia. *Am J Cardiol* 1971;**28**:428–35.

12 De la Cruz MV, Nadal-Ginard B. Rules for the diagnosis of visceral situs, truncoconal morphologies, and ventricular inversions. *Am Heart J* 1972;**84**:19–32.

13 Stanger P, Rudolph AM, Edwards JE. Cardiac malpositions. An overview based on study of sixty-five necropsy specimens. *Circulation* 1977;**56**:159–72.

14 Rao PS. Dextrocardia: systematic approach to differential diagnosis. *Am Heart J* 1981;**102**:389–403.

15 Freedom RM. The "anthropology" of the segmental approach to the diagnosis of complex congenital heart disease. *Cardiovasc Intervent Radiol* 1984;**7**:121–3.

16 Shinebourne EA, Macartney FJ, Anderson RH. Sequential chamber localization – logical approach to diagnosis in congenital heart disease. *Br Heart J* 1976;**38**:327–40.

17 Tynan MJ, Becker AE, Macartney FJ, Jimenez MQ, Shinebourne EA, Anderson RH. Nomenclature and classification of congenital heart disease. *Br Heart J* 1979;**41**:544–53.

18 Anderson RH, Becker AE, Freedom RM, et al. Sequential segmental analysis of congenital heart disease. *Pediatr Cardiol* 1984;**5**:281–7.

19 Anderson RH, Becker AE, Tynan M, Macartney FJ, Rigby ML, Wilkinson JL. The univentricular atrioventricular connection: getting to the root of a thorny problem. *Am J Cardiol* 1984;**54**:822–8.

20 Weinberg PM. Systematic approach to diagnosis and coding of pediatric cardiac disease. *Pediatr Cardiol* 1986;**7**:35–48.

21 Van Praagh R. Diagnosis of complex congenital heart disease: morphologic-anatomic method and terminology. *Cardiovasc Intervent Radiol* 1984;**7**:115–20.

22 Van Praagh R. The importance of segmental situs in the diagnosis of congenital heart disease. *Semin Roentgenol* 1985;**20**:254–71.

23 Anderson RH, Razavi R, Taylor AM. Cardiac anatomy revisited. *J Anat* 2004;**205**:159–77.

24 Beland MJ, Franklin RC, Jacobs JP, et al. Update from the International Working Group for Mapping and Coding of Nomenclatures for Paediatric and Congenital Heart Disease. *Cardiol Young* 2004;**14**:225–9.

25 Jacobs JP, Franklin RC, Jacobs ML, et al. Classification of the functionally univentricular heart: unity from mapped codes. *Cardiol Young* 2006;**16**(Suppl 1):9–21.

26 Bergersen L, Everett AD, Giroud JM, et al. Report from The International Society for Nomenclature of Paediatric and Congenital Heart Disease: cardiovascular catheterisation for congenital and paediatric cardiac disease (Part 1 – Procedural nomenclature). *Cardiol Young* 2011;**21**:252–9.

27 Geva T, Vick GW, 3rd, Wendt RE, Rokey R. Role of spin echo and cine magnetic resonance imaging in presurgical planning of heterotaxy syndrome. Comparison with echocardiography and catheterization. *Circulation* 1994;**90**:348–56.

28 Van Praagh R, Van Praagh S. Atrial isomerism in the heterotaxy syndromes with asplenia, or polysplenia, or normally formed spleen: an erroneous concept. *Am J Cardiol* 1990;**66**:1504–6.
29 Sutherland MJ, Ware SM. Disorders of left-right asymmetry: heterotaxy and situs inversus. *Am J Med Genet C* 2009;**151C**:307–17.
30 Cantrell JR, Haller JA, Ravitch MM. A syndrome of congenital defects involving the abdominal wall, sternum, diaphragm, pericardium, and heart. *Surg Gynecol Obstet* 1958;**107**:602–14.
31 Uemura H, Ho SY, Devine WA, Anderson RH. Analysis of visceral heterotaxy according to splenic status, appendage morphology, or both. *Am J Cardiol* 1995;**76**:846–9.
32 Van Praagh R, Van Praagh S. Anatomically corrected transposition of the great arteries. *Br Heart J* 1967;**29**:112–19.
33 Geva T, Powell AJ, Crawford EC, Chung T, Colan SD. Evaluation of regional differences in right ventricular systolic function by acoustic quantification echocardiography and cine magnetic resonance imaging. *Circulation* 1998;**98**:339–45.
34 Wong PC, Sanders SP, Jonas RA, et al. Pulmonary valve-moderator band distance and association with development of double-chambered right ventricle. *Am J Cardiol* 1991;**68**:1681–6.
35 Van Praagh R, Perez-Trevino C, Lopez-Cuellar M, et al. Transposition of the great arteries with posterior aorta, anterior pulmonary artery, subpulmonary conus and fibrous continuity between aortic and atrioventricular valves. *Am J Cardiol* 1971;**28**:621–31.
36 Geva T, Van Praagh S, Sanders SP, Mayer JE, Jr., Van Praagh R. Straddling mitral valve with hypoplastic right ventricle, crisscross atrioventricular relations, double outlet right ventricle and dextrocardia: morphologic, diagnostic and surgical considerations. *J Am Coll Cardiol* 1991;**17**:1603–12.
37 Geva T, Sanders SP, Ayres NA, O'Laughlin MP, Parness IA. Two-dimensional echocardiographic anatomy of atrioventricular alignment discordance with situs concordance. *Am Heart J* 1993;**125**:459–64.
38 Pasquini L, Sanders SP, Parness IA, et al. Conal anatomy in 119 patients with d-loop transposition of the great arteries and ventricular septal defect: an echocardiographic and pathologic study. *J Am Coll Cardiol* 1993;**21**:1712–21.
39 Van Praagh S, Geva T, Lock JE, Nido PJ, Vance MS, Van Praagh R. Biatrial or left atrial drainage of the right superior vena cava: anatomic, morphogenetic, and surgical considerations – report of three new cases and literature review. *Pediatr Cardiol* 2003;**24**:350–63.

CHAPTER 4

The Normal Pediatric Echocardiogram

Wyman W. Lai[1] and Jacqueline Wheatley[2]

[1] CHOC Children's Heart Institute, Orange, CA; University of California, Irvine School of Medicine, Irvine, CA, USA

[2] The Hospital for Sick Children, Toronto, ON; Mohawk College, Hamilton, ON, Canada

Examination principles

The basic elements of a standard transthoracic echocardiography (TTE) examination are 2D images supplemented by Doppler and color Doppler information in multiple orthogonal imaging planes [1]. The use of M-mode echocardiography is reserved primarily for the assessment of ventricular performance [2], although some current pediatric recommendations call for 2D assessment of left ventricular size and function [3]. Any laboratory performing a pediatric echocardiogram should have a written examination protocol that outlines the views to be obtained, the imaging modalities to be deployed for each view, and the preferred methods for recording and display. Whenever possible, the initial pediatric echocardiogram should be a complete study. A list of the structures to be examined with each view is helpful, and the required versus optional measurements should be clearly defined. A complete transthoracic pediatric echocardiogram should include a quantitative assessment of left ventricular size and systolic function (see later) [4].

Pediatric TTE is organized by acoustic "windows" from which the heart is examined. Many pediatric echocardiography laboratories begin the examination with subxiphoid, or subcostal, imaging instead of left parasternal views. This allows for the determination and display of visceral situs (site and/or location) at the beginning of an examination. Regardless of where the examination starts, the segmental approach is used to describe all of the major cardiovascular structures in sequence [5–7].

Complete sweeps of the heart should be made during the examination to rule out abnormalities at its base or apex or on one of its surfaces. The study information should be recorded as a combination of complete sweeps and multiple selected single-plane images [8–10]. Most ultrasound systems are configured so that a notch, or some other marking, on the side of a transducer corresponds to the side of a symbol displayed at the top of the image sector, usually to the right side of the screen (from the viewer's perspective). Therefore, when the transducer is positioned with the notch to the patient's left (at the 3 o'clock position), the left side of the patient will be displayed on the right of the screen. When the transducer is counterclockwise rotated so that the notch is directed superiorly (at 12 o'clock), the superior structures are displayed on the right of the screen. In the course of a routine sweep, the transducer notch position is held in a fixed position, and the transducer is angled to obtain a series of images in the desired imaging plane.

Because of the wide range of complex pathology that may be seen on a pediatric echocardiogram, images should be shown in their correct spatial, or "anatomically correct," position on the display screen. Therefore, the anterior and superior structures are displayed at the top of the screen, and the rightward structures are generally placed on the left side of the image display (with the exception being the parasternal long-axis view where the cardiac apex is displayed by convention on the left of the screen).

The diagnostic accuracy of an examination depends greatly on the image quality. Technical adjustments should be made throughout the examination by the operator to improve signal-to-noise ratio and image resolution. The appropriate probe and optimal transducer frequency are selected to image the structures in question, and adjustments of the electronic (acoustic) focus depth are made throughout the study as necessary. Centering of structures of interest, using an appropriate degree of magnification, and optimizing of windows for imaging and Doppler interrogation are critical for image quality. The optimal window should allow the ultrasound beam to be directed perpendicularly to structures of interest for 2D imaging. The ultrasound beam should be parallel to flow for Doppler interrogation and color flow mapping. The appropriate color box size should be used in order to maintain an adequate frame rate (the smaller the color box, the higher the frame rate), and selecting the proper color velocity range for the region of interest is crucial for accurate assessment. Patient position, comfort, and level of anxiety are important considerations during the examination.

In the usual performance of an echocardiogram, the goals from each view should be: (i) imaging of cardiovascular structures; (ii) color and/or spectral Doppler interrogation of each valve and other major cardiovascular structures; and (iii) a complete evaluation of any suspicious chamber, vessel, or flow

Echocardiography in Pediatric and Congenital Heart Disease: From Fetus to Adult, Third Edition. Edited by Wyman W. Lai, Luc L. Mertens, Meryl S. Cohen and Tal Geva.

Companion website: www.wiley.com/go/lai-echo3

Table 4.1 Structures viewed from subxiphoid (subcostal) sweep/views

Inferior vena cava
Hepatic veins
Abdominal aorta
Diaphragm
Superior vena cava
Left atrium
Right atrium
Atrial septum
Coronary sinus
Pulmonary veins
Mitral valve
Tricuspid valve
Left ventricle
Right ventricle
Ventricular septum
Left ventricular papillary muscles
Left ventricular outflow tract
Aortic valve
Right ventricular outflow tract
Pulmonary valve
Ascending aorta
Coronary arteries
Main and branch pulmonary arteries
Pericardium

Table 4.2 Structures viewed from apical sweep/views

Inferior vena cava
Left atrium
Right atrium
Atrial septum
Coronary sinus
Selected pulmonary veins
Mitral valve
Tricuspid valve
Left ventricle
Right ventricle
Ventricular septum
Left ventricular papillary muscles
Left ventricular outflow tract
Aortic valve
Right ventricular outflow tract
Pulmonary valve
Ascending aorta
Main and branch pulmonary arteries

Table 4.3 Structures viewed from left parasternal sweep/views

Inferior vena cava
Superior vena cava
Left atrium
Right atrium
Atrial septum
Coronary sinus
Pulmonary veins
Mitral valve
Tricuspid valve
Left ventricle
Right ventricle
Ventricular septum
Left ventricular papillary muscles
Left ventricular outflow tract
Aortic valve
Right ventricular outflow tract
Pulmonary valve
Ascending aorta
Coronary arteries
Main and branch pulmonary arteries
Pericardium

Table 4.4 Structures viewed from suprasternal notch sweep/views

Superior vena cava
Left atrium
Pulmonary veins
Ascending aorta
Superior thoracic aorta
Main and branch pulmonary arteries
Aortic arch
Proximal brachiocephalic arteries
Left innominate vein

Table 4.5 Structures viewed from right parasternal views

Inferior vena cava
Superior vena cava
Right atrium
Atrial septum
Right pulmonary veins
Ascending aorta
Right pulmonary artery

jet identified during the course of the examination. Tables 4.1–4.5 list the structures that should be visualized from the standard examination views. During the progress of pediatric TTE, the sonographer or echocardiographer must keep in mind the indications for the study and the need to address potential issues that may affect treatment. A complete examination may require that custom, or "in between," planes be used to investigate or display an abnormality.

Extracardiac structures are also visualized during a standard TTE examination. Mediastinal abnormalities such as masses or cysts, if present, should be noted [11,12]. The presence or absence of the thymus may be seen in young children. Careful attention to symmetry and amplitude of diaphragm motion and screening for pleural effusions from subxiphoid and flank windows is particularly important in postoperative cardiac patients.

Standard orthogonal imaging views

The five standard views of a pediatric TTE, as defined by the American Society of Echocardiography, are all employed as part of a routine examination including subxiphoid (subcostal), apical, parasternal (left parasternal), suprasternal notch, and right parasternal (Tables 4.1–4.5) [13]. These imaging planes provide unique information regarding cardiovascular malformations that

are often seen in childhood. A complete examination requires that the cardiovascular structures be imaged from multiple orthogonal planes. This practice minimizes artifacts due to false "dropout" of structures imaged parallel to the beam of interrogation, "shadowing" from reflective structures proximal to the area of interest, or "mirroring" from the reflection of ultrasound on tissue layers.

The imaging planes are identified by transducer location (subxiphoid, apical, left parasternal, suprasternal notch, and right parasternal) and by the plane of examination relative to the heart (four chamber, two chamber, long axis, and short axis) (Figure 4.1). In addition, imaging planes may be described as anatomic planes (sagittal, transverse/axial, or coronal). The views and structures presented in the following sections are described as seen in a patient with normal or near-normal cardiovascular anatomy.

Subxiphoid (subcostal) views

This imaging plane provides a great deal of information, particularly in young children who tend to have good acoustic windows. The child is placed in the supine position. For larger children, placing a pillow under their bent knees may help to relax the abdominal muscles. Subxiphoid imaging [14–16] begins with the determination of abdominal visceral situs in the transverse plane. The transducer is positioned with the notch at the 3 o'clock position as viewed from inferiorly with anterior structures displayed at the top of the screen. In addition to visualization of the liver and stomach, the spleen should be sought in patients with suspected abnormal abdominal visceral situs (e.g., heterotaxy syndrome). The location of the hepatic segment of the inferior vena cava and descending aorta in relation to the midline and one another are determined from this view (Figure 4.2, Video 4.1). The patency, size, and collapsibility of the inferior vena cava should be documented in its long axis (the transducer is rotated counterclockwise so that the notch is at the

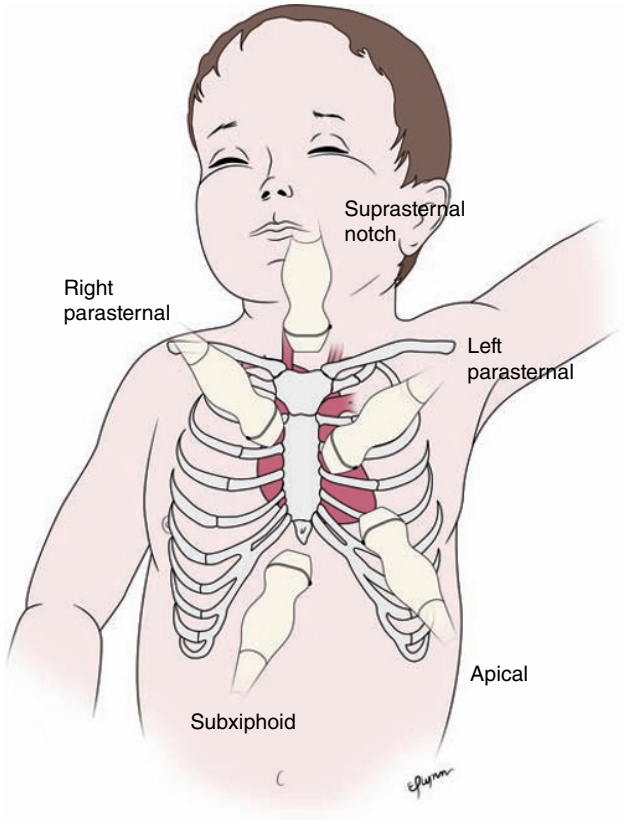

Figure 4.1 Line drawing of transducer locations for standard imaging windows.

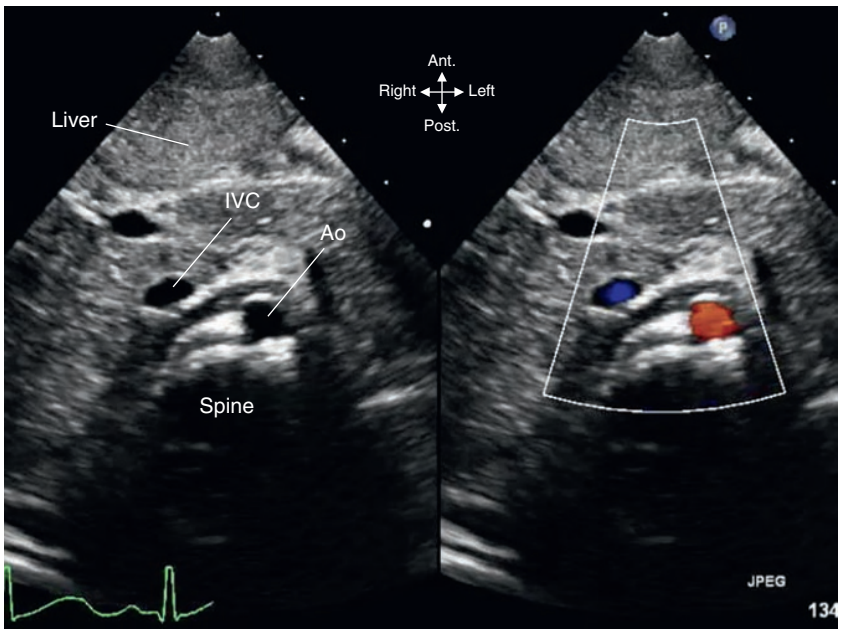

Figure 4.2 Axial view in color compare mode demonstrating 2D and color Doppler images of a child with normal abdominal visceral situs. Ao, aorta; IVC, inferior vena cava.

12 o'clock position), and the abdominal descending aorta should also be demonstrated (Figure 4.3, Videos 4.2 and 4.3). If a dilated azygos vein is seen posterior to the descending aorta, interruption of the inferior vena cava should be suspected. Inadvertent compression of the inferior vena cava, mimicking interruption, may be avoided by reducing the amount of abdominal pressure used to obtain the image.

With the notch again at 3 o'clock, the plane of imaging is angled from the abdomen to the thorax to obtain the "situs sweep" (Videos 4.4 and 4.5). The connections of the hepatic veins to the inferior vena cava are visualized, followed by the connection of the inferior vena cava to the right atrium. The position of the heart in the left thorax may also be determined in this sweep. The descending aorta at the level of the diaphragm should be identified, and any additional vascular structures crossing the diaphragm should be fully investigated by 2D imaging and color flow mapping. It is useful to visualize both hemidiaphragms at the same time in the subxiphoid long-axis (transverse) view to document normal diaphragmatic motion with respiration.

The image is then inverted so that the superior structures are displayed at the top of the screen. The subxiphoid long-axis (coronal, frontal) sweep begins in the transverse plane and utilizes the liver as an acoustic window to the heart (Figure 4.4, Video 4.6). The connections of the hepatic veins to the inferior vena cava should be documented, as well as the entrance of the inferior vena cava to the right atrium. As the sweep passes the inferior/posterior surface of the heart, the coronary sinus is often well visualized along the left posterior atrioventricular groove, and the posterior descending coronary artery may be seen in the posterior interventricular groove. The long-axis view allows for good visualization of the atrial septum and characterization of right versus left atrial and ventricular morphology. As imaging transitions into a nearly coronal plane, the ventricular outflow tracts are well displayed, as is the right atrial appendage and the proximal portion of the normal right superior vena cava to the right of the ascending aorta. The position of the left coronary artery ostium may be visualized as the sinuses of Valsalva and ascending aorta are imaged. The bifurcation of the main pulmonary artery into the branch pulmonary arteries should be documented during the sweep. Color flow mapping in the subxiphoid long axis may be advantageous for interrogation of the atrial septum and the anterior muscular septum (Video 4.7). To visualize the true long axis of the atrial septum, the transducer should be rotated in between the subxiphoid long- and short-axis views (left anterior oblique plane, see later). Sweeping from this plane can further elucidate defects in the inferior atrial septum that might be underappreciated in the standard subxiphoid views.

The subxiphoid short-axis (sagittal) sweep (Figure 4.5, Videos 4.8 and 4.9) starts in a sagittal plane with the transducer notch positioned inferiorly (6 o'clock). The short-axis "reference view" includes the atria (including the right atrial appendage), the atrial septum, and the superior and inferior venae cavae. The Eustachian valve – the venous valve of the inferior vena cava – is frequently seen in this view as an extension of the anterior wall of the inferior vena cava and should not be confused with the atrial septum [17]. The imaging sweep normally begins to the right of the patient, allowing visualization of the right upper pulmonary vein as it passes lateral and posterior to the superior vena cava and then proceeds from the base to the apex of the heart. The right pulmonary artery is seen in cross-section posterior to the superior vena cava and above the roof of the left atrium. The arch of the azygos vein above the right pulmonary artery and into the superior vena cava may also be visualized in this sweep. Atrial septal morphology, including the apposition

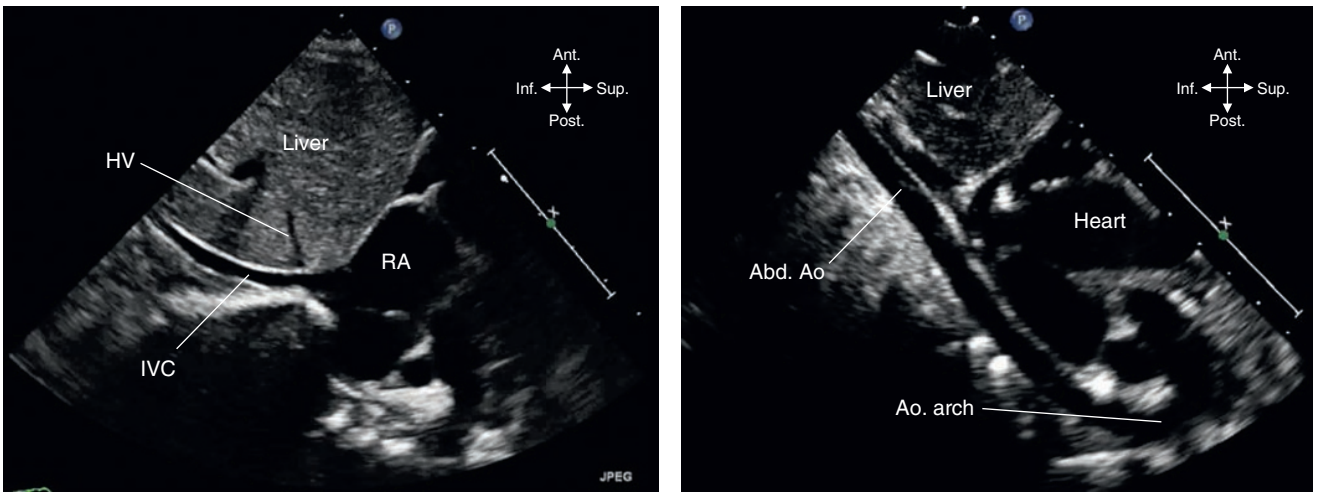

Figure 4.3 Long-axis composite image of uninterrupted inferior vena cava and descending aorta. **(a)** IVC, inferior vena cava; HV, hepatic vein; RA, right atrium. **(b)** Abd. Ao, abdominal aorta; Ao. arch, aortic arch.

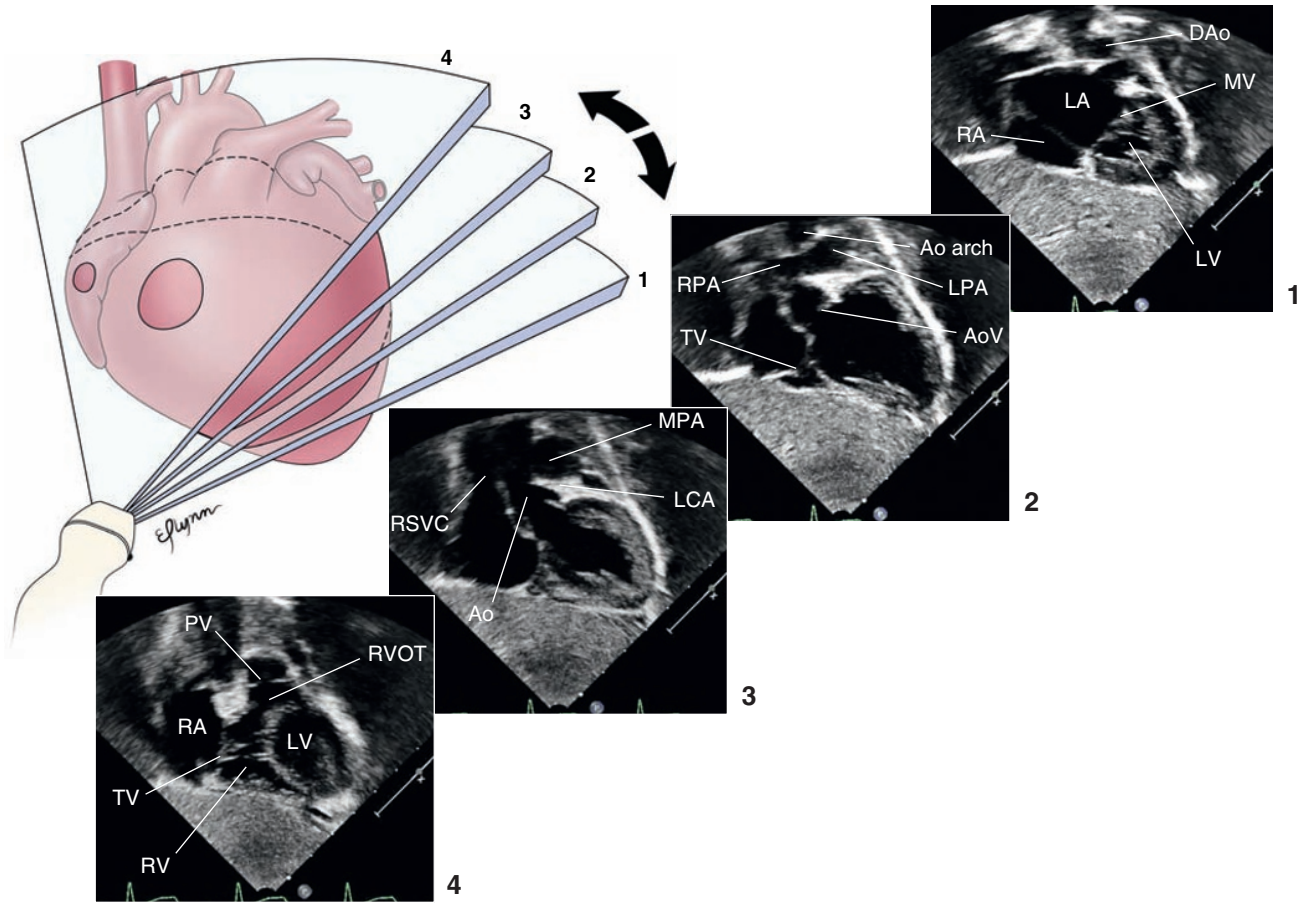

Figure 4.4 Line drawing and serial images of subxiphoid long-axis (coronal, frontal) sweep. **(1)** DAo, descending aorta; LA, left atrium; LV, left ventricle; MV, mitral valve; RA, right atrium. **(2)** Ao arch, aortic arch; AoV, aortic valve; LPA, left pulmonary artery; RPA, right pulmonary artery; TV, tricuspid valve. **(3)** Ao, aorta; LCA, left coronary artery; MPA, main pulmonary artery; RSVC, right superior vena cava. **(4)** LV, left ventricle; PV, pulmonary valve; RA, right atrium; RV, right ventricle; RVOT, right ventricular outflow tract; TV, tricuspid valve.

of the septum primum and septum secundum, is often well seen in the short-axis plane. The tricuspid valve is imaged before the mitral valve as the transducer passes from right to left. The morphology of the atrioventricular valves, including fibrous continuity between the atrioventricular and aortic valves, can be identified as the imaging plane passes the atrioventricular canal region. The transducer position may need to be repositioned during the sweep (generally more rightward on the abdomen, taking advantage of the right-sided liver as an acoustic window) to maintain a short-axis imaging plane as the apex of the heart is visualized. A list of structures that should be identified on the subxiphoid views is provided in Table 4.1. Color flow mapping of the atrial and ventricular septa, particularly in smaller children, is often best visualized in the subxiphoid short-axis sweep. It is important to lower the color flow Doppler scale due to the poor angle of interrogation for flow across portions of the ventricular septum and to capture low-velocity shunts. Doppler interrogation of the descending aorta at the level of the diaphragm, the hepatic vein, and the superior vena cava is recommended as part of a complete examination in all patients.

Apical views

Standard apical four-chamber and long-axis ("three-chamber") – as well as, in many laboratories, apical two-chamber – views are obtained [18]. The child is placed in a partial left lateral decubitus position with the left arm raised to bring the apex of the heart closer to the chest wall, and the apical impulse may be palpated for transducer placement. The notch of the transducer is directed toward the left axilla, at the 2–3 o'clock position as viewed from the apex. The four-chamber sweep (Figure 4.6, Video 4.10) begins posteriorly to demonstrate the length of the coronary sinus [19], the entrance of the inferior vena cava into the right atrium bordered anteriorly/inferiorly by the Eustachian valve, and the thoracic descending aorta posterior to the left atrium in the nearly transverse plane. The sweep covers the anterior surface of the heart after passing through the atrioventricular valves and the left ventricular outflow tract (Table 4.2). Careful color flow mapping of the ventricular septum can help to discern any ventricular septal defects, particularly in the apical muscular septum (Video 4.11). Importantly, this view should not be used to interrogate the

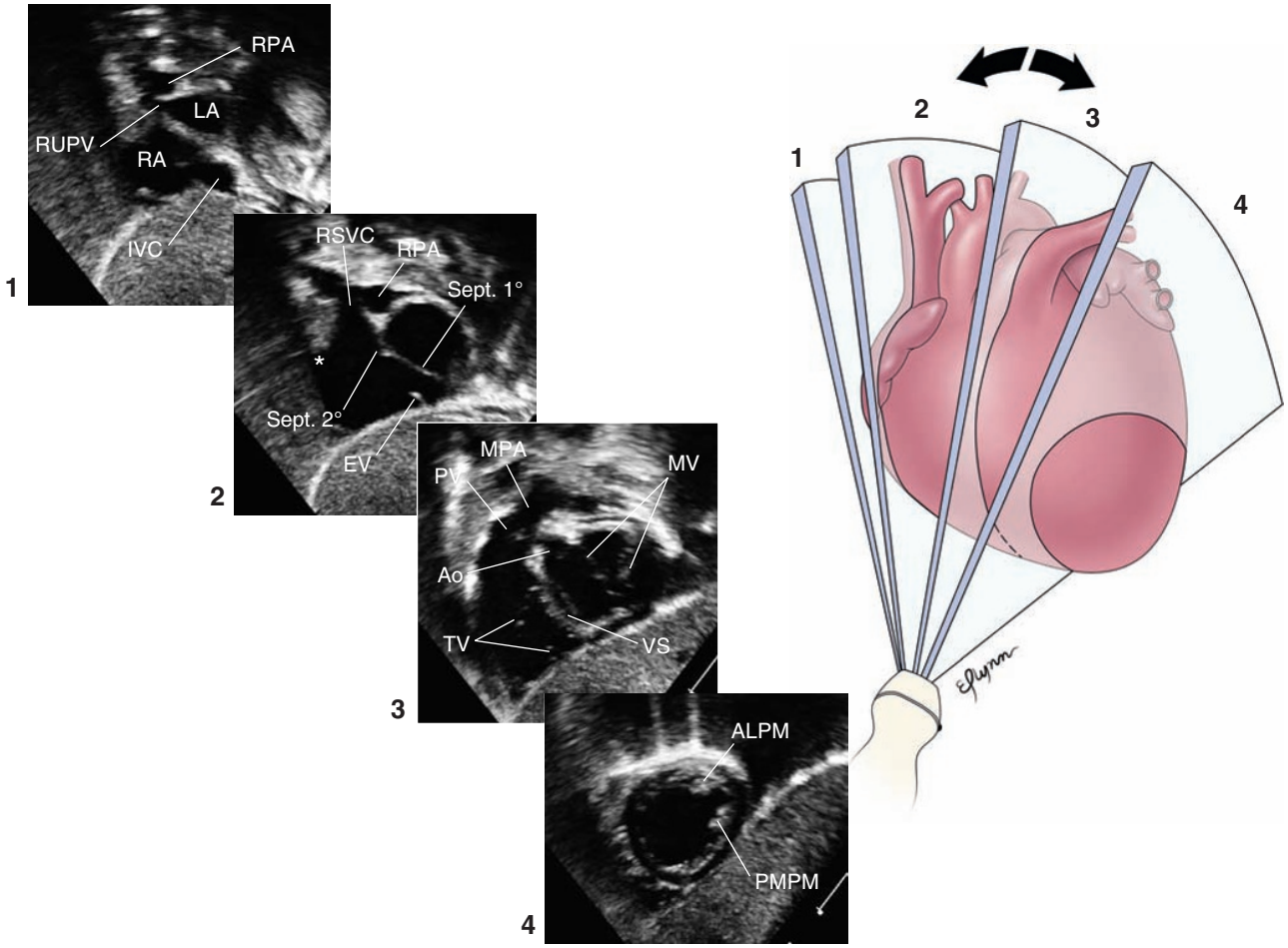

Figure 4.5 Line drawing and serial images of subxiphoid short-axis (sagittal) sweep. **(1)** IVC, inferior vena cava; LA, left atrium; RA, right atrium; RPA, right pulmonary artery; RUPV, right upper pulmonary vein. **(2)** EV, Eustachian valve; RPA, right pulmonary artery; RSVC, right superior vena cava; Sept. 1°, septum primum; Sept. 2°, septum secundum; *, region of the right atrial appendage. **(3)** Ao, aorta; MPA, main pulmonary artery; MV, mitral valve; PV, pulmonary valve; TV, tricuspid valve; VS, ventricular septum. **(4)** ALPM, anterolateral papillary muscle; PMPM, posteromedial papillary muscle.

atrial septum as it is parallel to the ultrasound beam and false dropout can occur.

The apical four-chamber reference view allows for spectral and color Doppler interrogation of the atrioventricular valves and the characterization of ventricular morphology (Video 4.12). With the proper adjustments, the apical displacement of the normal tricuspid annulus relative to the mitral annulus, ventricular trabeculations, and the moderator band may be well visualized. Angling anteriorly from the standard four-chamber view, the "five-chamber" view highlights the left ventricular outflow tract and ascending aorta (Figure 4.6(1)). Repositioning of the transducer medially toward the lower left sternal border and moving up one or two rib spaces brings the right ventricular inflow and right ventricular free wall more into alignment with the beam of interrogation (Video 4.13). Superior and anterior angulation from this position brings the right ventricular outflow tract into alignment and often offers an optimum angle for Doppler interrogation of the right ventricular outflow tract and color flow mapping of the pulmonary valve (Figure 4.7, Video 4.14).

The apical long-axis ("three-chamber") view is obtained by rotation of the transducer clockwise approximately 60° from the four-chamber view (Figure 4.8, Video 4.15), with the transducer notch at 4 o'clock. Some laboratories image the "three-chamber" view by rotating the transducer counterclockwise from the four-chamber view to place the transducer notch at approximately 10 o'clock (Video 4.16). Imaging of the left ventricular outflow tract from the apex allows for visualization of subaortic structures oriented perpendicular to the plane of insonation [20]. The long-axis view allows for optimal Doppler interrogation of the left ventricular outflow tract and ascending aorta as well as color flow mapping of the aortic valve. Modified views foreshortening the left ventricle may allow clearer visualization of the left ventricular outflow tract.

The two-chamber view is utilized for quantification of left atrial size, global left ventricular function [21], or assessment of

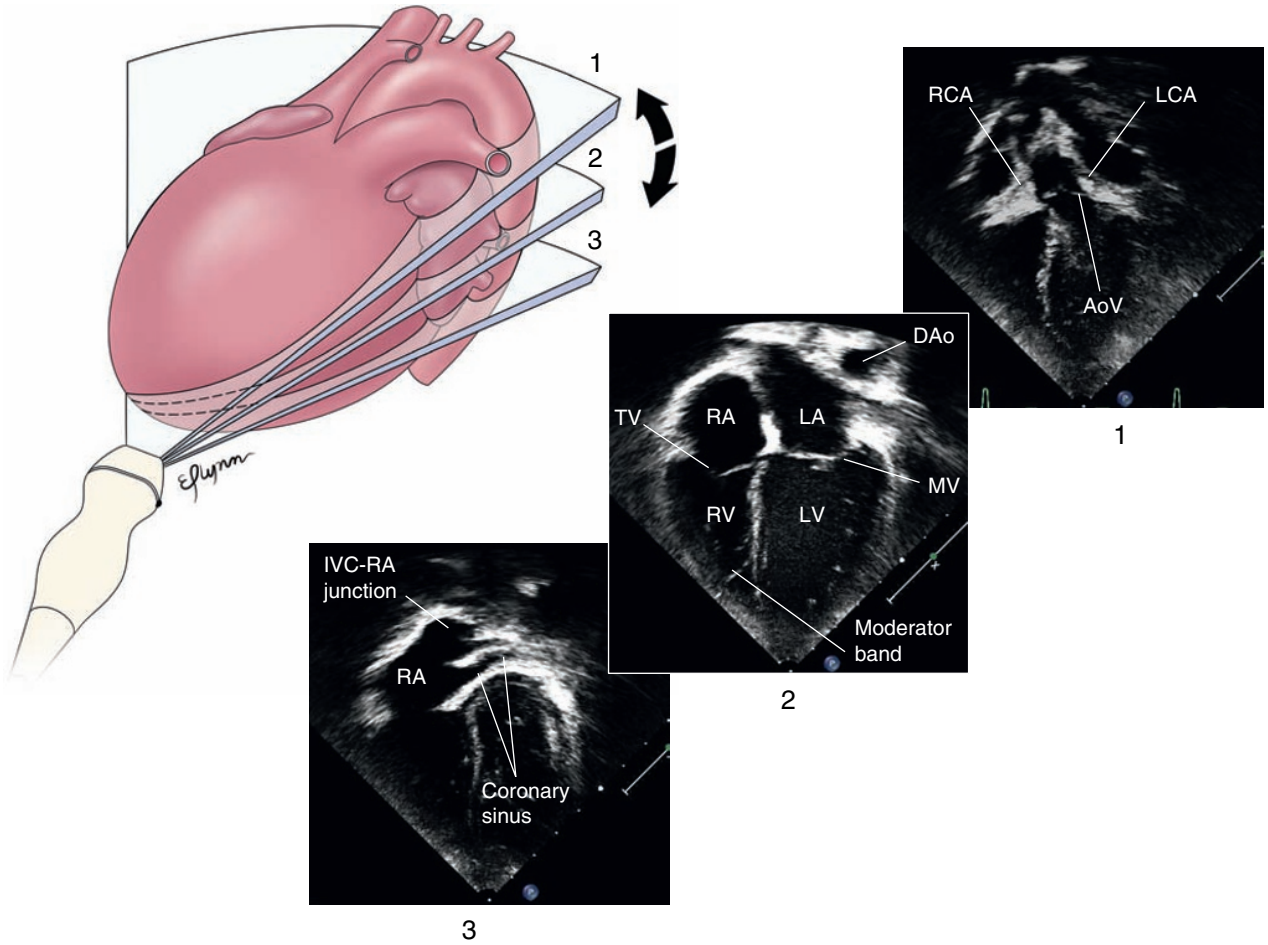

Figure 4.6 Line drawing and serial images of apical four-chamber sweep. **(1)** AoV, aortic valve; LCA, left coronary artery; RCA, right coronary artery. **(2)** DAo, descending thoracic aorta; LA, left atrium; LV, left ventricle; MV, mitral valve; RA, right atrium; RV, right ventricle; TV, tricuspid valve. **(3)** IVC-RA junction, inferior vena cava–right atrial junction; RA, right atrium.

regional wall motion. This view is obtained by rotation of the transducer counterclockwise approximately 60° from the four-chamber view, with the transducer notch at 12–1 o'clock. The anterior wall is displayed on the right side of the screen and inferior wall on the left (Figure 4.9, Video 4.17).

Parasternal (left parasternal) views

With the child still in a partial left lateral decubitus position, the transducer is placed on the upper to mid left sternal border with the transducer notch directed toward the right shoulder (10 o'clock) to provide a parasternal long-axis view [19,22]. The long-axis sweep, without and with color flow mapping of the ventricular septum, begins anteriorly at the pulmonary outflow and sweeps inferiorly towards the tricuspid inflow (Figure 4.10, Videos 4.18 and 4.19). The coronary sinus ostium may also be visualized with this sweep. The long-axis reference view is obtained with the transducer positioned over the left ventricular outflow tract (Video 4.20), allowing visualization of the aortic valve, mitral valve, and the basal to mid inferolateral wall of the left ventricle. The fibrous continuity between the mitral and aortic valves is easily demonstrated, and the phasic motion of the valve leaflets is well visualized. The transducer is angled toward the right hip to visualize the tricuspid valve and right ventricular inflow (Video 4.21). The transducer is then angled anteriorly toward the left shoulder to visualize the right ventricular outflow tract, pulmonary valve, and main pulmonary artery (Video 4.22). Color flow mapping of each of the valves should be performed from the parasternal window. Repositioning of the transducer superiorly may be required to provide a long-axis or sagittal oblique view of the aorta (Video 4.23), which best demonstrates the proximal ascending aorta in its long axis for diameter measurement and also allows for visualization of the right coronary artery ostium relative to the sinotubular junction.

The parasternal short-axis view at the base of the heart can provide detailed imaging of aortic valve morphology [23] as well as views of the right ventricular infundibulum (conus) and pulmonary valve. From the long-axis view, the transducer is clockwise rotated so that the transducer notch is directed toward

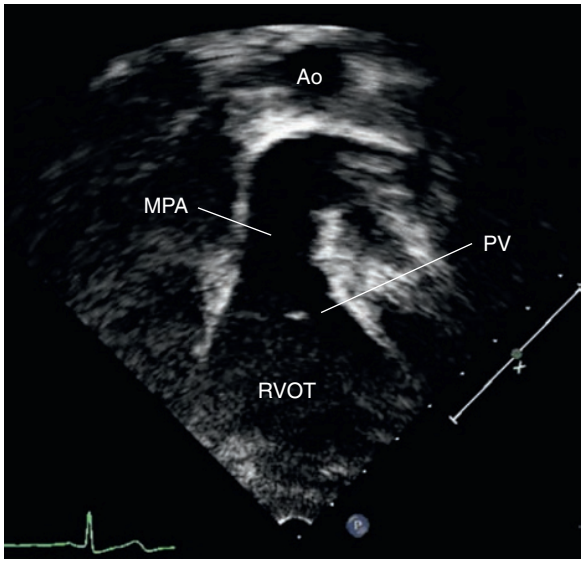

Figure 4.7 Modified apical view demonstrating the right ventricular outflow tract. Ao, aorta; MPA, main pulmonary artery; PV, pulmonary valve; RVOT, right ventricular outflow tract.

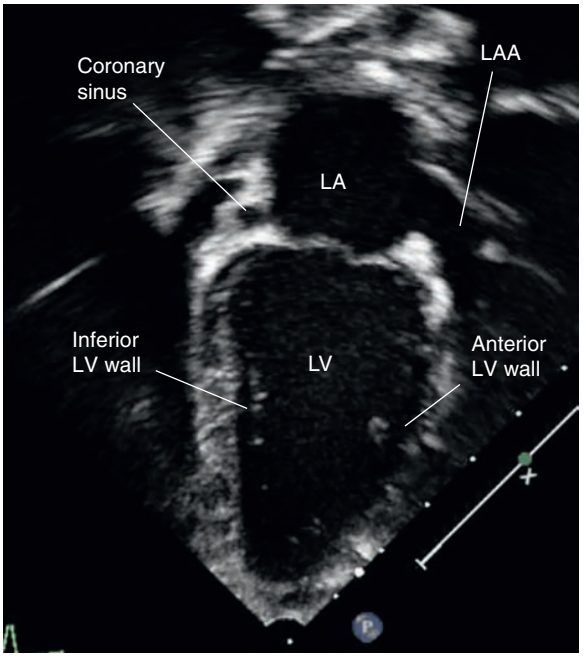

Figure 4.9 Apical two-chamber view. LA, left atrium; LAA, left atrial appendage; LV, left ventricle.

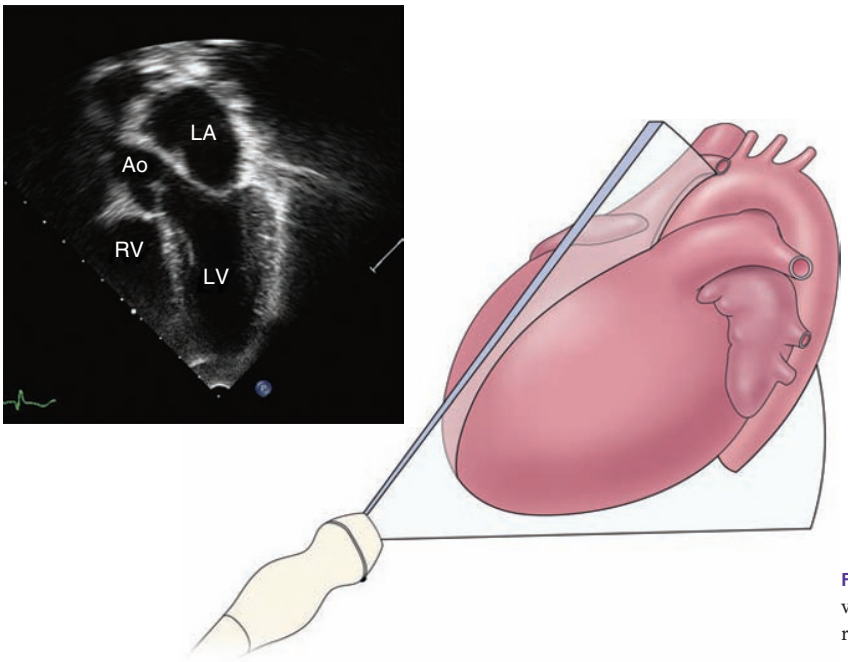

Figure 4.8 Line drawing and image of apical long-axis view. Ao, aorta; LA, left atrium; LV, left ventricle; RV, right ventricle.

the left shoulder (2 o'clock). The short-axis reference view (Figure 4.11(1), Video 4.24) consists of: the aorta centered in the imaging sector; the right ventricular inflow; the right ventricular outflow tract and main pulmonary artery; and the atria. Although relatively parallel to the beam of insonation, the atrial septum may be visualized in a modified short-axis view obtained by slight clockwise rotation (3 o'clock) and repositioning the transducer one or two rib notches inferiorly; this view may be especially useful in larger children with poor subxiphoid windows. Examination of the coronary artery ostia should be obtained from the short-axis views, as well as imaging and color flow mapping of the proximal coronary arteries (Figures 4.12 and 4.13, Videos 4.25 and 4.26) [24–26]. It is important to use clips rather than stillframe images to determine coronary artery anatomy. Clockwise rotation of the transducer (also 3 o'clock) into a transverse view elongates the left main and anterior

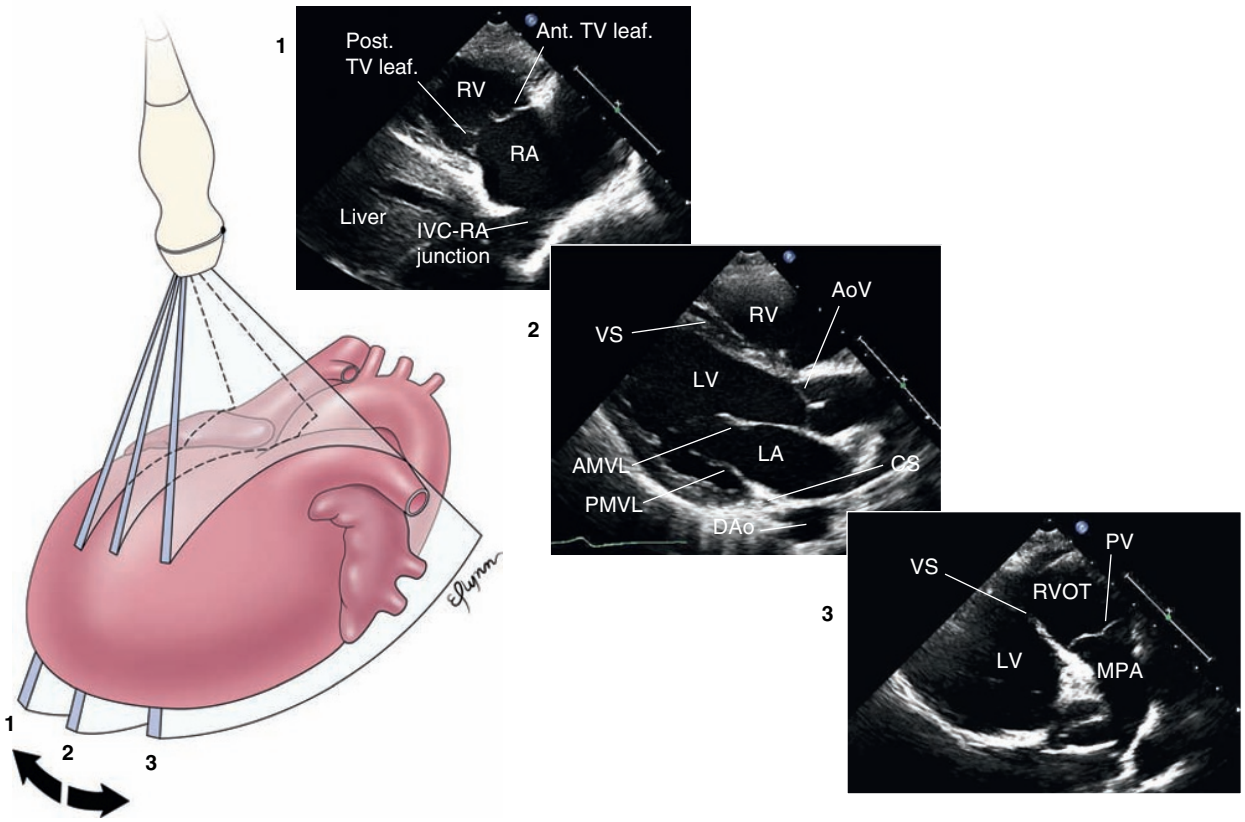

Figure 4.10 Line drawing and serial images of parasternal long-axis sweep. **(1)** Ant. TV leaf., anterior tricuspid valve leaflet; IVC-RA junction, inferior vena caval–right atrial junction; Post. TV leaf., posterior tricuspid valve leaflet; RA, right atrium; RV, right ventricle; **(2)** AMVL, anterior mitral valve leaflet; AoV, aortic valve; CS, coronary sinus; DAo, descending aorta; LA, left atrium; LV, left ventricle; PMVL, posterior mitral valve leaflet; RV, right ventricle; VS, ventricular septum. **(3)** LV, left ventricle; MPA, main pulmonary artery; PV, pulmonary valve; RVOT, right ventricular outflow tract; VS, ventricular septum.

descending coronary arteries, and often demonstrates the bifurcation of the left main coronary artery. The great cardiac vein may also be well visualized from this transverse left parasternal window [27]. Slight counterclockwise rotation (1 o'clock) may elongate the right coronary artery and improve its visualization.

The parasternal short-axis sweep (Videos 4.27 and 4.28) begins with the transducer tilted toward the right shoulder to demonstrate better the main and branch pulmonary arteries. Detailed imaging of the pulmonary valve and proximal main pulmonary artery may require repositioning of the transducer inferiorly, as well as tilting and clockwise rotation (to 3 o'clock) to provide a nearly coronal plane of imaging directed superiorly. Imaging of the pulmonary valve in this angled short-axis view should be optimized for pulmonary annulus diameter measurement. The parasternal short-axis sweep progresses from the base of the heart to the apex. On the left border of the heart at the base, the sweep shows the branch pulmonary arteries, followed by the left atrial appendage positioned anterior to the left upper pulmonary vein, and then the left lower pulmonary vein proximal to the atrioventricular groove. The right lower pulmonary vein is found near the entrance of the inferior vena cava separated by the atrial septum. Color and spectral Doppler are often helpful in distinguishing the left atrial appendage (bidirectional flow) from the left upper pulmonary vein (unidirectional flow). The morphology of the mitral leaflets and valve apparatus, including the position of the left ventricular papillary muscles, is often best seen on short-axis views of the ventricles (Videos 4.29–4.32). In larger hearts, color flow mapping of the ventricular septum may require separate sweeps of the anterior and posterior portions of the septum to assess for muscular ventricular septal defects. Examination of the apical muscular septum may require repositioning of the transducer toward the apex during the short-axis sweep. A list of structures that should be identified on the left parasternal views is provided in Table 4.3.

A "ductal view" is obtained from imaging in a parasagittal plane from a high left parasternal window, with the transducer notch at 12 o'clock. This window lines up the ultrasound beam with the main pulmonary artery–ductus–descending aorta continuum and allows for the exclusion of a normally located small patent ductus arteriosus (Figure 4.14, Videos 4.33 and 4.34). On

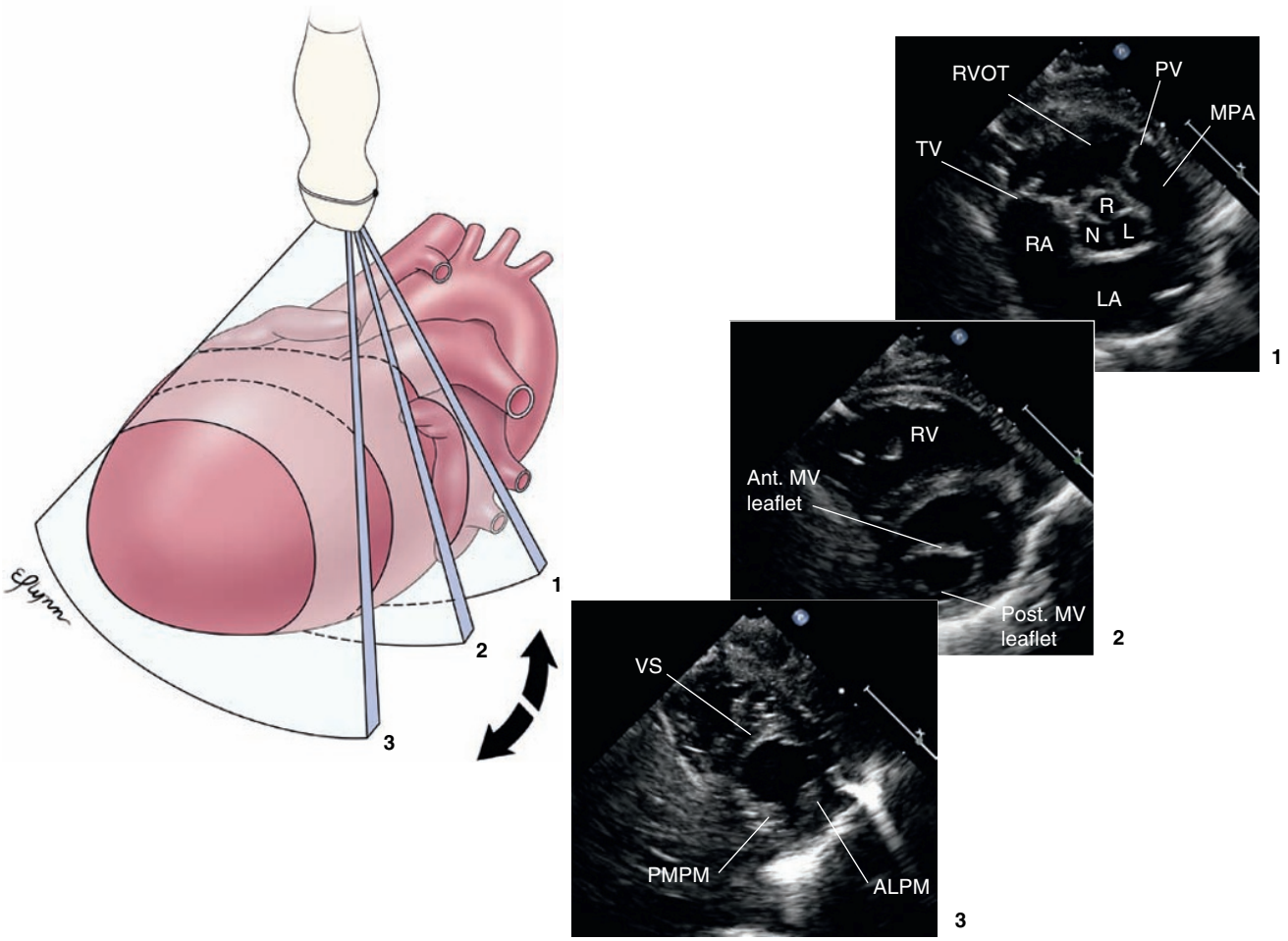

Figure 4.11 Line drawing and serial images of parasternal short-axis sweep. **(1)** L, left coronary cusp; LA, left atrium; MPA, main pulmonary artery; N, noncoronary cusp; PV, pulmonary valve; R, right coronary cusp; RA, right atrium; RVOT, right ventricular outflow tract; TV, tricuspid valve. **(2)** Ant. MV, anterior mitral valve; Post. MV, posterior mitral valve; RV, right ventricle. **(3)** ALPM, anterolateral papillary muscle; PMPM, posteromedial papillary muscle; VS, ventricular septum.

a larger patient, the position of the transducer may need to be adjusted to a lower window. The distal aortic arch and superior thoracic aorta may also be visualized through the heart and the main pulmonary artery, and, in larger individuals, the aortic isthmus is sometimes best seen from this position. The heart may be used as an acoustic window for the rest of the thoracic descending aorta. Clockwise rotation of the transducer to a high left sternal border transverse plane (transducer notch at 3 o'clock) may better demonstrate the left pulmonary veins in some larger individuals. Angling the transducer slightly posterior from the pulmonary veins can demonstrate the bifurcation of the pulmonary arteries (Video 4.35).

Suprasternal notch views

The child is placed in a supine position, and the neck and upper back may be slightly arched with the assistance of a rolled towel or pillow under the shoulders. Imaging from the suprasternal notch [28–30] includes positioning of the transducer in the right supraclavicular region and occasionally in the left supraclavicular region. In the coronal or short-axis plane with the transducer notch at 3 o'clock, the connection or absence of the left innominate vein to the right superior vena cava may be visualized. This view also demonstrates the right pulmonary artery in its long axis posterior to the aorta (Figure 4.15(2), Video 4.36). In smaller individuals, both the right and left pulmonary venous connections to the left atrium are well visualized in the far field of the suprasternal notch or left infraclavicular transverse view ("crab view") (Figure 4.16, Videos 4.37 and 4.38). Repositioning the transducer over the right supraclavicular or infraclavicular regions may better reveal the right pulmonary artery or right pulmonary veins. Flow in the superior vena cava may also be best seen in this plane. Finally, in a sweep one can see the aorta descend on one side of the mediastinum thus helping to determine arch sidedness.

The leftward extent of the left innominate vein should be examined by color flow mapping to exclude a left superior vena

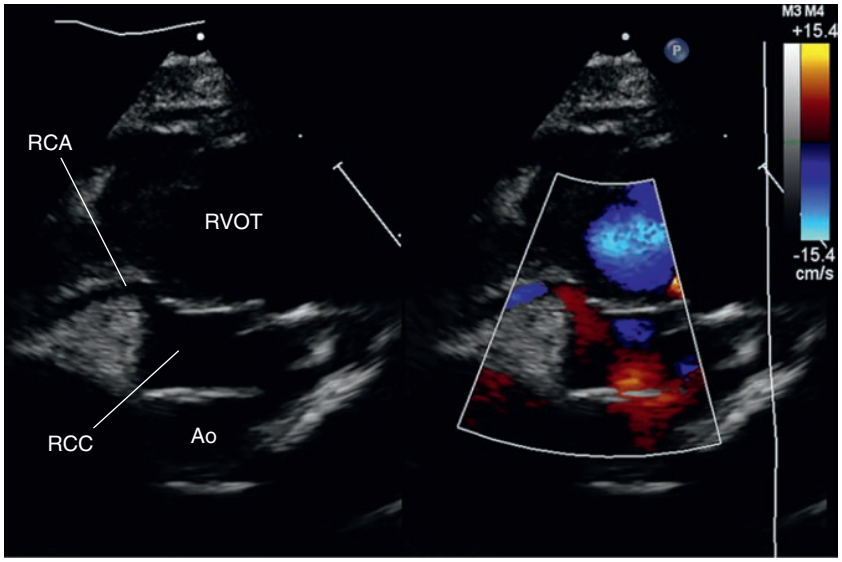

Figure 4.12 Parasternal short-axis 2D and color Doppler images of axial right coronary artery. Ao, aorta; RCA, right coronary artery; RCC, right coronary cusp; RVOT, right ventricular outflow tract.

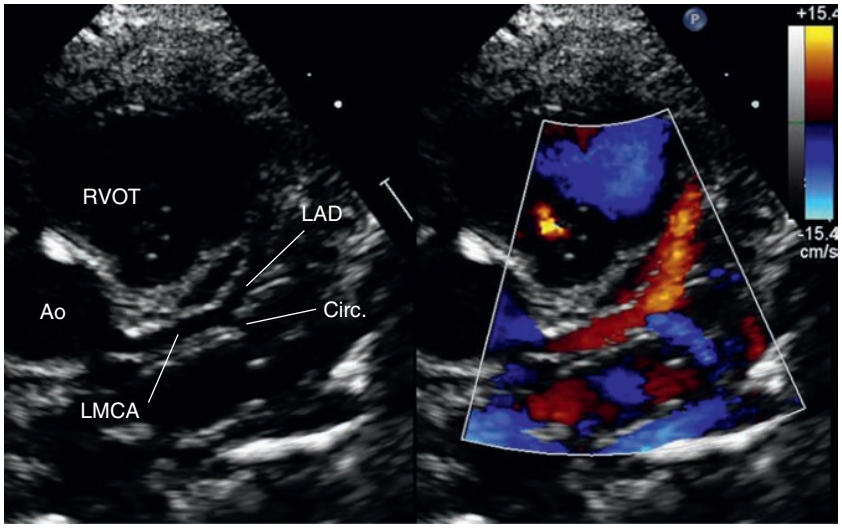

Figure 4.13 Parasternal short-axis 2D and color Doppler images of an axial left coronary artery. Ao, aorta; Circ., circumflex; LAD, left anterior descending; LMCA, left main coronary artery; RVOT, right ventricular outflow tract.

cava or an anomalous pulmonary venous connection by way of a vertical vein (Video 4.39). Infrequently, small tributaries of the left innominate vein, such as the left superior intercostal vein or left internal thoracic vein, may be seen draining normally by color flow mapping.

From the suprasternal notch short-axis view, superior (cranial) angulation of the transducer demonstrates the branching pattern of the aorta (Figure 4.17, Videos 4.40 and 4.41) [31]. The sidedness of the aortic arch may be determined in almost all cases as opposite of the direction, or sidedness, of the first brachiocephalic artery. Visualization of the aorta relative to the trachea or acoustic shadowing from the tracheal air column may help confirm arch sidedness. A normal branching pattern of the aortic arch should be documented by demonstration of a normally bifurcating first brachiocephalic artery; if the first branch does not bifurcate normally and/or the first and second branches are the same size, an aberrant origin of the subclavian artery should be suspected.

Demonstration of the left aortic arch in its long axis (Figure 4.18, Video 4.42) is achieved by counterclockwise rotation, resulting in a transducer notch position of 1–2 o'clock from the coronal plane in the suprasternal notch window. The axis is from left shoulder to right anterior hip. As noted earlier, the distal aortic arch and aortic isthmus are sometimes best seen from a "ductal view." Further leftward angulation often best demonstrates the left pulmonary artery (Figure 4.19, Video 4.43). A list of structures that should be identified on the suprasternal notch views is provided in Table 4.4.

Right parasternal views

The rightward extent of the atrial septum and nearby structures may be well visualized in a parasagittal imaging plane from the

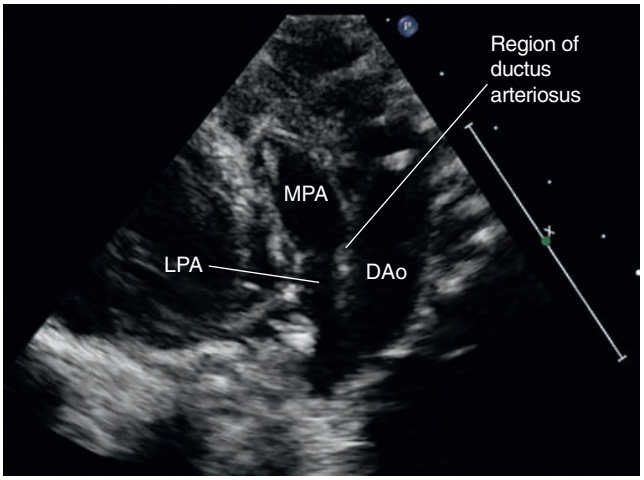

Figure 4.14 High parasternal "ductal" view. DAo, descending aorta; LPA, left pulmonary artery; MPA, main pulmonary artery.

right parasternal border with the transducer notch at 12 o'clock (Table 4.5) [32]. Positioning of the patient in a right lateral decubitus position with the right arm raised above the head is often helpful. From a window at the mid to upper right sternal border (Figure 4.20, Video 4.44), the structures imaged are similar to the subxiphoid short-axis reference view, including the atria, the atrial septum, and the superior and inferior venae cavae. The unique feature of the right parasternal window is that the superior portion of the atrial septum is oriented perpendicular to the plane of insonation, resulting in less "dropout" artifact. This view is therefore useful to assess for a superior sinus venosus defect. A sweep is made initially toward the right to demonstrate the rightward extent of the atrial septum and the right upper pulmonary vein. The azygos vein is often seen by imaging and color flow mapping as it arches over the right pulmonary artery and connects to the superior vena cava. The sweep then is directed leftward to image and color flow map the overlapping septum primum and septum secundum (Videos 4.45 and 4.46). Doppler interrogation of the left ventricular outflow tract can also be performed from the superior right upper parasternal window if indicated. In larger children, a separate inferior window one or two rib spaces lower may be utilized to demonstrate the more inferior structures at the rightward extent of the heart.

Rotation into a short-axis (transverse) imaging plane from a superior right parasternal window, with the transducer notch then positioned at 3 o'clock, allows visualization and color flow mapping of the right upper pulmonary vein. Sweeping from cranial to caudal, the relative positions of the right superior vena cava and ascending aorta are seen, followed by the right pulmonary artery in its long axis. The right upper pulmonary vein is visualized just below the right pulmonary artery bifurcation. Frequently, the right upper pulmonary vein is best demonstrated by imaging or color flow mapping in the transverse plane (Figure 4.21, Videos 4.47 and 4.48).

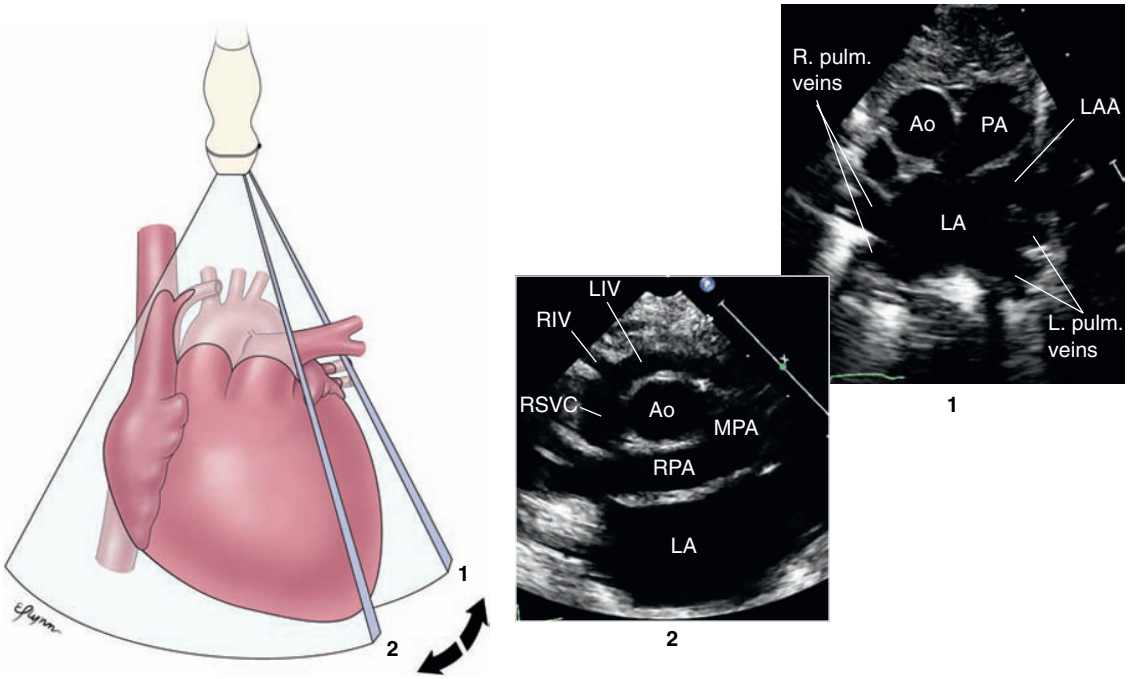

Figure 4.15 Line drawing and images of suprasternal short-axis views. **(1)** Ao, aorta; LA, left atrium; LAA, left atrial appendage; L. pulm. veins, left pulmonary veins; PA, pulmonary artery; R. pulm. veins, right pulmonary veins. **(2)** Ao, aorta; LA, left atrium; LIV, left innominate vein; MPA, main pulmonary artery; RIV, right innominate vein; RPA, right pulmonary artery; RSVC, right superior vena cava.

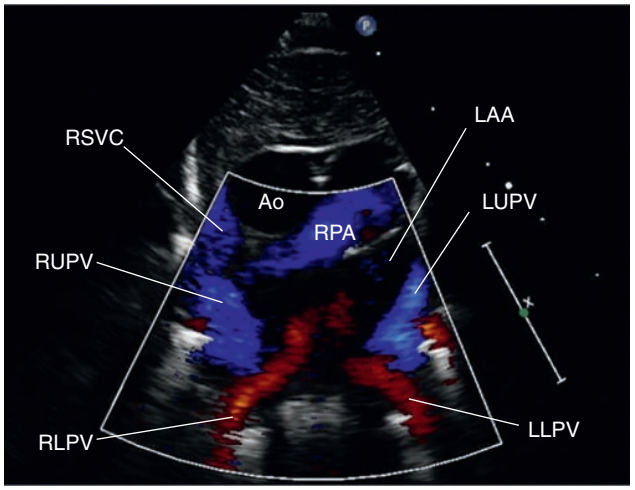

Figure 4.16 Color Doppler image of pulmonary veins to the left atrium. Ao, aorta; LAA, left atrial appendage; LLPV, left lower pulmonary vein; LUPV, left upper pulmonary vein; RLPV, right lower pulmonary vein; RPA, right pulmonary artery; RSVC, right superior vena cava; RUPV, right upper pulmonary vein.

Additional or supplemental imaging views

In some pediatric echocardiography laboratories, "in-between" imaging views are routinely performed as part of a normal echocardiogram. Two of these in-between views may be described as analogs of the right anterior oblique and the left anterior oblique, or long axial oblique, angiographic views used in cardiac catheterization procedures. Performance of these views is particularly important when cardiovascular malformations are suspected in the regions of interest.

Right anterior oblique view

The right anterior oblique view [33,34] is acquired by rotation of the transducer approximately 45° counterclockwise from the standard subxiphoid long-axis view, resulting in the transducer notch being positioned at 1–2 o'clock (Figure 4.22, Video 4.49). This plane simultaneously images the inflow and outflow portions of the right ventricle and highlights abnormalities of conal septum, particularly when there is anterior malalignment. It also demonstrates the right ventricular outflow tract and the connection to the branch pulmonary arteries. No sweep is involved with this view.

Left anterior oblique view

The left anterior oblique view [35–37] is a sweep acquired by rotation of the transducer approximately 30–45° clockwise from the standard subxiphoid long-axis view, resulting in the transducer notch being positioned at 4–5 o'clock, and scanning from base to apex (normally from right hip to left shoulder). This plane produces an en face view of the atrioventricular valves that best demonstrates any abnormal attachment of the atrioventricular valve leaflets and the chordal and papillary muscle positions (Figure 4.23, Video 4.50). It also highlights the left ventricular outflow tract.

"Flank" views

Supplemental imaging from the "flanks" is indicated when early postoperative examinations are performed. These views are obtained along the right and left posterior axillary lines near the level of the diaphragm with the transducer notch at 12 o'clock, resulting in a coronal imaging plane (with the superior structures to the right of the display screen and the inferior structures to the left) (Figure 4.24). Whenever possible, the liver or the spleen should be used as an acoustic window in order to visualize

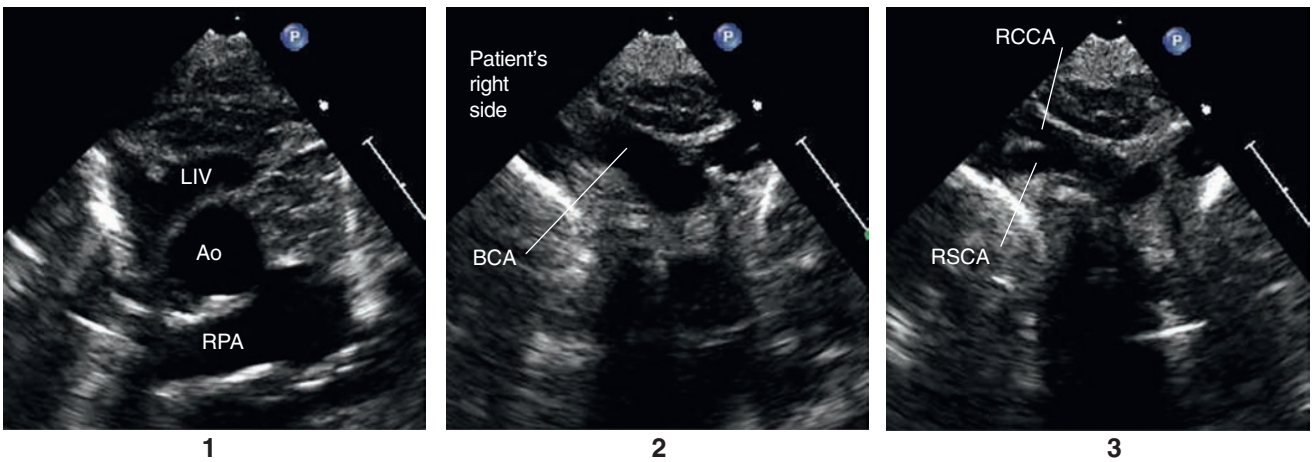

Figure 4.17 Serial images of suprasternal notch short-axis sweep for arch branching and sidedness. **(1)** Short axis reference image of the aorta in its short axis. Ao, aorta; LIV, left innominate vein; RPA, right pulmonary artery. **(2)** Sweeping superiorly, the brachiocephalic artery courses rightward of the patient from the aorta. BCA, brachiocephalic artery. **(3)** Continuing to sweep superiorly, the bifurcation of the brachiocephalic artery is seen. RCCA, right common carotid artery; RSCA, right subclavian artery.

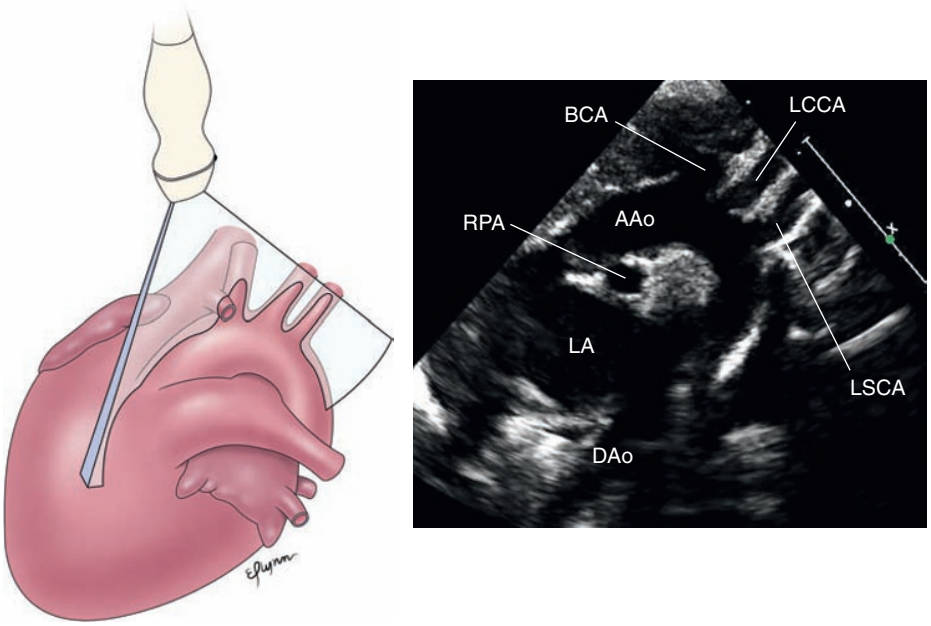

Figure 4.18 Line drawing and image of suprasternal notch aortic arch view. AAo, ascending aorta; BCA, brachiocephalic artery; DAo, descending aorta; LA, left atrium; LCCA, left common carotid artery; LSCA, left subclavian artery; RPA, right pulmonary artery.

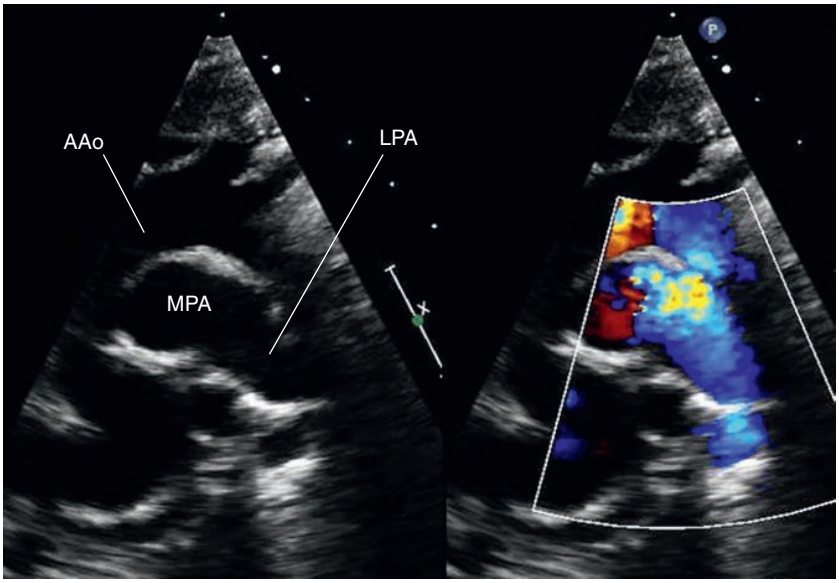

Figure 4.19 Suprasternal notch left pulmonary artery view. AAo, ascending aorta; LPA, left pulmonary artery; MPA, main pulmonary artery.

the costophrenic margin and beyond to observe diaphragmatic motion as well as to rule out pleural effusion.

Measurements

The measurement of cardiac structures and flows is critical to the interpretation of a pediatric echocardiogram. An abnormally small or large structure can be a clue to otherwise silent pathology, and is important to the planning of surgical procedures. Mild forms of obstruction can be diagnosed only by accurate measurement of flow velocities.

In general, it is recommended that all relevant measurements be made as part of a complete pediatric echocardiogram, as outlined in Chapters 5–9 on quantitative methods. Recommendations for quantification methods for a pediatric echocardiogram have been published [3]. In addition, guidelines have been published for the echocardiographic assessment of valvar

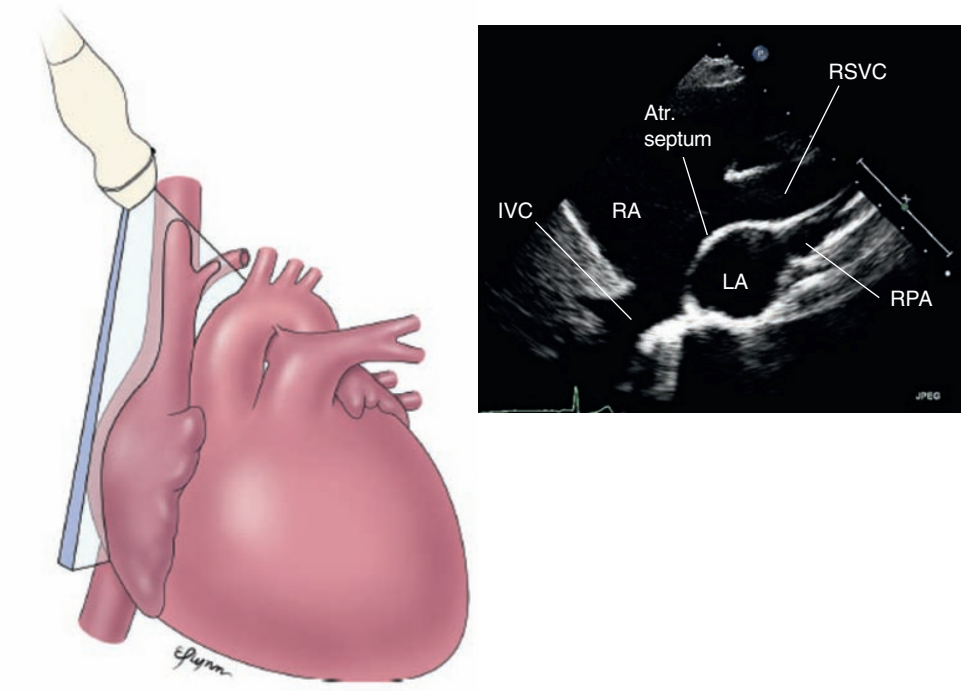

Figure 4.20 Line drawing and image of right parasternal longitudinal view. Atr. septum, atrial septum; IVC, inferior vena cava; LA, left atrium; RA, right atrium; RPA, right pulmonary artery; RSVC, right superior vena cava.

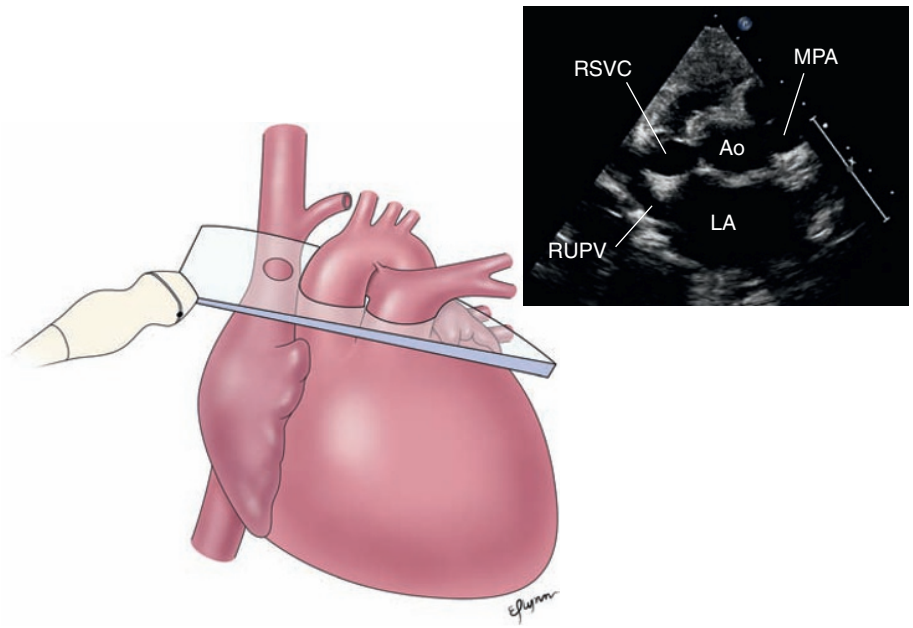

Figure 4.21 Line drawing and image of right parasternal short-axis view. Ao, aorta; LA, left atrium; MPA, main pulmonary artery; RSVC, right superior vena cava; RUPV, right upper pulmonary vein.

regurgitation [38] and quantitative methods in adult patients [21]. The measurements that are "relevant" in pediatric patients, however, will vary depending upon the specifics of their cardiovascular anatomy. The examination protocol of a laboratory should specify which measurements to perform and the laboratory procedure for obtaining each measurement for internal consistency.

Recommended measurements may be grouped into measurements of cardiovascular structures, ventricular size and function measurements, hemodynamic measurements, and miscellaneous/

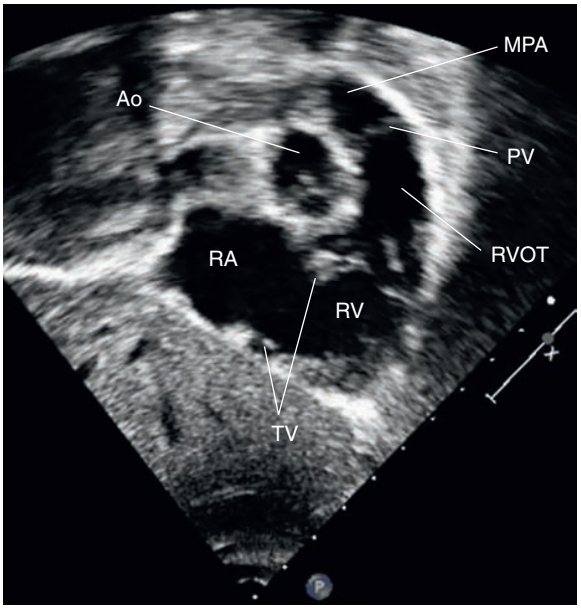

Figure 4.22 Subxiphoid right anterior oblique view. Ao, aorta; MPA, main pulmonary artery; PV, pulmonary valve; RA, right atrium; RV, right ventricle; RVOT, right ventricular outflow tract; TV, tricuspid ventricle.

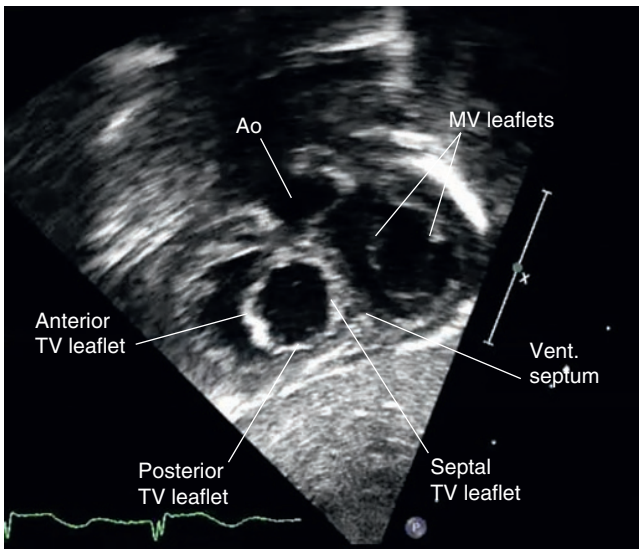

Figure 4.23 Subxiphoid left anterior oblique view. Ao, aorta; MV leaflets, mitral valve leaflets; TV, tricuspid valve; Vent. septum, ventricular septum.

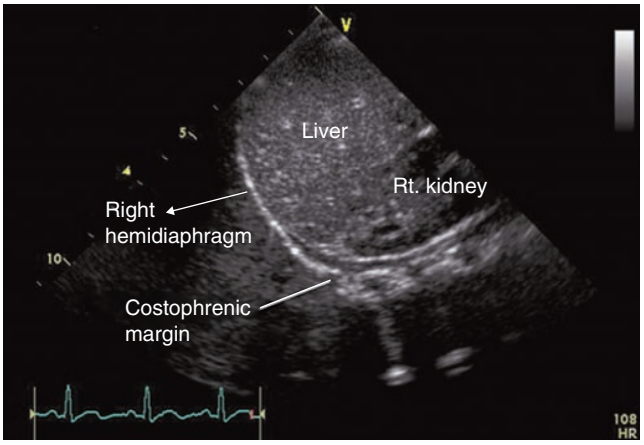

Figure 4.24 Flank view. Rt., right.

Table 4.6 Minimal elements for a pediatric echocardiography report

Demographic data
Name
Date of birth
Gender
Medical record identifier
Appointment information
Date of study
Location of study
Referring physician
Performing sonographer
Sedation used
Interpreting physician
Clinical data
Study indications
Patient height and weight
Body surface area
Blood pressure
Findings section
Structural features (morphologic diagnoses)
Measurements of cardiovascular structures (with z-scores for comparison with normal data), including aortic root dimension
Doppler (hemodynamic) findings
Ventricular function assessment, including quantitative assessment of left ventricular dimensions; wall thickness or mass; and systolic function (with some exceptions)
Summary section
Summary of the results, including any pertinent positive and negative findings

pathology-related measurements. The reader is referred to the appropriate sections of this textbook for a discussion of each of these measurement categories.

Reporting

The minimum elements of a pediatric echocardiography report have been defined in guidelines published by the American Society of Echocardiography [13] and in the accreditation standards of the Intersocietal Accreditation Commission [4]. An adapted version of the reporting requirements is provided in Table 4.6. Basic identifier information should be listed, and a statement relating to the indication for the study is required. The patient's height and weight should be recorded for body surface area calculation. Conveyance of the echocardiographic findings in a clear and cogent manner is important. The final report must be completely typewritten, and must include the

name of the sonographer, ordering physician, and interpreting physician. Abbreviations should be generally avoided or, when used, should be clearly noted and/or unambiguous.

The report findings section can be configured in a variety of ways but should include information on: (i) structural findings; (ii) measurements made of cardiovascular structures; (iii) Doppler echocardiographic data; and (iv) ventricular function assessment. Positive findings and pertinent negative findings should be listed.

Information pertaining to cardiovascular anatomy and structure can be conveyed utilizing the segmental approach. In addition to reporting the absolute values, it is useful to report quantitative measures within the context of age- or size-appropriate norms (e.g., z-score values) [39–41].

The hemodynamic and ventricular function measurements are discussed in other sections of this textbook. Relevant Doppler information concerning the atrioventricular valves, semilunar valves, and any shunt sites should be provided. Quantitative Doppler and ventricular function information, when appropriate, should be included in the report.

A summary section should be provided, including any pertinent positive or negative findings. If possible, important changes from the previous study should be noted. Any technical or other limitations – such as lack of patient cooperation – that might compromise the diagnostic accuracy of the echocardiographic examination should be specified in the report. Examples include suboptimal acoustic windows, heart rate constraints, and excessive patient motion during the examination.

Videos

To access the video clips for this chapter, please go to wiley.com/go/lai-echo3.

Video 4.1 Subxiphoid: abdominal situs color compare. Color compare subxiphoid axial view demonstrating a right-sided inferior vena cava (blue) and left-sided descending aorta (red).

Video 4.2 Subxiphoid: inferior vena cava with color Doppler. Subxiphoid long-axis view of the inferior vena cava in 2D and color Doppler. Note the normal collapsibility of the inferior vena cava.

Video 4.3 Subxiphoid: abdominal aorta with color Doppler. Subxiphoid long-axis view of the descending abdominal aorta in 2D and color Doppler.

Video 4.4 Subxiphoid: situs sweep. Subxiphoid axial situs sweep with the transducer at the top of the screen.

Video 4.5 Subxiphoid: situs sweep color Doppler. Subxiphoid axial color Doppler situs sweep with the transducer at the top of the screen. Note the hepatic veins connecting normally to the inferior vena cava.

Video 4.6 Subxiphoid: long-axis sweep. Subxiphoid long-axis sweep with the transducer at the bottom of the screen.

Video 4.7 Subxiphoid: long-axis sweep color Doppler. Subxiphoid long-axis color Doppler sweep with the transducer at the bottom of the screen.

Video 4.8 Subxiphoid: short-axis sweep. Subxiphoid short-axis sweep from base to apex. Note that the sweep starts to the right of the superior vena cava, demonstrating the right upper pulmonary vein.

Video 4.9 Subxiphoid: short-axis sweep color Doppler. Subxiphoid short-axis color Doppler sweep from base to apex. Note the color Doppler jet of a patent foramen ovale with left-to-right flow.

Video 4.10 Apical: four-chamber sweep. Apical four-chamber sweep from posterior to anterior. Note the coronary sinus.

Video 4.11 Apical: four-chamber sweep color Doppler. Apical four-chamber color Doppler sweep from anterior to posterior.

Video 4.12 Apical: four-chamber reference view with color Doppler. Apical four-chamber reference view with color Doppler of the left and right ventricular inflows. Note the trivial mitral and tricuspid regurgitation color Doppler jets.

Video 4.13 Apical: four-chamber with focus on the right ventricle with color Doppler. Apical four-chamber view with focus on the right ventricle in 2D and color Doppler. Note the trivial tricuspid regurgitation color Doppler jet.

Video 4.14 Apical: right ventricular outflow. Apical right ventricular outflow tract view in 2D and color Doppler. Note the trivial pulmonary regurgitation color Doppler jet.

Video 4.15 Apical: three-chamber with color Doppler (clockwise rotation). Apical three-chamber view in 2D and color Doppler. Clockwise rotation of the transducer from the four-chamber view results in display of the left ventricular outflow tract on the left of the screen.

Video 4.16 Apical: three-chamber with color Doppler (counterclockwise rotation). Apical three-chamber view in 2D and color Doppler. Counterclockwise rotation of the transducer from the four-chamber view results in display of the left ventricular outflow tract on the right of the screen. Note the trivial mitral regurgitation color Doppler jet.

Video 4.17 Apical two-chamber view. Note the left atrial appendage on the right of the screen.

Video 4.18 Parasternal: long-axis sweep. Left parasternal long-axis sweep from the right ventricular outflow tract to the right ventricular inflow.

Video 4.19 Parasternal: long-axis sweep color Doppler. Left parasternal long-axis color Doppler sweep from the right ventricular outflow tract to the right ventricular inflow.

Video 4.20 Parasternal: long-axis reference view with color Doppler. Left parasternal long-axis reference view with magnified color Doppler views of the aortic and mitral valves.

Video 4.21 Parasternal: right inflow with color Doppler. Left parasternal view of the right ventricular inflow in 2D and color Doppler. Note the trivial tricuspid valve regurgitation color Doppler jets.

Video 4.22 Parasternal: right outflow with color Doppler. Left parasternal view of the right ventricular outflow tract in 2D and color Doppler. Note the trivial pulmonary regurgitation color Doppler jet.

Video 4.23 Parasternal: ascending aorta with color Doppler. Superior left parasternal view of the ascending aorta in 2D and color Doppler.

Video 4.24 Parasternal: short-axis reference view. Left parasternal short-axis reference view.

Video 4.25 Parasternal: right coronary artery color compare. Color compare left parasternal short-axis magnified view of the right coronary artery.

Video 4.26 Parasternal: left coronary artery color compare. Color compare left parasternal short-axis magnified view of the left coronary artery. Note the bifurcation of the left main coronary artery into the left anterior descending (red) and circumflex (blue) coronary arteries.

Video 4.27 Parasternal: short-axis sweep. Left parasternal short-axis sweep from base to apex.

Video 4.28 Parasternal: short-axis sweep color Doppler. Left parasternal short-axis color Doppler sweep from base to apex.

Video 4.29 Parasternal: short-axis view of the mitral valve with color Doppler. Left parasternal short-axis view of the mitral valve in 2D and color Doppler.

Video 4.30 Parasternal: short-axis view of the left ventricle, basal level. Left parasternal short-axis view at the left ventricular basal level.

Video 4.31 Parasternal: short-axis view of the left ventricle, mid-ventricular level. Left parasternal short-axis view at the mid-ventricular level. Note the position of the left ventricular papillary muscles.

Video 4.32 Parasternal: short-axis view of the left ventricle, apical level. Left parasternal short-axis view of the left ventricle at the apex.

Video 4.33 High parasternal: ductal view with color Doppler. "Ductal view" in 2D and color Doppler.

Video 4.34 High parasternal: ductal view sweep with color Doppler. "Ductal view" color Doppler sweep from right to left.

Video 4.35 High parasternal: branch pulmonary arteries with color Doppler. High left parasternal view of the main and branch pulmonary arteries in 2D and color Doppler.

Video 4.36 Suprasternal: short-axis view with color Doppler. Suprasternal notch short-axis view in 2D and color Doppler.

Video 4.37 Left infraclavicular: "crab view." Left infraclavicular "crab view."

Video 4.38 Left infraclavicular: "crab view" color Doppler. Left infraclavicular "crab view" with color Doppler. Note the four pulmonary veins draining into the left atrium.

Video 4.39 Suprasternal: left innominate vein sweep with color Doppler. Suprasternal notch color Doppler sweep of the left innominate vein.

Video 4.40 Suprasternal: arch sidedness sweep. Suprasternal notch arch sidedness sweep with superior angulation. Note the bifurcation of the first brachiocephalic artery to the patient's right.

Video 4.41 Suprasternal: arch sidedness sweep with color Doppler. Suprasternal notch arch sidedness color Doppler sweep with superior angulation. Note the bifurcation of the right brachiocephalic artery into the right common carotid (red) and right subclavian (blue) arteries.

Video 4.42 Suprasternal: aortic arch with color Doppler. Suprasternal notch long-axis view of the aortic arch in 2D and color Doppler. Note the origins of the three aortic branches.

Video 4.43 Suprasternal: long-axis left pulmonary artery color compare. Color compare suprasternal notch long-axis view of the left pulmonary artery.

Video 4.44 Right parasternal: long-axis reference view. Superior right parasternal long-axis reference view.

Video 4.45 Right parasternal: long-axis sweep. Superior right parasternal long-axis sweep to the right and then left.

Video 4.46 Right parasternal: long-axis sweep with color Doppler. Superior right parasternal long-axis color Doppler sweep from right to left. Note the false dropout of the inferior portion of the atrial septum.

Video 4.47 Right parasternal: short-axis sweep. Right parasternal short-axis sweep from posterior to anterior.

Video 4.48 Right parasternal: short-axis sweep with color Doppler. Right parasternal short-axis color Doppler sweep from posterior to anterior.

Video 4.49 Subxiphoid right anterior oblique view. Note the right ventricular inflow and right outflow tract.

Video 4.50 Subxiphoid left anterior oblique view. Note the en face images of the atrioventricular valves.

References

1 Henry WL, DeMaria A, Gramiak R, et al. Report of the American Society of Echocardiography Committee on Nomenclature and Standards in Two-dimensional Echocardiography. *Circulation* 1980;**62**:212–17.

2 Snider AR, Serwer GA, Ritter SB. *Echocardiography in Pediatric Heart Disease*, 2nd edn. St. Louis, MO: Mosby, 1997.

3 Lopez L, Colan SD, Frommelt PC, et al. Recommendations for quantification methods during the performance of a pediatric echocardiogram: a report from the Pediatric Measurements Writing Group of the American Society of Echocardiography Pediatric and Congenital Heart Disease Council. *J Am Soc Echocardiogr* 2010;**23**:465–95.

4 IAC (Intersocietal Accreditation Commission). The IAC Standards and Guidelines for Pediatric Echocardiography Accreditation, 2017. https://www.intersocietal.org/echo/standards/IACPediatricEchocardiographyStandards2017.pdf (accessed December 2020).

5 Lev M. Pathologic diagnosis of positional variations in cardiac chambers in congenital heart disease. *Lab Invest* 1954;**3**:71–82.

6 Van Praagh R. Diagnosis of complex congenital heart disease: morphologic-anatomic method and terminology. *Cardiovasc Intervent Radiol* 1984;**7**:115–20.

7 Anderson RH, Becker AE, Freedom RM, et al. Sequential segmental analysis of congenital heart disease. *Pediatr Cardiol* 1984;**5**:281–7.

8 Thomas JD, Adams DB, Devries S, et al. Guidelines and recommendations for digital echocardiography. *J Am Soc Echocardiog* 2005;**18**:287–97.

9 Frommelt PC, Whitstone EN, Frommelt MA. Experience with a DICOM-compatible digital pediatric echocardiography laboratory. *Pediatr Cardiol* 2002;**23**:53–7.

10 Mathewson JW, Dyar D, Jones FD, et al. Conversion to digital technology improves efficiency in the pediatric echocardiography laboratory. *J Am Soc Echocardiog* 2002;**15**:1515–22.

11 Chandraratna PA, Littman BB, Serafini A, et al. Echocardiographic evaluation of extracardiac masses. *Br Heart J* 1978;**40**:741–9.

12 O'Laughlin MP, Huhta JC, Murphy DJ, Jr. Ultrasound examination of extracardiac chest masses in children. Doppler diagnosis of a vascular etiology. *J Ultrasound Med* 1987;**6**:151–7.

13 Lai WW, Geva T, Shirali GS, et al. Guidelines and standards for performance of a pediatric echocardiogram: a report from the Task Force of the Pediatric Council of the American Society of Echocardiography. *J Am Soc Echocardiog* 2006;**19**:1413–30.

14 Bierman FZ, Williams RG. Subxiphoid two-dimensional imaging of the interatrial septum in infants and neonates with congenital heart disease. *Circulation* 1979;**60**:80–90.

15 Lange LW, Sahn DJ, Allen HD, Goldberg SJ. Subxiphoid cross-sectional echocardiography in infants and children with congenital heart disease. *Circulation* 1979;**59**:513–24.

16 Sanders SP, Bierman FZ, Williams RG. Conotruncal malformations: diagnosis in infancy using subxiphoid 2-dimensional echocardiography. *Am J Cardiol* 1982;**50**:1361–7.

17 Limacher MC, Gutgesell HP, Vick GW, et al. Echocardiographic anatomy of the Eustachian valve. *Am J Cardiol* 1986;**57**:363–5.

18 Silverman NH, Schiller NB. Apex echocardiography. A two-dimensional technique for evaluating congenital heart disease. *Circulation* 1978;**57**:503–11.

19 Tajik AJ, Seward JB, Hagler DJ, et al. Two-dimensional real-time ultrasonic imaging of the heart and great vessels. Technique, image orientation, structure identification, and validation. *Mayo Clin Proc* 1978;**53**:271–303.

20 DiSessa TG, Hagan AD, Isabel-Jones JB, et al. Two-dimensional echocardiographic evaluation of discrete subaortic stenosis from the apical long axis view. *Am Heart J* 1981;**101**:774–82.

21 Lang RM, Badano LP, Mor-Avi V, et al. Recommendations for cardiac chamber quantification by echocardiography in adults: an update from the American Society of Echocardiography and the European Association of Cardiovascular Imaging. *J Am Soc Echocardiogr* 2015;**28**:1–39.e14.

22 Tanaka M, Neyazaki T, Kosaka S, et al. Ultrasonic evaluation of anatomical abnormalities of heart in congenital and acquired heart diseases. *Br Heart J* 1971;**33**:686–98.

23 Zema MJ, Caccavano M. Two dimensional echocardiographic assessment of aortic valve morphology: feasibility of bicuspid valve detection. Prospective study of 100 adult patients. *Br Heart J* 1982;**48**:428–33.

24 Jureidini SB, Marino CJ, Waterman B, et al. Transthoracic Doppler echocardiography of normally originating coronary arteries in children. *J Am Soc Echocardiog* 1998;**11**:409–20.

25 Zeppilli P, dello Russo A, Santini C, et al. in vivo; detection of coronary artery anomalies in asymptomatic athletes by echocardiographic screening. *Chest* 1998;**114**:89–93.

26 Clouse M, Cailes C, Devine J, et al. What is the feasibility of imaging coronary arteries during routine echocardiograms in children? *J Am Soc Echocardiog* 2002;**15**:1127–31.

27 Harada K, Tamura M, Toyono M, Takada G. Noninvasive visualization and measurement of great cardiac vein flow by transthoracic Doppler echocardiography in normal children. *Am J Cardiol* 2001;**88**:710–13.

28 Allen HD, Goldberg SJ, Sahn DJ et al. Suprasternal notch echocardiography. Assessment of its clinical utility in pediatric cardiology. *Circulation* 1977;**55**:605–12.

29 Sahn DJ, Allen HD, McDonald G, Goldberg SJ. Real-time cross-sectional echocardiographic diagnosis of coarctation of the aorta: a prospective study of echocardiographic-angiographic correlations. *Circulation* 1977;**56**:762–9.

30 Snider AR, Silverman NH. Suprasternal notch echocardiography: a two-dimensional technique for evaluating congenital heart disease. *Circulation* 1981;**63**:165–73.

31 Murdison KA. Ultrasonic imaging of vascular rings and other anomalies causing tracheobronchial compression. *Echocardiography* 1996;**13**:337–56.

32 McDonald RW, Rice MJ, Reller MD, et al. Echocardiographic imaging techniques with subcostal and right parasternal longitudinal views in detecting sinus venosus atrial septal defects. *J Am Soc Echocardiog* 1996;**9**:195–8.

33 Marino B, Ballerini L, Marcelletti C, et al. Right oblique subxiphoid view for two-dimensional echocardiographic visualization of the right ventricle in congenital heart disease. *Am J Cardiol* 1984;**54**:1064–8.

34 Isaaz K, Cloez JL, Danchin N, et al. Assessment of right ventricular outflow tract in children by two-dimensional echocardiography using a new subcostal view. Angiocardiographic and morphologic correlative study. *Am J Cardiol* 1985;**56**:539–45.

35 de Leva F, Caso P, Calabro R, et al. Tetralogy of Fallot. Subcostal approach in bidimensional echocardiography. *G Ital Cardiol* 1984;**14**:113–20.
36 Chin AJ, Yeager SB, Sanders SP, et al. Accuracy of prospective two-dimensional echocardiographic evaluation of left ventricular outflow tract in complete transposition of the great arteries. *Am J Cardiol* 1985;**55**:759–64.
37 Cohen MS, Jacobs ML, Weinberg PM, Rychik J. Morphometric analysis of unbalanced common atrioventricular canal using two-dimensional echocardiography. *J Am Coll Cardiol* 1996;**28**:1017–23.
38 Zoghbi WA, Enriquez-Sarano M, Foster E, et al. Recommendations for evaluation of the severity of native valvular regurgitation with two-dimensional and Doppler echocardiography. *J Am Soc Echocardiog* 2003;**16**:777–802.
39 Fisher SD, Easley KA, Orav EJ, et al. Mild dilated cardiomyopathy and increased left ventricular mass predict mortality: the prospective P2C2 HIV Multicenter Study. *Am Heart J* 2005;**150**:439–47.
40 Daubeney PE, Blackstone EH, Weintraub RG, et al. Relationship of the dimension of cardiac structures to body size: an echocardiographic study in normal infants and children. *Cardiol Young* 1999;**9**:402–10.
41 Sluysmans T, Colan SD. Theoretical and empirical derivation of cardiovascular allometric relationships in children. *J Appl Physiol* 2005;**99**:445–57.

PART II

Quantitative Methods

CHAPTER 5

Structural Measurements and Adjustments for Growth

Steven D. Colan[1] and Leo Lopez[2]

[1] Harvard Medical School; Boston Children's Hospital, Boston, MA, USA

[2] Stanford University School of Medicine Stanford, CA; Lucile Packard Children's Hospital Standford, Palo Alto, CA, USA

Introduction

Observations of the developing cardiovascular system date from antiquity, with Aristotle's description of the beating heart in a chicken egg. However, quantitative description of the cardiovascular system was a key step on the path to modern cardiology. The development of measurement techniques, beginning in the nineteenth century, combined with the ability to treat heart lesions beginning in the mid-twentieth century, spurred interest in accurate diagnosis and in methods correlating structure and function of the cardiovascular system with clinical outcomes.

Determination of the sizes of cardiovascular structures is mandatory for adequate diagnosis and treatment of acquired and congenital cardiac disease [1]. For many cardiac disorders, these quantitative variables are highly predictive of outcome and provide critical information about response to therapy, timing of intervention, and, most importantly, which type of intervention is likely to have the optimum outcome. However, changes in the size and shape of cardiovascular structures can be secondary to factors other than the disease process, and methods are therefore required to differentiate these potential confounders. These issues are particularly evident in children, where somatic growth and maturation can potentially confound detection of disease or treatment effects.

Recommendations for standardization of measurements in children were published in 2010 by the American Society of Echocardiography [2]. These recommendations included reporting the size and function of cardiovascular structures as the number of standard deviations from the population mean value (z-score) relative to age or body size, depending on which of these independent variables is the primary physiologic determinant. Normative values for echocardiographic measurements that are derived from data collected at Boston Children's Hospital, measured in accordance with the American Society of Echocardiography recommendations are available at https://zscore.chboston.org. The methods of data collection and analysis have been previously published [3,4]. Essential to understanding the reliability of these measurements is documentation of their reproducibility, and the intraobserver, interobserver, and interacquisition variability has also been systematically evaluated [5]. These studies provide the foundation for a recently established normative database of echocardiographic measurements in a large cohort of healthy children in North America as part of the Pediatric Heart Network (PHN) Echo Z-Score Project [6]. Here we present a general discussion of the issues surrounding adjustment of cardiovascular structures for age and body size and the methods that were used in the derivation of the models in the PHN project.

The application and clinical utility of normative data (z-scores) ultimately depend on the ability to predict outcomes. A severely dilated left ventricle (LV) with a z-score >4 standard deviations (SD) above the normal mean can be compatible with long-term survival and normal functional capacity, whereas ventricular hypoplasia with a z-score <-4 is not tolerated even in the short term. An additional caveat to the interpretation of z-score values is that the relationship between degree of abnormality and outcome is highly variable and disease specific, and evolves continuously depending on available therapies. For example, based on data in patients with neonatal critical aortic valvar stenosis, in 1991 we derived an equation based on the sizes of the mitral valve, aortic root, and length of the LV relative to body surface area (BSA) that predicted survival after balloon dilation of the aortic valve with 95% accuracy [7]. However, this predictive capacity was rapidly rendered obsolete due to therapeutic advancements in the field that achieved survival in patients who were previously considered candidates only for single ventricle repair or cardiac transplantation. Ultimately, the statistical degree of abnormality of size and function of a cardiovascular structure is a mathematically determinable, static quantity.

Echocardiography in Pediatric and Congenital Heart Disease: From Fetus to Adult, Third Edition. Edited by Wyman W. Lai, Luc L. Mertens, Meryl S. Cohen and Tal Geva.

Companion website: www.wiley.com/go/lai-echo3

In contrast, the implications these abnormalities have for outcomes are disease specific, continuously evolving, and associated with an evolving predictive capacity.

Physiologic principles underlying cardiovascular dimensions

The relation of cardiovascular dimensions to body size and age can be observed empirically and analyzed statistically, based on measurements of cardiac and vascular structures derived from imaging data such as echocardiography. The study of the relative growth of a part of an organism in relation to the growth of the entire organism is known as allometry, and therefore here we are concerned with cardiovascular allometry. Although cardiac computed tomography, magnetic resonance imaging, and catheterization also provide quantitative assessment of cardiac structures, these modalities involve greater risk and cost. Therefore, echocardiography remains the primary source of empirical normative pediatric allometric data. Allometric relations can also often be predicted theoretically from basic physiologic principles. These two approaches can be used for purposes of reciprocal verification. A higher level of confidence can be attached to conclusions that are based on concordance of established physiologic principles and empirical methods. We have previously performed such a comprehensive analysis focused primarily on vascular structures [3] and summarize the results here.

The development and maintenance of optimum geometric properties of the vascular pathways is essential to provide adequate blood flow over a wide range of body activities, while simultaneously avoiding excess hemodynamic stress. Optimized design of biological structures as a result of the environmental pressure exerted by natural selection is an established principle of biology that explains the curvilinear relation of the weight of a tree and the size of its branches [8], the relation between the diameters of pulmonary bronchi and bronchial air flow, and the shape of eggs [9–11]. Energy efficiency for the vascular system is maximized when the vascular size minimizes the energy required to propel blood through the vascular system by optimizing the relationship between vessel radius and flow rates. Theoretical foundations of the principle of minimum work [12,13] and optimality of the vascular system based on Murray's law [14–19] have been validated by the quantitative studies of coronary [20] and cerebral arterial dimensions [21]. The theoretical aspects and details of these calculations have been described in detail [14,20,21].

The principle of minimum work

The energy cost of phasic blood flow is determined by two components. Viscous energy loss [22,23] in blood vessels is related to friction between flowing blood and the vessel wall at the endothelial vessel–blood interface. This energy loss decreases with increasing vessel diameter due to the geometric relationship between vascular cross-sectional area and vascular surface area. The volume of blood within a cylindrical blood vessel increases in proportion to the square of the radius whereas the surface area increases in direct proportion to the radius. Therefore, the proportion of blood in contact with a viscous interface decreases as the radius increases, which means there is proportionally less resistance to flow in large vessels. The second component of energy loss is due to the oscillatory nature of blood flow in the central arterial tree. The oscillatory component of energy loss is related to the need to accelerate flow with every beat (kinetic energy that is lost during the deceleration phase), and this oscillatory component increases in proportion to the volume of blood that undergoes cyclic acceleration and deceleration. The optimal vascular dimension is that at which the sum of these two competing energy costs is minimized (Figure 5.1a). We estimated the viscous energy loss and the inertial energy content of blood flow for the aorta and the main pulmonary artery over the typical range of body surface area (BSA, 0.2–1.8 m^2) and over the range of cardiac output (CO) encountered during physical activity (from 3.5 L/min/m^2 to 17.5 L/min/m^2) in order to determine the optimal vessel size [3]. We found that the size of the aorta that we observed in our normal population corresponded to the theoretical optimal value in terms of energy dissipation for CO up to two times the resting CO in infants, increasing to values that were optimal for three to four times the resting CO for older children (Figure 5.1b). Data obtained from athletes and hypertensive subjects indicate that cardiac structures adapt to peak levels of pressure and volume demand. Heart rate response is the primary determinant of CO increase with exertion, and infants have an approximately twofold magnitude of heart rate reserve, a value that increases to three- to fourfold in older children and young adults. Thus, the difference between observed diameters that are optimal in terms of energy dissipation in infants versus children corresponds to the expected difference in CO associated with age-appropriate physical activity and range of intensity of exertion.

Allometric modeling

Many disease processes result in a change in the size or function of cardiovascular structures, and quantitative assessment of these changes is diagnostically and prognostically useful. However, the usefulness of these measurements is limited by the confounding effects of growth and other factors that influence LV size. In general, cardiovascular structures are highly plastic and are known to remodel in response to variations in the hemodynamic state related to a large number of interacting factors such as growth, development, exercise participation, genetics, body composition, basal metabolic rate, and hematocrit, in addition to many environmental factors such as altitude and ambient temperature. Although many of these factors are difficult to quantify, body size and age are two of the most potent determinants, particularly in children, and are readily quantifiable. Therefore, considerable effort has been devoted to the study

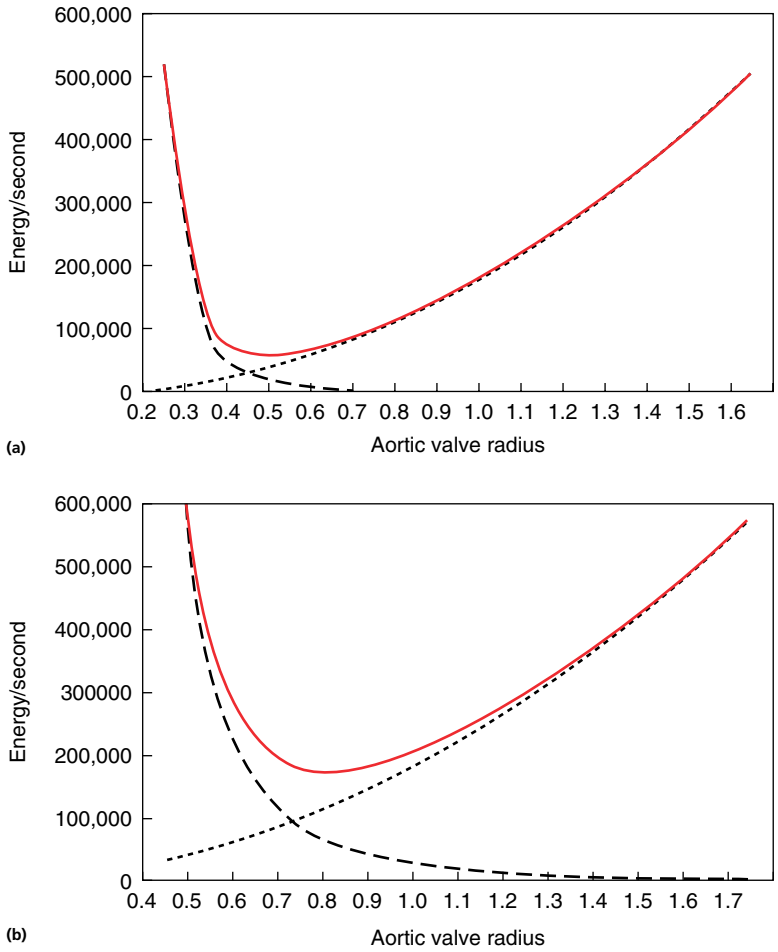

Figure 5.1 Optimal aortic valve radius calculated according to the principle of minimal work for two levels of cardiac output. Energy loss per second (erg/s) secondary to viscous friction (descending dashed line) is plotted against the radius of the aortic valve (cm). On the same scale, the inertial energy content of blood (ascending dashed line) and the total energy loss calculated as the sum of viscous energy loss and inertial energy content loss (continuous red line) are plotted for theoretical cardiac outputs (QS) of 3.5 L/min **(a)** and 17.5 L/min **(b)**, representing the theoretical cardiac output at rest and at maximal exercise of a normal subject with a body surface area (BSA) of 1 m^2. The least amount of total energy loss per unit time corresponds to the minimum of the total energy loss curve. The corresponding radius for 3.5 L/min flow is 0.45 cm and for 17.5 L/min it is 0.8 cm. These values represent the theoretical range of normal optimal aortic valve radius for this BSA. *Source*: Sluysmans T, Colan SD. Theoretical and empirical derivation of cardiovascular allometric relationships in children. *J Appl Physiol* 2005;99:445–57. The American Physiological Society.

of the relationship between the size of cardiovascular structures and both age and body size.

In addition to the implications of allometry for patient care, adjustment for the effects of changes in body size also has important implications for clinical research. Although clinical investigators attempt to avoid potential confounders by selection of a properly matched control group, if the disease or the therapeutic intervention can impact growth, detection of beneficial effects due to the therapeutic intervention can be confounded by differences in somatic growth between the intervention and control groups. For example, consider a study undertaken to determine if a novel medical therapy can favorably alter the severity of LV dilation in infants with dilated cardiomyopathy. We know that treatments may have different effects on somatic growth, either directly or secondary to improved cardiovascular status. Even if active and placebo treated cohorts are matched for age and BSA at the time of study enrollment, the differential impact of somatic growth on LV size could confound the interpretation of the direct effects of disease treatment on LV size if the proportion of change in LV size attributable to somatic growth cannot be quantified. Thus, adjusting for the effects of somatic size is critical to evaluating therapeutic benefit.

The fallacy of indexing for body surface area (BSA): the so-called "per-BSA method"

Historically, the most common approach to adjusting cardiovascular structures for body size has been to calculate their ratio relative to BSA. For example, "cardiac index" is calculated as CO divided by BSA, and "left ventricular mass index" is frequently calculated as LV mass (LVM) divided by BSA, although alternative methods of adjusting LVM for body size have been

recommended. Because the term "left ventricular mass index" is ambiguous, it is not used in this chapter and the specific formula is shown, such as LVM/BSA, LVM/BSA$^{1.33}$, LVM/height$^{2.7}$, etc. Current recommendations in the adult guidelines published by the American Society of Echocardiography are to adjust LV mass and volumes in adults using these "per-surface area standards" [24] despite their demonstrated lack of validity [25–28]. For "indexing" to be successful, the indexed variable must be invariant with changes in the indexing variable.

The genesis of the "per-BSA" approach is the observation that in numerous intra- and inter-species studies, body heat production and CO are linearly related to BSA over a broad range of body sizes [29,30]. Consequently, cardiac index has been adopted as a reasonably valid method of comparing the CO of individuals of varying BSA. Next, based on regression models that found a nearly linear relationship between CO and the size of other cardiac and vascular structures in adults, the per-BSA method was extrapolated and adopted by many as a general method for adjusting for the effects of body size on all cardiovascular structures.

Unfortunately, although the relationship between two variables can often be described as nearly linear, this does not mean that this is the best descriptor of their relationship. The mathematical inadequacy of this method can be readily recognized by a simple example. There are many studies documenting a statistically significant linear relationship between LV volume and BSA, and a statistically significant linear relationship between LV short-axis dimension and BSA. However, volume and dimension are related by a cubic function, and it is therefore mathematically impossible for both volume and dimension to have a true linear relationship to BSA. The delusion that the per-BSA method is adequate in adjusting for the effects of body size is based on excess reliance on simple linear regression analysis performed over short ranges of the independent variable (BSA) in the absence of critical examination of how well the mathematical model actually describes the data and whether these results align with physiological underpinnings [31,32].

It is reasonably straightforward to statistically test whether an allometric model provides an adequate description of the relationship between body size and the size of the body part. The intent of "indexing" or "normalizing" a variable such as CO for BSA is to permit valid comparisons between individuals of differing BSA by eliminating any residual dependence of the indexed variable on BSA. Therefore, if the method of indexing or adjusting for body size fully accounts for the effect of body size on the cardiovascular measurement, then the indexed variable will have the same mean value regardless of body size.

It is worth considering a concrete example of how easily one can be misled by a high correlation coefficient obtained by linear regression. Figure 5.2a presents the strong linear relationship ($R^2 = 0.88$) between the diameter of the aortic valve annulus (AVD) and BSA in 1365 normal children evaluated at Boston Children's Hospital varying in age from newborn to 18 years of age and varying in BSA from 0.18 to 2.3 m^2. Such observations, in the absence of careful testing for whether this linear model eliminates residual dependence of AVD on BSA, have led to the common method of a per-BSA approach with "indexed aortic valve diameter" calculated as AVD divided by BSA. However, Figure 5.2b demonstrates the inadequacy of the per-BSA method for this variable because a curvilinear (power) function provides a significantly better correlation for the AVD diameter versus BSA relationship. Figure 5.2c illustrates the mathematically equivalent form of the relation in Figure 5.2b as the regression of AVD versus BSA$^{0.5}$, which results in a linear fit with the intercept passing through the origin. The aortic valve dimensions

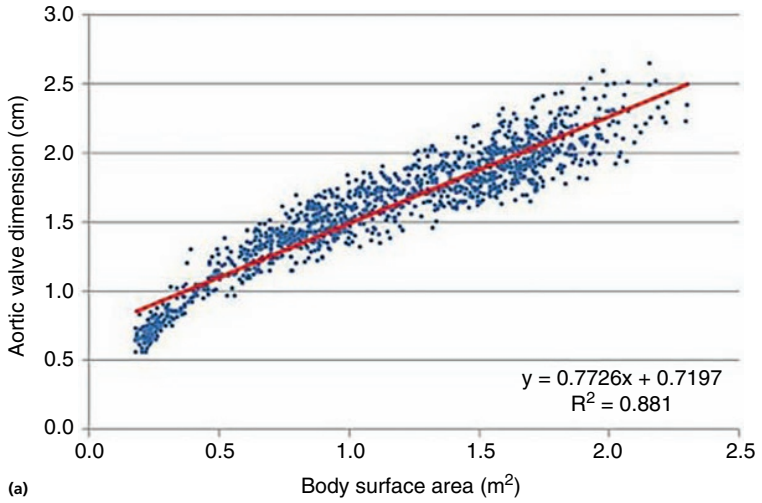

Figure 5.2 **(a)** The linear regression line for aortic valve dimension (AVD) versus body surface area (BSA) in normal children shows a high correlation with a non-zero intercept. **(b)** The regression for AVD versus BSA is optimal for the nonlinear function AVD = a × BSA$^{0.5}$. **(c)** The regression of AVD versus BSA$^{0.5}$ is linear with a zero intercept. **(d)** The regression of AVD/BSA$^{0.5}$ versus BSA demonstrates a constant mean and standard deviation.

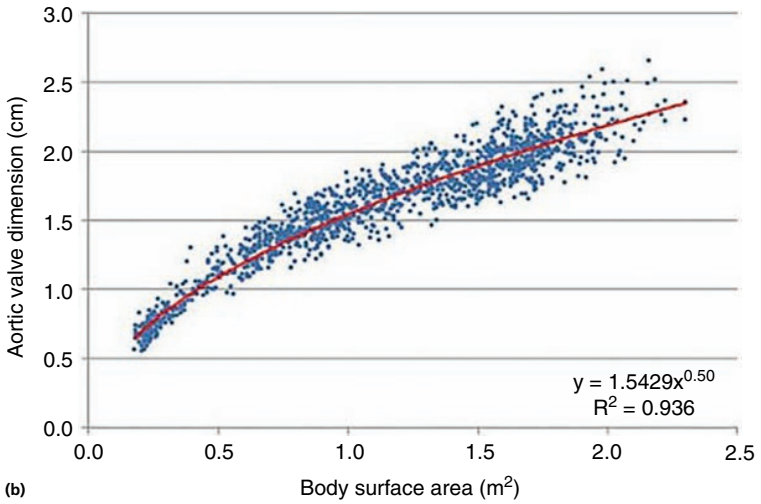

(b)

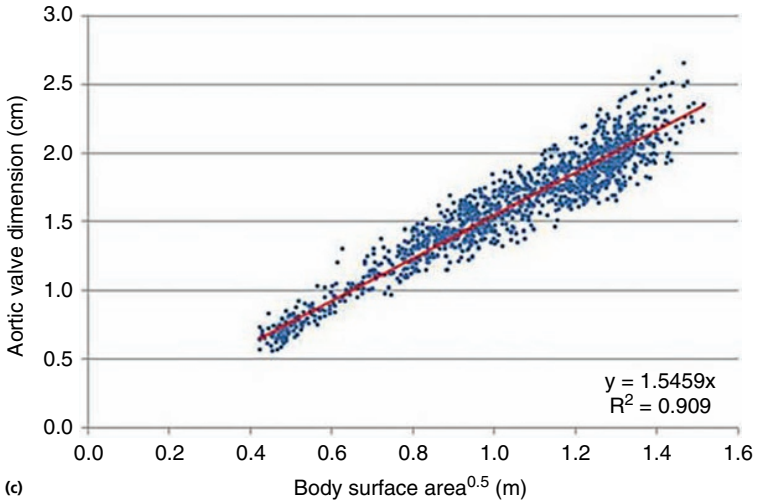

(c)

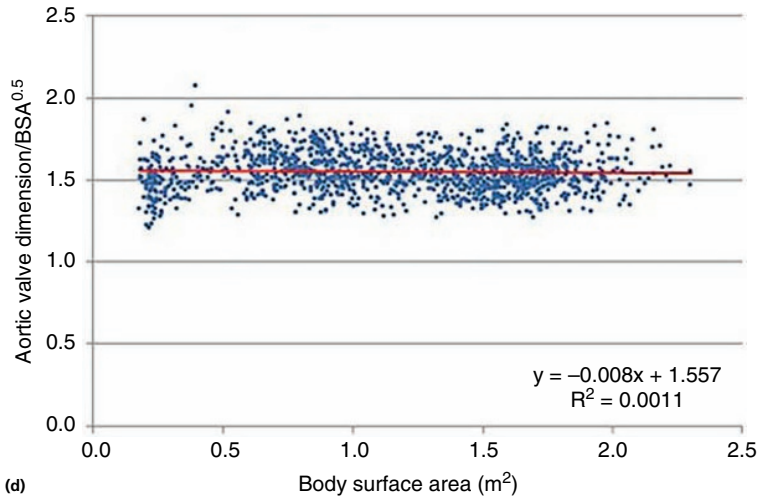

(d)

Figure 5.2 (Continued)

are seen to have a progressive increase in the residuals (the distance of the points from the regression line). When AVD/BSA$^{0.5}$ is regressed against BSA (Figure 5.2d), there is no significant residual relation between the "indexed" AV dimension and BSA (that is, the slope of the regression line is not significantly different from zero), and there is also no significant relation between the residuals and BSA, indicating that heteroscedasticity (variability of the predicted variable) across the range of BSA has also been eliminated. This is the goal for a correctly "indexed" variable – the mean and standard deviation are constant over the data range.

Alternative "indexing" methods

The inadequacy of the per-BSA method has led investigators to evaluate other approaches to adjusting for the effect of body size on the size of cardiovascular structures. The first and simplest is to attempt to linearize the relationship by mathematically transforming either the cardiovascular structure, BSA, or both. The observation that the cross-sectional areas of vascular structures relate linearly to BSA predicts that their diameters should relate linearly to the square root of BSA (BSA$^{0.5}$). It has also been suggested that this approach can be generalized [3] such that linear measurements should be normalized to BSA$^{0.5}$, area measurements should be normalized to BSA$^{1.0}$, and volume measurements should be normalized to BSA$^{1.5}$. Although this approach fails with cardiac chamber measurements (as discussed in the section "Adjustment of cardiac chamber size and LV mass for somatic growth"), the relationships of the central arterial dimensions follow this paradigm for dimensions and cross-sectional areas. As shown in Figure 5.2c, AVD versus BSA$^{0.5}$ is indeed highly linear with a zero intercept, and the graph of AVD/BSA$^{0.5}$ versus BSA (Figure 5.2d) shows that indexing AVD to BSA$^{0.5}$ eliminates residual dependence of the aortic valve diameter on BSA.

Adjustment of cardiac chamber size and left ventricular mass for somatic growth

Although vascular and valvar dimensions scale to BSA$^{0.5}$ and vascular and valvar cross-sectional areas scale to BSA$^{1.0}$, chamber sizes, specifically atrial and ventricular volumes and ventricular mass, do not scale to BSA$^{1.5}$, which would be the anticipated result if all normalized variables were dimensionless (cm/m, cm^2/m^2, and cm^3/m^3) [4].

However, despite the assertion by some investigators [33] that the relation between BSA and both LV mass (LVM) and volume must be BSA$^{1.5}$, in fact the empirically observed relation documented by numerous investigators is that LV end-diastolic volume (EDV) and LVM relate most closely to BSA^b where mean b ~1.33 (range 1.25–1.35) [3,6]. For 1436 normal children evaluated at Boston Children's Hospital, we found BSA$^{1.33}$ to be the optimum scaling transform for left ventricular EDV (Figure 5.3), which is in close agreement to the exponent (1.3) identified in the larger multicenter PHN study [6]. The explanation for this failure to follow the same scaling paradigm is the nonlinear decrease in heart rate associated with increasing BSA and age. In the normal population the relations of age and BSA to heart rate are similar, although BSA is likely the more important physiologic determinant based on the impact of height on pulse wave reflections [34]. The mathematics of this relationship are as follows: CO = ejection fraction × EDV × heart rate, and since (i) ejection fraction is invariant with age and BSA, and (ii) CO varies in proportion to BSA$^{1.0}$, it follows that heart rate × EDV must vary in proportion to BSA$^{1.0}$. Therefore, the empirically observed

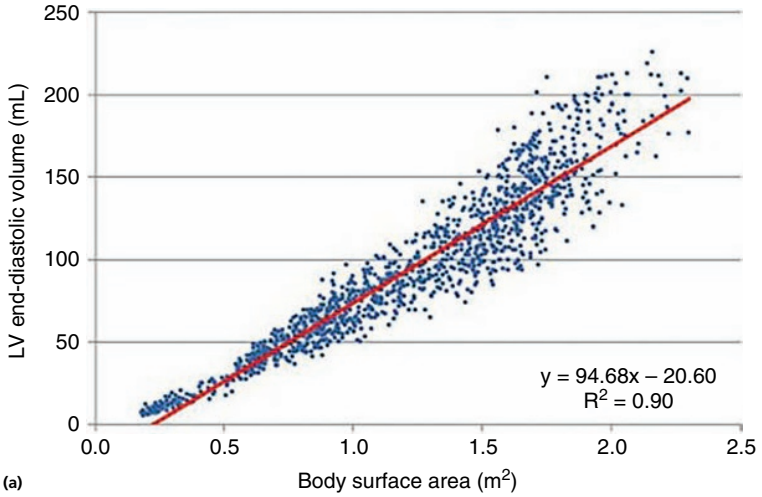

Figure 5.3 **(a)** The relationship between left ventricular (LV) end-diastolic volume (EDV) and body surface area (BSA) is nearly linear but the intercept is non-zero. **(b)** EDV/BSA has a significant residual correlation with BSA. **(c)** EDV has a higher linear correlation coefficient to BSA$^{1.33}$ and a zero intercept. **(d)** Regression of EDV/BSA$^{1.33}$ versus BSA eliminates the dependence of the normalized variable on BSA.

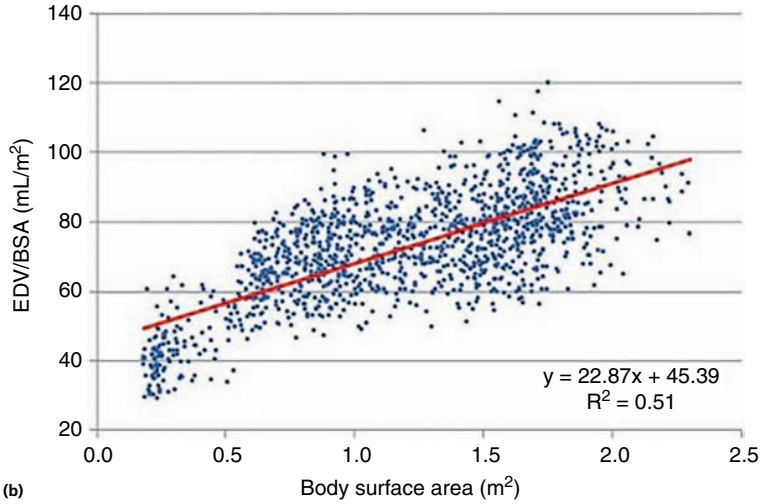

(b)

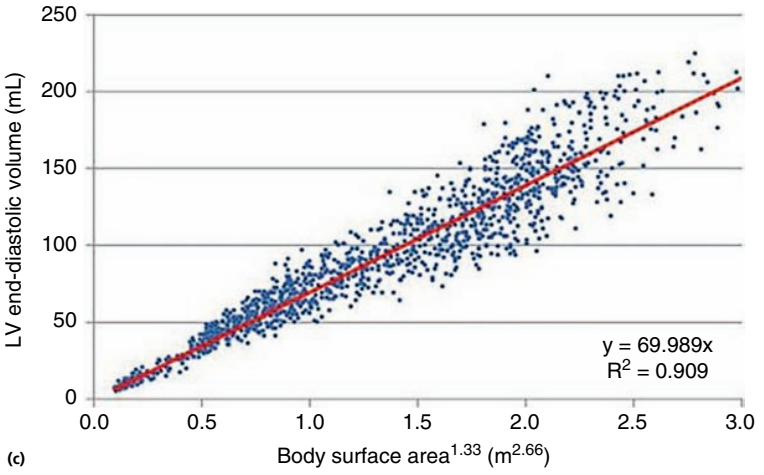

(c)

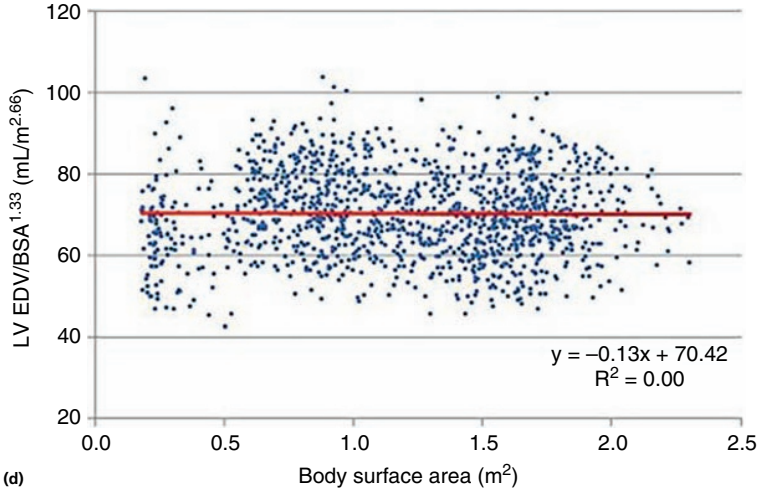

(d)

Figure 5.3 (Continued)

fact that EDV varies in proportion to $BSA^{1.33}$ means that heart rate must vary in proportion to $BSA^{-0.33}$ in order for their product to vary in proportion to $BSA^{1.0}$. As seen in Figure 5.4, adjusting heart rate for body size as $HR/BSA^{-0.33}$ eliminates any significant residual relationship between heart rate and BSA.

The normal relationship between LVM and body size has been an area of considerable interest due to the documented adverse impact of LV hypertrophy (LVH) associated with a variety of disorders, particularly hypertension [35]. As illustrated in Figure 5.5a, LVM has virtually the same relationship to $BSA^{1.0}$ as that of EDV, with a correlation coefficient of 0.9. Nonetheless, as shown in Figure 5.5b, LVM/BSA has significant persistent residual dependence on BSA. When LVM is indexed to $BSA^{1.33}$ (Figure 5.5c) rather than $BSA^{1.0}$, the linear regression line passes through the intercept but the correlation coefficient is not significantly improved. Nonetheless, as shown in Figure 5.5d, despite the marginal improvement in the correlation coefficient, indexing LVM to $BSA^{1.33}$ eliminates any residual dependence of LVM on BSA, demonstrating that excessive reliance on correlation coefficient rather than residuals analysis can be misleading. Similarly, and perhaps more importantly, as shown in Figure 5.5e, despite the fact that indexing LVM to $BSA^{1.5}$ results in a higher correlation coefficient than the regression against $BSA^{1.33}$, indexing LVM relative to $BSA^{1.5}$ fails to eliminate the dependence of indexed LVM on BSA and results in a significant inversely linear relationship, again demonstrating that excessive reliance on the correlation coefficient can be misleading when trying to define the optimum normalizing variable. A successfully "indexed" variable will have a mean value that is invariant over the range of the indexing variable.

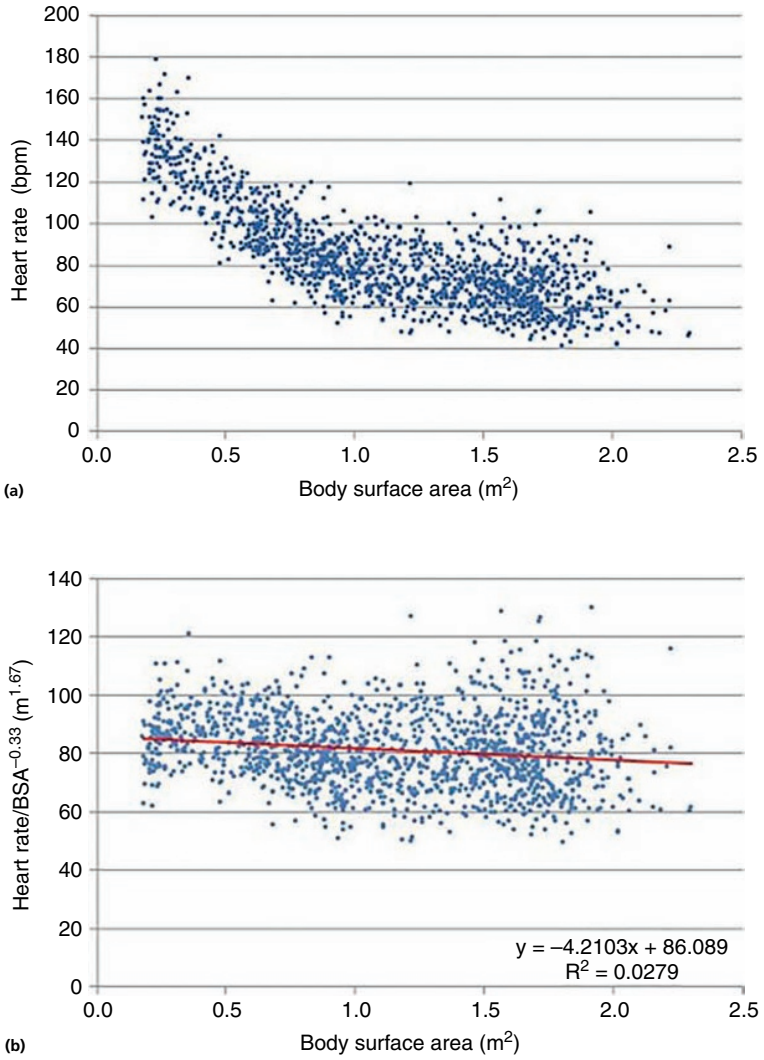

Figure 5.4 **(a)** Heart rate has an inverse, nonlinear relationship to body surface area (BSA) which is upwardly concave. **(b)** When heart rate is indexed by $BSA^{-0.33}$, the significant residual dependence on BSA is eliminated.

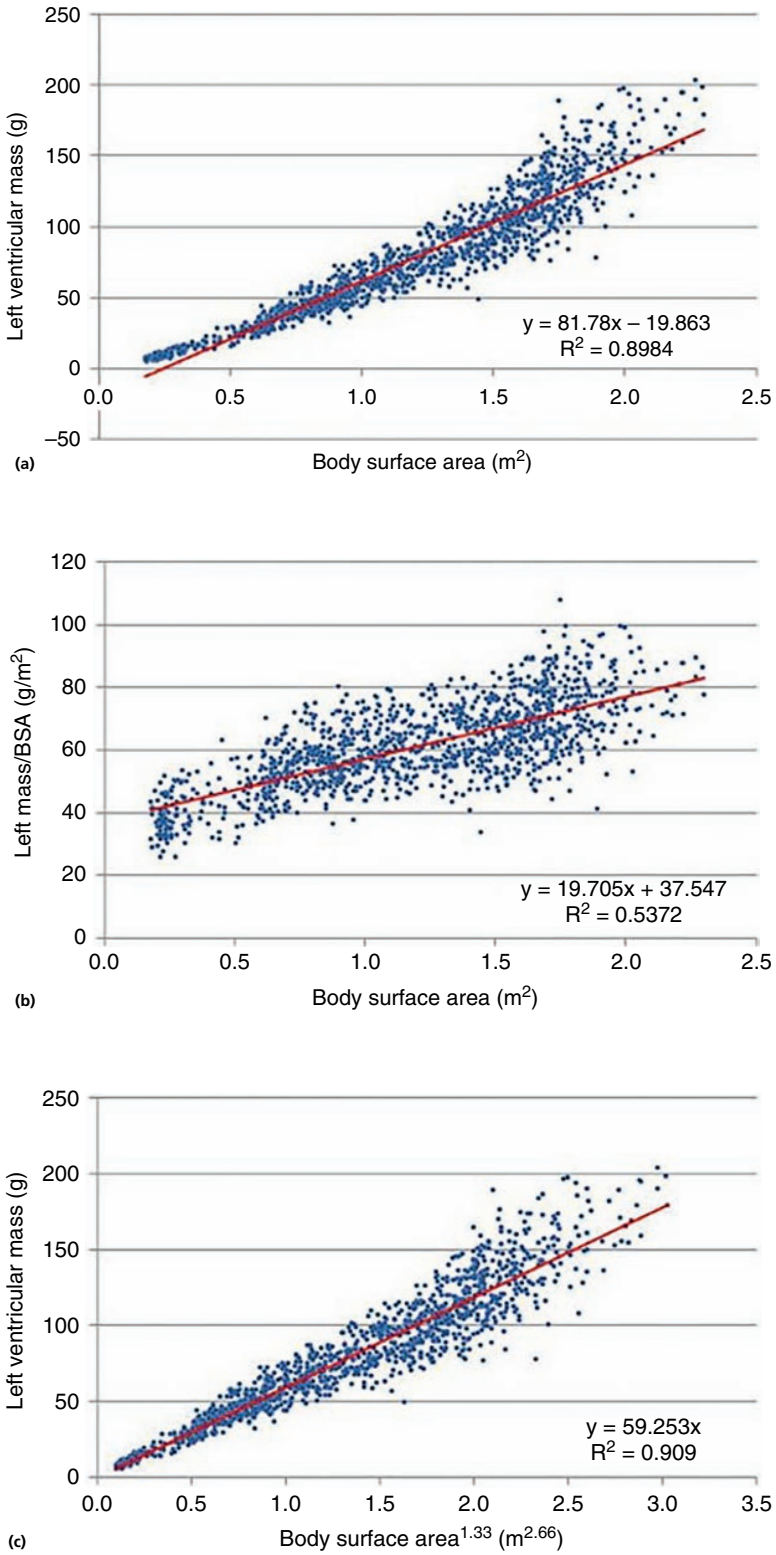

Figure 5.5 **(a)** Left ventricular mass (LVM) has a nearly linear relationship to body surface area (BSA) with a correlation coefficient of 0.9. **(b)** LVM/BSA has significant persistent dependence on BSA. **(c)** LVM has a highly linear relationship to $BSA^{1.33}$ with a correlation coefficient that is not significantly improved compared to $BSA^{1.0}$. **(d)** Despite the marginal improvement in the correlation coefficient, $LVM/BSA^{1.33}$ has no residual dependence on BSA. **(e)** $LVM/BSA^{1.5}$ has a higher correlation coefficient than the regression relative to $BSA^{1.33}$. **(f)** Despite a higher correlation coefficient, $LVM/BSA^{1.5}$ is significantly dependent on BSA.

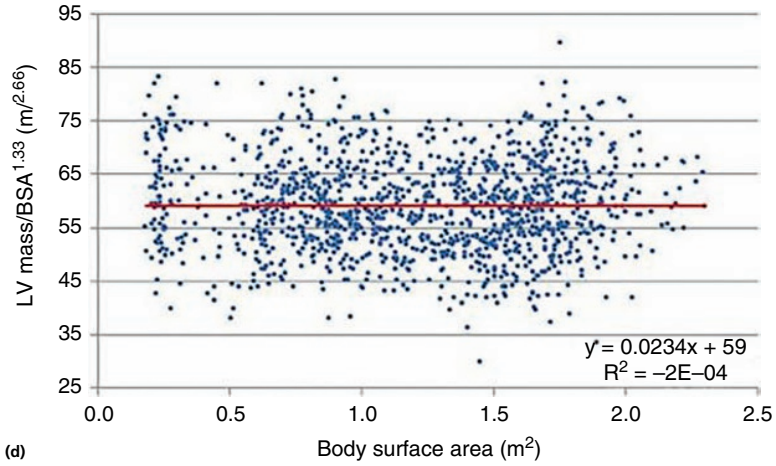

(d)

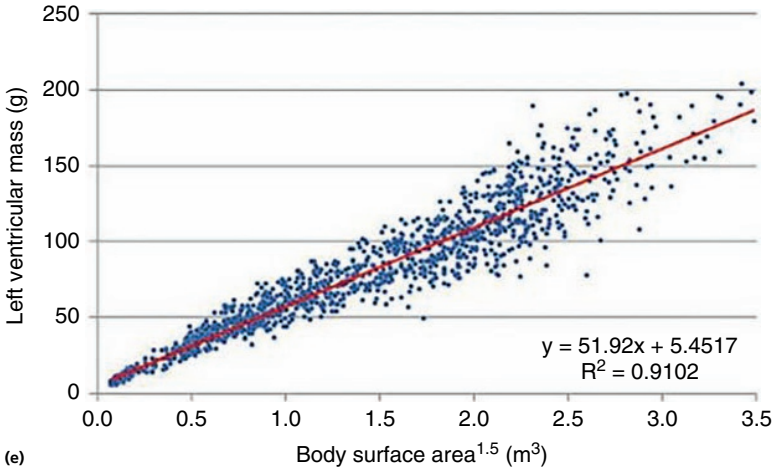

(e)

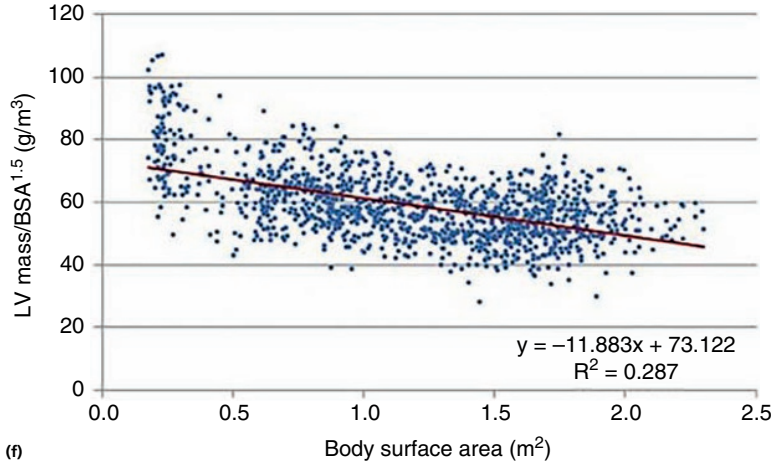

(f)

Figure 5.5 (Continued)

The relationship of LVM to BSA is empirically the same as EDV, as shown in Figures 5.3 and 5.5, where 1.33 is the scaling exponent for BSA that eliminates residual dependency of LVM/$BSA^{1.33}$ on BSA, whereas $BSA^{1.0}$ and $BSA^{1.5}$ fail to eliminate the dependency of the "indexed" variable on body size.

Z-score methods

The failure of simpler methods (such as BSA-indexing) to adequately account for the relationships between body size and the sizes of cardiovascular structures has resulted in an expanding reliance in the pediatric community on the use of *z-scores*, also known as *normal deviates* or *standard scores*, to adjust for the effect of age and/or body size on the size of cardiovascular structures [36]. The z-score of a variable is the position, expressed in SD, of the observed case relative to the mean of the population distribution. For cardiovascular structures, the calculation of z-scores is performed relative to the distribution of the structure in the normal population in order to adjust for the normal relationship to age or some parameter of body size.

Z-scores are normalized variables such that a z-score of zero represents a value at the normal population mean and a z-score of 1 or −1 represents a value that is 1 SD above or below the normal mean. The z-score can be mathematically converted to a percentile and the interpretation of z-scores is parallel to the use of percentiles. In the case of height and weight, calculation of percentiles adjusts for the normally expected age-related change in height or weight, permitting comparison of subjects at varying ages. Although z-scores can be readily converted to percentiles, their reporting as SD is generally preferable as they avoid range compression in the higher and lower ranges. For example, a z-score of 4 (4 SD above the normal population mean) has a percentile of 99.8, whereas a z-score of 10 (10 SD above the population mean) has a percentile of 99.9. At values outside of the normal range, it is much easier to appreciate the magnitude of abnormality of a structure when it is expressed as a z-score. The z-score approach represents the most powerful and flexible approach to normalizing cardiovascular parameters for the effects of age and BSA and has therefore become the standard approach in pediatric cardiology [36].

There are, however, a number of potential confounders that can invalidate z-score calculations and must be accounted for. Nonconstant variance (heteroscedasticity) with respect to both age and body size has been demonstrated for virtually all echocardiographic measurements. Although the term "heteroscedasticity" is unfamiliar to most clinicians, the concept is not. As shown in Figure 5.3c, the data spread for EDV increases as the absolute value of BSA increases. This phenomenon of a nonconstant, continuously increasing variance of the dependent variable over the range of the independent variable is one type of heteroscedasticity. This pattern is seen with virtually all anatomic measurements, where the data spread increases progressively in conjunction with increasing values for the independent variable (age, height, weight, BSA, etc.).

Statistical methods for dealing with this phenomenon have received considerable attention, as discussed in some detail by Abbott and Gutgesell [31]. There are several statistical methods that can be used to reduce nonconstant variance when constructing confidence and prediction intervals. These methods include multivariable regression techniques [37], variance stabilizing transformations [31,36–39], and weighted least squares analysis [40]. Such statistical methods, although improving the accuracy of prediction intervals, are invariably ad hoc and lack a sound physiologic basis for choosing one method over another. In heart growth, data are skewed to the right, and logarithmic transformation is probably the most common type of transformation used in medical research for correcting heteroscedasticity and rightward skewed data [31]. For residuals that demonstrate a reasonably regular relationship to the independent variable, the method of Altman [41] has particular appeal of simplicity both in terms of calculation and interpretation. Regardless of the method that is selected, the end result must be tested to confirm that the final model results in an equal and constant distribution around the mean value over the full range of the independent variable, and that 96% of all data are included in the interval going from −2SD to +2SD.

Parametric versus statistical derivation of z-scores

The methods described in the foregoing assume that it is possible to define a continuous parametric equation that adequately describes the relationship between the size of the cardiovascular structure and either age or a measure of body size over the full range of the independent variable. This approach has the unique advantage of permitting conclusions concerning the nature of the physiologic relationship between somatic and cardiovascular growth. The fact that the cross-sectional areas of the central arteries and cardiac valves are highly correlated with BSA, and that BSA is highly correlated with CO, supports the concept that flow is a primary and reproducibly constant determinant of the growth of these structures. An alternative to this "physiologic" approach that has also been pursued is a purely statistical description of the data, which permits derivation of z-scores but does not provide any implications concerning the underlying physiologic mechanisms. For example, multiple linear regressions and the lambda-mu-sigma (LMS) method can be used to describe nonlinear data and have been used to calculate the z-scores and percentiles for height and weight data that are used in the Centers for Disease Control and World Health Organization growth charts for children [42–45]. The LMS method evaluates the population distribution over discrete intervals of the independent variable and then applies a smoothing function to the derived ranges to yield a description of the data that is a continuously varying function over the range of

the independent variable. The complex relationships between both height and weight lend themselves well to this approach. This technique is most advantageous when the determinants of the change in size of a cardiovascular structure are sufficiently heterogeneous that a single, physiologically-based relationship that adequately describes the data over the full range of the independent variable cannot be identified. The other advantage is that the variance of the data is determined locally rather than as a global function and nonconstant variance can be correctly reflected in the confidence intervals.

Several caveats concerning the determination of z-scores are in order. A number of recent reports have documented differences in published z-scores systems and have noted a failure on the part of some to meet criteria for clinical and statistical validity [46]. There are several important issues that arise in the determination of valid normative z-scores:

1 Selecting an appropriate population for determination of "normal" values is obviously critical, including assurance in addition to a "normal" echocardiogram that the patient is free of systemic disorders. For example, phenotypically "normal" subjects who carry pathogenic genes known to be associated with hypertrophic cardiomyopathy manifest patterns of high normal wall thickness and low normal tissue velocity, and inclusion of patients in this category could skew the normative ranges [47,48].
2 The population needs to include an appropriate normative range for BSA, BMI, and age as well as consideration of other potential demographic confounders such as sex and race.
3 The BSA formula used to calculate an individual z-score must be the same BSA formula used to establish the z-score model, a requirement that is often neglected. There are a number of published methods for calculating BSA and they yield different results, particularly at lower values. The formula with the soundest experimental basis is that of Haycock et al. [49]. In a systematic analysis of the normative data at Boston Children's Hospital in which we compared the amount of variance of the cardiovascular structures relative to BSA that could be explained by each of these formulas, we found that the Haycock formula performed best [3]. Unfortunately, the Du Bois formula, whose derivation included no children and yields invalid results in this population, remains in common use [50].
4 The method of measurement must be the same for the population from which the z-score regressions are derived and the population to which they are applied. For example, it is clear from a number of publications evaluating differences between echocardiographic and magnetic resonance imaging measurements of LV volume that values derived from magnetic resonance imaging are systematically larger than those from echocardiography, precluding the use of a common set of normative values [51]. Other issues include use of z-scores derived from M-mode for 2D LV dimension data, diastolic (the standard in adult labs) versus systolic (the standard in pediatric labs) measurement of aortic dimensions, leading edge-to-leading edge versus inner edge-to-inner edge measurements of vascular structures, and the multiple methods to calculate LV mass and volumes (from M-mode versus 2D measurements using the area–length approach versus single-plane or biplane Simpson's rule) that yield different values.
5 The resulting z-score algorithms need to optimize the quality of the data fit, and nonconstant variance (heteroscedasticity, as illustrated in Figure 5.3c) must be accounted for.
6 Finally, z-score methods that have both a physiologic justification and statistical validity are preferable to those that are based on statistical considerations alone. For example, higher order polynomial curve fits can be used to describe virtually any dataset, often with more significant correlation coefficients, but they are devoid of any physiologic justification. One of the primary uses of z-scores is not merely to evaluate the position of an individual within the population in which the z-scores were derived, but also to evaluate the presence and degree of abnormality in a new population. Extrapolation of the z-score values to a population other than that in which they were originally derived is more likely to be valid if there is a defined physiologic basis for the relationship that can be expected to be found in the new population. These two issues (physiologic validity and heteroscedasticity) are discussed in more detail in a subsequent section.

The Pediatric Heart Network Echo Z-Score Project

With many of these issues in mind, the PHN established z-score models using a normative echocardiographic database from 3215 healthy North American children [6]. The study population encompassed the full range of body sizes encountered in pediatrics divided equally by sex and by race (whites, African Americans, and an "other" category to account for all other racial groups). In addition, significant efforts were made to exclude children with systemic disorders or risk factors associated with heart disease or abnormal cardiovascular measurements. Using a physiologically valid approach to describe the relationship between cardiovascular size and body size by determining the appropriate BSA transformation (BSA^b), models were established that accounted for the nonconstant variance that is characteristic of cardiovascular growth. The most important study finding was that, in children, sex, race, and ethnicity do not have a clinically significant effect on z-scores adjusted for BSA, and this conclusion was achieved using a novel approach to distinguish statistical significance from clinical significance. Because of the large study sample size, confounding factors like age, sex, race, and ethnicity proved to have statistically significant effects on many of the z-score models. However, previously published estimates of echocardiographic measurement variability [5] provided thresholds of measurement differences that could be attributable to random error. In other words, a measurement difference that achieved statistical significance

may be within the range of expected variability for that particular measurement and is unlikely to represent a clinically meaningful difference.

Choice of normalizing variable and impact of adiposity on left ventricular mass

The selection of which parameter of body size, such as height, weight, or BSA, is optimal for the purposes of normalizing the size of cardiovascular structures has been controversial [52,53]. There is a large body of data indicating that in normal children and adults BSA performs better than height or weight alone [3]. However, use of BSA as the normalizing variable for LVM has been noted to result in underdetection of LVH in the presence of obesity [54–56]. The physiologic basis for this is well documented, and it relates to the fact that adipose tissue is less metabolically active than other tissues and therefore receives less blood flow [57]. Since CO is normally the primary determinant of the growth of cardiovascular structures, abnormal adiposity disrupts the normal relationship between BSA and CO such that, in obese individuals, CO (and therefore LVM) is actually lower than predicted for BSA. Therefore, adjusting LVM relative to BSA results in an underestimation of the severity of hypertrophy in the obese. Although less intensively investigated, this physiology predicts that abnormally low adiposity should be associated with an overestimate of LVH if LVM is adjusted for BSA.

The potential for LVM adjusted for BSA to underestimate severity of LVH has led to the recommendation in the 2017 guidelines for management of hypertension in children that, in the presence of obesity, LVM should be adjusted for height$^{2.7}$ (height-indexed LVM = LVM/height$^{2.7}$) instead of relative to BSA [58]. As seen in Figure 5.6a, LVM has a highly nonlinear relation to height. When LVM is "indexed" relative to height$^{2.7}$ (Figure 5.6b), there is a persistent, marked, nonlinear relation between LVM/height$^{2.7}$ and height, with a steep initial negative slope, indicating that this mode of indexing does not eliminate the dependence of LVM on height in young children. However, when the range of height is restricted to the adolescent and adult range (height >1.2 m), as seen in Figure 5.6c, the dependence of

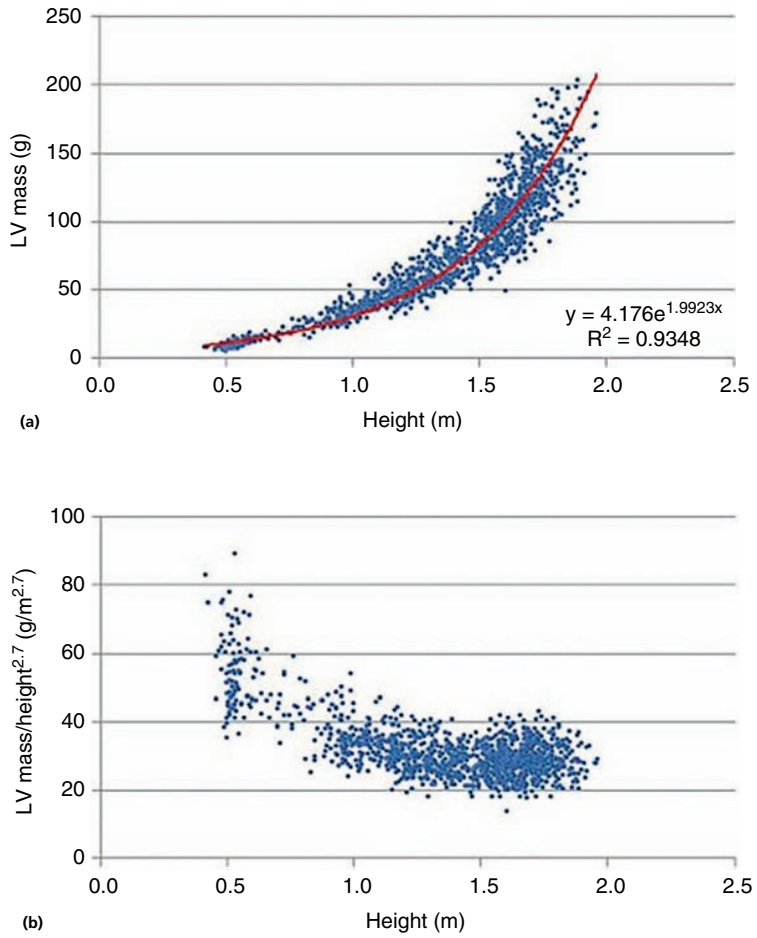

Figure 5.6 **(a)** Left ventricular (LV) mass has a direct, nonlinear dependence on height. **(b)** When the full range of height is included, LV mass/height$^{2.7}$ has a significant relationship to height. **(c)** When height is restricted to the near-adult range (>1.2 m), the residual dependence of LV mass/height$^{2.7}$ on height is eliminated. **(d)** LV mass/height$^{2.7}$ has a significant direct relationship to body mass index.

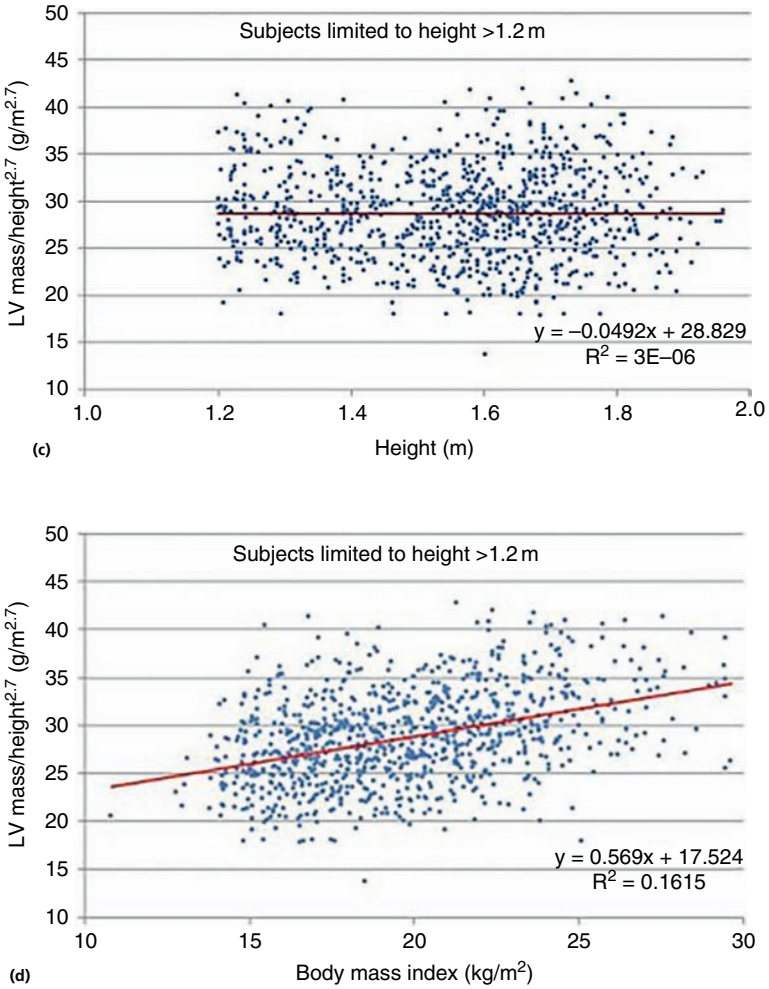

Figure 5.6 (Continued)

LVM/ height$^{2.7}$ on height is nearly eliminated. This observation has resulted in the recommendation that this method of adjusting LVM for body size be used in the obese. In fact, as shown in Figure 5.6d, when height$^{2.7}$ is used as the scaling variable, LVM/ height$^{2.7}$ demonstrates a progressive increase over the normal range of body mass index (BMI), which is the opposite of the physiologically predicted relationship where increasing adipose tissue is predicted to result in a lower cardiac index.

Alternatively, stroke volume and CO have been reported to relate more closely to fat-free mass [59]. Therefore fat-free mass has also been suggested as a potential allometric scaling variable in the obese [53]. However, fat-free mass is not generally measured in clinical practice, and normative data relative to this variable are not available. Furthermore, although the blood flow requirement of adipose tissue is less than lean tissue, adipose tissue is not inert and therefore the impact of adipose tissue on CO is non-zero. Indeed, both fat and fat-free body mass are independent, positive predictors of LVM in children [60], and, although the latter is the stronger determinant, adjustment for height alone cannot be predicted from first principles to represent an improved method of predicting LVM. A major obstacle to ascertaining the best method to adjust LVM for body size is the difficulty in determining percent body fat in routine clinical care. Although commonly used, BMI appears to be a rather poor predictor of obesity, with one study demonstrating a false negative rate for obesity of 25% in men and 48% in women [61]. Nevertheless, it remains the most readily available method and is therefore the most commonly used. Several other methods of assessing adiposity are available, including use of more complex computational methods [62], dual-energy x-ray absorptiometry (DEXA) [61], bioelectric impedance analysis [63], and hydrostatic underwater weighing. Bioelectric impedance is inexpensive and easy to implement but concerns persist about its accuracy. DEXA scanning is widely available and radiation exposure is low (about twice that of an airport scanner), but it takes 10–20 minutes and incurs additional expense. Hydrostatic underwater weighing is quite accurate but difficult to implement as a routine procedure. As a result, the modeling of the impact of obesity on LVM has relied primarily on BMI as an estimate of adiposity, despite the limitations of this measure.

Left ventricular mass z-score versus mass-to-volume ratio for detection of left ventricular hypertrophy

Adjusting LVM relative to body size ignores the fact that changing body size and the proportional changes in CO only indirectly impact LVM and do not represent the primary determinants of changes in LVM. The primary hemodynamic determinant of changes in LVM is LV wall stress, which is a function of pressure × (mass/volume) [64]. An increase in either pressure or volume results in higher wall stress, which stimulates a hypertrophic response that persists until wall stress is normalized. In normal children up to age 18, the mass-to-volume ratio (MVR) is constant with age and BSA (Figure 5.7a and b). Any sustained rise in ventricular volume results in compensatory hypertrophy until wall stress is normalized, resulting in similar elevation of LVM and LV volume, known as eccentric hypertrophy. Increased pressure without higher ventricular volume loading stimulates a hypertrophic response that results in a rise in LVM until wall stress is normalized, leading to a higher MVR, known as concentric hypertrophy. Thus, increases in MVR reflect hypertension-induced hypertrophy in contrast to the proportional increase in LVM associated with physiologic (growth, aerobic exercise) or pathologic (anemia, aortic or mitral regurgitation) conditions that cause an increase in LV volume. Obesity does not change the physiologic relationship between blood pressure and LVH, and detection of LV concentric hypertrophy (an increase in MVR) therefore in theory remains the best physiologic measure of the adverse impact of obesity-associated hypertension on LVM. This approach avoids the issue as to what should be the "correct" body size variable for indexing of LVM. Indeed, for detection of hypertension-induced increases in LVM, EDV is in theory the best indexing variable.

The primary limitation to this approach is the accuracy with which the MVR can be measured. The two variables used for this calculation are endocardial volume (EDV_{endo}) and epicardial volume (EDV_{epi}). Since left ventricular myocardial volume

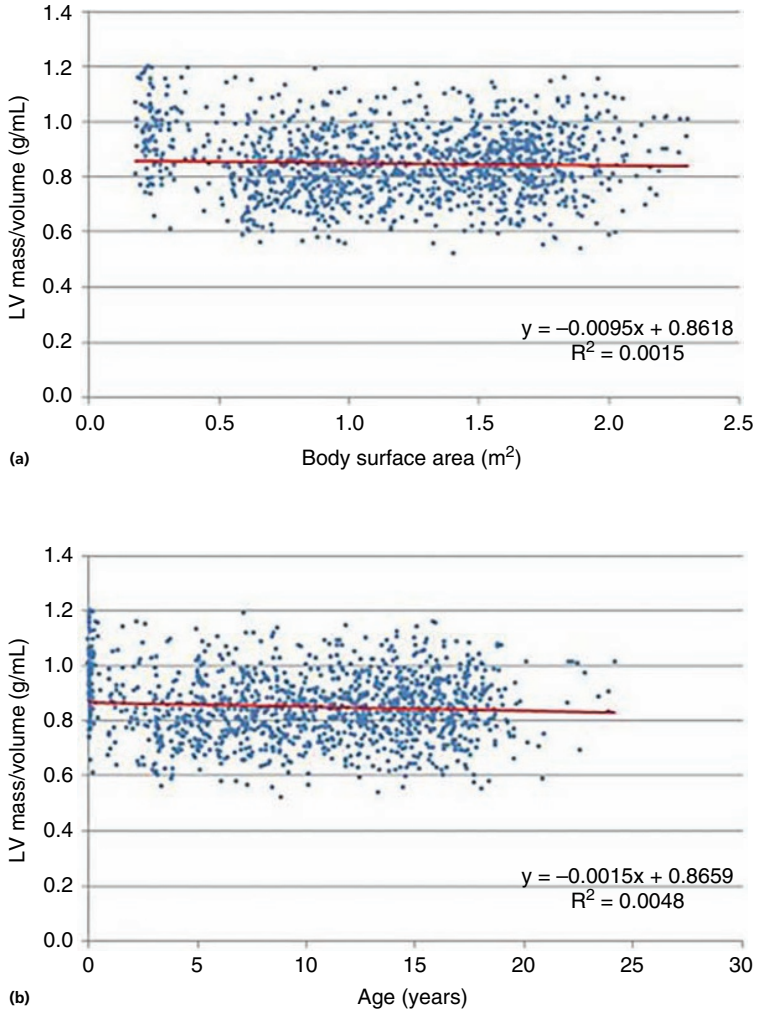

Figure 5.7 **(a)** The left ventricular (LV) mass/volume relationship, a direct measure of the presence or absence of concentric hypertrophy, is constant versus body surface area and age **(b)**.

(= EDV_{epi} – EDV_{endo}) and EDV (= EDV_{endo}) are calculated from the same two measurements as MVR, one might assume that the reproducibility of LVM (which is calculated as the product of myocardial density and volume) and MVR should be similar, but in fact MVR will always have poorer reproducibility compared to LVM due to "propagation of uncertainty" or "propagation of error," whereby reproducibility of the derived variable is always worse than the reproducibility of the independent variables. In this case, propagation of error predicts that the error in calculating myocardial volume = EDV_{epi} – EDV_{endo} is less than the error in calculating MVR = (EDV_{epi} – EDV_{endo})/EDV_{endo}. Empirically, in a prior study of the reproducibility of LV mass and volume measurements in pediatric patients with dilated cardiomyopathy, we found that the intraobserver variability for EDV was 6.6% and the intraobserver variability for LVM was 10%, resulting in an observed MVR intraobserver variability that was 17% [5], as predicted when the propagated error is calculated for this formula. Ultimately, the trade-off here is whether a parameter with a superior physiologic basis (MVR) will prove more predictive of outcomes than a parameter that can be measured more reproducibly.

Conclusion

The progress in therapeutic options available to the pediatric cardiology community has made it requisite that we identify meaningful risk and outcome variables for evaluating our interventions, an effort that often requires the ability to differentiate between the effects of body size and the effects of disease. Echocardiographic imaging techniques have made this information available on an unprecedented scale, enabling analyses that permit both improved understanding of the control mechanisms of cardiovascular growth and the routine application of normative data to clinical practice. Advances in information technology have permitted incorporation of calculation of these normative data into routine laboratory reporting. The intersection of these driving forces makes universal adoption of the z-score techniques requisite for optimal care delivery.

References

1 Lipshultz SE, Miller TL. Establishing norms for echocardiographic measurements of cardiovascular structures and function in children. *J Appl Physiol* 2005;**99**:386–8.

2 Lopez L, Colan SD, Frommelt PC, et al. Recommendations for quantification methods during the performance of a pediatric echocardiogram: a report from the Pediatric Measurements Writing Group of the American Society of Echocardiography Pediatric and Congenital Heart Disease Council. *J Am Soc Echocardiogr* 2010;**23**:465–95.

3 Sluysmans T, Colan SD. Theoretical and empirical derivation of cardiovascular allometric relationships in children. *J Appl Physiol* 2005;**99**:445–57.

4 Colan SD, Parness IA, Spevak PJ, Sanders SP. Developmental modulation of myocardial mechanics: age- and growth-related alterations in afterload and contractility. *J Am Coll Cardiol* 1992;**19**:619–29.

5 Colan SD, Shirali G, Margossian R, et al. The ventricular volume variability study of the Pediatric Heart Network: study design and impact of beat averaging and variable type on the reproducibility of echocardiographic measurements in children with chronic dilated cardiomyopathy. *J Am Soc Echocardiogr* 2012;**25**:842–54.

6 Lopez L, Colan S, Stylianou M, et al. Relationship of echocardiographic *Z* scores adjusted for body surface area to age, sex, race, and ethnicity: The Pediatric Heart Network Normal Echocardiogram Database. *Circ Cardiovasc Imaging* 2017;**10**;e006979.

7 Rhodes LA, Colan SD, Perry SB, Jonas RA, Sanders SP. Predictors of survival in neonates with critical aortic stenosis. *Circulation* 1991;**84**:2325–35.

8 Murray CD. A relationship between circumference and weight in trees and its bearing on branching angles. *J Gen Physiol* 1927;**11**:431–41.

9 Horsfield K. Diameters, generation, and orders in the bronchial tree. *J Appl Physiol* 1990;**68**:457–61.

10 Thompson DW. On the shape of eggs and on certain other hollow structures. In: Press CU (ed.) *On Growth and Form*. New York: Macmillan, 1943, pp. 935–57.

11 Weibel ER. *Morphometry of the Human Lung*. New York: Springer Verlag/Academic Press, 1963.

12 Murray CD. The physiologic principle of minimal work applied to the angle of branching arteries. *J Gen Physiol* 1926;**6**:835–41.

13 Murray CD. The physiologic principle of minimum work: I. The vascular system and the cost of blood volume. *Proc Natl Acad Sci USA* 1926;**12**:207–14.

14 Pollanen MS. Dimensional optimization at different levels of the arterial hierarchy. *J Theor Biol* 1992;**159**:267–70.

15 Kamiya A, Togawa T. Theoretical relationship between the optimal models of the vascular tree. *Bull Math Biophys* 1974;**36**:311–23.

16 Kamiya A, Togawa T. Optimal branching structures of the vascular tree. *Bull Math Biophys* 1972;**34**:431–8.

17 Zamir M. The role of shear forces in arterial branching. *J Gen Physiol* 1976;**67**:213–22.

18 Uylings HBM. Optimization of diametres and bifurcation angles in lungs and vascular tree structures. *Bull Math Biol* 1977;**39**:509–20.

19 Sherman TF. On connecting large vessels to small: the meaning of Murray's law. *J Gen Physiol* 1981;**78**:431–53.

20 Seiler C, Kirkeeide RL, Gould KL. Basic structure-function relations of the epicardial coronary vascular tree: Basis of quantitative coronary arteriography for diffuse coronary artery disease. *Circulation* 1992;**85**:1987–2003.

21 Rossitti S, Löfgren J. Vascular dimensions of the cerebral arteries follow the principle of minimum work. *Stroke* 1993;**24**:371–7.

22 Caro CC, Pedley TJ, Schroter RC, Seed WA. Flow in pipes and around objects. In: Caro CG, Pedley TJ, Schroter RC, Seed WA (eds) *The Mechanics of the Circulation*. New York: Oxford University Press, 1978, pp. 44–78.

23 Yoganathan AP, Cape EG, Sung H-W, Williams FP, Jimoh A. Review of hydrodynamic principles for the cardiologist: Applications to the

study of blood flow and jets by imaging techniques. *J Am Coll Cardiol* 1988;**12**:1344–53.
24 Zoghbi WA, Adams D, Bonow RO, et al. Recommendations for noninvasive evaluation of native valvular regurgitation: a report from the American Society of Echocardiography developed in collaboration with the Society for Cardiovascular Magnetic Resonance. *J Am Soc Echocardiogr* 2017;**30**:303–71.
25 Graham TP, Jr., Jarmakani JM, Canent RVJ, Morrow MN. Left heart volume estimation in infancy and childhood. Reevaluation of methodology and normal values. *Circulation* 1971;**43**:895–904.
26 Gutgesell HP, Rembold CM. Growth of the human heart relative to body surface area. *Am J Cardiol* 1990;**65**:662–8.
27 Henry WL, Ware J, Gardin JM, Hepner SI, McKay J, Weiner M. Echocardiographic measurements in normal subjects. Growth-related changes that occur between infancy and early adulthood. *Circulation* 1978;**57**:278–84.
28 Tanner JM. Fallacy of per-weight and per-surface area standards, and their relation to spurious correlation. *J Appl Physiol* 1949;**2**:1–15.
29 Grollman A. Physiologic variations in the cardiac output in man. *Am J Physiol* 1929;**90**:210–17.
30 Lange PE, Onnasch DG, Schaupp GH, Zill C, Heintzen PH. Size and function of the human left and right ventricles during growth. Normative angiographic data. *Pediatr Cardiol* 1982;**3**:205–11.
31 Abbott RD, Gutgesell HP. Effects of heteroscedasticity and skewness on prediction in regression: modeling growth of the human heart. *Methods Enzymol* 1994;**240**:37–51.
32 El Habbal M, Somerville J. Size of the normal aortic root in normal subjects and in those with left ventricular outflow obstruction. *Am J Cardiol* 1989;**63**:322–6.
33 de Simone G, Galderisi M. Allometric normalization of cardiac measures: producing better, but imperfect, accuracy. *J Am Soc Echocardiogr* 2014;**27**(12):1275–8.
34 London GM, Guerin AP, Pannier BM, Marchais SJ, Metivier F. Body height as a determinant of carotid pulse contour in humans. *J Hypertens Suppl* 1992;**10**:S93–5.
35 Baker-Smith CM, Flinn SK, Flynn JT, et al. Diagnosis, evaluation, and management of high blood pressure in children and adolescents. *Pediatrics* 2018;**142**:e20182096.
36 Kirklin JW, Blackstone EH, Jonas RA, Kouchoukos NT. Anatomy, dimensions, and terminology. In: Kirklin JW, Barrat-Boyes BG (eds) *Cardiac Surgery*. New York: Churchill Livingstone, 1993, pp. 21–60.
37 Bates DM, Watts DG. *Nonlinear Regression Analysis and its Applications*. New York: John Wiley and Sons, 1988.
38 Zar JH. *Biostatistical Analysis*, 2nd edn. Englewood Cliffs: Prentice-Hall, 1974.
39 Montgomery DC, Peck EA. *Introduction to Linear Regression Analysis*, 2nd edn. New York: John Wiley and Sons, 1992.
40 Theil H. *Principles of Econometrics*. New York: John Wiley and Sons, 1971.
41 Altman DG. Construction of age-related reference centiles using absolute residuals. *Stat Med* 1993;**12**:917–24.
42 Ward R, Schlenker J, Anderson GS. Simple method for developing percentile growth curves for height and weight. *Am J Phys Anthropol* 2001;**116**:246–50.
43 Flegal KM. Curve smoothing and transformations in the development of growth curves. *Am J Clin Nutr* 1999;**70**:163S–5S.
44 Cole TJ, Freeman JV, Preece MA. British 1990 growth reference centiles for weight, height, body mass index and head circumference fitted by maximum penalized likelihood. *Stat Med* 1998;**17**:407–29.
45 Cole TJ, Green PJ. Smoothing reference centile curves: the LMS method and penalized likelihood. *Stat Med* 1992;**11**:1305–19.
46 Cantinotti M, Scalese M, Molinaro S, Murzi B, Passino C. Limitations of current echocardiographic nomograms for left ventricular, valvular, and arterial dimensions in children: a critical review. *J Am Soc Echocardiogr* 2012;**25**:142–52.
47 Ho CY, Day SM, Colan SD, et al. The burden of early phenotypes and the influence of wall thickness in hypertrophic cardiomyopathy mutation carriers: findings from the HCMNet Study. *JAMA Cardiol* 2017;**2**:419–28.
48 Ho CY, Cirino AL, Lakdawala NK, et al. Evolution of hypertrophic cardiomyopathy in sarcomere mutation carriers. *Heart* 2016;**102**:1805–12.
49 Haycock GB, Schwartz GJ, Wisotsky DH. Geometric method for measuring body surface area: a height-weight formula validated in infants, children, and adults. *J Pediatr* 1978;**93**:62–6.
50 Du Bois D, Du Bois EF. A formula to estimate the approximate surface area if height and weight be known. *Arch Intern Med* 1916;**17**:863–71.
51 Leonardi B, Margossian R, Colan SD, Powell AJ. Relationship of magnetic resonance imaging estimation of myocardial iron to left ventricular systolic and diastolic function in thalassemia. *JACC Cardiovasc Imaging* 2008;**1**:572–8.
52 Winter EM, Brooks GA. From euclid to molecular biology and gene expression: where now for allometric modeling? *Exerc Sport Sci Rev* 2007;**35**:83–5.
53 Batterham AM, George KP, Whyte G, Sharma S, McKenna W. Scaling cardiac structural data by body dimensions: A review of theory, practice, and problems. *Int J Sports Med* 1999;**20**:495–502.
54 De Simone G, Daniels SR, Devereux RB, et al. Left ventricular mass and body size in normotensive children and adults: Assessment of allometric relations and impact of overweight. *J Am Coll Cardiol* 1992;**20**:1251–60.
55 Daniels SR, Kimball TR, Morrison JA, Khoury P, Meyer RA. Indexing left ventricular mass to account for differences in body size in children and adolescents without cardiovascular disease. *Am J Cardiol* 1995;**76**:699–701.
56 Mahgerefteh J, Linder J, Silver EJ, et al. The prevalence of left ventricular hypertrophy in obese children varies depending on the method utilized to determine left ventricular mass. *Pediatr Cardiol* 2016;**37**:993–1002.
57 Frayn KN, Karpe F, Fielding BA, Macdonald IA, Coppack SW. Integrative physiology of human adipose tissue. *Int J Obes Relat Metab Disord* 2003;**27**:875–88.
58 Flynn JT, Kaelber DC, Baker-Smith CM, et al. Clinical practice guideline for screening and management of high blood pressure in children and adolescents. *Pediatrics* 2017;**140**:e20171904.
59 Collis T, Devereux RB, Roman MJ, et al. Relations of stroke volume and cardiac output to body composition: the strong heart study. *Circulation* 2001;**103**:820–5.
60 Dai S, Harrist RB, Rosenthal GL, Labarthe DR. Effects of body size and body fatness on left ventricular mass in children and adolescents: Project HeartBeat! *Am J Prev Med* 2009;**37** (1 Suppl):S97–104.

61 Shah NR, Braverman ER. Measuring adiposity in patients: the utility of body mass index (BMI), percent body fat, and leptin. *PLoS One* 2012;**7**:e33308.
62 Foster BJ, Platt RW, Zemel BS. Development and validation of a predictive equation for lean body mass in children and adolescents. *Ann Hum Biol* 2012;**39**:171–82.
63 Kyle UG, Bosaeus I, De Lorenzo AD, et al. Bioelectrical impedance analysis-part II: utilization in clinical practice. *Clin Nutr* 2004;**23**:1430–53.
64 Colan SD. Ventricular function in pressure overload lesions. In: Fogel MA (ed.) *Ventricular Function and Blood Flow in Congenital Heart Disease*. Malden: Blackwell Publishing, 2005, pp. 187–204.

CHAPTER 6

Hemodynamic Measurements

Mark K. Friedberg and Olivier Villemain
The Hospital for Sick Children; University of Toronto, Toronto, ON, Canada

Introduction

Hemodynamics refers to the physiology of blood flow. Pressure and flow are commonly assessed in clinical echocardiography to evaluate ventricular performance and pressure, shunt lesions, valvar and vascular stenosis, and valvar regurgitation. Hemodynamic assessment by echocardiography is very useful to diagnose, follow, and manage children with congenital and acquired heart disorders. In this chapter, the principles underlying the clinical use of Doppler echocardiography as well as its important limitations are reviewed. Hemodynamic measurements to evaluate ventricular systolic and diastolic function as well as hemodynamic assessment of specific lesions are covered in the chapters pertaining to those subjects.

Table 6.1 lists the abbreviations used in this chapter.

Blood flow and its assessment by Doppler echocardiography

Blood flow refers to the amount of blood passing a given point during a specified length of time and is expressed as units of volume per unit of time, for example, liters/minute. Flow velocity refers to the rate at which the blood changes position, and is expressed in distance per unit time, for example, meters/second. Laminar flow refers to flow that occurs at a relatively homogeneous velocity and direction across the vessel. Acceleration refers to the rate of change in flow velocity, expressed as units of distance per time squared, for example, meters/second^2 [1,2]. Blood flow velocity can be measured noninvasively using Doppler, while flow and acceleration must be calculated. With the rapidly developing field of high frame-rate echocardiography, blood flow and various associated hemodynamic parameters can now be measured directly by speckle-tracking echocardiography [3].

The periodic nature of the cardiac cycle has a number of implications for blood flow in the heart and central vasculature. The rise in pressure caused by the heart's contraction generates the force that accelerates the blood and generates flow. Because of inertial effects, the increase in flow velocity lags behind the pressure event. Doppler flow across the mitral valve, with a simultaneous pressure recording in the left atrium and ventricle, provides a good illustration of this phenomenon (Figure 6.1). When pressure in the left ventricle falls below that in the left atrium, the pressure difference between the left atrium and ventricle drives flow acceleration into the left ventricle. The flow accelerates as long as pressure is higher in the atrium than in the ventricle. However, peak velocity actually occurs when the pressure has already equalized in both chambers. When the pressure gradient reverses and becomes lower in the atrium, flow decelerates. For a period of time the inertial forces cause blood to flow against the pressure difference, from the atrium into the ventricle.

The Doppler insonation angle

The Doppler insonation angle is the angle between the ultrasound beam and the direction of blood flow. To reliably measure flow velocity by Doppler the insonation angle should be as narrow as possible, that is, the ultrasound beam must be oriented as closely as possible to the direction of flow. When the direction of flow is not parallel to the insonation angle, the flow velocity will be underestimated as a function of the cosine of the insonation angle as per the equation $v_{measured} = v \times \cos(\alpha)$, where v is the blood velocity and α is the angle between the Doppler beam and the direction of flow. When the Doppler beam is at 90° to the direction of flow, the detected flow velocity is zero and therefore invisible to the ultrasound. It is theoretically possible to calculate the true velocity of flow by correcting for the angle between the ultrasound beam and direction of flow. In practice, however, the calculation is suboptimal, and it is far preferable to align the ultrasound beam with the direction of flow. This is facilitated by using color Doppler flow to visualize the flow orientation before placing the pulsed- or continuous-wave Doppler sample. For clinical practice, angles of less than 15–20° between the insonation beam and blood flow are acceptable. In addition, multiple views should be obtained to ensure that the optimal insonation angle and highest velocity are captured.

Echocardiography in Pediatric and Congenital Heart Disease: From Fetus to Adult, Third Edition. Edited by Wyman W. Lai, Luc L. Mertens, Meryl S. Cohen and Tal Geva.

Companion website: www.wiley.com/go/lai-echo3

Table 6.1 Symbols and abbreviations for hemodynamic variables and other parameters

2D – two-dimensional
3D – three-dimensional
C_c – coefficient of contraction
E – energy
g – gravitational constant
h – height
m – mass
P – pressure
ρ – density of blood
v – velocity
AOA – anatomic orifice area
BSI – blood speckle flow imaging
CSA – cross-sectional area
CW – continuous wave
EOA – effective orifice area
EROA – effective regurgitant orifice area
LV – left ventricle or left ventricular
LVOT – left ventricular outflow tract
MR – mitral regurgitation
PAH – pulmonary arterial hypertension
PISA – proximal isovelocity surface area
PRF – pulse repetition frequency
PW – pulsed wave
Qp/Qs – ratio of pulmonary to systemic flow
RA – right atrium or right atrial
ROA – regurgitant orifice area
RF – regurgitant flow
RV – right ventricle or right ventricular
TVI – time-velocity integral
VFI – vector flow imaging

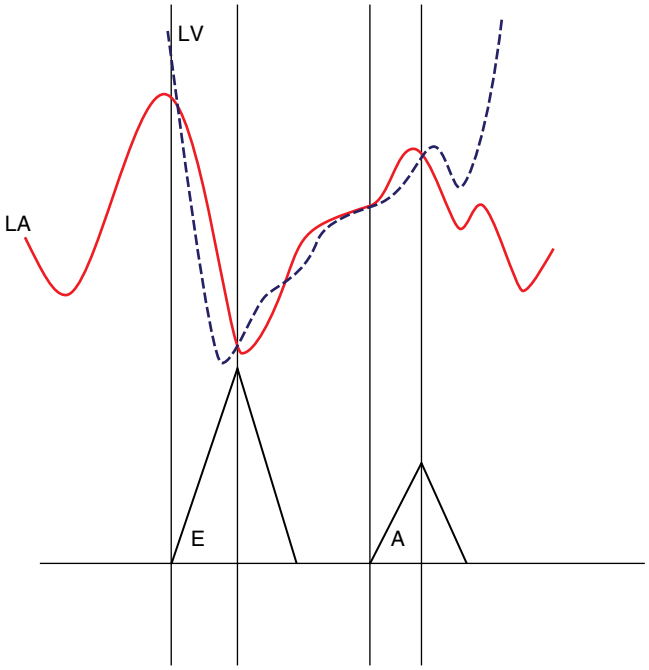

Figure 6.1 The relationship between the mitral inflow velocity and the pressure difference between the left atrium (LA) and left ventricle (LV). Flow acceleration of the E wave on the mitral inflow Doppler tracing begins with the first pressure crossover and corresponds with a period when LV pressure is higher than pressure in the LA. Peak velocity of the E wave corresponds to the second pressure crossover and the deceleration phase of the E wave corresponds to flow against the pressure gradient when LA pressure is higher than LV. This pattern is repeated during the A wave.

Blood flow profiles

Flow is calculated as the product of the average velocity and cross-sectional area (CSA) of the vessel. If flow was constant, laminar, and homogenous across the vessel this would be relatively easy to do. However, in the cardiovascular system, flow is pulsatile and the flow velocity varies across the cross-section of the vessel or orifice. The distribution of flow velocities across the vessel is called the flow velocity profile. In a straight, rigid tube with steady laminar flow, flow velocities are highest in the center and lowest in the periphery. This yields a parabolic velocity profile across the vessel with the highest velocities in the center of the spectral Doppler envelope and the lowest velocities at its edges. In contrast, flow entering a tube from a reservoir has a relatively flat velocity profile at the vessel inlet, that is, all velocities are similar across the vessel cross-sectional area. The flat flow velocity profile at the inlet of the vessel gradually becomes parabolic as flow propagates through the vessel. Because the velocity profile at the vessel inlet is flat, spectral Doppler measurement of the peak velocity at the vessel inlet is more representative of the average velocity. The transition from a flat to a parabolic velocity profile occurs because of the viscous drag between the vessel wall and the adjacent fluid with concomitant acceleration of flow in the center of the vessel. Consequently, when the velocity profile is parabolic, the maximum velocity significantly overestimates the mean velocity, which is the parameter needed to calculate flow. For example, in the branch pulmonary arteries, the flow velocity profile is parabolic and a three-dimensional assessment would be required to derive the true average velocity for flow calculations [1,2]. Likewise, a small Doppler sample volume that captures local velocities may not represent the average velocity across the entire cross-sectional area of the vessel if it is placed either in a region of local turbulence or in a region of local high-velocity laminar flow. One can picture this as a river with fast flow in the center and slow flow at the edges. Sampling the flow in one region will not reflect the average velocity across the entire width of the river. Likewise, sampling flow velocity in a region where the water is turbulent due to rocks does not represent the average velocity of the river across its width. Over the coming years, assessment of blood flow using echocardiography is expected to change rapidly as high frame-rate speckle tracking imaging noninvasively directly assesses the velocity and direction of flow [4].

Other factors also influence flow profiles. At vascular bifurcations, such as the carotid artery bifurcation [5], the greater central velocity in the carotid artery results in a skewed velocity profile in the internal carotid artery, with greater velocity flow adjacent to the bifurcation. In curved vessels, such as the aortic

arch, the flow profile in the curved segment depends on the flow profile at the entrance to the curve. If parabolic, the maximum velocity is shifted toward the outer wall with flow velocity slowing along the inner wall and vortex development or even flow reversal [6] (Video 6.1). In contrast, if the flow profile is flat at the entrance to the curve, centrifugal forces produce higher pressure (lower velocities) at the outer aspect of the curve, and lower pressures (higher velocities) at the inner curvature of the vessel. For example, the flow profile in the ascending aorta is generally flat (velocities are equal across the whole cross-sectional area), and therefore the flow velocities are generally highest along the inner curvature of the aortic arch.

The Coanda effect

The Coanda effect refers to a flow profile where the tendency of a stream of fluid is to follow a convex surface, rather than a straight line. In the heart, the Coanda effect causes jets to adhere to the chamber or vessel wall and can significantly affect Doppler assessment of valvar regurgitation and shunts. Examples include aortic regurgitation jets that track along the valve cusp or the ventricular septal surface and mitral regurgitation (MR) jets that hug the atrial wall (Figure 6.2, Video 6.2). The Coanda effect is actually a manifestation of the Bernoulli principle, which is described in further detail later. The larger decrease in flow velocity along the inner surface of the jet, away from the vessel wall, increases the pressure relative to the outer surface of the jet where velocities are higher, thereby pushing the jet toward the vessel wall. Because of the Coanda effect, and in general because of eccentric jets, multiple echocardiographic views should be obtained in order to achieve the narrowest insonation angle between the ultrasound beam and direction of flow and hence capture the highest velocity.

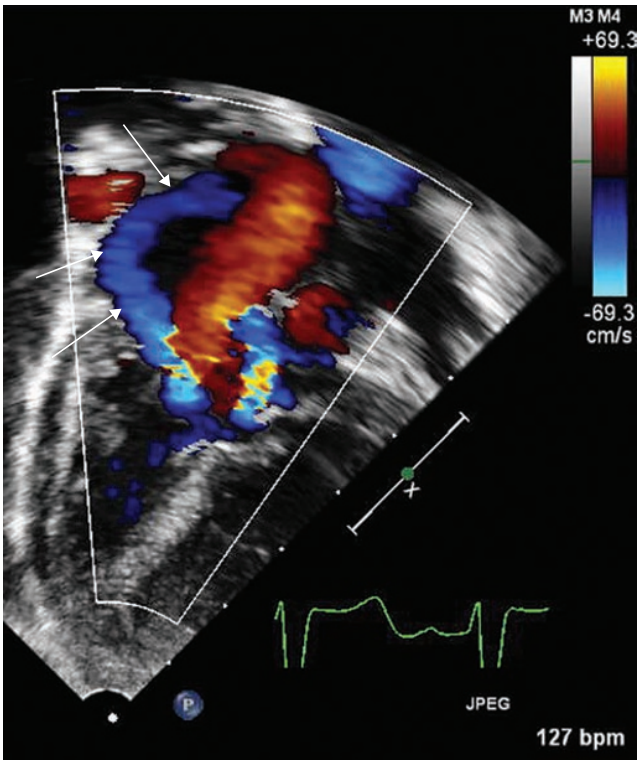

Figure 6.2 Left atrioventricular valve regurgitation on an apical three-chamber (long-axis) view with color flow Doppler in a patient after repair of atrioventricular septal defect. Note the eccentric regurgitant jet going away from the transducer (blue) which then tracks along the left atrial wall (arrows) due to the Coanda effect.

Characteristics of flow through a narrow orifice, the vena contracta, and the phenomenon of pressure recovery

When flow approaches a narrowing, the flow streamlines converge to enter the orifice. This pushes the streamlines close together so that the diameter of the jet passing through the orifice is smaller than the size of the anatomical orifice itself (known as the *anatomic orifice area* (AOA)). The narrowest region of the jet at or immediately after it emerges from the orifice is called the *vena contracta*. Because the vena contracta is the smallest CSA through which the flow passes it is also known as the *effective orifice area* (EOA). The flow velocity is highest and pressure lowest at this point. It is the EOA and not the AOA that determines the hemodynamic importance of a narrowing. Therefore, the hemodynamic effect of a stenosis can be significantly greater than would be predicted on the basis of the actual orifice size. The size of the vena contracta is relatively independent of flow rate and driving pressure for a fixed orifice [7]. The vena contracta is measured from color Doppler [8–10], correlates closely with the actual EOA [11] and severity of valve regurgitation [12], and is therefore used to judge the severity of valvar regurgitation. Downstream of the vena contracta, the streamlines begin to diverge at the periphery of the jet, forming a central core of laminar flow that persists for a variable distance (Figure 6.3).

The high-velocity edges of the central core shear against the stagnant flow around the central jet, creating eddies that gradually engulf the central core and the surrounding area (Figure 6.4). A common error is to assume that aliasing of the color Doppler signal distal to the orifice implies turbulence when in reality it is the turbulent flow of the parajet region creating the aliasing, not high flow velocity. More distally in the vessel, downstream from the stenotic orifice, the phenomenon of pressure recovery becomes important. Let us dwell on this for a moment as pressure recovery impacts Doppler measurements. The Bernoulli equation, which is subsequently discussed, implies that the conversion of pressure to velocity is reversible, and that velocity can be converted to pressure. When blood flows across a narrow orifice, velocity rises and pressure falls, with the lowest pressure associated with the narrowest portion of the jet at the vena contracta. Distal to this point, as the flow stream widens and the flow velocity diminishes, the pressure rises again, a phenomenon known as pressure recovery [13]. In essence,

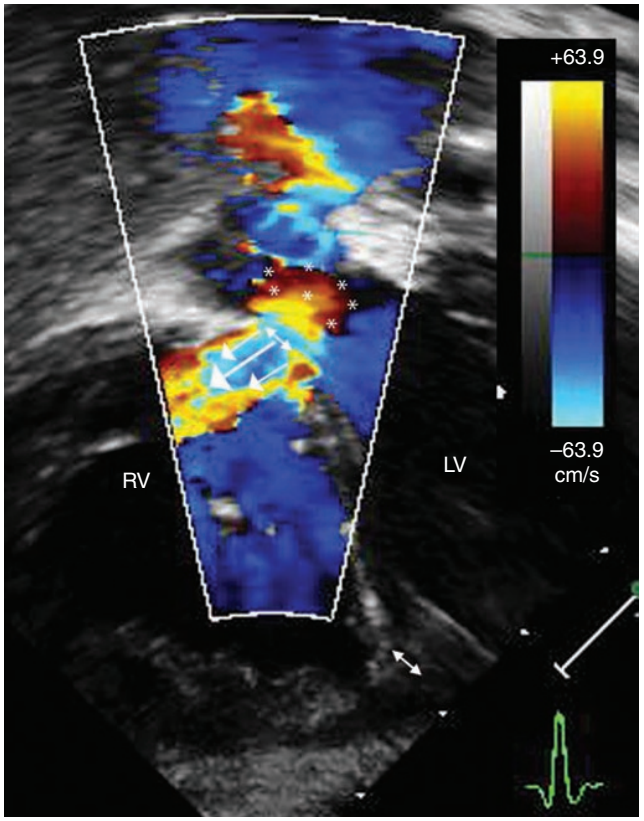

Figure 6.3 Color flow Doppler of shunting through a ventricular septal defect (VSD) depicting flow characteristics of a jet. Proximal to the VSD in the left ventricle (LV), flow is seen converging onto the VSD orifice in concentric semicircles of increasing velocity (proximal isovelocity surface acceleration (PISA)) (asterisks). The jet streamlines form the narrowest diameter at or just beyond the anatomic orifice of the VSD – at the vena contracta (double-headed arrow). Distal to the VSD orifice, the jet is seen with the highest velocity at its center (long arrow) and lower velocities at its edges (short arrows). More distally the flow re-laminarizes and can be seen as the solid orange color at the edge of the sample box in the right ventricle (RV).

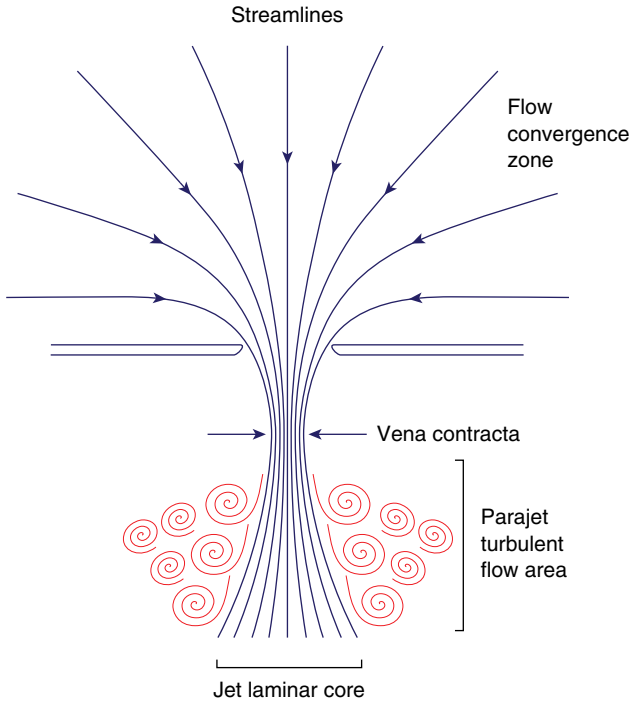

Figure 6.4 Flow through an orifice in a flat surface. The flow convergence area is characterized by nonturbulent flow that follows streamlines converging in a symmetric pattern. The inertial forces of the peripheral streamlines are directed toward the center of the orifice and exert forces in a direction that narrows the jet to a minimum cross-sectional area at the level of the vena contracta; the streamlines then diverge in the jet laminar core. The parajet area is characterized by turbulent flow eddies.

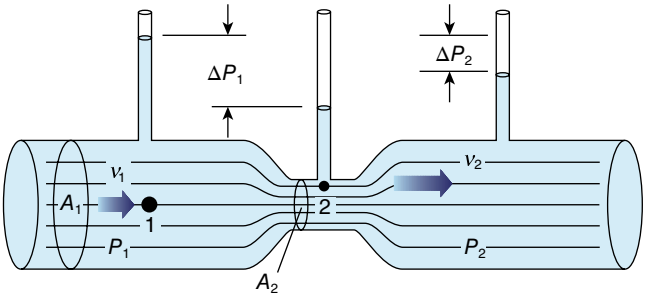

Figure 6.5 The Venturi tube (after Giovanni Venturi, 1746–1822) is a cylindrical pipe with a streamlined constriction designed to minimize energy losses in the fluid flowing through it. The pressure drop between the inlet and area of greatest constriction (ΔP_1) can be used to calculate flow and is the basis of the Venturi meter. The shape of the outlet is optimized to avoid turbulence. With optimal geometry of the tube, pressure recovery can lead to a net loss of pressure as small as 10% (ΔP_2) if turbulent flow is avoided and the only energy loss is due to the viscous effects at the walls of the chamber. A_1 and A_2 are the initial and minimum cross-sectional areas, v_1 and v_2 are the initial and final velocities, and P_1 and P_2 are the initial and final pressures.

pressure recovery occurs because not all kinetic energy across the stenosis is dissipated as turbulence, and some of the flow becomes laminar again. However, pressure recovery is always incomplete because some energy is lost due to friction along the boundaries of the outflow jet (Figure 6.5). The amount of energy lost in this transition depends on the shape of the outlet chamber and can be clinically significant. For example, in aortic stenosis there is an inverse relationship between the size of the aortic root (which is often dilated) and the amount of pressure recovery distal to the stenotic aortic valve [14]. The larger the aortic root, the less the pressure recovery, and the higher the gradient across the valve. Similarly, pressure recovery is less in eccentric jets [14] (Video 6.1). Therefore, for any given orifice size, the functional severity of stenosis is greater in eccentric jets, both because of a greater pressure loss (smaller effective orifice area) and because of diminished pressure recovery.

When a Doppler sample is placed at, or immediately distal to the vena contracta, pressure recovery has not yet occurred and even though the measured gradient is true, it will overestimate